Global examination of papillomavirus protein-protein interactions: the intraviral interactome of HPV31 and the cellular binding partners of cutaneous papillomaviruses

Dissertation

der Mathematisch-Naturwissenschaftlichen Fakultat

der Eberhard Karls Universitat Tübingen

zur Erlangung des Grades eines

Doktors der Naturwissenschaften

(Dr. rer. nat.)

vorgelegt von

Giada Corradini Bartoli

aus Rom/Italien

Tübingen

2017

Gedruckt mit Genehmigung der Mathematisch-Naturwissenschaftlichen Fakultat der

Eberhard Karls Universitat Tübingen.

Tag der mundlichen Qualifikation:	16.10.2017
Dekan:	Prof. Dr. Wolfgang Rosenstiel
1. Berichterstatter:	Prof. Dr. Thomas Iftner
2. Berichterstatter:	Prof. Dr. Peter G. Kremsner

Table of Contents

1. Summary

Human papillomaviruses (HPVs) comprise a large group of small DNA viruses that infect mucosa and epithelia. Infections can be either asymptomaticand cleared by the immune system or they can persist and cause cancer. Many studies supported the causative role of HR-HPVs in cervical carcinoma, whereas the HPV-related causality of non-melanoma skin cancer (NMSC), where HPV is thought to act as a co-carcinogen, is not fully understood.

Protein-protein interactions were studied in this work to get more insights into cutaneous PV tumor development and to obtain a comprehensive intraviral interactome of HPV31.

Since expression of the two viral oncoproteins E6 and E7 are associated with the progression of HPV-related tumors, cutaneous E6 proteins of HPV5, 38 as well as CRPV were used as baits to perform mass-spectometry (MS)-based assays to identify new cellular interaction partners. Analysis of the MS data led to the confirmation of previously published interactors and to the identification of new proteins. Among them, the 17-Beta-Hydroxysteroid Dehydrogenase isoforms 4 (17βHSD4) was validated as an interactor of both CRPV and 38E6.

A flow cytometry-based FRET assay (FACS-FRET) was used to unravel the intraviral interactome of the HR type HPV31. Nine viral proteins were fluorophore-tagged and then tested for interactions between each other via FACS-FRET. The screening revealed new interactions besides confirming the previously reported ones. For the first time, we show an interaction between the E6 and E7 oncoproteins.

These findings contribute to a better understanding of the molecular mechanisms by which cutaneous PV interfere with the host. The data might furthermore be the basis for future research elucidating mechanisms by which cutaneous PVs cause cancer and ultimately pave the path for new therapeutic options for the treatment of PV-induced malignancies.

Zusammenfassung

Humane Papillomaviren (HPVs) umfassen eine große Gruppe von kleinen DNA-Viren, die die Schleimhaut und das Epithel infizieren. Infektionen können entweder asymptomatisch sein und durch das Immunsystem kontrolliert werden oder sie können persistieren und Krebs verursachen. Viele Studien unterstützen eine ursächliche Rolle von HR-HPVs in der Entstehung von Gebärmutterhalskrebs, während die HPV-bezogene Kausalität von Non-Melanoma-skin cancer (NMSC), wo HPV als Co-Karzinogen wirkt, nicht vollständig geklärt ist.

In dieser Arbeit wurden Protein-Protein-Wechselwirkungen untersucht, um Einblicke in die Tumor-Entwicklung durch kutane PV und in das intravirale Interaktom von HPV31 zu erhalten.

Da die Expression der beiden viralen Onkoproteine E6 und E7 mit der Progression von HPV-induzierten Tumoren korreliert, wurden die kutanen E6-Proteine von HPV5, 38 sowie CRPV als Baits verwendet, um Massenspektrometrie (MS) -basierte Assays durchzuführen, um neue zelluläre Interaktionspartner zu identifizieren. Die Analyse der MS-Daten führte zur Bestätigung von bisher veröffentlichten Bindungspartnern und zur Identifizierung neuer Proteine. Unter ihnen befindet das Protein 17-Beta-Hydroxysteroid Dehydrogenase Isoformen 4 (17βHSD4), welches als neuer Interaktor von CRPV und 38E6 validiert wurde.

Ein Flüssigzytometrie-basierter FRET-Assay (FACS-FRET) wurde verwendet, um das intravirale Interaktom des HR-Typs HPV31 zu analysieren. Neun virale Proteine wurden mit Fluorophoren markiert und dann auf Wechselwirkungen miteinander mittels FACS-FRET getestet. Das Screening zeigte neben der Bestätigung von zuvor beschriebenen, auch bisher unbekannte Interaktionen. Zum ersten Mal konnte somit eine Interaktion zwischen den E6- und E7-Onkoproteinen gezeigt werden.

Diese Erkenntnisse tragen zu einem besseren Verständnis der molekularen Mechanismen bei, durch welche kutane PV den Wirtsorganismus beeinflussen. Weiterhin stellen diese Ergebnisse das Fundament für zukünftige Forschungsvorhaben zur Aufklärung der molekularen Mechanismen dar, durch welche kutane PV Krebs verursachen, und ebnen letztlich den Weg für neue therapeutische Ansätze für die Behandlung von PV-induzierten Malignitäten.

2. Introduction

2.1 Papillomaviruses

Papillomaviruses (PVs) are small DNA viruses, belonging to the *papillomaviridae* family. They are able to infect mucosal and cutaneous epithelia and are characterized by a high tissue- and host-specificity. PVs classification is based on the comparison of the nucleotide sequence of the major capsid proteins L1 open reading frame (ORF). L1 is the most conserved gene in the viral genome and its sequence is used to differentiate new types (>10% different to the closest type), subtypes (2-10%) and variants (< 2%) [1]. More than 200 PVs were identified so far, 174 of which are known to infect humans and are divided in 5 genera: alpha, beta, gamma, mu and nu (Fig. 1). HPVs can be further divided in mucosal (Alpha) and cutaneous (Beta, Alpha4, Gamma, Mu, Nu) types based on their tissue tropism [2].

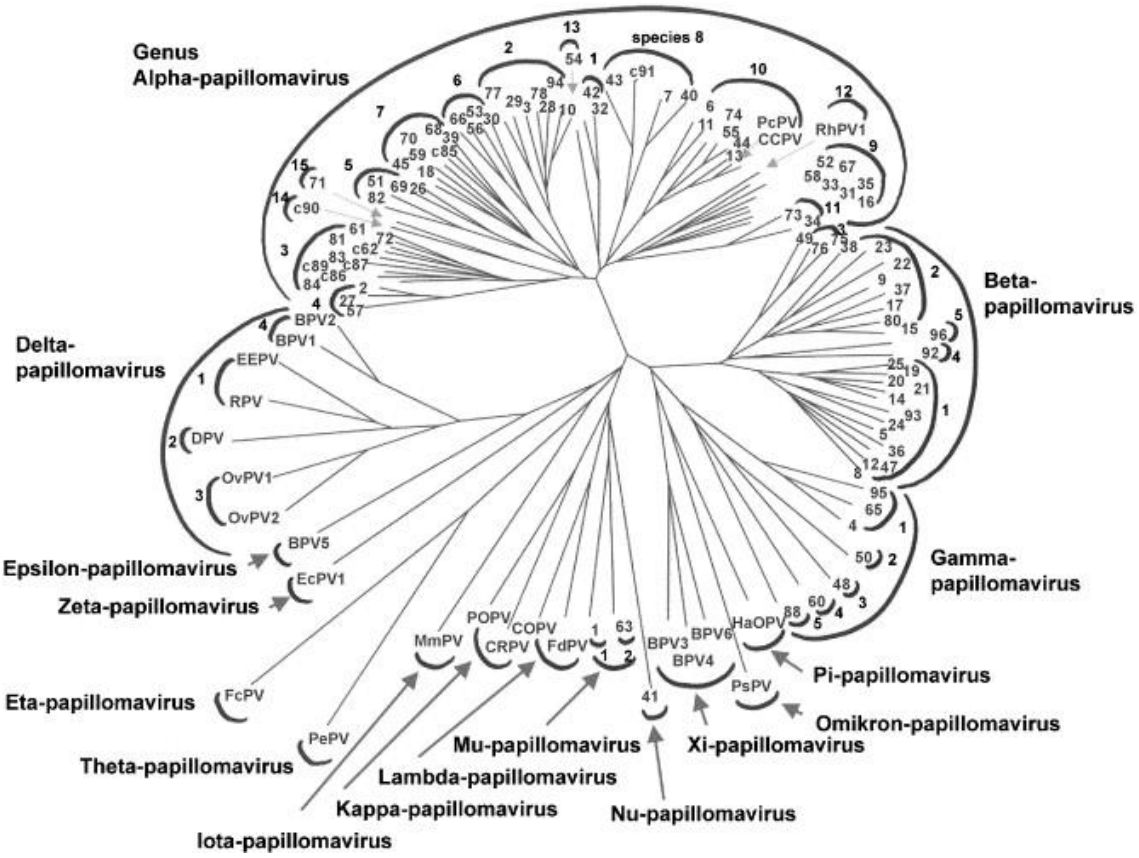

Fig. 1 Classification of papillomaviruses (Figure adapted from de Villiers E. et al., 2004 [1])

1.1.1 Clinical relevance

Several HPV types inhabit skin and mucosa asymptomatically but some HPVs can lead to lesions ranging from self-limiting benign warts to abnormal malignant growth. Because of their documented association with tumors, some HPV types were classified as carcinogens by the International Agency for Research on Cancer (IARC) [3] (Fig. 2)

Fig. 2 Classification of carcinogenicity of different HPV types made by IARC (Figure adapted from Bravo I.G. & Félez-Sánchez, M., 2015 [3])

Mucosal α-HPV types, because of their varying carcinogenic potential, can be subdivided in high risk (HR, associated with cervical cancer, other genital cancers and oropharyngeal cancers) and low risk (LR, related to genital warts and papillomas) [4]. Cervical cancer is the 4th most common cancer in women worldwide with approximately 500,000 new cases every year (World cancer research fund: http://www.wcrf.org/). Cervical HPV infections are the most common sexually transmitted infections and HPV16 (50%), followed by HPV18, 45 and 31 are the most common types detected in Europe [5]. It was shown that the majority of the

women are infected during their first sexual contact [6] and that women younger than 25 years have the highest prevalence [7], [8]. Approximately 90% of cervical infections are cleared by the immune system within two years [9], however, a persistent infection can progress to cervical intraepithelial neoplasia (CIN), that is differentiated in mild (CIN1), moderate (CIN2) and severe (CIN3/carcinoma in situ) dysplasia. The pre-malignant lesions CIN1 and CIN2 can spontaneously regress over the years in 57% and 47% of the cases respectively [10], whereas an untreated CIN3 can develop cancer in 30-50% of the cases within 30 years [11]. A common feature of cervical cancers is the integration of the viral DNA into the host genome with the resulting disruption of the E2 gene, which is the viral regulator of transcription, replication, genome maintenance and partitioning, and the consequent constitutive expression of the E6 and E7 oncogenes that favor tumor growth [12].

Although mucosal HPVs were documented to be the causative agents of virtually all cervical carcinomas [13], it is still controversial whether cutaneous HPVs are causally involved for skin cancer development.

The first reports showed that the β1-HPVs 5 and 8 are associated with skin cancers in patients with the autosomal recessive hereditary disease Epidermodysplasia verruciformis (EV) [14], [15]. Squamous cell carcinoma (SCC) can arise within 10-30 years after the first manifestation of benign lesions in 30-50% of EV-affected patients on sun-exposed sites [15] and 90% of these cancers are positive for HPV5 and 8 [16].

Nonmelanoma skin cancer (NMSC) is the most common cancer worldwide in the Caucasian population and accounts for almost 40% of all cancer cases [17]. NMSC comprises actinic ketatosis and Bowen's disease but also squamous cell carcinoma (SCC) basal cell carcinoma and (BCC) that account for 16% and 80% of all skin cancers, respectively [18], [19]. For the development of NMSC, age, skin, UV light exposure and immunosuppression are major risk factors [20]. Concerning the immune status of the host, organ transplant recipients under immune suppression were documented to have a 50-100 times higher risk for NMSC [21]. Although HPV involvement in NMSC remains unclear in healthy individuals, β_2-HPV infection is thought to be associated with NMSC since HPV DNA was found in approximately 50% of SCCs in immunocompetent individuals whereas it reached 80% in immunocompromised people [22], [23]. Unlike HR, cutaneous HPVs are most likely co-carcinogens since they may contribute to cancer cooperating with other factors such as UV radiation and/or immunosuppression. The other main difference is that only a small number of NMSC cells contain viral DNA [24], [25] pointing towards a role of cutaneous HPVs in the beginning of tumorigenesis whereas in cervical cancer the viral oncoproteins are constitutively expressed [26].

1.1.2 Genome organization

The HPV genome is a circular double-stranded DNA comprising approximately 8 kb which contains a coding region of 8 or 9 ORFs (depending on the type) and an upstream regulatory region (URR) also known as long control region (LCR) which contains the origin of replication and regulatory elements (Fig. 3) [27]. The coding region encodes for early (E) and late (L) proteins. Early proteins play a role in replication, transcription, maintenance of the viral genome, cell cycle and apoptosis control while the late genes are transcribed and then translated in the structural proteins composing the icosahedral capsid.

Two promoters and two different poly-adenylation sites control transcription of the polycistronic HPV mRNAs according to the differentiation status of the infected cell [28].
In the beginning of the infection, only the early promoter (p97 for HPV31 and 16; p105 for HPV18), located in the URR, is activated and can guide the expression of E1 and E2, for the establishment of the stable viral episomes, and E6 and E7, to control the cell cycle [27]. At the time of differentiation, the late promoter (p742 for HPV31; p670 for HPV16) is activated and this increases the transcription of E1 and E2 proteins [29], responsible for genome amplification [29]. At the same time it leads to the expression of E1^E4, E5, L2 and L1, responsible for genome packaging into viral particles and virion release [27]. Polyadenylation sites contribute to transcription regulation as well: the early polyadenylation site (pAE) drives the polyadenylation of the mRNAs produced in the first steps of the viral life cycle by the early promoter. Upon cellular differentiation, polyadenylation occurs via the late polyadenylation site (pAL) on the late promoter transcripts. Alternative splicing is another way how HPV regulates its gene expression [30].

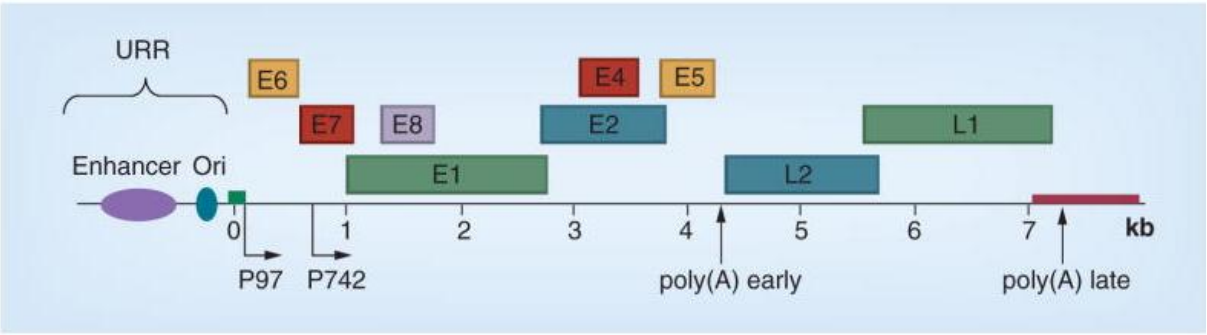

Fig. 3 Linearized HPV31 genome showing the URR followed by the promoters and the polyadenylation sites that are directing transcription of the viral genes (figure taken from [27]).

1.1.3 Viral proteins

The only enzyme expressed by papillomaviruses is the E1 protein, an ATP-dependent helicase expressed at low levels in HPV-positive cells [31]. E1 recognizes AT-rich sequences in the origin (ori) of replication, next to the early promoter and its binding is strengthened by complex formation with E2. Upon binding, E1 assembles into double hexamers, its active form, and can recruit a complex for DNA replication on the viral ori where it unwinds the DNA, making it accessible for replication [32], [33].

The DNA binding protein E2 is the viral regulator of transcription, replication, genome maintenance and partitioning [34]. E2 acts mainly by recruiting cellular proteins to specific DNA sequences, called E2 binding sites (E2BS), which are predominantly present next to the E1BS at the ori. In this way E2 controls transcription in a dose-dependent manner and enhances E1 function in the initial phase of replication [35]. Another important function of E2 is to ensure proper genome partitioning to each daughter cell during mitosis, by tethering the viral DNA to the segregating chromosomes [36].

The ORF of E4, the most expressed HPV protein, is located within the E2 ORF and is expressed as a splice variant, E1^E4 [37]. Historically, E4 was classified as an early protein, however many studies have demonstrated that it is involved in the late stages especially taking into account that the capsid proteins, L1 and L2, are expressed only in E4-positive cells and that the expression of E4 temporarily precedes the one of L2 and L1 [38]. Moreover, during its accumulation in the upper epithelial layers, E4 associates and disrupts the keratin network, pointing towards a possible role in virion release [39].

Many papillomaviruses, except the beta, gamma and mu genera, encode the E5 ORF, a small hydrophobic protein with transforming activity. E5 function was studied mainly in BPV, where it shows a strong tumorigenic activity, and in HPV16 where this activity is rather weak [40]. The role of E5 is not yet totally understood but it can stimulate cell growth by influencing mitogenic signals stemming from EGFR-mediated pathways: since E5 localizes on the membrane, it can bind EGF receptors, thus causing receptor dimerization and signaling activation [41], [42]. Moreover, by association with the vacuolar ATPase, E5 can delay the endosomal acidification which affects EGFR recycling with a consequent increased transmission of growth signals to the nucleus [43], [44]. By simultaneous endosomal alkalinisation, E5 contributes to immune escape by accumulating MHC class I molecules in the Golgi and thus reducing its expression on the membrane [40].

The two structural proteins L1 and L2, generated by alternative splicing, are expressed during the late phases of the viral life cycle, engaging the late promoter and the pAL [45]. Virions are non-enveloped particles and the icosahedral capsids, approximately 55 nm in diameter, are composed by 360 molecules, organized in 72 pentamers, of the major capsid protein L1 and an unknown number of the minor capsid protein L2, which mainly resides in the central cavity of the L1 pentamer [46], [47]. An important feature of the L1 protein is that it is able to modulate its conformation depending on the viral cycle stage: in the beginning of the infection L1 guarantees viral attachment but after entry allows viral genome to enter the cell [48]. Although the L2 protein is hidden into the capsid during the first stages of infection, is thought to have a crucial role during viral attachment [49], [50]. Moreover, it has been shown that L2 contributes in later steps: following entry it could mediate transition to the Golgi network, and entrance of the viral genome into the cell nucleus [51].

1.1.4 Viral oncoproteins

During the productive phase of viral life cycle the early proteins E6 and E7 play a key role in enhancing cell proliferation and delaying cellular terminal differentiation. By interfering with the host cell, the viral genome is amplified and an increased number of infectious viral particles can be produced [52]. When the viral genome integrates, as it is in the case of cervical cancer, E6 and E7 are constitutively expressed and, acting as oncoproteins, they favor cell proliferation and inhibition of apoptosis thereby sustaining cellular transformation (Bedell et al. 1987; Vousden et al. 1988). Earlier studies showed that HR-E6 and E7 are responsible for keratinocytes's transformation [55], [56] and that E6, unlike E7, is not able to immortalize cells alone. However, when E6 is co-expressed, it increases the efficiency of immortalization. Compared to HR, LR-E6 and E7 have little or no immortalizing activity [57]. E6 and E7 can influence different cellular processes, ranging from cell cycle to cell death and, due to the fact that they were never been shown to possess enzymatic activity, they use mainly protein interactions to alter cellular protein functions [58], [59]. HR viral oncoproteins collaborate to favor cell growth and avoid apoptosis: they were both shown to contribute to genomic instability [60] which is needed for malignant progression and to interact with the BRCA1 (BReast CAncer 1) protein with the consequent release of hTERT (human Telomerase reverse transcriptase) repression [61]. On the other hand, HR-HPV E6 proteins were also shown to increase telomerase activity by interacting with the NFX1 (Nuclear Transcription Factor, X Box-Binding Protein 1) proteins [62].

Since cutaneous HPVs are mainly associated with benign warts, they were not so extensively studied like the α-HPVs. Previous reports, however, showed that HPV38 and 49 have immortalizing activity [63], [64] and that the EV-associated types, HPV5 and 8, can activate telomerase [65].

Exclusive for HR E6 proteins' structure is a dimerization domain at the N-terminus and a PDZ (PSD-95, Dlg, ZO-1 proteins) binding domain at the C-terminus. E6 proteins, in addition, contain two zinc-finger domains, formed by four Cys-X-X-Cys motifs [66], connected by a helical linker that together form a pocket able to bind LXXLL sequences, contained in cellular proteins that bind E6 of both mucosal and cutaneous HPVs [67] (Fig. 4). The most thoroughly studied property of HR-E6 is its interaction with the tumor suppressor protein p53 [68], [69]. p53 regulates several cellular processes and is responsible for cell cycle arrest, apoptosis and senescence [70]. In normal cells p53 is inactive and constantly degraded by the proteasome, but its activation by DNA damage or cellular stress leads to cell cycle arrest or cellular apoptosis [71]. HR-E6 has been shown to form a ternary complex with p53 and with the ubiquitin ligase E6AP (E6 associated protein), which contains an LXXLL motif. E6, via E6AP, ensures cell cycle progression through p53 poly-ubiquitination and proteasomal degradation [72]. Also the cutaneous HPV38 E6 can interfere with p53 signaling by accumulating the p73 isoform which inhibits p53 activity [73]. Moreover, β-HPVs HPV5, HPV8, and HPV38 were shown to prevent stabilization of p53 in presence of genome instability [74].

E6 proteins of cutaneous PVs interact with the LXXLL-peptide containing MAML (Mastermind-like) family of transcription activators [75], [76]. MAML proteins regulate Notch pathway activation and it has been shown that Notch signaling acts as a tumor suppressor in the skin [77]–[79]. HPV8 E6, by interacting with MAML1, can delay Notch-induced keratinocytes's terminal differentiation and therefore favor HPV life cycle progression [80].

Cutaneous and HPV16 E6 can regulate p53 also through its association with the acetyltransferase p300 (Muench et al. 2010b; Zimmermann et al. 1999). By binding p300, E6 blocks p53 acetylation and consequently inhibits the transcription of p53 regulated genes [83]. HPV5 and 8 bind p300 much more efficiently if compared to HPV16 or HPV38 and this binding leads to p300 in an E6AP-independent manner [81].

PDZ domain-containing proteins have tumor suppression functions and can interact with the C-terminus of HR-E6. HDlg1, hDlg4 [84], MAGI-1, -2, -3 [85], [86] and MUPP1 [87] are PDZ proteins known to be targeted by E6. However, E6-mediated inactivation or degradation of PDZ proteins does not seem to be directly related to the carcinogenic potential of HPV [88], [89].

E6 can inhibit apoptosis in different ways: LR, HR and the cutaneous HPV5 and 8 E6 interact with Bak (Bcl-2 homologous antagonist/killer), a pro-apoptotic protein, and induce its E6AP-dependent degradation in response to UV DNA damage [90], [91]; FADD (Fas-associated death domain), a protein involved in the extrinsic apoptosis pathway, can also be degraded by E6 [92].
Moreover, through alternative splicing a short isoform of HR-E6 named E6* is produced. This protein, which comprises the N-terminus of E6, does not interact with LXXLL, but instead interacts with full length E6 and E6AP [93] and inhibits p53 degradation thereby controlling E6 activity.

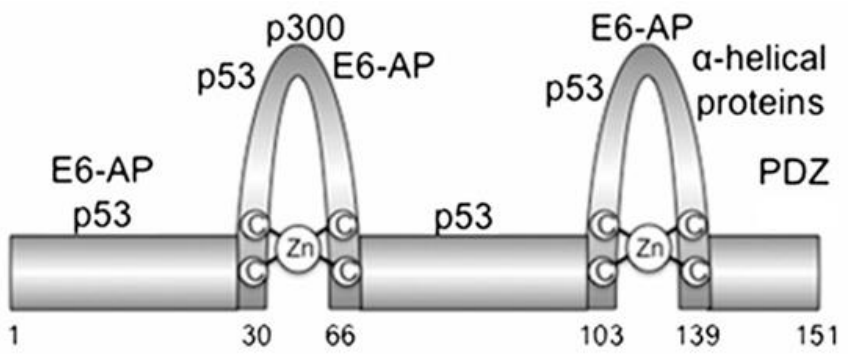

Fig. 4 HPV16 E6 structure (Figure adapted from [94])

E7 proteins consist of approximately 100 amino acids and their structure is characterized by a zinc-finger motif at the C-terminus, which is also a dimerization domain [66]. The amino terminus of E7 share sequence similarity with the Simian virus 40 large T antigen (SV40 T-Ag) and the Adenovirus E1A protein (Ad-E1A) in two regions called conserved regions (CR) 1 and 2 [95], [96]. The CR1 and 2 domains, as for SV40 T-Ag and Ad-E1A, are responsible for the transforming activity of HR-E7 [97] (Fig. 5).

HR-E7s interact with the pocket protein family (pRb, p107, p130) through the LXCXE motif in the CR2 domain and this interaction is stronger in HR-HPVs when compared to LR- and EV-associated HPVs [98]–[100].
pRb is an oncosuppressor that normally limits the activity of the E2F transcription factor, thus inhibiting cell cycle progression from G1 to S phase until the cell is prepared to divide. In the absence of pRb, E2F activates the transcription of genes involved in cell growth [101]. In the context of a HPV infection, the E7 protein abrogates pRb-E2F interaction by degrading or

just binding pRb, leading to deregulated cell cycle and thus contributing to cancer development [102].

E7 proteins from different types bind UBR4 (p600), an E3 ubiquitin ligase [103], and for HPV16 it was shown to be involved in transformation and anchorage-independent growth [104]. For HPV16 E7 it was also documented that pRb degradation is obtained via E7 interaction with ZER1. The ternary complex pRb-16E7-ZER1 can then associate with the cullin2 complex that targets pRb for degradation [103], [105].

Moreover, HR-E7 can induce chromatin remodeling through interactions with histone acetyltransferases (HATs) and histone deacetylases (HDACs) as well as histone methyltransferases (HMTs) and demethylases [106], [107].

Like E6, E7 contributes indirectly to hTERT transcription, since hTERT promoter contains an E2F binding site that can be activated once pRb is blocked [108].

Telomerase activation and pRb inactivation are essential for immortalization [109].

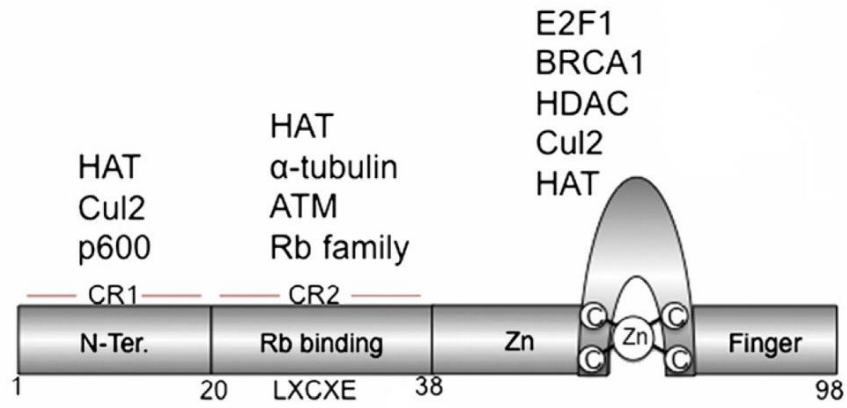

Fig. 5 HPV16 E7 structure (Figure modified from [94])

1.1.5 Cottontail Rabbit PapillomaVirus (CRPV)

The relationship between papilloma virus and cancer was first demonstrated by infection of domestic rabbits with CRPV [110]. CRPV, also known as Shope rabbit papillomavirus, is a kappa PV and was first found in warts of cottontail rabbits [111]. Former studies showed that CRPV could infect different rabbit strains, where it promotes skin tumor formation within 3 to 6 weeks post infection [110]. However, only in domestic rabbits these papillomas progress in 80% of the cases to invasive carcinoma in 6-12 months without any other co-factor, whereas in cottontail rabbits, its natural host, they generally regress spontaneously [112], [113]. Clearly, infection of domestic rabbits with CRPV is a suitable method to study several aspects of PV infections *in vivo* and, in particular, to understand the complex mechanisms behind PV-induced skin tumors.

1.1.6 CRPV genome and viral proteins

The CRPV genome is similar to HPV in organization and protein sequence conservation (Fig. 6). It consists of 7,868 nucleotides encoding 10 genes [114] that follow the same time- and space-dependent expression pattern as it is for HPVs. Viral transcription is regulated by three early promoters (PE-1, PE-2, PE-3) and one late promoter (PL). Two polyadenylation sites (poly-AE, poly-AL) and alternative splicing are also involved in regulating transcription. As for other PVs, early genes are transcribed as polycistronic mRNAs in the initial phase of infection but transcription starts from three different early promoters; the transcripts are poly-adenylated at the poly-AE site and are subjected to alternative splicing. In the last stage of differentiation, when only L1 and L2 are produced, transcription begins at the PL and the resulting mRNAs are poly-adenylated at the poly-AL.

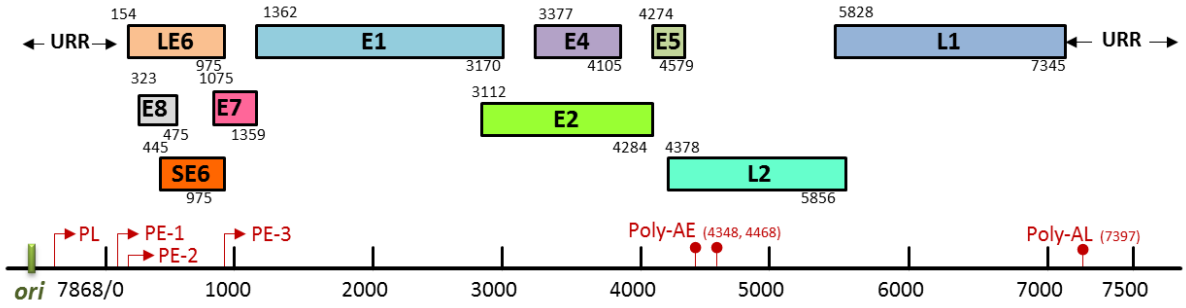

Fig. 6 Linearized CRPV genome showing the URR, the promoters and the polyadenylation sites that are directing transcription of the viral genes (figure taken and modified from [115]).

Protein sequences and functions are also conserved among PVs. There are, however, few exceptions. In HR-HPVs, the E6* isoform derives from alternative splicing while the two CRPVE6 proteins (Long and Short E6) are expressed by two different promoters [116], [117]. Long E6 (LE6) transcription initiates at the first ATG and Short E6 (SE6) is translated from a second transcript that starts at the second ATG contained within the LE6 sequence [116]. Unlike HR-HPVs, CRPVE6 proteins are not able to bind and degrade p53, however by binding p300 they indirectly interfere with p53-mediated apoptosis [63]. CRPVE7 shares some functional similarities with HR-HPVE7: among other things, both bind pRb resulting in the release of E2F that stimulates cell cycle progression [118].

1.2 HPV life cycle

1.2.1 Attachment and viral entry

It has been suggested that the initial infection takes place in proliferating cells of the basal layer after a micro lesion of the epithelium has occurred [29]. Several studies investigated the entry step of HPV life cycle leading to the conclusion that the first contact is between the major capsid protein L1 and a receptor present on the cell surface or on the extracellular matrix (ECM). The majority of the studies demonstrated that HPVs use heparin sulfate proteoglycans (HSPGs) [119], [120] as their main attachment receptors. HSPGs are complex glycoproteins composed of a core protein with covalently attached heparan sulfate chains. They are either expressed on the cell surface on the cell surface (Syndecan-1 and glypicans) or secreted into the ECM (agrin, perlecan, type XVIII collagen) [121]. During wound healing, basal keratinocytes highly express a specific HSPG, Syndecan-1, that was also demonstrated to be mainly expressed in the epithelial tissue, specifically in proliferating keratinocytes making it a perfect candidate as a potential attachment receptor (Sapp & Bienkowska-Haba 2009; Shafti-Keramat et al. 2003).

However, other studies propose that the primary binding might take place at the basement membrane, excluding an involvement of a cell membrane receptor but rather suggesting that a secreted HSPG might be required. Laminin 5, highly expressed during wound healing by migrating keratinocytes and released into the ECM, is a putative protein for this role as it might act as a transient receptor that allows HPV capsid proteins to bind the attachment receptors on neighboring cells [123], [124].

The nature of the primary attachment receptor is still controversial but it is certain that the binding of L1 to the receptor leads to the exposure of the hidden N-terminus of the minor capsid protein L2, a process mediated by the cell chaperone cyclophilin B. This conformational change leads to the cleavage of the L2 amino-terminal domain by a furin convertase [47] which might result in a loss of affinity for the primary receptor and the subsequent exposure of a secondary receptor binding site in L1 [49], [50] (Fig. 7).

Although the nature of the secondary receptor, responsible for HPV internalization is still controversial, there are a few candidates that seem to form a protein complex to help HPV in entering the cell: α6 integrins (α6β1, specifically expressed in the cells of the basal layer, and α6β4, mainly expressed during wound healing on epithelial cells) and epidermal growth factor receptors (EGFRs, highly expressed in the epithelial basal layer) were shown to be

able to bind HPV. Moreover, after the binding, α6 integrins and EGFRs may collaborate in assembling an entry platform in association tetraspanins [125].

Previous studies showed that viral particles co-localize with the tetraspanins CD151 and CD63. Tetraspanins can form complexes, called tetraspanin-enriched microdomains (TEMs), associating with other membrane proteins, such as α6 integrins and EGFRs. The hypothesis is that TEMs may be responsible of transferring HPV binding from the primary to the secondary receptor complex [125], [126].

After cell surface binding, to initiate a productive infection, HPV particles are internalized into the cell. It is evident that HPV entry occurs by endocytosis [127].

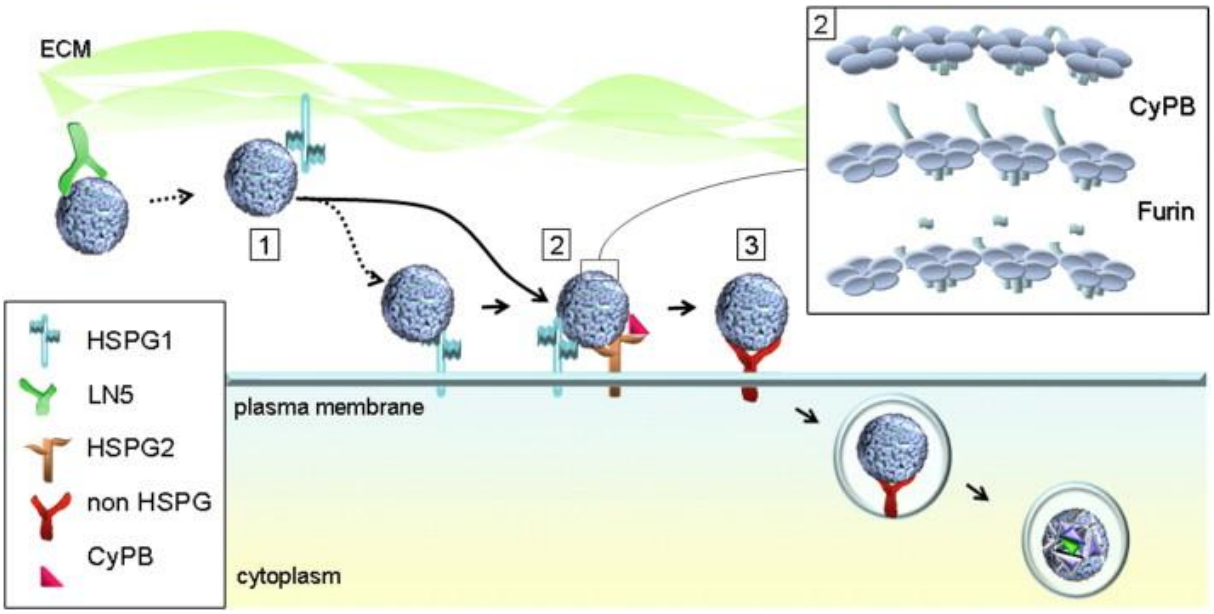

Fig. 7 HPV internalization model. The process shows primary and secondary receptor binding. (1) The virion binds to the primary attachment receptor, HSPG1. (2) The binding is transferred to secondary HSPG binding sites present on the cell surface (HSPG2) and this results in conformational changes leading to the exposure of the L2 amino terminus and furin cleavage. (3) Another conformational change triggers endocytosis. Extracellular matrix (ECM); Laminin 5 (LN5); HeparanSulfate ProteoGlycan (HSPG); cyclophilin B (CyPB). (Figure taken from [49]).

Non-enveloped viruses's preferred endocytosis pathways are the clathrin- and the caveolae-mediated pathways [128]. Although earlier studies confirmed the same for HPV [129], [130], a lot of recent data are supporting the idea of a clathrin- and caveolae-independent mechanism [131], [132]. This new alternative pathway has not been fully characterized but it requires the tetraspanin CD151, the tyrosine kinase and actin activities [125], and it might use TEMs as an entry platform [132].

1.2.2 Uncoating and intracellular trafficking

Internalized intact viral particles exceed the size to pass through the nuclear pore, so they must undergo capsid disassembly before entering into the nucleus [133]. It was shown that capsids are directed to the endosomal compartment upon arrival in the cytoplasm [132], [134]. HPV virions are trafficked in perinuclear CD63 containing vescicles, that are acidified by a vacuolar ATPase [135], a process that helps the uncoating of the virions and leads to the release of the L2/Genome complex [131], [136]. As soon as viral uncoating occurs, L1 and L2 are separated by cellular chaperones, such as cyclophilin, in different compartments. The minor capsid protein, along with the viral DNA is retrogradely transported to the Golgi network [137], [138] by the retromer complex that enables recycling of factors to the cell surface. From the Golgi compartment, the L2/viral DNA complex is transported to the nucleus along microtubules: the L2 protein interacts with the microtubule motor protein dynein and this allows the movement to the nucleus [139], [140]. It is well established that L2 accompanies the viral genome and the complex accumulates in specific nuclear structures responsible for viral transcription and replication, known as promyelocytic leukemia (PML) nuclear bodies or nuclear domain 10 (ND10) [141], [142] (Fig. 8).

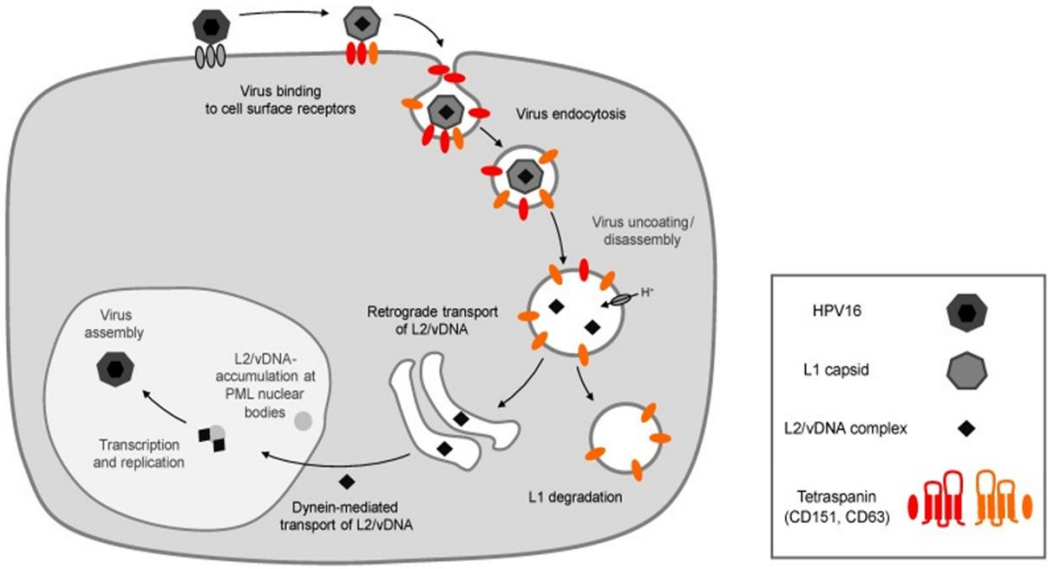

Fig. 8 Viral uncoating and endocytosis (Figure modified from [125])

1.2.3 Viral genome maintenance, amplification and virions production

The HPV life cycle is tightly dependent on cellular differentiation. After a micro lesion the viral particles enter the basal layer, where wound healing occurs and infection presumably takes place in stem-cells in the basal layer, granting a long-term maintenance of the viral DNA in the tissue [143]. As with most viruses, PV replication is totally dependent on the cell and viral genome is replicated with the cellular DNA. HPV gene expression follows a spatial and temporal pattern (Fig. 9). Upon infection, viral genomes are replicated and, after being established as episomes, are kept at low copy number in the basal layer [29]. In this first replication step the viral proteins E1 and E2 are thought to play a major role: E2 binds to the viral DNA and recruits the helicase E1 to the viral origin where it can assemble the cellular replication machinery; to ensure the viral genome maintenance, E2 can anchor the newly synthesized viral genomes to the segregating cellular chromosomes [31]. The virus has to overcome the loss of proliferation due to the natural differentiation process every epithelial cell undergoes. On one hand HPV needs proliferating cells to use the cellular replication machinery, on the other hand, it cannot totally inhibit differentiation since other viral proteins need differentiation-related transcription factors [143]. This delicate balance is mainly maintained in the upper layer by the viral proteins E6, E7 (and presumably E5) and E2. The viral oncogenes, E7 and E6, act mainly on cell cycle progression and downregulation of apoptosis as described before.

E2 has a central role in regulating the expression of all the viral genes in a dose-dependent manner: if high levels of E2 are present it behaves like a repressor of the early promoter (all the early genes are downregulated) but when E2 is not abundant transcription through the early promoter is activated and as a result E2 regulates both its own expression and, consequently, the viral copy number [27]. During neoplastic progression to cervical cancer, this subtle regulation is abolished because HPV integrates its DNA into the host genome causing deletion of the E2 gene and therefore leading to an increased expression of the viral oncogenes E6 and E7 [144]. Once the genome has been amplified and the infected cells have differentiated, infectious viral particles have to be build and released with dead skin cells. Upon differentiation, the late promoter is activated and the late proteins L1 and L2 can be produced. L2, the first protein synthesized, is localized in the PML bodies where it can recruit the capsomeres formed by L1 in the cytosol and, although it has been shown that viral particles can be formed without L2, when L2 is present both packaging and infectivity were demonstrated to be more efficient [31]. Once the virions are ready, it was hypothesized that

E4 might help the viral particles in egressing from the cell surface by disrupting the keratin network [39].

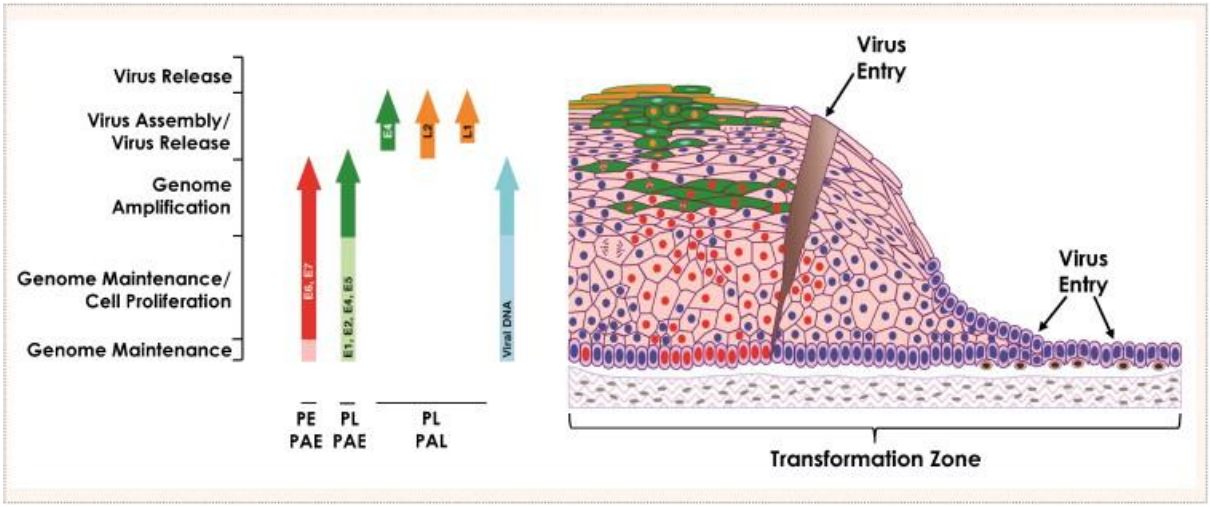

Fig. 9 HPV temporal and spatial protein expression pattern (Figure adapted from [29])

3. Aim of the work

The molecular mechanisms that HPV uses to promote tumorigenesis in HPV-related cancers outside of the cervix uteri are not yet understood. While cervical HPV oncoprotein interactions were investigated in several studies, much less is known about the interactions of cutaneous HPV oncoproteins and only few studies refer to the intraviral interactome of the HPV. Protein-protein interaction studies are strong tools to gain more insights into the pathogenicity of viruses and, therefore, the objectives of this study were to identify new viral-host interaction partners of the cutaneous E6 oncoproteins, in particular of CRPV and HPV38, and to create a network of HPV31 intra-viral protein interactions.

4. Materials and methods

4.1 Materials

4.1.1 Media for bacteria

LB Medium (Luria Bertani Bouillon): 25 g of high salt LB Broth Base (Fluka) dissolved in 1 l of H_2O.

LB Agar: 15 g of Select Agar (Gibco®) dissolved in 1 l of LB Medium.

SOC Medium: 2% (w/v) Bactotryptone, 0.5% (w/v) BactoYeast Extract, 10 mM NaCl, 2.5 mM KCl, 10mM $MgCl_2$, 10 mM MgSO4 and 20 mM Glucose.

Freezing Medium: 50 % LB Medium, 50 % Glycerin.

4.1.2 Bacteria

E.coli DH5α (Clontech) Genotype F- 80dlacZ M15 (lacZYA-argF) U169 recA1 endA1 hsdR17 (rk-, mk+) phoA supE44-thi-1 gyrA96 relA1

4.1.3 Media and solutions for eukaryotic cells

DMEM + FBS: Dulbecco's Modified Eagle Medium (Gibco® by Life Technologies) supplemented with 10% of fetal bovine serum (FBS, PAA) and with 50 mg/l of Gentamicin (Sigma-Aldrich).

DMEM + CS: Dulbecco's Modified Eagle Medium (Gibco® by Life Technologies) with 50 mg/l Gentamicin (Sigma-Aldrich) and 10% Calf Serum (CS) (Gibco by Life Technologies)

F-Medium: Ham's F-12 GlutaMAX and DMEM/Ham's F-12 (1:1 v/v) supplemented with 1.8 mM Adenin, 417 µg/ml Hydrocortison, 50 µg/ml Insulin, 50 µg/ml Transferrin, 0.02 µM Triiodthyronin T3, 10 µM Cholera toxin, 1% v/v Penicillin/Streptomycin, 10% HyClone (HC, HyClone Laboratories, Inc.)

N/Terts Medium: DMEM + DMEM/Ham's F12 (3:1 v/v) (Gibco® by Life Technologies) with 10% fetal bovine serum, 1% L-glutamine, 1% Penicillin/Streptomycin and supplemented with

RM+ (0.4 µg/ml Hydrocortisone, 5 µg/ml Insulin, 0.01 µg/ml EGF, 10 µM Cholera toxin, 1.8 mM Adenine, 5 µg/ml Transferrin and 0.0013 µg/ml Lyothyronine (L4)

Freezing Medium:

- C33A, HeLa, SiHa, CaSki, HEK293T, A431, Phoenix: DMEM supplemented with 20% FBS and 10% DMSO
- NIH3T3-J2 with DMEM+CS supplemented with 10% CS and 10% DMSO
- NIKs with N/Terts medium supplemented with 10 % HC and 10 % DMSO

PBS: Dulbecco's Phosphate-Buffered Saline without $CaCl_2$ und $MgCl_2$ (Gibco® by Life Technologies)

Opti-MEM®: Reduced-Serum and antibiotic-free medium used for DNA and siRNA transfection (Gibco® by Life Technologies)

G418: Stock solution 100 mg/ml in ddH_2O (Biochrom)

Puromycin: Stock solution 1 mg/ml in ddH_2O (Calbiochem)

Penicillin-Streptomycin (10,000 U/ml): solution containing 10,000 units/ml of penicillin and 10,000 µg/ml of streptomycin (Gibco® by Life Technologies)

Trypsin-EDTA: solution containing 2.5 g/l of trypsin and 0.38 g/l of EDTA with Phenol red (Gibco® by Life Technologies)

Versene Solution: PBS (Gibco® by Life Technologies) with 0.5 mM EDTA

Mitomycin C: Stock solution 0.4 mg/ml (Medac) in PBS (Gibco® by Life Technologies)

Polybrene (Hexadimethrine bromide) solution: Stock solution 5 mg/ml (1000x) (Sigma-Aldrich)

Glucose: Solution with ≥ 99.5% of D-(+)-Glucose (Sigma-Aldrich)

Fugene HD: transfection reagent (Promega)

HiPerfect: siRNA transfection reagent (Qiagen)

4.1.4 Eukaryotic cell lines

Cell lines	Description
HeLa	HPV18-positive cervix carcinoma cell line [145]
NHK	Normal human keratinocytes [146]
NIH3T3-J2	Murine Fibroblasts cell line [147]
C33a	Human HPV-negative cervical carcinoma cells mutated in p53 and pRb proteins [148]
SiHa	HPV16-positive cervix carcinoma cell line [149]
HEK 293T	Human embryonal kidney cell line with adenovirus E1A ad SV40 Large-T-Antigen [150]
NIKS	Spontaneously immortalized human keratinocytes cell line [151]
Phoenix	Retroviral packaging cell line based on 293T [152]
CaSki	HPV16-positive cervix carcinoma cell line [153]
A431	Epidermoid carcinoma cell line overexpressing EGFR and mutated in p53 [154]
AVS	Primary keratinocytes, harboring the whole CRPV genome, immortalized with CRPV particles [155]
N/Terts	Human foreskin keratinocytes immortalized with the catalytic subunit of human telomerase [156]

4.1.5 Commercial kits

Kit	Catalogue number	Brand
QIAquick Gel Extraction Kit	28706	Qiagen
QIAprep Spin Miniprep Kit	27106	Qiagen
QIAprep Spin Midiprep Kit	12945	Qiagen
Rneasy Mini Kit	74106	Qiagen
QIAshredder	79656	Qiagen
QuantiTect Reverse Transcription Kit	205311	Qiagen
LongRange PCR Kit	206401	Qiagen
LightCycler 480 SYBR Green I Master	04707516001	Roche
µMACS HA Isolation Kit	130-091-122	Miltenyi Biotec
Rapid I Ligation Kit	K1422	Thermo scientific
Protein detection Pierce 660nm	22660	Thermo Scientific
SuperSignal West Dura Extended Duration Pierce	34075	Thermo Scientific
SuperSignal West Femto Maximum Sensitivity Substrate Pierce	34095	Thermo Scientific
NE-PER Nuclear and Cytoplasmic Extraction Reagents	78833	Thermo Scientific
Gaussia Juice Kit	102541	P.J.K.

4.1.6 Enzymes

Restriction endonucleases: Thermo Scientific, NEB

DNA polymerases:

- GoTaqR DNA Polymerase (Promega)
- Pyrobest DNA polymerase (Takara)

Fast AP (Thermo Scientific, EF0654)

4.1.7 Reference ladders

Protein ladders:

- Spectra Multicolor Broad Range Protein Ladder (Thermo Scientific)
- Pageruler Prestained Protein Ladder (Thermo Scientific)

DNA ladder:

- 1 kB Plus DNA Ladder (Invitrogen)

4.1.8 Buffers and solutions

DNA loading buffer: 20% Ficoll 400, 0.1 M Na2EDTA pH 8.0, 1% SDS, 0.25% bromophenol blue or 0.25% xylene cyanol.

Protein loading buffer (4X): ROTI®-LOAD 1 reducing (Roth).

MCLB (Mammalian Cell Lysis Buffer): 50mM Tris, 150mM NaCl, 0.5% (v/v) NP-40 (IGEPAL CA-630, Sigma Aldrich), cOmplete Protease Inhibitor Cocktail (Roche)

RIPA buffer: 10 mM NaF, 10 mM Tris-HCl pH 7.5, 150 mM NaCl, 1 mM EDTA, 1% (v/v) Triton X-100, 1.5% (v/v) SDS, 0.5% (w/v) Deoxycholate, cOmplete Protease Inhibitor Cocktail (Roche)

Coomassie staining solution: 2.5 g Coomassie-Brilliant-Blue R-250(Merck), 454 ml H_2O, 92 ml acetic acid

Coomassie destaining solution: 454 ml Methanol, 471 ml H2O, 75 ml acetic acid

TAE buffer (50X): 2 M Tris, 1 M Acetic acid, 100 mM Na_2EDTA, pH 8.5

Ethidiumbromid: solution ready-to-use 500 µg/ml (Roth)

TBS (10X): 500 mM Tris, 1.5 M NaCl, pH 7.5

TBS-T: 1XTBS with 0.1% TWEEN® 20

PBS: 137 mM NaCl, 2.7 mM KCl, 1.5 mM KH_2PO4, pH 7.2

PBS-T: 1xPBS buffer + 0.1% (v/v) Tween 20

Ponceau S solution: 0.1% (w/v) Ponceau S in 5% (v/v) acetic acid

4.1.9 Antibodies

4.1.9.1 Primary antibodies

Antigen	Species	Manufacturer	Dilution WB/IF
α-tubulin	mouse monoclonal	Calbiochem (DM1A, #CP06)	1:1000
17β-HSD4	mouse monoclonal	Santa Cruz (A-6, sc-365167)	1:1000/1:400
Actin	mouse monoclonal	Sigma-Aldrich (AC-40, A3853)	1:1500
E6AP	rabbit polyclonal	Santa Cruz (H-182, sc-25509)	1:1500
EGFR	mouse monoclonal	Dako (M7239, Clone E30)	-/1:500
FLAG	rabbit monoclonal	Cell Signaling (#2368)	1:1000
HA	mouse monoclonal	Covance (16B12)	1:1500/1:1000
HA	rabbit monoclonal	Cell signaling (C29F4, #3724)	1:1000/1:1600
HDAC1	mouse monoclonal	Santa Cruz (10E2, sc-81598)	1:500
HDAC2	mouse monoclonal	Santa Cruz (F-6, sc-55542)	1:1000
HSP90	mouse monoclonal	Santa Cruz (sc-69703)	1:2000
KRIP-1	rabbit polyclonal	Transduction Laboratories (#610680)	1:1000
LSD1/KDM1A	rabbit monoclonal	Cell Signaling (C69G12, #2184)	1:1000/1:400
MAML1	rabbit polyclonal	Cell Signaling (#4608)	1:1000
p300	rabbit polyclonal	Santa Cruz (C-20, sc-585)	1:1000
p53	mouse monoclonal	Santa Cruz (DO-1, sc-126)	1:1000
pRb	mouse monoclonal	Cell signaling (4H1, #9309)	1:2000/1:200

4.1.9.2 Secondary antibodies

Antigen	Species	Manufacturer	Dilution
anti-rabbit IgG	swine polyclonal	Dako (P0399)	1:1000
anti-mouse IgG	rabbit polyclonal	Dako (P0260)	1:2500
anti- goat IgG	rabbit polyclonal	Dako (P0449)	1:1000
anti-mouse (green)	goat anti-mouse, IRDye 800	Odyssey Infrared Imaging (926-32210D)	1:15000
anti-mouse (red)	goat anti-mouse, IRDye 680	Odyssey Infrared Imaging (926-32211D)	1:15000
anti-rabbit (green)	goat anti-rabbit IRDye 800	Odyssey Infrared Imaging (926-32211D)	1:15000
anti-rabbit (red)	goat anti-rabbit IRDye 680	Odyssey Infrared Imaging (926-32221D)	1:15000
anti- goat (red)	donkey anti goat IRDye 680	Odyssey Infrared Imaging (926-68071)	1:15000

4.1.10 DNA constructs

4.1.10.1 Expression vectors

pMSCVpuro-L3HA: at the C-terminus of the multiple cloning site of the pMSCVpuro vector a 12 amino acids linker followed by 3 HA-Tag epitopes (with stop codon) was cloned via XhoI/EcoRI; after digestion with BglII/XhoI a sequence can be inserted which will then be expressed as a 3xHA-tagged protein (internal database # 2384, Amp^R) (Fig. 10) .

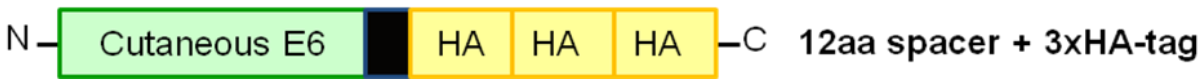

Fig. 10 pMSCVpuro-L3HA. Scheme showing how the viral proteins were 3xHA-tag cloned. aa: amino acids; 3xHA: triple HA tag.

pMSCV-CRPVLE6M98S-L3HA: CRPVLE6M98S (amplified from # 2138, the mutation Methionine to Serine at position 98 ensures the exclusive expression of CRPVLE6) was cloned into pMSCV-L3HA (#2384) via BglII and XhoI. The new generated vector was registered in the internal database as # 2431, Amp^R.

pMSCV-CRPVSE6-L3HA: CRPVSE6 was cloned into pMSCV-L3HA (# 2384) via BglII and XhoI. The new generated vector was registered in the internal database as # 2432, Amp^R.

pMSCV-HPV5E6-L3HA: HPV5E6 (# 595) was cloned into pMSCV-L3HA (# 2384) via BglII and XhoI. The new generated vector was registered in the internal database as # 2433, Amp^R.

pMSCV-HPV38E6-L3HA: HPV38E6 (amplified from # 2048) was cloned into pMSCV-L3HA (# 2384) via BglII and XhoI. The new generated vector was registered in the internal database as # 2433, Amp^R.

pCMV-N-Flag_linker_HA: expression vector kindly given by Karl Munger, based on pCMV-Bam-Neo with the addition of a N-terminal Flag-linker-HA tag. The multiple cloning site contains an EcoRV and a BamHI site (Internal database # 2509, Amp^R).

pCMV-N-Flag_linker_HA-CRPVLE6M98S: CRPVLE6M98S (amplified from # 2138, the mutation Methionine to Serine at position 98 ensures the exclusive expression of CRPVLE6), was cloned into pCMV-N-Flag_linker_HA (# 2509) via EcoRV. The new generated vector was registered in the internal database as # 2511, Amp^R.

pCMV-N-Flag_linker_HA-CRPVSE6: CRPVSE6 was cloned into pCMV-N-Flag_linker_HA (# 2509) via EcoRV. The new generated vector was registered in the internal database as # 2512, Amp^R.

pCMV-N-Flag_linker_HA-HPV5E6: HPV5E6 (amplified from # 595) was cloned into pCMV-N-Flag_linker_HA (# 2509) via EcoRV. The new generated vector was registered in the internal database as # 2513, Amp^R.

pCMV-N-Flag_linker_HA-HPV38E6: HPV38E6 (amplified from # 2048) was cloned into pCMV-N-Flag_linker_HA (# 2509) via BamHI. The new generated vector was registered in the internal database as # 2514, Amp^R.

Notch Intracellular Domain (NICD): Notch Intracellular Domain received from Scott Vande Pol (Internal database # 2536, Amp^R).

pBabe-puro: Retroviral vector kindly given from Scott Vande Pol [75] (Internal database # 2755, Amp^R).

pBabe-puro BPVE6: Retroviral vector containing BPV1 E6 kindly given from Scott Vande Pol [75] (Internal database # 2756, Amp^R).

pBabe-puro CRPVLE6 M98S: CRPVLE6 M98S was PCR amplified, using # 2511 as template, adding EcoRI restriction sites and then cloned into the pBabe-puro vector (# 2536). The new generated vector was registered in the internal database as # 2757, Amp^R.

pBabe-puro CRPVLE6 M98S Flag_linker_HA: The Flag_linker_HA-CRPVLE6 M98S was excised from pCMV-N-Flag_linker_HA-CRPVLE6M98S (# 2511) and then cloned into the pBabe-puro vector (# 2536). The new generated vector was registered in the internal database as # 2758, Amp^R.

peYFP-C1: Clontech vector encoding for eYFP, kindly donated by Prof. Schindler. Using NheI/AgeI and XhoI/EcoRI it is possible to insert sequences that will be C- and N-terminally tagged, respectively (Fig. 11, internal database # 2590, Kan^R).

pmTagBFP-C1: Clontech vector encoding for mTagBFP, kindly donated by Prof. Schindler. Using NheI/AgeI and XhoI/EcoRI it is possible to insert sequences that will be C- and N-terminally tagged, respectively (Fig. 11, internal database # 2598, Kan^R).

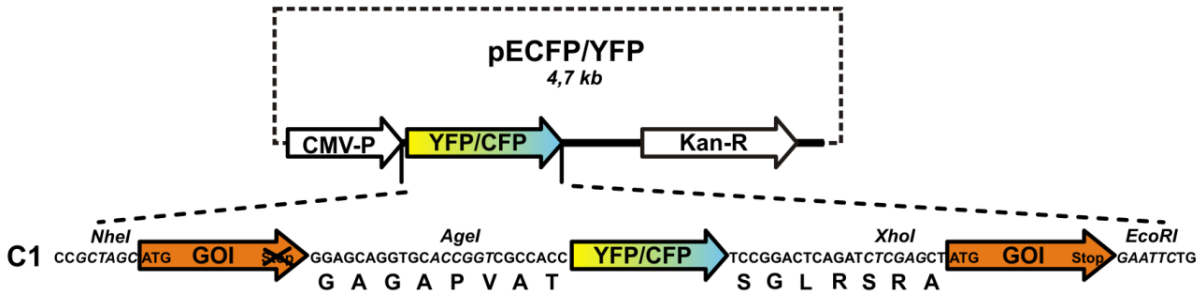

Fig. 11 **pmTagBFP-C1 and peYFP-C1 vectors** (Clontech, given by Prof. Schindler) figure adapted by [157]. HPV31 sequences were cloned into the vectors via NheI/AgeI for the C-terminal tag and via XhoI/EcoRI or Kpn2I/SmaI for the N-terminal tag.

peYFP-mTagBFP: expression vector encoding for eYFP-mTagBFP in a single protein constitutively giving a positive FRET signal, kindly donated by Prof. Schindler, used as positive control for FACS-FRET experiments (Internal database # 2750, Kan^R).

peYFP-HPV31 E1 N-Ter: The new generated vector was registered in the internal database as # 2589, Kan^R.

pmTagBFP-HPV31 E1 N-Ter: HPV31 E1 was PCR amplified and cloned into pmTagBFP via Kpn2I/SmaI. The new generated vector was registered in the internal database as # 2725, Kan^R.

peYFP-HPV31 E2co N-Ter: HPV31 E2co (codon-optimized version synthesized by Invitrogen) was PCR amplified and cloned into peYFP via Kpn2I/SmaI. The new generated vector was registered in the internal database as # 2726, Kan^R.

pmTagBFP-HPV31 E2co N-Ter: HPV31 E2co (codon-optimized version synthesized by Invitrogen) was PCR amplified and cloned into pmTagBFP via Kpn2I/SmaI. The new generated vector was registered in the internal database as # 2727, Kan^R.

peYFP-HPV31 E8^E2Cco N-Ter: HPV31 E8^E2co (codon-optimized version synthesized by Invitrogen) was PCR amplified and cloned into peYFP via Kpn2I/SmaI. The new generated vector was registered in the internal database as # 2728, Kan^R.

pmTagBFP-HPV31 E8^E2Cco N-Ter: HPV31 E8^E2co (codon-optimized version synthesized by Invitrogen) was PCR amplified and cloned into pmTagBFP via Kpn2I/SmaI. The new generated vector was registered in the internal database as # 2729, Kan^R.

peYFP-HPV31 E1^E4 N-Ter: HPV31 E1^E4 was PCR amplified and cloned into peYFP via Kpn2I/SmaI. The new generated vector was registered in the internal database as # 2730, Kan^R.

pmTagBFP-HPV31 E1^E4 N-Ter: HPV31 E1^E4 was PCR amplified and cloned into pmTagBFP via Kpn2I/SmaI. The new generated vector was registered in the internal database as # 2731, Kan^R.

peYFP-HPV31 E5 N-Ter: HPV31 E5 was PCR amplified and cloned into peYFP via Kpn2I/SmaI. The new generated vector was registered in the internal database as # 2734, Kan^R.

pmTagBFP-HPV31 E5 N-Ter: HPV31 E5 was PCR amplified and cloned into pmTagBFP via Kpn2I/SmaI. The new generated vector was registered in the internal database as # 2735, Kan^R.

peYFP-HPV31 E6sm N-ter: HPV31 E6 was PCR amplified and a silent mutation (T→G) within the splicing donor site at position 105 was inserted into the E6 ORF via overlapping PCR. E6sm was then cloned into peYFP via Kpn2I/SmaI. The new generated vector was registered in the internal database as # 2738, Kan^R.

pmTagBFP-HPV31 E6sm N-Ter: HPV31 E6 was PCR amplified and a silent mutation (T→G) within the splicing donor site at position 105 was inserted into the E6 ORF via

overlapping PCR. E6sm was then cloned into pmTagBFP via Kpn2I/SmaI. The new generated vector was registered in the internal database as # 2739, Kan^R.

peYFP-HPV31 E7 N-Ter: HPV31 E7 was PCR amplified and cloned into peYFP via Kpn2I/SmaI. The new generated vector was registered in the internal database as # 2740, Kan^R.

pmTagBFP-HPV31 E7 N-Ter: HPV31 E7 was PCR amplified and cloned into pmTagBFP via Kpn2I/SmaI. The new generated vector was registered in the internal database as # 2741, Kan^R.

peYFP-HPV31 L1co C-Ter: HPV31 L1co (codon-optimized version synthesized by Invitrogen) was PCR amplified and cloned into peYFP via NheI/AgeI. The new generated vector was registered in the internal database as # 2746, Kan^R.

pmTagBFP-HPV31 L1co C-Ter: HPV31 L1co (codon-optimized version synthesized by Invitrogen) was PCR amplified and cloned into pmTagBFP via NheI/AgeI. The new generated vector was registered in the internal database as # 2747, Kan^R.

peYFP-HPV31 L2co C-Ter: HPV31 L2co (codon-optimized version synthesized by Invitrogen) was PCR amplified and cloned into peYFP via NheI/AgeI. The new generated vector was registered in the internal database as # 2748, Kan^R.

pmTagBFP-HPV31 L2co C-Ter: HPV31 L2co (codon-optimized version synthesized by Invitrogen) was PCR amplified and cloned into pmTagBFP via NheI/AgeI. The new generated vector was registered in the internal database as # 2749, Kan^R.

4.1.10.2 Reporter vectors

Hes1-luc: Hes1-Luciferase (Notch responsive) reporter gene from Annika Wallenberg (internal database # 2535, Amp^R).

pGL 31URR luc: reporter plasmid containing HPV31 nt 7067 to 107 in pGL3 basic [158] (internal database # 752, Amp^R).

pCMV Gluc (Gaussia): commercial artificial reporter containing the sequence for the secreted Gaussia Luciferase (GLuc) under the control of the Cytomegalovirus (CMV) promoter (New England Biolabs, internal database # 1770, Amp^R).

4.1.11 Oligonucleotides

4.1.11.1 Cloning primers

Cloning in pMSCV:

Primer name	**Sequence (5' →3')**	**Position (nt)**
CRPVLE6 BglII F	aacgaaAGATCTatggagaactgcctgccacg	154-173
CRPVSE6 BglII F	gcaaggAGATCTatgcgttgtacagtttgcgg	445-464
CRPVLE6_SE6 XhoI R	gcggccCTCGAGtctaaattctgtgaagttaa	972-953
HPV5E6 BglII F	ggtaatAGATCTatggctgagggagccgaaca	200-219
HPV5E6 XhoI R	ccgacgCTCGAGccaatcatgataaaaatgct	670-651
HPV38E6 BglII F	ggccggAGATCTatggaactaccaaaacctca	200-219
HPV38E6 XhoI R	aaggccCTCGAGttctattgctttgcaatgcc	622-603

Cloning in pCMV:

Primer name	**Sequence (5' →3')**	**Position (nt)**
CRPVLE6 EcoRV F	ctttatGATATCgagaactgcctgccacgctc	157-180
CRPVSE6 EcoRV F	cgccagGATATCcgttgtacagtttgcggaag	448-467
CRPVLE6_SE6 EcoRV R	cggcgcGATATCtcatctaaattctgtgaagt	975-956
HPV5E6 BamHI F	ctaaatGGATTCgctgagggagccgaacacca	203-222
HPV5E6 BamHI R	cgggcgGGATTCttaccaatcatgataaaaat	673-654
HPV38E6 BamHI F	cgccagGGATCCgaactaccaaaacctcaaac	203-222
HPV38E6 BamHI R	cgggcgGGATCCtcattctattgctttgcaat	625-606

Cloning in peYFP and pmTagBFP:

Primer name	Sequence (5' →3')	Position (nt)
HPV31E1 Kpn2I F	gattatTCCGGAgctgatccagcaggtacaga	1865-1881
HPV31E1 SmaI R	cgccggCCCGGGtcataatgttctaatatttt	2751-2732
HPV31E2 co Kpn2I F	aattatTCCGGAgagacactgagccagcggct	2696-2715 (codon-optimized)
HPV31E2 co SmaI R	atactaCCCGGGtcagatggtcatgtagccgg	3811-3792 (codon-optimized)
HPV31 E8 Kpn2I F	atataTCCGGAgccggatctggcggagg	1262-1281 (codon-optimized)
HPV31 E2C SmaI R	accgatCCCGGGctagatggtcatgtagc	3811-3790 (codon-optimized)
HPV31E1^E4Kpn2I F	gattatTCCGGAgctgatccagcagtgacgaaata tcctt	865-884
HPV31E1^E4SmaI R	cgctgtCCCGGGttataggtgtagttgcagga	3578-3559
HPV31E5Kpn2I F	cgcggcTCCGGAattgaactaaatatttctac	3819-3838
HPV31E5SmaI R	agcgtaCCCGGGttactgttgacttaaaaaag	4070-4051
HPV31E6Kpn2I F	agcgatTCCGGAttcaaaaatcctgcagaaag	111-130
HPV31E6SmaI R	gattatCCCGGGttacacttgggtttcagtac	557-538
HPV31E6sm 95 F	actgcaaaggGcagttaaca	206-225
HPV31E6sm 115 R	tgttaactgCcctttgcagt	225-206
HPV31E7Kpn2I F	agctatTCCGGAcgtggagaaacacctacgtt	563-582
HPV31E7SmaI R	atcgcaCCCGGGttacagtctagtagaacagt	856-837
HPV31L1co NheI F	agctatGCTAGCatgagcctgtggaggcccag	5552-5571 (codon-

		optimized)
HPV31L1co AgeI R	ataaACCGGTgcacctgctcccttcttggtcttcttcct ct	7063-7044 (codon-optimized)
HPV31L2 co NheI F	aatcatGCTAGCatgcggagcaagcggagcac	4171-4190 (codon-optimized)
HPV31L2 co AgeI R	atattaACCGGTgcacctgctccggcagccac	5568-5549 (codon-optimized)

4.1.11.2 Sequencing primers

Primer name	**Sequence (5' →3')**	**Position (nt)**
pMSCV 1333 F	CCCTTGAACCTCCTCGTTCGACC	1333-1356
pMSCV_1473 R	CAGCGGGGCTGCTAAAGCGCATGC	1473-1449
HPV5E6 379 F	TTAGATTGCTGTGGCAGAGG	579-601
HPV5E6 450 R	ACACTGCCTACAGATTCCCTTC	650-628
HPV38E6 257 F	TTGAACAGGTGGAGCAACAG	457-477
HPV38E6 395 R	CCTTTCCAATTGCCTCTAACC	595-574
pCMV-Flag-F	GGACTACAAGGATGACGATG	Standard sequencing primer
pCMV-Flag-R	GATCCGTCGAGGAATTCAC	Standard sequencing primer
pBabe puro 5 F	CTTTATCCAGCCCTCAC	Standard sequencing primer
pBabe-puro 3 R	ACCCTAACTGACACACATTCC	Standard sequencing primer
BFP-YFP seq 511 F	CCCATTGACGCAAATGGGCG	Standard

		sequencing primer
BFP-YFP seq 1400 R	ATGATCAGTTATCTAGATCCG	Standard sequencing primer
HPV31L2 co 565 F	CATCAGCACCCACAACTACG	6117-6137
HPV31L2 co 805 R	TGTGGCTGGTGTTGCTGAAG	6357-6337
HPV31E1 823 F	AACAATTGAAAAATTATTAG	2688-2708
HPV31E1 1213 R	TTTGTCACATCTACTTTTAA	3078-3058
HPV31L1co 728 F	CGGCGACACCCTGTTCTTCT	4899-4919
HPV31L1co 935 R	TAGGGCTTGTTGAAGATCTG	5106-5086

4.1.11.3 siRNAs

- AllStar Negative control siRNA Negative control siRNA (1027281, Qiagen)
- si18E6 [159] CACTTCACTGCCAAGACATA (Qiagen)

4.2 Cell Culture

4.2.1 Cell cultures and cell lines storage

Cells were maintained at 37°C, 5% CO2 and 99% of relative humidity on plastic plates (Nunc, all except NIKS with Primaria).

C33A, HeLa, SiHa, CaSki, HEK293T, Phoenix cell lines were maintained in cell culture with DMEM + FBS, N/Terts with N/Terts Medium, 3T3 J2 with DMEM + CS medium, NIKS cells were cultured in F-medium together with growth-arrested feeder cells, 3T3 J2. The feeder cells were treated with 80 ng/ml mitomycin C (Medac) for 1-2 h in order to arrest their growth, then were washed 3 times with 5 ml PBS to be added to NIKS cells.

When cells were confluent, the medium was removed, the plate was washed with 5 ml PBS and incubated at 37°C with 1 ml of Trypsin (Gibco® by Life Technologies). After few minutes trypsin was inactivated by adding as much medium as needed to split the cells and the cells were then transferred to new culture dishes.

To store the cells, medium was removed from confluent plates, cells were washed with 5 ml PBS, trypsinized and spun down at 250 x g for 5 min at 20°C. Cell pellets were re-suspended in freezing medium using 1 ml for one original 10 cm plate. Each ml was then transferred in a cryotube and stored at -80°C in a freezing box (Nalgene) for at least 24 h.

Cells were thawed using a water bath at 37°C. Cell suspension was transferred to a 10 cm dish together with 9 ml of medium. The day after the medium was exchanged with 10 ml of fresh new medium.

4.2.2 DNA transfection

The day before transfection, cells were counted in a Neubauer chamber and seeded depending on the cell type and the plate format. Exogenous DNA was transfected using the nonliposomal transfection reagent Fugene HD (Promega), according to the manufacturer´s protocol. Briefly, 24 h after seeding, DNA and Fugene were mixed at a ratio of 5:1 (C33a), 5:2 (HeLa, HEK293T) or 4:1 (N/Terts) in the serum-free medium, OptiMEM (Life technologies), vortexed, and after a 15 min of incubation at RT the complexes were added drop-wise to the cells.

4.2.3 Establishment of stable cell lines

To establish NIKS cells stably expressing different E6s the packaging cell line Phoenix was used. Transient transfections were performed with Fugene using a Fugene/DNA ratio of 5:2. The process was divided in three different steps:

1. Retroviruses generation

3×10^6 Phoenix cells were seeded in 10 cm plates and were transfected with 4 µg of DNA (pMSCVpuro-L3HA, pMSCV-CRPVLE6M98S-L3HA, pMSCV-CRPVSE6-L3HA, pMSCV-HPV5E6-L3HA, pMSCV-HPV38E6-L3HA) the day after. 24h later the medium was exchanged to 7 ml of DMEM with 10% FCS and gentamicin and the plates were incubated at 32°C. At the same time 1.5×10^6 NIKS cells were seeded in 60 mm plates in F-medium without feeder cells.

2. Transduction

Supernatant from Phoenix cells was sterile-filtered, Polybrene was added to a final concentration of 10 µg/ml. NIKS cells were then incubated with the supernatant for 4 h and afterwards 4 ml of F-medium were added for 24 h.

3. Selection

NIKS cells were then split onto of 3T3 J2 feeder cells in 10 cm plates. 24 h later antibiotic selection was started (150 µg/ml Neomycin and 0.4 µg/ml Puromycin) and was continued for at least 10 days.

4.3 Molecular Cloning and DNA/RNA methods

4.3.1 Agarose gel electrophoresis

DNA and RNA fragments were separated with agarose gel electrophoresis. Agarose gels, in this study, were made with 0.8 – 1.2% of agarose dissolved in electrophoresis buffer (TAE buffer) with the addition of ethidium bromide (Roth). Once solidified, the agarose gel was placed in the electrophoresis unit to run at 80-110 V for 40-60 min.

4.3.2 DNA purification from agarose gels

DNA fragments, after separation in an agarose gel, were cut out with a scalpel under a 320 nm UV light and the bands were purified with QIAquick Gel Extraction Kit (Qiagen).

4.3.3 Nucleic acid concentration determination

Nucleic acid concentrations were measured after purification of plasmids (QIAprep Spin Miniprep Kit, Qiagen) or DNA fragments (QIAquick Gel Extraction Kit, Qiagen) with the Nanodrop® ND-1000 (Thermo scientific) according to the manufacturer´s instructions. For measuring nucleic acids, the ratio of absorbance at 260 nm and 280 nm is used as a measure of nucleic acids purity. A 260/280 ratio of ~1.8 was considered as “pure” for DNA; a ratio of ~2.0 was accepted as “pure” for RNA. For this purpose 2 µl of water were used as blank and, after that, then samples were measured.

4.3.4 DNA digestion with restriction enzymes

Restriction endonucleases were used for digestion of plasmids or PCR amplicons following the manufacturer´s protocol. In the case of digested vectors, an additional step of dephosphorylation with FastAP (Fermentas) was performed, in order to avoid re-ligation during the process of plasmid- insert ligation. The digested fragments were then purified, after their separation during an agarose gel electrophoresis.

4.3.5 Plasmid-insert Ligation

For transformation of competent bacteria, digested plasmids and fragments were ligated using the Rapid DNA Ligation Kit (Thermo scientific). For each transformation reaction, 30 ng of the vector were used and DNA and inserts were ligated following the molar ratio 1:3. The reaction mixture was incubated for 10 min at 22 °C and then used to transform competent bacteria.

4.3.6 Generation of competent bacteria

DH5α were cultured overnight in 100 ml of LB medium without antibiotics. On the next day 20 ml of the overnight culture were grown in 400 ml of LB medium for 1.5-2 hours until the OD_{600} reached 0.45-0.55. All the following steps were carried out at 4°C.

The bottle containing the 420 ml of culture was incubated on ice for 30 minutes and then the culture was divided in 50 ml tubes and centrifuged at 4000 rpm for 10 min at 4°C. The supernatant was then removed and the remaining pellets were re-suspended in 100 ml of ice-cold TFB1 buffer. An incubation of 15 minutes on ice followed and then the tubes were centrifuged at 4000 rpm for 10 min at 4°C. Supernatants were discarded, pellets were re-suspended in 20 ml of ice-cold TFB2 and incubated on ice for 15 min. In the end, the suspension was aliquoted in 1.5 ml microcentrifuge tubes, shock-frozen in liquid nitrogen and immediately stored at -80°C.

The efficiency of transformation was assessed by transforming 10 ng of DNA in 100µl bacteria and counting the number of colonies the day after on the plate. The best achievable efficiency was 10^8 colonies / µg of DNA.

TFB1 pH 5.8 with NaOH	**TFB2** pH 6.5
MES 10mM	MOPS 10mM
RbCl 100mM	RbCl 10mM
$CaCl_2$ x $2H_2O$ 10mM	$CaCl_2$ x $2H_2O$ 75mM
$MnCl_2$ x $4H_2O$ (Only after pH 5.8)	

4.3.7 Bacteria transformation

To transform bacteria, 15 µl of the ligation reaction were added to 100 µl of competent bacteria, incubated on ice for 30 min and then heat-shocked at 42°C for 90 seconds. Immediately after they were put back on ice and 350 µl of SOC medium were added before growing the bacteria, while shaking, at 37°C for 45 minutes. Bacteria were then plated on antibiotic containing LB-plates and were incubated overnight at 37°C.

4.3.8 Selection of clones, DNA extraction and sequencing

The day after transformation, the antibiotic resistant plates were checked for the presence or absence (plates with the cleaved and dephosphorilated empty vector re-ligated) of colonies. For each new generated plasmid, few colonies were picked and grown overnight. The following day DNA was extracted from the overnight cultures using the Miniprep Kit (Qiagen), DNA was digested with suitable restriction endonucleases and only the positive clones were prepared to be sequenced by the GATC Biotech (Konstanz) company.

4.3.9 PCR

Primer design was in accordance with the general criteria [160]:

- unique oligonucleotide sequence in the template

- primer length inbetween 18-25 nt

- optimal annealing temperature around 60°C

- GC content at least 50%

For the PCR reactions the following polymerases were used: the proof reading Pyrobest DNA polymerase (Takara) was used for cloning and the GoTaq Polimerase (Promega) was used for testing mycoplasma contamination in cell culture and to screen clones.

For the PCR reactions with the Pyrobest DNA polymerase (Takara), according to the manufacturer's protocol, the reaction mixture contained 10X of supplied Pyrobest buffer, 4 µl of 10 µM dNTPs mix, 1 µl of 100µM primer forward and reverse, < 500 ng of DNA template and 0.25 µl of polymerase in a final volume of 50 µl.

Step	Temperature	Time	Number of Cycles
Initial Denaturation	98°C	3 minutes	1 cycle
Denaturation	98°C	30 sec	
Annealing	42–65°C	0.5–1 minute	25–35 cycles
Extension	72°C	1min/kb	
Final Extension	72°C	10 minutes	1 cycle
Final Hold	4°C	Indefinite	1 cycle

4.4 Protein methods

4.4.1 Cellular lysis

Proteins were isolated from cell culture dishes by removing the medium, washing with cold PBS and either trypsinizing or scraping the cells from the plate. The samples were shortly spun down in a table top centrifuge at 13.000 rpm for 5 minutes at 4°C and, after discarding the supernatants, pellets were re-suspended in MCLB buffer supplemented with protease inhibitor (cOmplete Protease Inhibitor Cocktail Tablets, Roche). Lysis took place on ice for 15-30 minutes and afterwards the samples were centrifuged at 13.000 rpm for 5 minutes at 4 °C to separate the cell debris. The protein loading buffer (4X ROTI®-LOAD 1, Roth) was added to the collected supernatants and samples were denatured for 5 min at 95°C. The ready-to-use lysates were stored at -20°C.

MCLB (Mammalian Cell Lysis Buffer)

50mM Tris

150mM NaCl

0.5% (v/v) NP-40 (IGEPAL® CA-630, Sigma Aldrich)

cOmplete Protease Inhibitor Cocktail (Roche)

4.4.2 Western blot

For western blot analysis, samples were run on 6-12 % SDS–polyacrylamide gels [162], the proteins were then transferred for 90 minutes at 90 Volts in CAPS buffer to a nitrocellulose membrane (0.22 µM Potran, Schleicher & Schuell). The membrane was then blocked with 5% nonfat dry milk dissolved in 1X TBS-T at RT for 1 hour to reduce unspecific binding of the primary antibody. Unless otherwise specified, primary antibodies (4.1.9.1) were diluted in TBS-T and the membrane was incubated on a shaker at 4°C, after being washed three times with TBS-T. The following day the membrane was washed three times with TBS-T and the secondary antibody (4.1.9.2) was incubated for 1 h at RT on a shaker. After rinsing the membrane from the excess of not bound antibody the bands were detected using either the SuperSignal West Dura Extended Duration Substrate (Thermo Scientific), in the case of the HRP-conjugated antibodies, or were directly acquired with the Odyssey Fc (LI-COR) and analyzed with the Image Studio Software (LI-COR). In rare cases, the membrane was re-

probed after removing the bound antibodies with a stripping buffer overnight at 4°C and blocked again, allowing a second incubation with different primary and secondary antibodies.

Resolving buffer	**Stacking buffer**	**SDS-PAGE running buffer (5X)**	**CAPS buffer**	**Stripping buffer**
1.5 M Tris pH 8.8	1.5 M Tris pH 6.8	125 mM Tris 0.96 M Glycine 0.5% (w/v) SDS	10 mM CAPS, 10% (v/v) Methanol pH 10.3	62.5 mM Tris pH 6.8 2% SDS 50 mM DTT

4.4.3 Dual-reporter luciferase assay

Luciferase assays are useful tools for reporter quantitation in cells. When luciferase catalyses the oxidation of D-luciferin, light is emitted and this can be measured with a luminometer in relative luciferase activity (RLUs). In a dual reporter luciferase assay two reporters encoding different luciferase enzymes are expressed at the same time. Generally, the second reporter is used as an internal control and helps to eliminate experimental fluctuations that may be due to differences in cell viability and transfection efficiency. In our assay activities of Firefly (Fluc, *Photinus pyralis*) and Gaussia (Gluc, *Gaussia princeps)* were measured and the Gaussia-Juice Luciferase Assay (P.J.K) was used.

The day before transfection $5x10^4$ C33A cells/well were seeded in the 24-well plate. First, the activity of the Gaussia luciferase released into the medium was measured. For this purpose 5 µl of the medium were pipetted in a tube to measure the turnover of the substrate Coelenterazine in the luminometer (LUMAT LB9507, EG&G Berthold). Afterwards the medium was removed and the cells were washed twice with 500 µl of cold PBS and lysed with 150µl of cold luciferase lysis buffer. After 10 minutes of lysis on ice, 100 µl of lysates were pipetted in tubes already containing 100 µl of luciferase assay buffer to determine the luciferase activity of the Firefly luciferase in the luminometer. Each condition was measured in duplicate (2 wells), and, after normalizing the firefly values to the Gaussia values

(Fluc/Gluc), the average of the two resulting values was taken to minimize the experimental variability.

Luciferase lysis buffer	**Luciferase assay buffer**
100 mM KPO4 pH 7.8	100 mM KPO4 pH 7.8
1% Triton-X-100	15 mM MgSO4
1 mM DTT	1 mM ATP
	1:50 Luciferin solution - 100 mM KPO4 pH 7.8 - 15 mM MgSO4 - 1 mM ATP - 50 mM Luciferin

4.4.4 Co-ImmunoPrecipitation (CoIP)

All the CoIPs were performed using the µMACS HA Isolation Kit (Miltenyi Biotec). One 10 cm dish of confluent cells was enough for a small scale CoIP, while for a big scale CoIP either ten 10 cm plates or four 15 cm plate were used. All steps were carried out at 4°C. What follows will describe the small scale CoIP, but in brackets are the volumes for the big scale.

Medium was removed from the dish, cells were washed with ice-cold PBS and 1 ml (4ml) of pre-cooled MCLB buffer supplemented with the cOmplete Protease Inhibitor Cocktail Tablets (Roche) was added. Cells were scraped with a rubber policeman from the dish, transferred to a microcentrifuge (falcon) tube, mixed well and incubated on ice for 30 min.

After this incubation period, samples were spun down at 10.000 x g for 10 min to sediment cell debris (in the case of the large scale, the centrifugation step was repeated more than once to have the supernatant as clean as possible from cell debris). Supernatants were transferred to a pre-chilled tube: 1/10 of the sample was kept as INPUT control sample and the rest was used for the pull down assay. 30 µl (120 µl) of anti-HA magnetic beads were added to the lysates and incubated in the cold room on an orbital shaker for 1 h. In the

meanwhile elution buffer (Roti-load, Roth) was heated to 95°C, the µ-columns placed in the magnetic field of the µMacs separator and 200µl lysis buffer were applied to the columns and let to flow through. After incubation with magnetic beads was finished, the suspensions were applied onto the columns and the lysates were left to run through ("FLOW THROUGH" sample). After washing the columns 5 times with the lysis buffer, the immunoprecipitates (IP) were collected applying 20 µl of pre-heated elution buffer and incubating for 5 minutes at room temperature. Another 50 µl (24 µl) of elution buffer were added and then samples were centrifuged at 1000 rpm for 1 min. 1/10 of the IP samples was used for western blot analysis and the rest for the mass spectrometry analysis.

4.4.5 Proteome analysis

4.4.5.1 Tryptic digestion of proteins

For proteome analysis, samples were given to the Proteome Center Tübingen (PCT) to proceed with the proteomics analysis. Samples were loaded on a NuPAGE Bis-Tris 4-12% gradient gel (Invitrogen). After short gel run and brief Coomassie staining each gel piece was cut into small pieces. Destaining was performed by washing three times with 10 mM ABC and acetonitrile (ACN) (1:1, v/v) and was followed by protein reduction with 10 mM DTT in 20 mM ABC for 45 minutes at 56°C, and alkylation with 55 mM iodoacetamide in 20 mM ABC for 30 minutes at room temperature in the dark. The gel pieces were then washed twice for 20 minutes in destaining solution followed by dehydration with ACN. The liquid was removed and gel pieces were swollen at room temperature by adding 13 ng/µl sequencing grade trypsin (Promega) in 20 mM ABC. Digestion of proteins was performed at 37°C overnight. The resulting peptides were extracted in three subsequent incubation steps with 30% ACN/3% TFA; with 80% ACN/0.5% acetic acid; and with 100% ACN. Supernatants were combined, ACN was evaporated in a vacuum centrifuge and peptides were desalted using C18 StageTips.

4.4.5.2 Nano LC-MS/MS analysis

All digested peptide mixtures were separated on the EasyLC nano-HPLC (Proxeon Biosystems) coupled to an LTQ-Orbitrap-XL (Thermo Fisher Scientific). Binding and chromatographic separation of the peptides was performed on a 15 cm fused silica emitter of 75 µm inner diameter (Proxeon Biosystems), in-house packed with reversed-phase ReproSil-Pur C18-AQ 3 µm resin (Dr. Maisch GmbH). The peptide mixtures were injected onto the column in HPLC solvent A (0.5% acetic acid) at a flow rate of 500 nl/min and subsequently

eluted with a 107 minute segmented gradient of 2-80% of HPLC solvent B (80% acetonitrile in 0.5% acetic acid) at a flow rate of 200 nl/min. Each sample was run once. The mass spectrometer was operated in the data-dependent mode to automatically switch between MS and MS/MS acquisition. Survey full scan MS spectra were acquired in the mass range from m/z 300 to 2000 in the orbitrap mass analyzer at a resolution of 60,000. Accumulation target value of 106 charges was set and the lock mass option was used for internal calibration (Olsen et al., 2005). The ten most intense ions were sequentially isolated and fragmented in the linear ion trap using collision-induced dissociation (CID) at the ion accumulation target value of 5000 and default CID settings. The ions already selected for MS/MS were dynamically excluded for 90 s. The resulting peptide fragment ions were recorded in the linear ion trap. In total, 4 LC-MS measurements were performed in the first experiment and 5 in the second experiment.

4.4.5.3 MS Data Processing and Analysis

Raw data were analyzed using MaxQuant (version 1.2.2.9) that, thanks to recently developed sophisticated normalization and matching algorithms [163], provided parts per million (ppm) level mass accuracy, confident identification of proteins (False Discovery Rate less than 1% on peptides and proteins level, with a minimum of 2 peptides per protein) and accurate intensity-based label-free quantification. The searched database was Uniprot (88,692 protein entries) and a common contaminant database of 247 proteins entries, allowing partial trypsin cleavage of 2 missed cleavages, was used. Additionally, one small database containing sequence of protein plasmids was created and used for search. Oxidation of methionines and N-terminal acetylation were specified as variable modifications, whereas carbamidomethylation on cysteines was defined as a fixed modification. The fragment mass tolerance was 6 ppm (monoisotopic mass), and the mass window for the precursor was set to 0.5 Da. The Maxquant output files were parsed for further analysis using the statistical tool suite Perseus (version.1.3.0.4). First, hits to the reverse database, contaminants and proteins only identified with modified peptides were eliminated. For every bait, a separate grouping was defined for valid values in the specific bait pull-downs. The interacting protein were identified and quantified only when present in the 2 biological replicates. The Label Free Quantification (LFQ) ratios were quantified using the intensity-based absolute quantification (iBAQ) algorithm [164] in order to identify interactors of LE6, SE6 and 38E6. The iBAQ ratios where normalized to fit a Gaussian normal distribution and at least two values were necessary to calculate the median, therefore, since HPV5 E6 was tested only once, the possible interactors of HPV5 E6 were not quantified. The one sided significance B statistical test ($p<0.05$) as described by MaxQuant [165] was applied in order

to identify significant proteins interactions compared to the empty vector control. To identify differential interactions between LE6 and SE6, the iBAQ ratios from each analysis were divided by each other's. Subsequently, the two sided Significance B statistical test ($p<0.05$) was applied in order to identify interactions disparities that significantly changed between LE6 and SE6.

4.4.6 SILAC

4.4.6.1 Introduction

Stable isotope labeling by amino acids in cell culture (SILAC) is a metabolic labeling approach that represents a powerful tool for quantitative proteomics. SILAC relies on metabolic incorporation of stable isotope-labeled amino acids provided in cell culture media into all newly synthesized proteins [166].

Custom-synthesized cell culture media without essential amino acids, such as arginine and lysine, are supplemented with isotope labeled arginine and lysine. Because there is no chemical difference between the labeled and the natural amino acid, cells behave exactly like cells grown in medium with unlabeled amino acids. Mammalian cells are not able to synthesize essential amino acids and, therefore, when labeled essential amino acids are supplied in the medium instead of the natural ones, cells use them for protein synthesis. All the natural amino acids will be replaced by the isotope labeled analogs as soon as the cells are gone through a certain number of cell divisions. Since serum contains free (unlabeled) amino acids, SILAC culture media were supplemented with commercially available dialyzed fetal bovine serum, where no detectable traces of amino acids are found [167], [168].

An important advantage of SILAC is that lysates from cells grown in different culture media can be mixed before analysis but only as long as their protein amounts are the same. During a mass spec experiment proteins are fragmented and peptides are detected based on their mass/charge ratio. Using isotopes, atoms with the same charge but different mass, will allow to differentiate the same protein coming from cells grown in different media by analyzing mass spectra. To quantify a change in protein amount in a certain condition, SILAC relies on ratios between isotope labeled proteins isolated from the same cell line grown in heavy, medium-heavy or light label media and to see a difference between the two samples, the starting samples have to have an equal protein amount [169] (Fig. 12). Protein amounts were equalized by measuring the total protein concentration in each sample with the Pierce™

660nm Protein Assay Reagent (ThermoFisher Scientific) and adjusting each sample volume in order to have the same total protein amount in each sample.

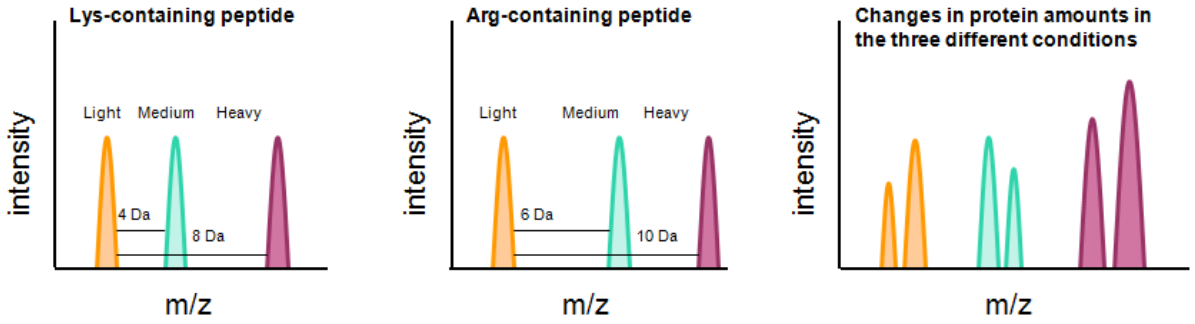

Fig. 12 Isotope mass differences and quantification. m: mass; z: charge.

4.4.6.2 Samples preparation

In our study (Fig. 13) C33a cells were grown in SILAC heavy label (Lys8Arg10), medium-heavy label (Lys4Arg6) or light label (Lys0Arg0) media in 60 mm dishes and after 14 days labeled amino acid incorporation rate, measured by the Proteome Center of Tübingen, was found higher than 95% in all cases. Moreover, cells grown in heavy and medium-heavy media behaved exactly the same as the ones grown in light medium, showing that there was no difference due to the isotope labeling amino acids substitution.

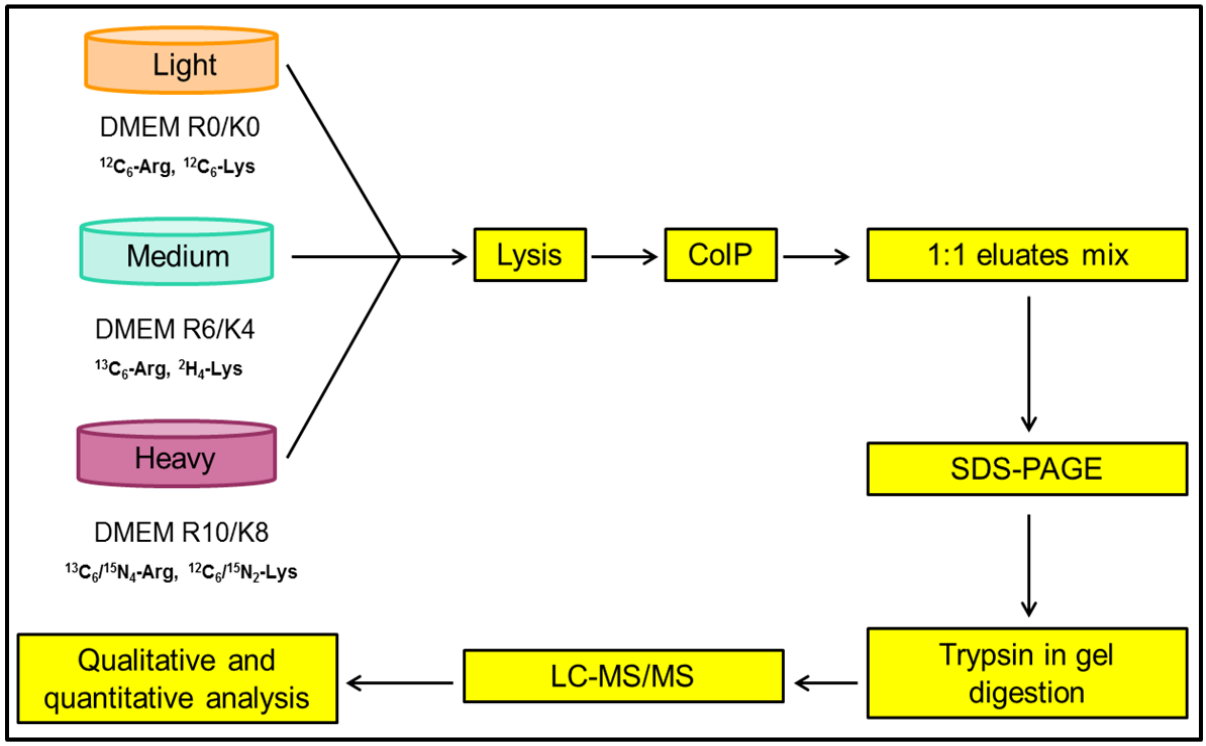

Fig. 13 SILAC work flow

For the Nano-LC-MS/MS analysis 5 x 10^6 cells were seeded into 4 x 15 cm plates. Expression vectors containing pCMV-Flag-Linker-HA alone, pCMV-Flag-Linker-HA+CRPVLE6 M98S or pCMV-Flag-Linker-HA+CRPVSE6 were transfected in cells grown in different media as shown in Table 1 and the experiment was performed in duplicate inverting the media.

Table 1

	pCMV+LE6	pCMV+SE6	pCMV
1st SILAC	Heavy label	Heavy-Medium label	Light label
2nd SILAC	Heavy-Medium label	Light label	Heavy label

Cells were harvested 48 h post transfection with a cell scraper in 4 ml of pre-chilled MCLB buffer supplemented with the cOmplete Protease Inhibitor Cocktail Tablets (Roche) and collected in falcon tubes on ice, where the lysis continued for 30 min. After lysis, tubes were centrifuged, supernatants were kept on ice and protein concentration was measured. Input samples with equivalent protein concentrations were incubated with 120 µl of magnetic anti-HA beads (Milteniy) and CoIP was performed as described. All the immunoprecipitates, except 1/10 kept to test the CoIP efficiency in a western blot, were then mixed 1:1:1 and given to the core facility, Proteome Center Tübingen (PCT), to proceed with the proteomics analysis.

4.4.6.3 Nano-LC-MS/MS

Immunoprecipitates from each cell line were mixed 1:1:1 (“light” to “heavy” to “medium”). Protein mixture was loaded on the gel and each of 6 gel slices was digested with Trypsin according to the protocol published by Macek et al.[170]. All peptides were measured on Easy-LC nano-HPLC (Proxeon Biosystems) coupled to an LTQ Orbitrap Elite mass spectrometer (Thermo Fisher Scientific). Liquid chromatography was done with a 15 cm fused silica emitter with an inner diameter of 75 µm and a tip diameter of 8 µm in-house made nano-HPLC column, packed with reversed-phase ReproSil-Pur C18-AQ 3 µm resin (Dr. Maisch GmbH). Peptides were flushed with HPLC solvent A (0.5 % acetic acid) at a flow rate of 500 nL/min with the maximum pressure of 280 Bar. Elution was done using segmented 90 min gradient (LTQ Orbitrap Elite) of 5 - 90 % HPLC solvent B (80 % ACN, 0.5 % acetic acid) at a flow rate of 200 nL/min. The eluted peptides were ionized in an electrospray ionization (ESI) source (Proxeon Biosystems) set to positive ion mode. Full scan MS spectra were acquired in the orbitrap analyzer in a mass range from m/z 300 - 2000 at a

resolution of 120,000 (LTQ Orbitrap Elite), followed by fragmentation in LTQ mass analyzer of the top 20 (LTQ Orbitrap Elite) most intense precursor ions with collision induced dissociation (CID) at a target value of 5000 charges. Dynamic exclusion was used to exclude fragmented masses for 90 sec.

4.4.6.4 Data processing and analysis

The mass spectrometer data were processed using MaxQuant suite V 1.2.2.9 [165], [171]. Spectra were searched using Andromeda search engine [172] against the proteome database of *Homo sapiens* (UniProt complete proteome database, taxonomy ID 9606), consisting of 88,692 protein entries and 247 commonly observed lab contaminants. Mass tolerance for first search was set to 20 ppm, and to 6 ppm for the main search. Multiplicity was set to three. Lys0, Arg0; Lys4, Arg6 and Lys8, Arg10 for “light”, “medium” and “heavy” samples, respectively. Full tryptic specificity was required and a maximum of two missed cleavages were allowed. Carbamidomethylation of cysteine was set as fixed modification while oxidation (M) and acetylation (on N-term) were chosen as variable modifications. Initial mass tolerance for the precursor ion was set to 6 parts per million (ppm) and 0.5 Da at the fragment ion level. For quantification of proteins, minimum two peptides with at least seven amino acids had to be detected. The maximum allowed posterior error probability (PEP) was set to 1 and the false discovery rate (FDR) to max 1 % for peptides and proteins. Re-quantification was enabled while second peptides disabled.

4.4.6.5 Bioinformatic analysis

Perseus V 1.3.0.4, a module from the MaxQuant suite [165], was used for calculation of the Pearson correlation for both proteome. This was done by extraction of the H/L ratios from ProteinGroups.txt file, generated in MaxQuant. Contaminants, reverse hits or identified by site were removed, values Log2 transformed and the Pearson correlation calculated for the H/L ratios of both replicates.

The calculation of significantly changing proteins and phosphorylation sites was also done in Perseus V 1.3.0.4 (two-tailed “Significance B” test; $p \leq 0.05$). H/L ratios were transformed to Log2, whereas intensities of peptides or phosphorylation sites were Log10 transformed.

We applied truncation based on Benjamini-Hochberg [173] corrected p-values with threshold value of 0.05 to test whether specific annotation terms are significantly enriched or depleted among the chosen set of proteins of interest.

4.4.7 Immunofluorescence (IF)

For Immunofluorescence assays, 200.000 cells were grown on coverslips contained in 6 well dishes. The day after medium was removed and they were rinsed with PBS. Cells were fixed with 100 µl Acetone + Methanol (1:1) for 2 min at RT. Coverslips were then washed 3 times with PBS and blocked for 1 hour at RT with 50 µl of PBS + 3% BSA. Primary antibody was diluted in PBS + 3% BSA and incubated overnight at 4°C in a humid chamber. The following day, the antibody solution was removed and the coverslips were washed 3 times with PBS-T. Incubation with the secondary antibody was done at RT for 1 hour in a dark and humid chamber. After washing the coverslips 3 times with PBS-T, a 20 sec DAPI staining was performed and 3 further washing steps followed. In the end, coverslips were mounted onto glass slides using one drop of FluoPrep (Biomerieux, REF 75521) and let to dry for at least 1 h. Microscopy analyses were performed using the fluorescence microscope Axiovert M200 (Zeiss).

4.4.8 FACS-FRET

Fluorescence resonance energy transfer (FRET), first described by Theodor Förster in 1946, is a phenomenon that describes the energy transition from a fluorophore (donor) in an excited state to a neighboring fluorophore (acceptor) by dipole-dipole interaction [174]. The efficiency of this energy transfer depends primarily on the distance between fluorophores that have to be less than 10 nm [175] thus making FRET a suitable method to determine direct interactions between two molecules in close proximity. The availability of several spectral variants of the Green Fluorescent Protein (GFP) [176] made FRET a suitable tool to investigate protein-protein interactions. By tagging the protein of interest with one of the GFP variants, FRET can be used to investigate interactions of native proteins in living cells. The spectral characteristics of the chosen fluorophores are also very important: the donor's emission spectrum have to overlap with the excitation spectrum of the acceptor, so that the energy released by the donor can excite the acceptor (Fig. 14). Combining FRET with FACS permits the evaluation of thousands of cells in a short time and minimizes the blurred signals resulting from the spectral overlap, making FACS-FRET a powerful technique to detect protein-protein interactions [157].

For FACS-FRET experiments, 150.000 C33a cells were seeded in 12 well plates, transfected with 1 µg of DNA the day after and harvested 48 h post-transfection. Cells were washed twice with PBS, after removing the medium from the wells, and, afterwards, they were re-

suspended in PBS + 1% FBS and kept on ice before analysis. The MACSQuant Analyzer (Miltenyi Biotec) was used to perform FACS-FRET measurements. First, viable cells were identified using the forward scatter (FSC) and the sideward scatter (SSC) gating strategy. A 405 nm laser was used to excite the donor (BFP) and the V1 channel was used to detect its emission through a 450/50 filter. The acceptor was excited with a 488 nm laser and its emission was quantified with the B1 channel via a 525/50 filter. FRET signals were measured with the V2 channel (525/50). To identify only FRET-positive cells the gating took into account the false positive signals deriving from the excitation of the acceptor (with the 405 nm laser) and combine it with the negative control (cells co-expressing donor and acceptor) (Fig. 14A) and the positive control (cells expressing a fusion construct of donor-acceptor) (Fig. 14B). The remaining cells are evaluated for FRET by adjusting the gate to define cells which are co-transfected with BFP and YFP only and should thus be FRET-negative and with a BFP-YFP fusion construct that represent the FRET-positive cell population.

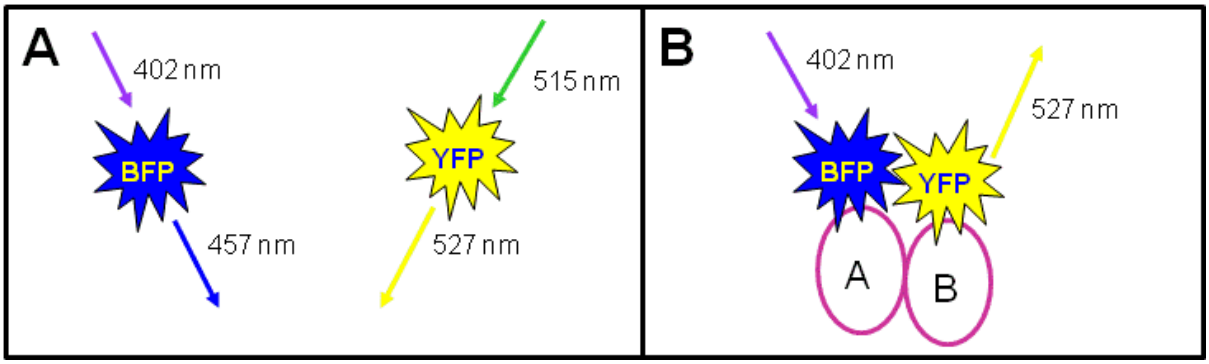

Fig. 14 FRET. When there´s an overlap between the donor emission and the acceptor excitation wavelength, if the two fluorophores are not close enough there will be any FRET (A), if the two proteins are in close proximity, there will be FRET (B).

4.4.9 Proximity ligation assay (PLA)

PLA is a method to investigate direct protein-protein interactions and the Duolink kit (Sigma Aldrich) was used for this purpose (Fig. 15) . Cells were processed as for an immunofluorescence until the incubation with the primary antibody. The step of the incubation with the secondary antibodies was substituted with the incubation with the PLA secondary antibody probes and all the following steps were performed following the manufacture's protocol. Briefly, the probes were ligated and, in case of close proximity of the two proteins investigated and consequently of the bound antibodies, the formation of a circle followed. A rolling circle amplification with fluorescently labeled nucleotides led to the formation of fluorescent spots, an indication of protein-protein interaction. Microscopy analyses were performed using the fluorescence microscope Axiovert M200 (Zeiss).

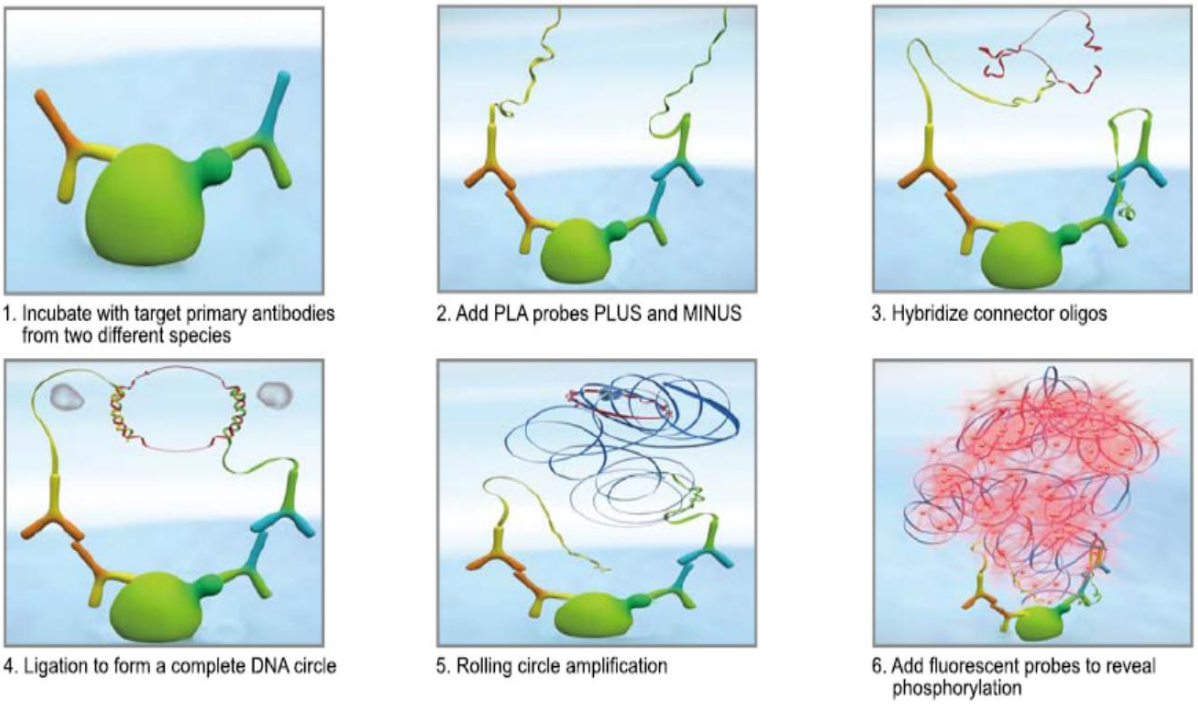

Fig. 15 PLA principle (Figure adapted from the Duolink kit manual, Sigma Aldrich)

5. Results

5.1 Identification of new cutaneous E6 interaction partners

Persistent infection of keratinocytes with high-risk types (HR) of human papillomavirus (HPV) is causally related to the development of cervical cancer. The deregulation of cellular processes by the viral oncoproteins E6 and E7 is essential for malignant transformation of the cells.

While much is known about the features of the HR-HPV oncoproteins and their contribution to the development of cancer, the role of E6 and E7 of cutaneous papillomaviruses related to nonmelanoma skin cancer (NMSC) remains not fully understood. Therefore, this part of the work aimed at evaluating the protein-binding characteristics of the E6 protein of different cutaneous types through liquid chromatography/mass spectrometry (LC/MS)-based proteomics.

5.1.1 Transient expression of E6 HA-tagged proteins

To investigate viral-host interactions of cutaneous E6 proteins, a system for exogenous protein expression had to be established. Therefore E6 proteins of HPV 5, 38 and CRPV were, HA (hemagglutinin) tagged and expressed in HPV negative cell lines. Since stable expression of the HA-tagged proteins did not result in the production of a sufficient protein amount for proteomic analysis in NIKS cells (Supplementary results, Fig. S1 and S2), the expression system was changed to a transient expression system. First, E6 genes were cloned into the pCMV vector containing an N-terminal Flag_Linker_HA tag (pCMV-N-Flag_Linker_HA, a kind gift from Dr. K. Munger). Subsequently, the HPV-negative cell line C33a was transfected with these constructs and protein expression was analyzed on a western blot (Fig. 16).

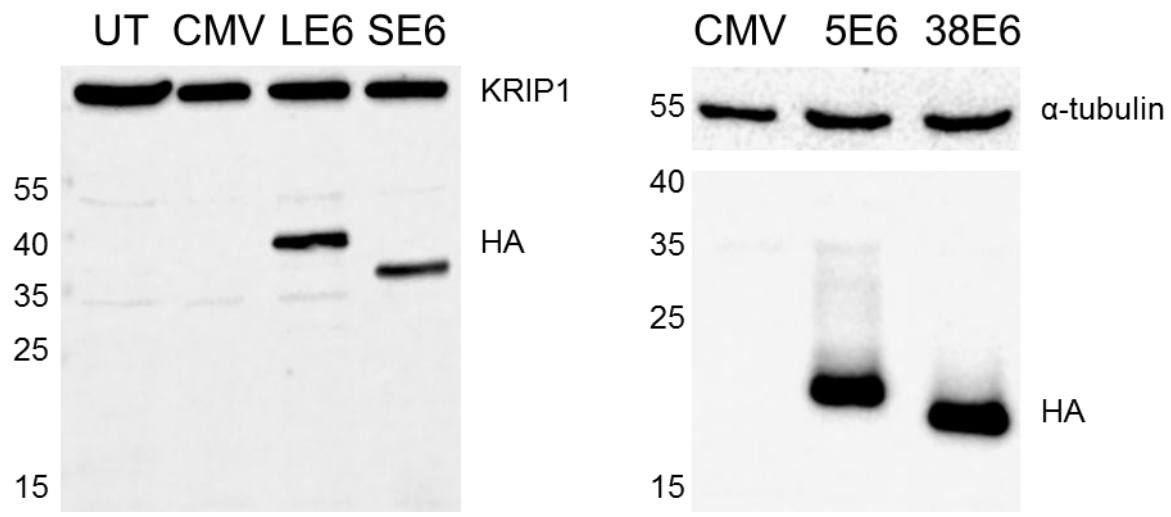

Fig. 16 Western blot showing HA-tagged E6 protein expression in transiently transfected C33a cells. Lysates were analyzed with an anti-HA antibody and either KRIP1 or α-tubulin were used as housekeeping proteins. On the left, molecular weights are indicated in kDa. UT: untransfected; CMV: pCMV-N-Flag_Linker_HA empty vector; LE6: pCMV-N-Flag_Linker_HA-CRPVLE6; SE6: pCMV-N-Flag_Linker_HA-CRPVSE6; 5E6: pCMV-N-Flag_Linker_HA-HPV5E6; 38E6: pCMV-N-Flag_Linker_HA-HPV38E6.

All the tagged E6 proteins transiently expressed in C33a cells were detected and a clear band at the expected molecular size was observed for CRPVLE6 and SE6 and for HPV5 and 38E6. Untransfected (UT) cells and the empty vector control showed no band.

An immunofluorescence was also performed to evaluate expression and localization of the tagged E6 proteins. In Fig. 17 an example of C33a cells transfected with the empty vector (CMV), CRPVLE6 (LE6) and HPV38E6 (38E6) is shown.

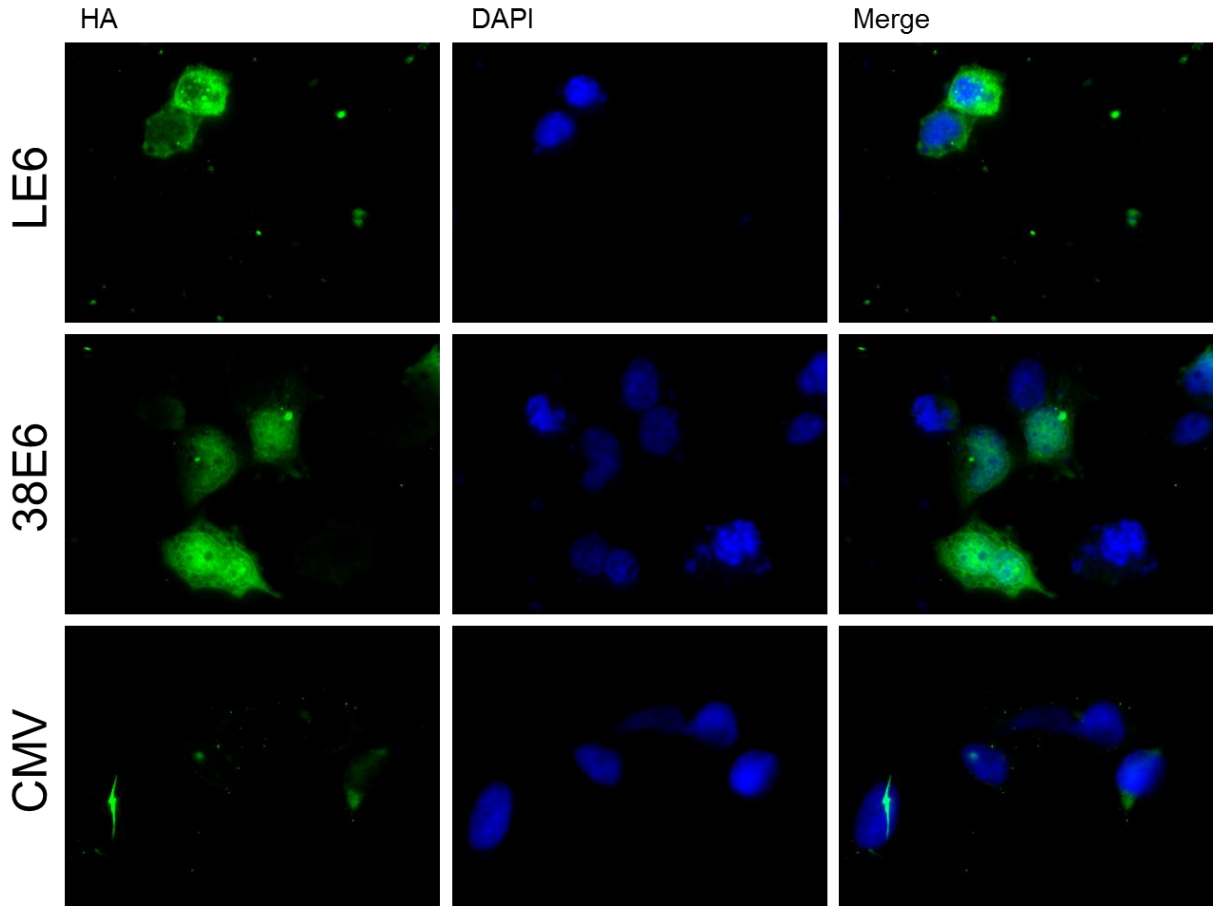

Fig. 17 Immunofluorescence showing expression of LE6 and 38E6. C33a cells were stained with an anti-HA antibody (green). Cell nuclei were stained with DAPI (blue). Merge shows the overlay of HA and DAPI stainings.

Immunofluorescence analysis revealed that both LE6 and 38E6 were expressed in C33a cells and that their localization was nuclear and cytoplasmic.

5.1.2 E6 HA-tagged proteins bind to their known interaction partners

In order to determine whether the HA-tagged E6 proteins are functional, a co-immunoprecipitation (CoIP) was performed to analyze the proteins' interacting protein-binding capabilities on known interaction partners (Fig. 18).

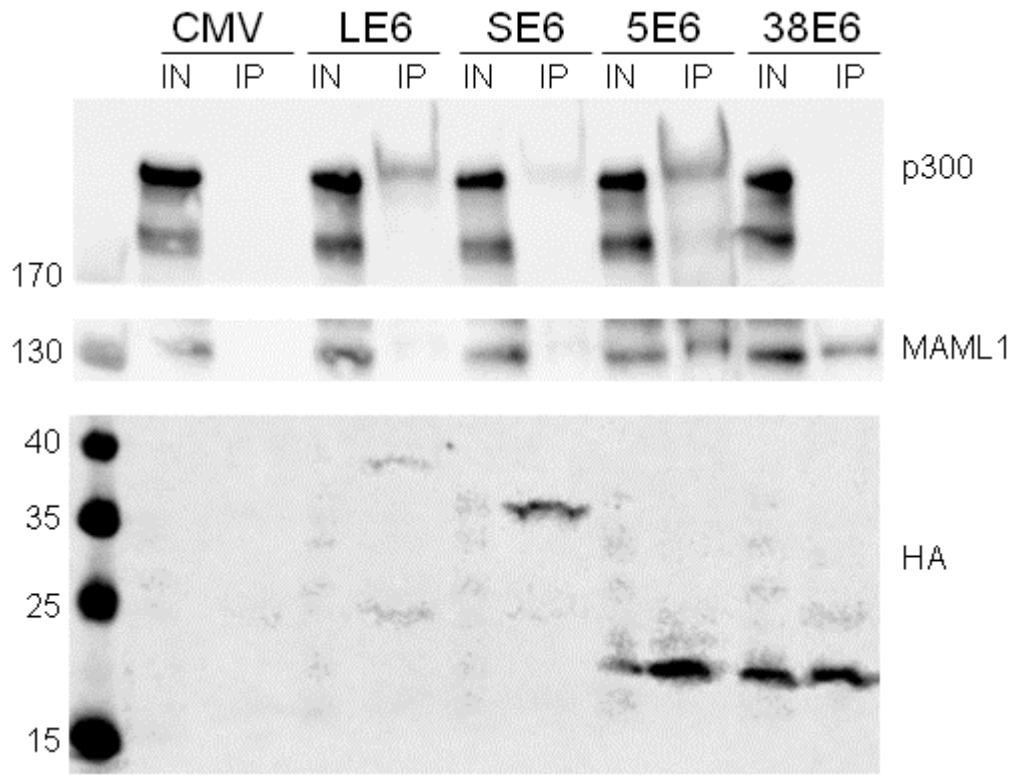

Fig. 18 CoIP of Flag_linker_HA tagged E6 proteins. HA-tagged proteins were tested for the binding to p300 (300 kDa, upper panel, IP) and MAML1 (130 kDa, middle panel, IP), that were used as positive controls for the pull down. Specific HA signals were detected for all the proteins (lower panel, LE6 ~40 kDa , SE6 ~35 kDa, 5E6 ~20 kDa, 38E6 ~19 kDa) in both inputs (IN) and immunoprecipitates (IP) with the exception of LE6 and SE6 that were only visible in the IP. CMV: pCMV-N-Flag_Linker_HA empty vector; LE6: pCMV-N-Flag_Linker_HA-CRPVLE6; SE6: pCMV-N-Flag_Linker_HA-CRPVSE6; 5E6: pCMV-N-Flag_Linker_HA-HPV5E6; 38E6: pCMV-N-Flag_Linker_HA-HPV38E6. Molecular sizes are shown in kDa on the left.

The western blot analysis of the CoIP experiment shows no band for the HA-tagged E6 proteins in the input (IN) samples and only appears in the immunoprecipitate (IP) samples. Bands for p300 were detected in the CRPV LE6, SE6 and 5E6 expressing cell lysates while5 and 38E6 pulled down MAML1.

The interaction of CRPVE6 and MAML1 remains elusive, because there might be a species-specificity incompatibility as a rabbit protein was expressed in human cells, meaning that CRPVE6 might not be able to bind human MAML1 (hMAML1) but could potentially be able to associate with rabbit MAML1 (rMAML1).

Because an anti-rabbit MAML1 antibody is not available and the anti- human MAML1-antibody does not recognize rabbit MAML1 (Fig. 19-A), due to protein sequence differences in the epitope targeted by the anti-human MAML1 antibody, described in the antibody

datasheet as a peptide surrounding His 810 residue (Fig. 19-B), a CoIP using rabbit cells, to test whether CRPVE6 was able to pull down rMAML1, could not be performed.

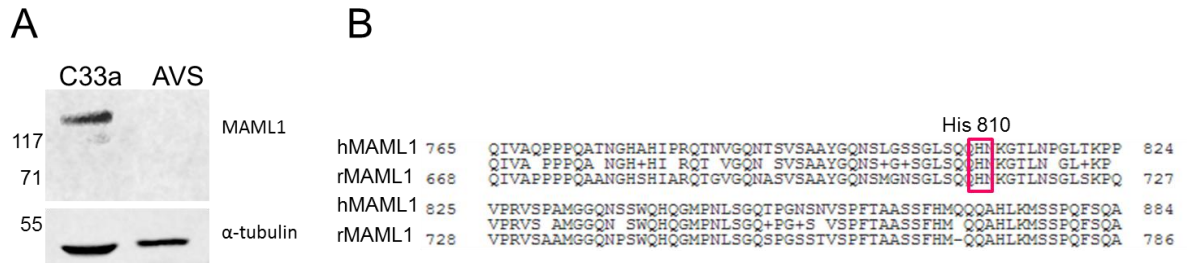

Fig 19 MAML1 antibody does not recognize rabbit MAML1. A: western blot showing that MAML1 was detected in C33a but not in AVS (Primary rabbit keratinocytes, harboring the whole CRPV genome) cells. α-tubulin was used as a loading control. On the left, molecular sizes are indicated in kDa. B: Blast alignment of MAML1 protein sequences of the human and rabbit isoform showing difference in the region where the antibody used is supposed to bind. Human MAML1 (hMAML1); rabbit MAML1 (rMAML1).

Although E6 protein expression levels revealed by the CoIP were variable, some E6 proteins were able to pull down their reported interacting partners. This confirmed that the tagged E6-proteins were functional at protein-protein interaction level.

5.1.3 CRPVLE6 downregulates Notch activation in C33a cells

E6 proteins of some types of β-HPVs and BPV1 were previously reported to be able to interfere with the Notch signaling pathway [75], [76]. CRPV resembles some of the cutaneous PV features and this led to the hypothesis that LE6 might also be able to affect Notch pathway activation. To investigate this, luciferase assays using a Notch-responsive luciferase plasmid were performed. For this reason LE6 was cloned into the retroviral vector pBabe-puro with and without the Flag-Linker-HA tag. C33a cells were co-transfected with a Notch-responsive luciferase plasmid expressing Hes1-luc, a known Notch transcriptional target, and Gaussia luciferase plasmid pCMV-Gluc, as well as with either BPV1E6, the CRPVLE6 expression plasmids or the empty vector. Notch-dependent transcription was activated upon co-expression of the Notch Intracellular Domain (NICD). As a result, BPV1E6 expression resulted in the repression of Notch activity. Moreover, LE6, with and without tag, seemed to able to downregulate Hes1-luc activity when Notch signaling was activated (Fig. 20).This suggests that the protein is both expressed and functional with and without the tag in C33a cells.

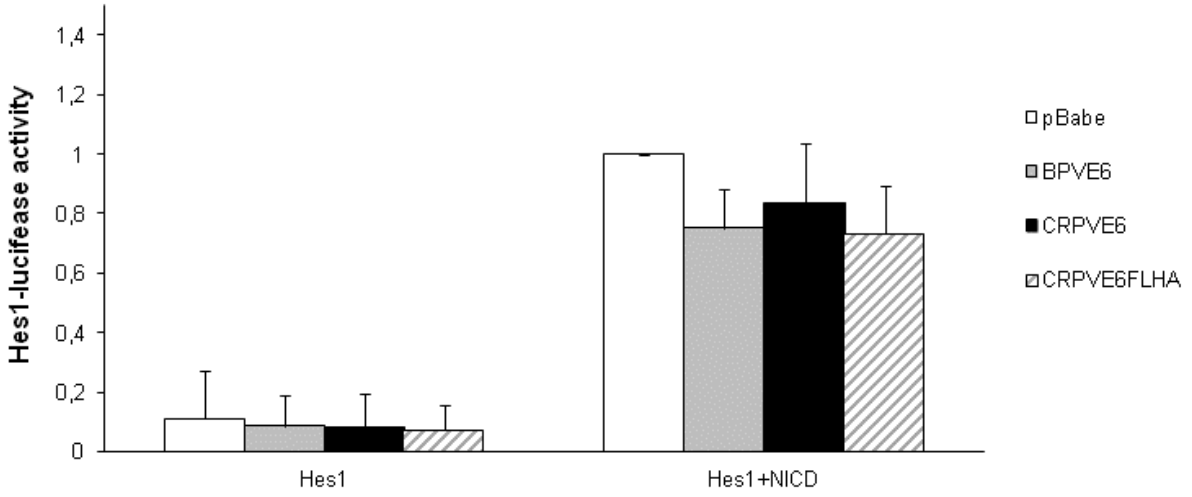

Fig. 20 Luciferase assay showing Notch repression by LE6. C33a cells were transiently transfected with Hes1 luciferase reporter plasmid, together with pBabe-puro-CRPVLE6 (LE6), CRPVLE6_Flag_Linker_HA (LE6 FLHA) or BPVE6, with or without the Notch IntraCellular Domain (NICD). Gaussia was used as an internal transfection control. The bars represent luciferase activities relative to the empty vector ± NICD transfected cells (pBabe). White bars represent luciferase activity in empty vector transfected cells, grey bars, black bars and striped bars show BPVE6, CRPVE6 and CRPVE6_Flag-linker-HA activity. On the left is shown Hes1 basal activity whereas on the right is the activity after co-transfection with NICD, and therefore Notch pathway activation. Data are presented as the average ± standard deviations of five different experiments.

Although a clear interaction between LE6 and MAML1 could not be demonstrated (Section 5.1.2), the luciferase assay demonstrates that LE6 interferes with Notch pathway, as other proteins do by interacting with MAML1 (i.e. BPV1 E6), with a mechanism that still has to be elucidated.

5.1.4 Proteome analysis of E6 tagged proteins using label free quantification

Once expression and functionality of the tagged E6 proteins was assessed, a protein interaction analysis was performed. Flag-HA-tagged proteins were transiently expressed in C33a cells and a CoIP was carried out after 48 hours using the whole cell lysate. A western blot was performed to verify the presence of the HA-tagged proteins and the efficiency of the Co-IP (Fig. 21). MAML1 was used as a control for the pull down efficiency of HPV5 and 38E6. The CoIP and the proteomic analysis were repeated twice in two independent

experiments, using different DNA preparations and different cell passages, to prove the reproducibility of the experiment.

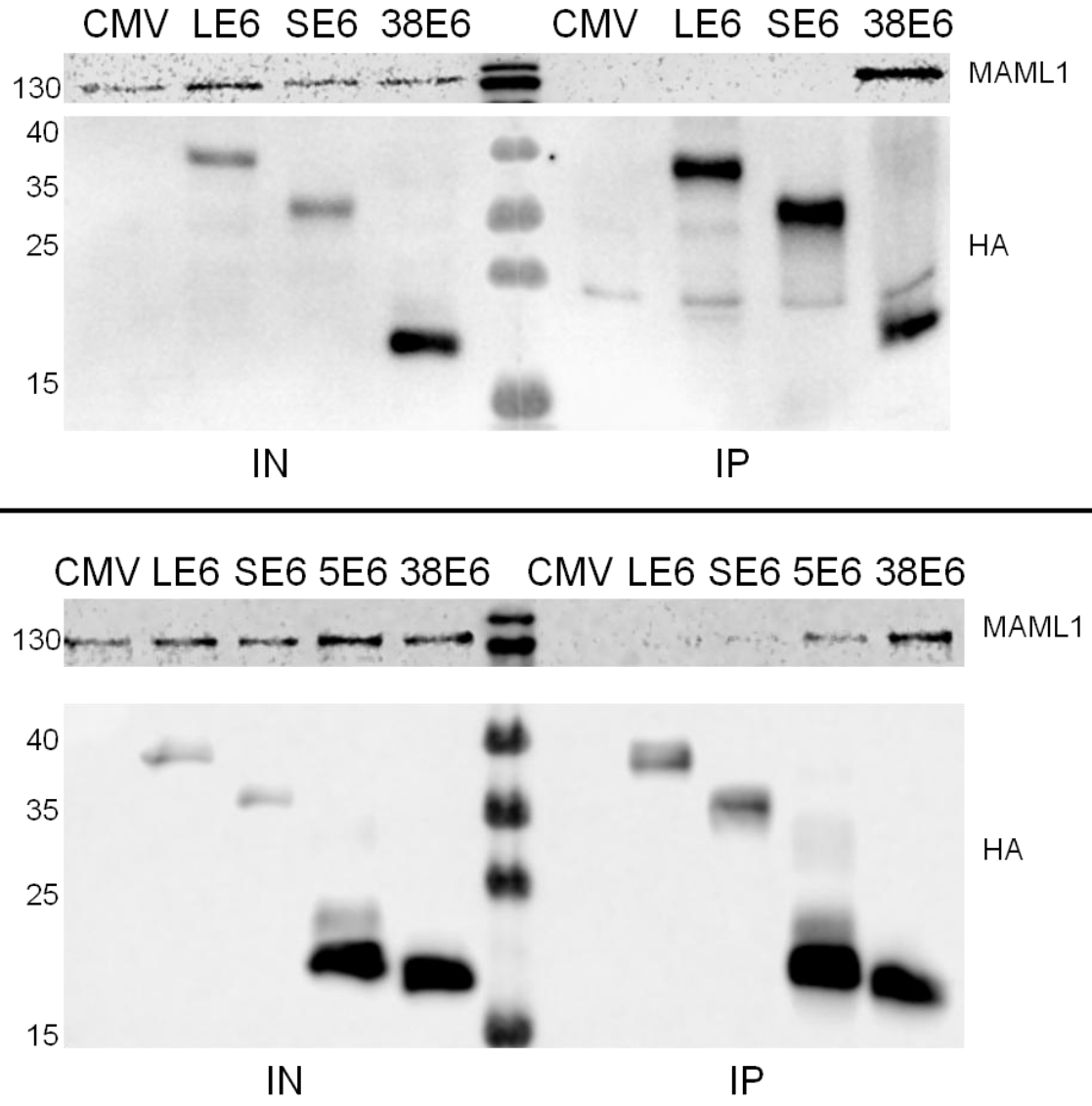

Fig. 21 CoIP of Flag_linker_HA tagged E6 proteins. HA-tagged E6 proteins were tested for the binding to MAML1 (upper panel) that was used as positive control for the pull down, in two independent experiments. Specific HA signals were detected for all the proteins (lower panels, LE6 ~40 kDa , SE6 ~35 kDa, 5E6 ~20 kDa, 38E6 ~19 kDa) in both inputs (IN) and immunoprecipitates (IP) at the expected sizes. CMV: pCMV-N-Flag_Linker_HA empty vector; LE6: pCMV-N-Flag_Linker_HA-CRPVLE6; SE6: pCMV-N-Flag_Linker_HA-CRPVSE6; 5E6: pCMV-N-Flag_Linker_HA-HPV5E6; 38E6: pCMV-N-Flag_Linker_HA-HPV38E6. Molecular sizes are shown in kDa on the left.

As shown by the western blot analysis, the specific bands detected with an anti-HA antibody demonstrated that proteins were expressed. Moreover, MAML1 was pulled down by HPV5 and 38E6 (Fig. 20, upper panels) indicating that the CoIP worked.

The next step was to perform a proteome analysis using the immunoprecipitates. With this aim, a label free quantitative mass spectrometry experiment was performed by the core facility Proteome Center of Tübingen (PCT). Using and analyzing the data obtained by the PCT, the cellular interaction partners of LE6, SE6 and 38E6 were identified.

Since more than 2000 proteins were identified in each experiment an analysis procedure was performed to sort and quantify them (Materials and methods, section 4.4.5.3). Briefly, raw data were analyzed with MaxQuant (version 1.2.2.9), and then further analyzed using the statistical tool suite Perseus (version.1.3.0.4). The label free quantification (LFQ) ratios were quantified using the intensity-based absolute quantification (iBAQ) algorithm in order to identify interactors of LE6, SE6 and 38E6.

A list of interaction partners for LE6, SE6 and 38E6 was generated (Supplementary results, Fig. S3, S4, S5 and S6). In Fig. 22-A, -B, -C, the distribution of the Log2 ratios of proteins' iBAQs from LE6, SE6 and 38E6 is represented using scatter plots, whereas in Fig. 23 are shown the differential interaction partners of LE6 and SE6.

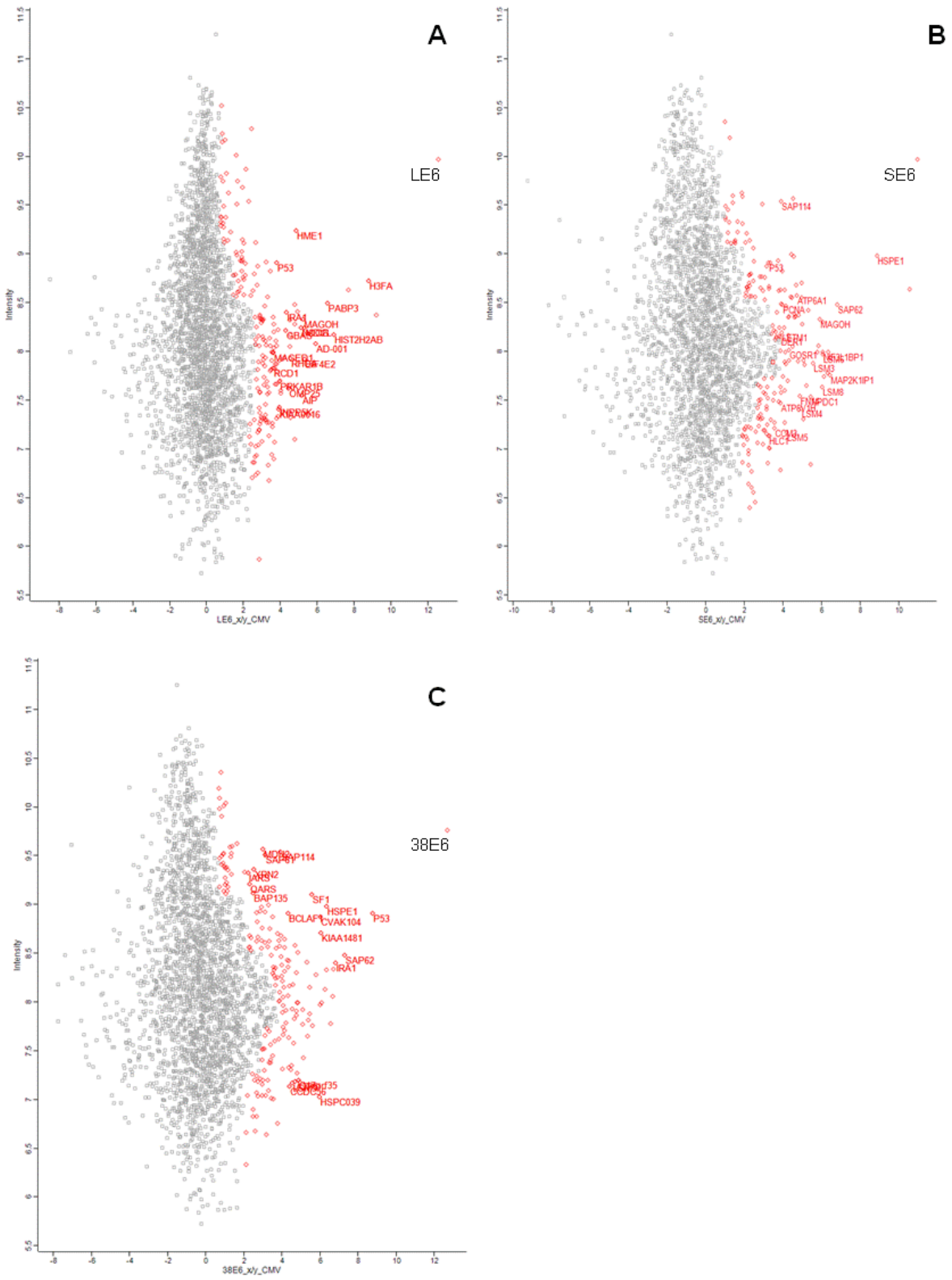

Fig. 22 Scatter plots of the Log2 ratios of proteins' iBAQs from LE6, SE6 and 38E6. The distribution is a Gaussian normal distribution with a median of 0 and a standard deviation of 1.The plot represent two independent experiments. Highlighted in red are the significantly interacting proteins with LE6, SE6 and 38E6, and the names of few important proteins described in literature.

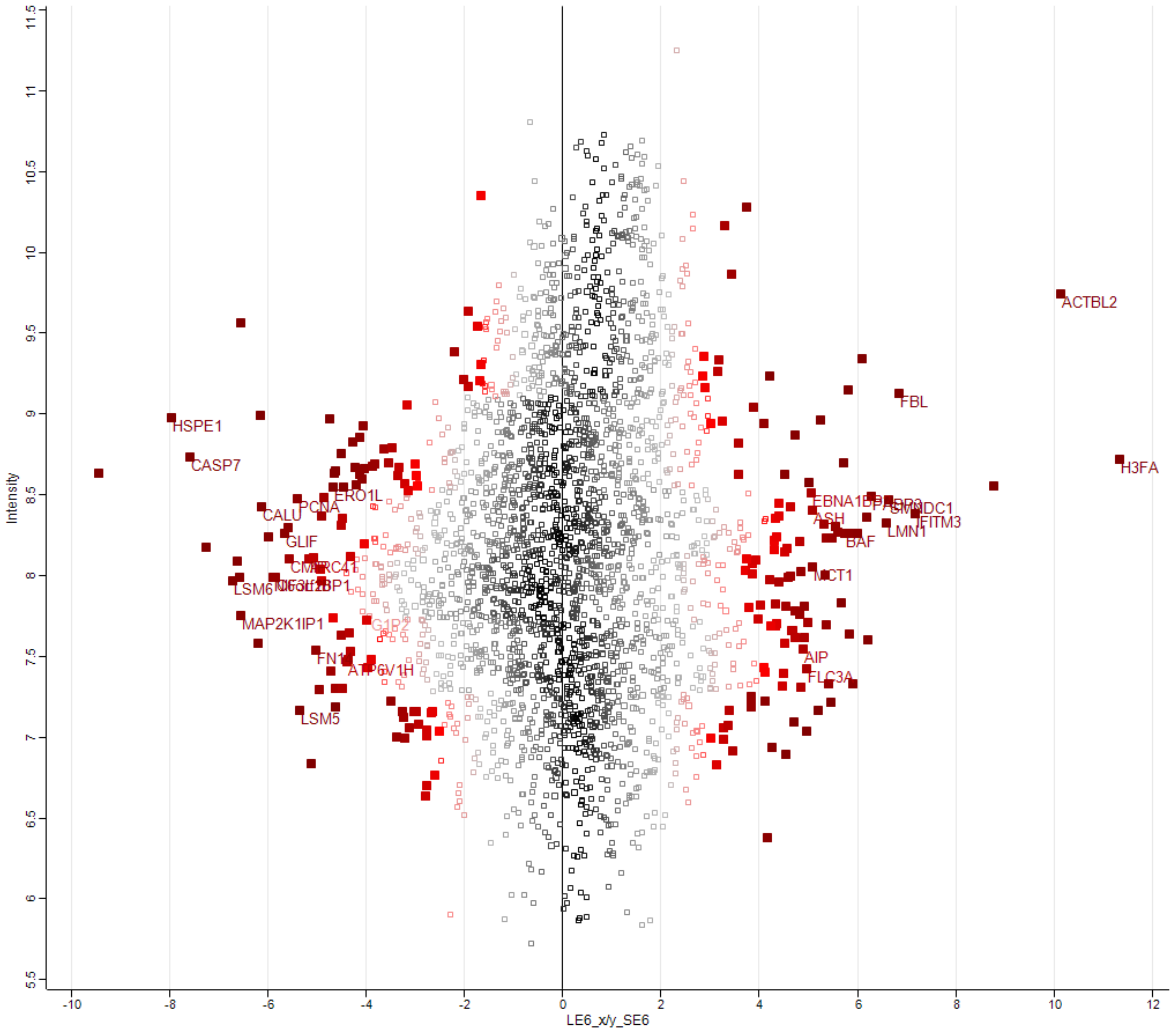

Fig. 23 Scatter plot of differential interaction partners of LE6 and SE6. The iBAQs distribution is a Gaussian normal distribution with a median of 0 and a standard deviation of 1. Highlighted in red are the significantly interacting proteins of SE6 (on the left) and LE6 (on the right) the names of few important proteins described in literature, where progressively dark red proteins are the most represented proteins interacting specifically with LE6 or SE6.

In total, 2792 proteins were identified and quantified from the 3 datasets, where 195 proteins, 186 proteins and 188 proteins were significantly identified as interactors of LE6, SE6 and 38E6 respectively (Fig. 24).

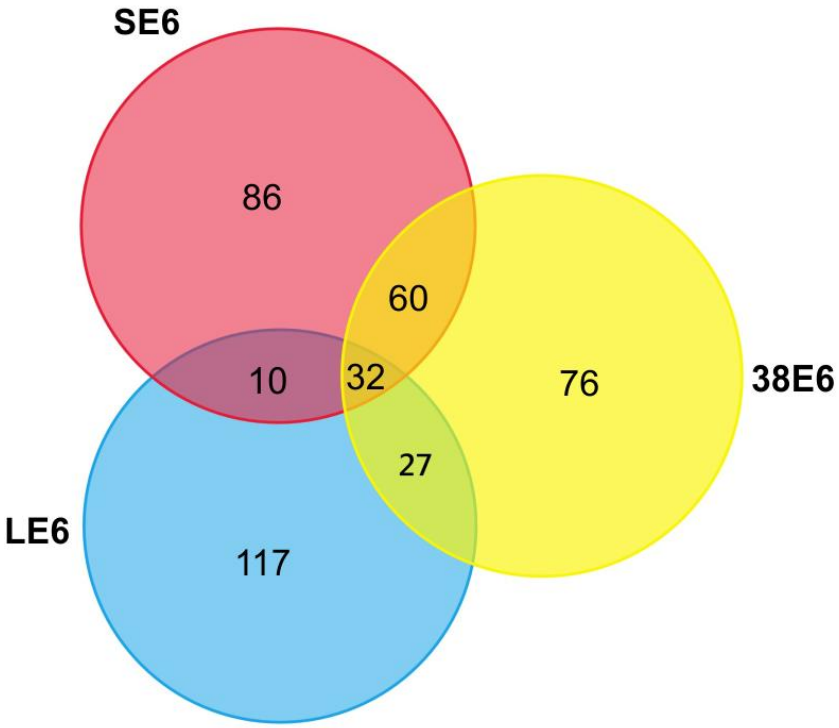

Fig. 24 Venn diagram showing the specific and common interacting proteins of 38E6, LE6, and SE6. The blue circle represents the interacting proteins identified for LE6, the pink circle represents the interacting proteins identified for SE6 and the yellow circle represents the interacting proteins identified for 38E6. The intersections among the colored areas show the common interacting proteins.

Furthermore it was found that 60, 27 and 10 proteins were exclusive common interactors of 38E6+SE6, 38E6+LE6 and LE6+SE6, respectively whereas 32 proteins were identified to interact with all the three baits (Table 5).

The common interacting proteins between LE6 and SE6, 38E6 and LE6, 38E6 and SE6, are summarized in Tables 2, 3 and 4 respectively. Additionally, in Table 5 the proteins common in the three datasets are also shown.

Table 2. Common proteins between LE6 and SE6. List of common interacting proteins, where Protein IDs represent the Uniprot identification numbers, Gene symbols are the abbreviated names of the genes, EntrezGene IDs are the Entrez gene identification numbers.

Uniprot ID	Gene Symbol	EntrezGene ID	Gene description
O75486	SUPT3H	8464	suppressor of Ty 3 homolog (S. cerevisiae)
Q9H9B4	SFXN1	94081	sideroflexin 1
Q15363	TMED2	10959	transmembrane emp24 domain trafficking protein 2
Q16878	CDO1	1036	cysteine dioxygenase type 1
E5KLJ5	OPA1	4976	optic atrophy 1 (autosomal dominant)
P30536	TSPO	706	translocator protein (18kDa)
Q96KC2	ARL5B	221079	ADP-ribosylation factor-like 5B
Q86W74	ANKRD46	157567	ankyrin repeat domain 46
Q9H2U2	PPA2	27068	pyrophosphatase (inorganic) 2
Q9NTG7	SIRT3	23410	sirtuin 3

Table 3. Common proteins between 38E6 and LE6. List of common interacting proteins, where Protein IDs represent the Uniprot identification numbers, Gene symbols are the abbreviated names of the genes, EntrezGene IDs are the Entrez gene identification numbers.

Uniprot ID	Gene Symbol	EntrezGene ID	Gene description
Q6NZY4	ZCCHC8	55596	zinc finger, CCHC domain containing 8
Q9Y5U9	IER3IP1	51124	immediate early response 3 interacting protein 1
Q9Y320	TMX2	51075	thioredoxin-related transmembrane protein 2
J3QR07	YTHDC1	91746	YTH domain containing 1
O60573	EIF4E2	9470	eukaryotic translation initiation factor 4E family member 2
Q92615	LARP4B	23185	La ribonucleoprotein domain family, member 4B
P63220	RPS21	6227	ribosomal protein S21
B4E2P2			
Q8N0U8	VKORC1L1	154807	vitamin K epoxide reductase complex, subunit 1-like 1
P14927	UQCRB	7381	ubiquinol-cytochrome c reductase binding protein
Q9NZE8	MRPL35	51318	mitochondrial ribosomal protein L35
Q9Y3C6	PPIL1	51645	peptidylprolyl isomerase (cyclophilin)-like 1
P57105	SYNJ2BP	55333	synaptojanin 2 binding protein
P49821	NDUFV1	4723	NADH dehydrogenase (ubiquinone) flavoprotein 1, 51kDa
Q8IUE6	HIST2H2AB	317772	histone cluster 2, H2ab
A6NHR9	SMCHD1	23347	structural maintenance of chromosomes flexible hinge domain containing 1
Q15388	TOMM20	9804	translocase of outer mitochondrial membrane 20 homolog (yeast)
O60831	PRAF2	11230	PRA1 domain family, member 2
P26196	DDX6	1656	DEAD (Asp-Glu-Ala-Asp) box helicase 6
P62487	POLR2G	5436	polymerase (RNA) II (DNA directed) polypeptide G
B3KY94	CDIPT	10423	CDP-diacylglycerol--inositol 3-phosphatidyltransferase
Q15436	SEC23A	10484	Sec23 homolog A (S. cerevisiae)
A7MAP1			
F5H3A1			
P78527	PRKDC	5591	protein kinase, DNA-activated, catalytic polypeptide
Q9UNL2	SSR3	6747	signal sequence receptor, gamma (translocon-associated protein gamma)
P05023	ATP1A1	476	ATPase, Na+/K+ transporting, alpha 1 polypeptide

Table 4. Common hits between 38E6 and SE6. List of common interacting proteins, where Protein IDs represent the Uniprot identification numbers, Gene symbols are the abbreviated names of the genes, EntrezGene IDs are the Entrez gene identification numbers.

Uniprot ID	Gene Symbol	EntrezGene ID	Gene description
P61604	HSPE1	3336	heat shock 10kDa protein 1
Q9UHA4	LAMTOR3	8649	late endosomal/lysosomal adaptor, MAPK and MTOR activator 3
Q9Y333	LSM2	57819	LSM2 homolog, U6 small nuclear RNA associated (S. cerevisiae)
Q9UDW1	UQCR10	29796	ubiquinol-cytochrome c reductase, complex III subunit X
P17677	GAP43	2596	growth associated protein 43
P62312	LSM6	11157	LSM6 homolog, U6 small nuclear RNA associated (S. cerevisiae)
P99999	CYCS	54205	cytochrome c, somatic
Q6I9Y2	THOC7	80145	THO complex 7 homolog (Drosophila)
O95777	LSM8	51691	LSM8 homolog, U6 small nuclear RNA associated (S. cerevisiae)
P38117	ETFB	2109	electron-transfer-flavoprotein, beta polypeptide
O95415	BRI3	25798	brain protein I3
P04181	OAT	4942	ornithine aminotransferase
A2A274			
P34897	SHMT2	6472	serine hydroxymethyltransferase 2 (mitochondrial)
G3V5Z7			
P00505	GOT2	2806	glutamic-oxaloacetic transaminase 2, mitochondrial
P40926	MDH2	4191	malate dehydrogenase 2, NAD (mitochondrial)
Q92688	ANP32B	10541	acidic (leucine-rich) nuclear phosphoprotein 32 family, member B
Q96HE7	ERO1L	30001	ERO1-like (S. cerevisiae)
O75390	CS	1431	citrate synthase
E7ESZ7			
Q8NBQ5	HSD17B11	51170	hydroxysteroid (17-beta) dehydrogenase 11
O95249	GOSR1	9527	golgi SNAP receptor complex member 1
P36551	CPOX	1371	coproporphyrinogen oxidase
Q9Y4Y9	LSM5	23658	LSM5 homolog, U6 small nuclear RNA associated (S. cerevisiae)
P50213	IDH3A	3419	isocitrate dehydrogenase 3 (NAD+) alpha
P12004	PCNA	5111	proliferating cell nuclear antigen
J3KPS3			
Q9BUN8	DERL1	79139	derlin 1
O75439	PMPCB	9512	peptidase (mitochondrial processing) beta
P00367	GLUD1	2746	glutamate dehydrogenase 1
P49419	ALDH7A1	501	aldehyde dehydrogenase 7 family, member A1
Q9BUL8	PDCD10	11235	programmed cell death 10
O15145	ARPC3	10094	actin related protein 2/3 complex, subunit 3, 21kDa
P55735	SEC13	6396	SEC13 homolog (S. cerevisiae)
P30519	HMOX2	3163	heme oxygenase (decycling) 2
J3KQ97			
Q9NYF8	BCLAF1	9774	BCL2-associated transcription factor 1
O75348	ATP6V1G1	9550	ATPase, H+ transporting, lysosomal 13kDa, V1 subunit G1
Q96MC6	HIAT1	64645	hippocampus abundant transcript 1
P24752	ACAT1	38	acetyl-CoA acetyltransferase 1
Q9UQ80	PA2G4	5036	proliferation-associated 2G4, 38kDa
P23434	GCSH	2653	glycine cleavage system protein H (aminomethyl carrier)
Q9NUP9	LIN7C	55327	lin-7 homolog C (C. elegans)
Q96S55	WRNIP1	56897	Werner helicase interacting protein 1
P00390	GSR	2936	glutathione reductase
P23368	ME2	4200	malic enzyme 2, NAD(+)-dependent, mitochondrial
P30044	PRDX5	25824	peroxiredoxin 5
P47897	QARS	5859	glutaminyl-tRNA synthetase
Q16643	DBN1	1627	drebrin 1
Q32Q12			
P35241	RDX	5962	radixin
P38919	EIF4A3	9775	eukaryotic translation initiation factor 4A3
P55072	VCP	7415	valosin containing protein
P06576	ATP5B	506	ATP synthase, H+ transporting, mitochondrial F1 complex, beta polypeptide
F8VQ10			
Q00610	CLTC	1213	clathrin, heavy chain (Hc)
P54136	RARS	5917	arginyl-tRNA synthetase
Q12931	TRAP1	10131	TNF receptor-associated protein 1
P10809	HSPD1	3329	heat shock 60kDa protein 1 (chaperonin)

Table 5. Common hits between 38E6, SE6 and LE6. List of common interacting proteins, where Protein IDs represent the Uniprot identification numbers, Gene symbols are the abbreviated names of the genes, EntrezGene IDs are the Entrez gene identification numbers.

Uniprot ID	Gene Symbol	EntrezGene ID	Gene description
Q7Z417	NUFIP2	57532	nuclear fragile X mental retardation protein interacting protein 2
O75381	PEX14	5195	peroxisomal biogenesis factor 14
P61326	MAGOH	4116	mago-nashi homolog, proliferation-associated (Drosophila)
P51970	NDUFA8	4702	NADH dehydrogenase (ubiquinone) 1 alpha subcomplex, 8, 19kDa
Q15428	SF3A2	8175	splicing factor 3a, subunit 2, 66kDa
Q96C36	PYCR2	29920	pyrroline-5-carboxylate reductase family, member 2
Q9BZK7	TBL1XR1	79718	transducin (beta)-like 1 X-linked receptor 1
O75323	GBAS	2631	glioblastoma amplified sequence
Q8WZ42	TTN	7273	titin
O75352	MPDU1	9526	mannose-P-dolichol utilization defect 1
Q9Y5S9	RBM8A	9939	RNA binding motif protein 8A
P04637	TP53	7157	tumor protein p53
P54819	AK2	204	adenylate kinase 2
Q9BSR8	YIPF4	84272	Yip1 domain family, member 4
Q96J01	THOC3	84321	THO complex 3
P00492	HPRT1	3251	hypoxanthine phosphoribosyltransferase 1
P62310	LSM3	27258	LSM3 homolog, U6 small nuclear RNA associated (S. cerevisiae)
Q9Y3E0	GOLT1B	51026	golgi transport 1B
P22695	UQCRC2	7385	ubiquinol-cytochrome c reductase core protein II
P78347	GTF2I	2969	general transcription factor IIi
P28331	NDUFS1	4719	NADH dehydrogenase (ubiquinone) Fe-S protein 1, 75kDa (NADH-coenzyme Q reductase)
P38606	ATP6V1A	523	ATPase, H+ transporting, lysosomal 70kDa, V1 subunit A
Q15459	SF3A1	10291	splicing factor 3a, subunit 1, 120kDa
P61803	DAD1	1603	defender against cell death 1
Q9Y2W1	THRAP3	9967	thyroid hormone receptor associated protein 3
O75306	NDUFS2	4720	NADH dehydrogenase (ubiquinone) Fe-S protein 2, 49kDa (NADH-coenzyme Q reductase)
Q12874	SF3A3	10946	splicing factor 3a, subunit 3, 60kDa
P13861	PRKAR2A	5576	protein kinase, cAMP-dependent, regulatory, type II, alpha
P09661	SNRPA1	6627	small nuclear ribonucleoprotein polypeptide A'
P08579	SNRPB2	6629	small nuclear ribonucleoprotein polypeptide B
P41252	IARS	3376	isoleucyl-tRNA synthetase
Q9ULV4	CORO1C	23603	coronin, actin binding protein, 1C

5.1.5 Identification of known interaction partners

After processing and sorting the putative interacting proteins, it was not possible to identify the interactions already described in literature, as p300 and MAML1.

Concerning p300, known to interact with LE6 and SE6, it was identified in both pull downs but not significantly. This result could be related to the fact that p300 is part of a protein family and therefore not enough unique peptides were identified. For this reason p300 was automatically eliminated by the software as it did not fit to the parameters set. Although the western blot shown in Fig. 17 demonstrates the interaction of p300 with LE6 or SE6, possibly due to the large homology between CBP (CREB-binding protein) and p300 (68%), the software was unable to distinguish which of the two proteins was the direct interactor and only detected that p300/CBP was involved.

MAML1, although shown to be a strong 38E6 binder by White et al. 2012, was never pulled down in the two aforementioned experiments. This might be explainable once more by the

fact that it belongs to a huge protein family which does not allow the generation of enough unique peptides.

Moreover, as the strict parameter significance B was applied to the whole analysis, this might have affected the entire quantification.

Except for the binding of 38E6 to p53, that was highly reproducible since it was present in both the experiments and was also shown by western blot (Fig. 25, this figure was previously shown as Fig. 18), p300 and MAML1 were only identified by western blot.

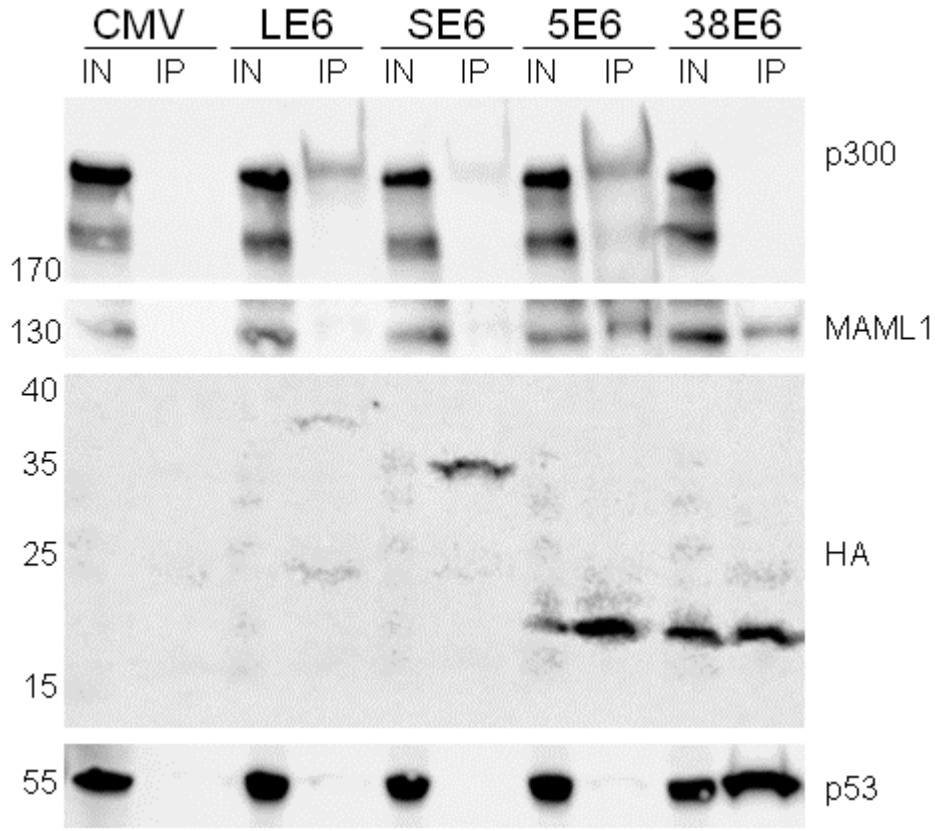

Fig. 25 Western blot showing 38E6 and p53 interaction. HA-tagged proteins were tested for the binding to p300 (upper panel, IP) and MAML1 (middle upper panel, IP), that were used as positive controls for the pull down. p53 was also shown to be pulled down by 38E6 (lower panel). Specific HA signals were detected for all the proteins (middle lower panel, LE6 ~40 kDa , SE6 ~35 kDa, 5E6 ~20 kDa, 38E6 ~19 kDa) in both in the inputs (IN) and immunoprecipitates (IP) with the exception of LE6 and SE6 that were only visible in the IP. CMV: pCMV-N-Flag_Linker_HA empty vector; LE6: pCMV-N-Flag_Linker_HA-CRPVLE6; SE6: pCMV-N-Flag_Linker_HA-CRPVSE6; 5E6: pCMV-N-Flag_Linker_HA-HPV5E6; 38E6: pCMV-N-Flag_Linker_HA-HPV38E6. Molecular sizes are shown in kDa on the left. Figure previously shown as Figure 18.

5.1.6 Functional analysis

A functional enrichment analysis was carried out using the tool suite FunRich [178]. The proteins identified were analyzed and, for each bait, it was identified in which biological pathway (Fig. 26), cell line (Fig. 27) and transcription factors (Fig. 28) they were involved in. Hypergeometric uncorrected p-values were used for statistics.

5.1.6.1 Biological pathways

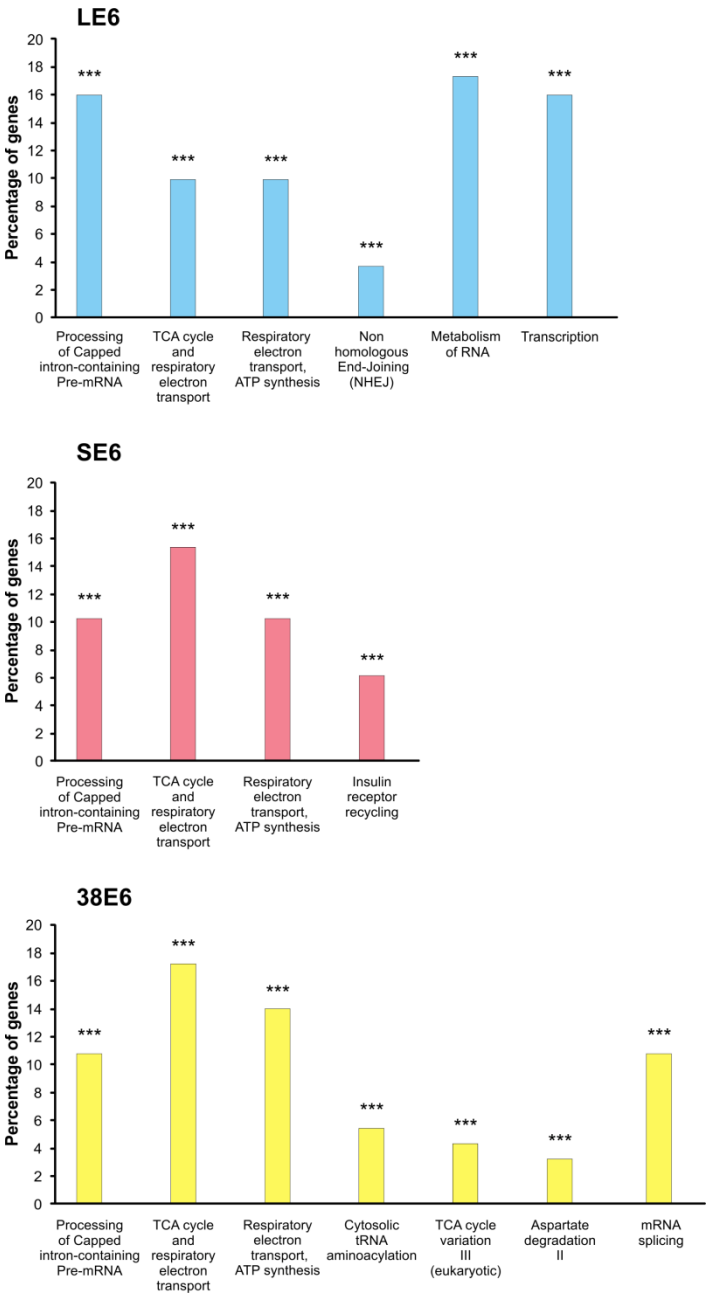

Fig. 26 Functional enrichment analysis of biological pathways using FunRich. Genes enriched in the highest probable pathways ($p < 0.001$) are showed.

Fold enrichment was calculated by comparing the identified proteins against all the proteins as background. In biological pathways, all the baits show an involvement in mRNA processing, respiratory electron transport, ATP synthesis and citric acid cycle, although at different levels. Moreover, LE6 and 38E6 share pathways involved in transcription while non homologous end-joining and the insulin receptor recycling pathways are exclusive of LE6 and SE6, respectively.

5.1.6.2 Sites of expression

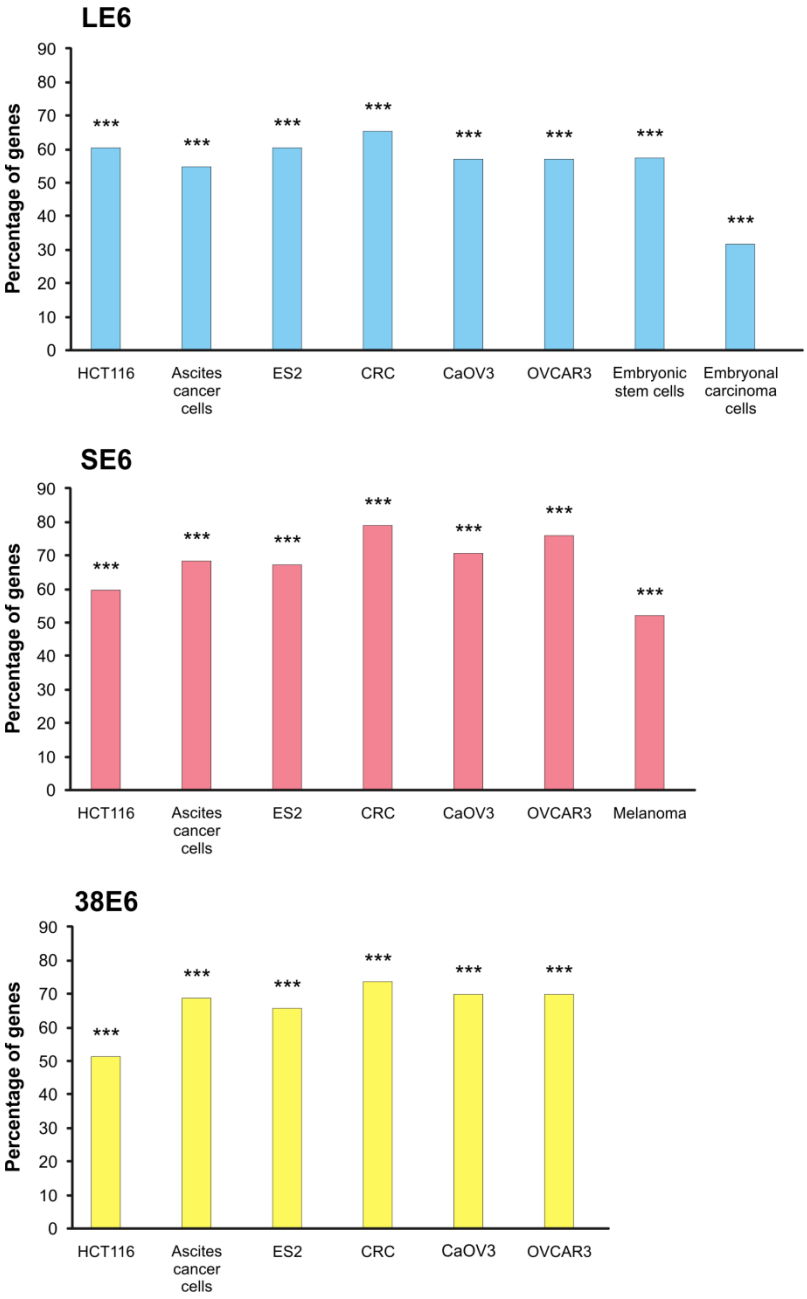

Fig. 27 Functional enrichment analysis of site of expression using FunRich. Genes enriched in the highest probable sites (p< 0.001) are showed.

Concerning the site of expression, the cell lines where the genes were found to be expressed, are showed in Fig. 27. For all the baits, consistent with their role as oncoproteins, the cell lines identified were all linked to cancer. Ovarian carcinoma (CaOV3, OVCAR3, ES2), colorectal carcinoma (HCT 116, CRC), ascites cancer cell lines were common to all, while the proteins enriched in SE6 pull downs showed a strong expression in melanoma cell line as well and LE6 also in embryonic stem cells and embryonal carcinoma cells.

5.1.6.3 Transcription factors

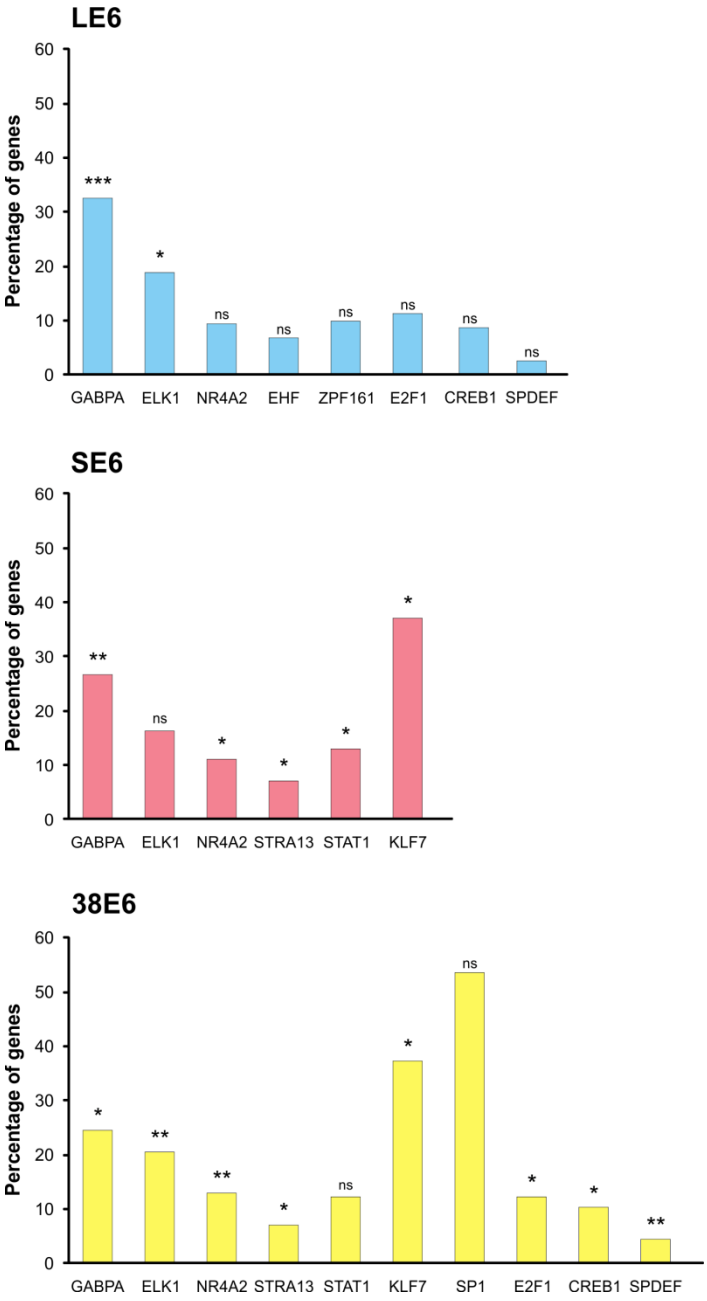

Fig. 28 Functional enrichment analysis of transcription factors using FunRich. Genes linked to the highest probable transcription factors are showed.

The putative transcription factors shared by LE6, SE6 and 38E6 are three: the GA Binding Protein Transcription Factor Alpha Subunit (GABPA), the member of ETS oncogene family (ELK1) and the Nuclear Receptor Subfamily 4, Group A, Member 2 (NR4A2).

Observing the graph in Fig. 28 it is possible to notice that, while the transcription factors involved with 38E6 and SE6 are highly significant, the ones of LE6, although highly represented, are not.

In addition, it is possible to see that LE6 and 38E6 have further common transcription factors, as the E2F Transcription Factor 1 (E2F1), the CAMP Responsive Element Binding Protein 1 (CREB1) and the SAM Pointed Domain Containing ETS Transcription Factor (SPDEF). On the other end, SE6 shares additional transcription factors only with 38E6: the Kruppel-Like Factor 7 (KLF7), the STimulated by Retinoic Acid 13 protein (STRA13) and the Signal Transducer and Activator of Transcription 1 (STAT1). Transcription factors exclusively associated to LE6 are the Zinc Finger and BTB Domain Containing 14 (ZFP161) and the ETS Homologous Factor (EHF) and of 38E6 is SP1.

5.1.7 Proteome analysis of CRPVE6 proteins using SILAC

For stronger validation, an additional approach was used. SILAC (Stable Isotope Labeling with Amino acids in cell Culture) is a metabolic labeling strategy which uses stable isotope labeled amino acids in the growth medium. First, SILAC is a quantitative method that allows the comparison of up to three different conditions in the same experiment. Moreover, the labeling allows the identification of hits in the empty vector-transfected cells that can be excluded and considered as background.

SILAC was used to perform a proteome analysis and this experiment focused on the rabbit proteins CRPVLE6 and SE6.

C33a cells were cultivated in SILAC DMEM medium until they reached a full incorporation of isotope labeled amino acids. Afterwards, C33a cells were transiently transfected with Flag-HA-tagged CRPVLE6 and SE6 and after 48 hours the whole cell lysate was used to perform a CoIP. A western blot was carried out to demonstrate the presence of the HA-tagged proteins and the efficiency of the Co-IP (Fig. 29). The protein amounts were kept constant in all input (IN) samples, as shown by the level of the housekeeping gene α-tubulin (~60kDa band). The efficiency of the CoIP was confirmed by the presence of the unique specific band detected by an anti-HA antibody.

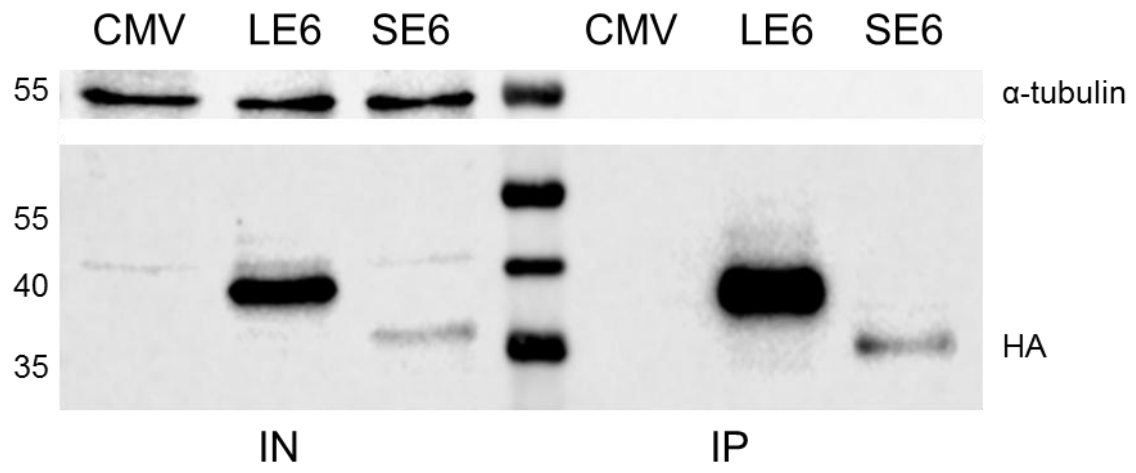

Fig. 29 CoIP of Flag_linker_HA tagged CRPV E6 proteins. CRPV LE6 and SE6, as well as the empty vector (CMV), were transiently expressed in C33a cells. The western blot shows the specific band for LE6 (~40 kDa) and SE6 (~35 kDa) using an anti-HA antibody (lower panel). An HA signal was detected for all the proteins (lower panel) in both inputs (IN) and immunoprecipitates (IP) at the expected sizes. On the left, equal amounts of IN, representing an aliquot of the cell extract from transfected cells before the CoIP, and on the right are shown the IP, 1/10 of the samples resulting from the CoIP. Samples were analyzed for the presence of a reference protein using an anti-α-tubulin antibody. Molecular weights are shown in kDa on the left.

Immunoprecipitates (IP) were analyzed by the PCT. In the first experiment, C33a cells transfected with the empty vector (CMV) were grown in the light medium (L), those transfected with LE6 in the heavy medium (H) and the SE6-transfected cells were labeled with the medium-heavy medium (M). In the first run, 2049 proteins were identified and they were plotted according to their intensities and ratios as shown in Fig. 30.

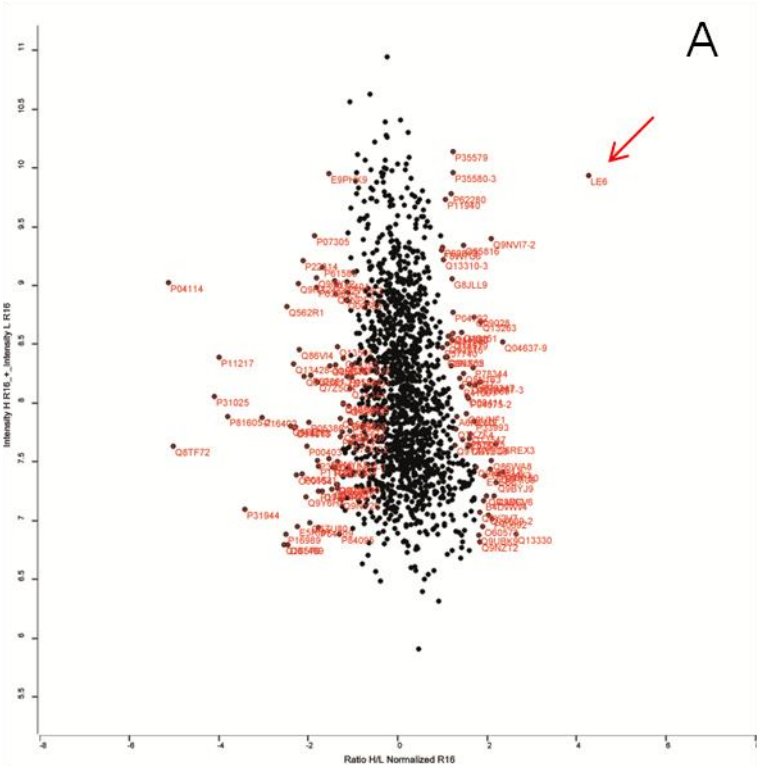
A
LE6
P35579
P35580-3
P07305
Q9NVI7-2
Q13310-3
G8JLL9
P04114
Q562R1
Q04637-9
P11217
P31025
Q8TF72
P31944
Q13330
Intensity H R16_+_Intensity L R16
Ratio H/L Normalized R16

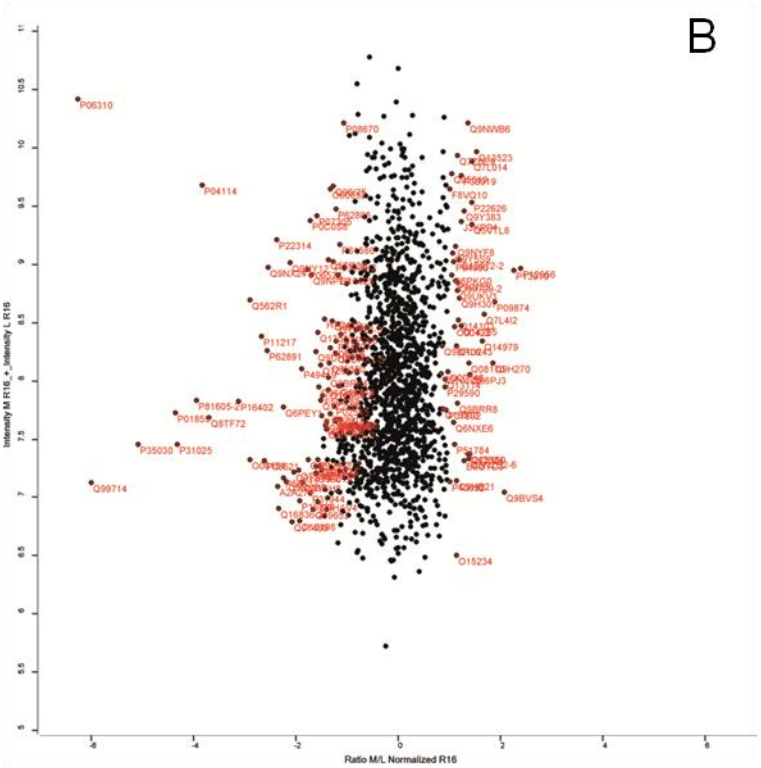
B
P06310
Q9NWB6
P04114
P22314
Q562R1
P11217
P62891
P81605-ZP16402
Q8TF72
P35030
P31025
Q99714
Q9BVS4
O15234
Intensity M R16_+_Intensity L R16
Ratio M/L Normalized R16

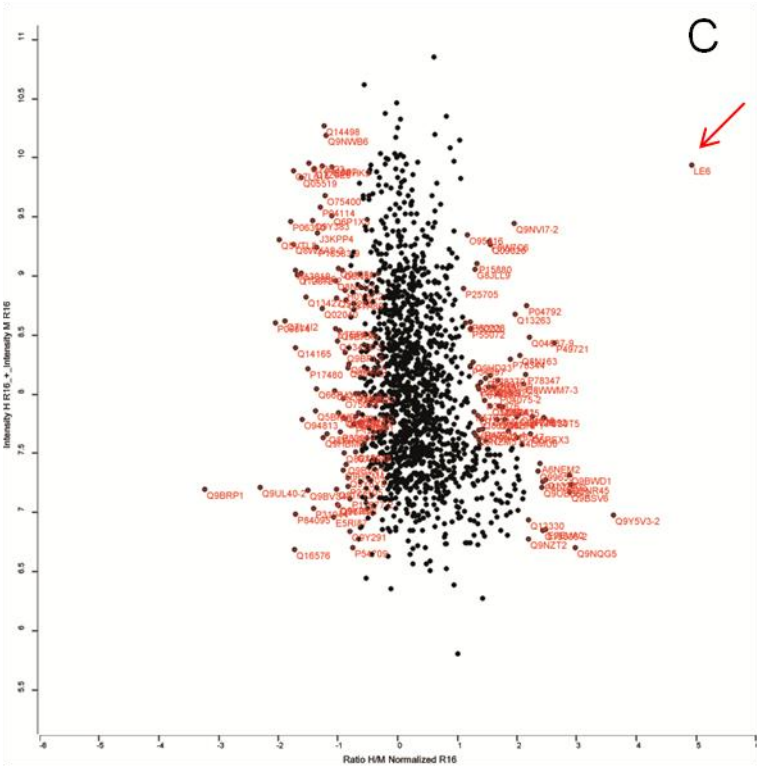

Fig. 30 Data analysis scatter plot of possible interaction partners. Peptide transformed intensities (Log_{10}) were plotted against SILAC ratios (Log_2) of protein groups normalized to their respective protein. Significant outliers are located on the left and right sides of the main distribution. The plots show protein abundance changes between CMV and LE6 (H/L) in A, CMV and SE6 (M/L) in B and LE6 and SE6 (H/M) in C.

In Fig. 30-A, where the proteins identified in LE6 are compared to the ones found in the empty vector pull down, it was possible to distinguish the typical bell-shaped distribution. In this graph, outliers, corresponding to highly significant SILAC ratios, surrounded the main population of unspecific binders. Since putative interaction partners are proteins with high ratios and high intensities, the dots in the upper right corner were representative of the proteins that mainly interact with LE6 whereas proteins on the left were enriched in the empty vector pull down.

The plot in Fig. 30-B show the distribution of the proteins found in the SE6 pull down compared to the empty vector. No proteins were detected in the upper right corner, enough distant from the distribution of nonspecific binding proteins, meaning that no possible binding candidates were identified. SE6 was also not significantly distant from the distribution, leading to the conclusion that its expression was not high enough.

LE6 and SE6 CoIP were compared as shown in Fig. 30-C. Since SE6 pull down did not correctly work, it was expected that no significant outliers could be found in this plot, where only LE6 was shown to be significantly distant from the main distribution.

The list of 2148 putative interaction proteins was analyzed. Only the proteins with a p-value ≤ 0.05 were taken into consideration and were sorted in descending order according to their intensities.

Although the western blot of SE6 did not show a high expression level (Fig. 29 and 30-B), an analysis was performed however to identify proteins involved in relevant pathways. As expected, no interesting proteins were detected. On the other hand, LE6 analysis yielded a selection of 60 proteins (Supplementary results, Fig. S7) and an interesting relation was found among some of them. Five proteins were selected (Table 5) as they all are part of the NuRD complex and therefore thought to be relevant for an oncoprotein.

Table 5 Relevant proteins detected in the first LE6 SILAC experiment. In the table are shown the intensities, the ratios, the p-values, the protein IDs (Uniprot) and the protein names of proteins detected in the first LE6 experiment that are linked to the NuRD complex. Proteins are sorted by descending intensity.

Intensity H+L	Ratio H/L	p value H/L	Protein IDs	Protein Names
8,729885	1,696261	0,001	Q09028	Chromatin assembly factor 1 subunit C
7,731814	1,598079	0,010	Q13547	Histone deacetylase 1; Histone deacetylase 2
7,698066	1,591201	0,010	F6S0T5	BRAF35-HDAC complex protein BHC110; Lysine-specific histone demethylase 1A
7,040725	2,022368	0,018	Q14839-2	ATP-dependent helicase CHD4
6,881898	2,631523	0,002	Q13330	Metastasis-associated protein MTA1; Metastasis-associated protein MTA3

The next step was to validate if LE6 binds to at least one of the detected proteins to assess a possible involvement of LE6 in the recruitment of the NuRD complex. Since KDM1A (Uniprot ID F6S0T5) was identified also in the label free approach, although not significant, this was the first protein investigated. First, the membrane of the western blot performed to determine the validity of the CoIP before processing the samples was re-probed with an anti-KDM1A antibody (Fig. 31, this figure was previously shown as Fig. 29).

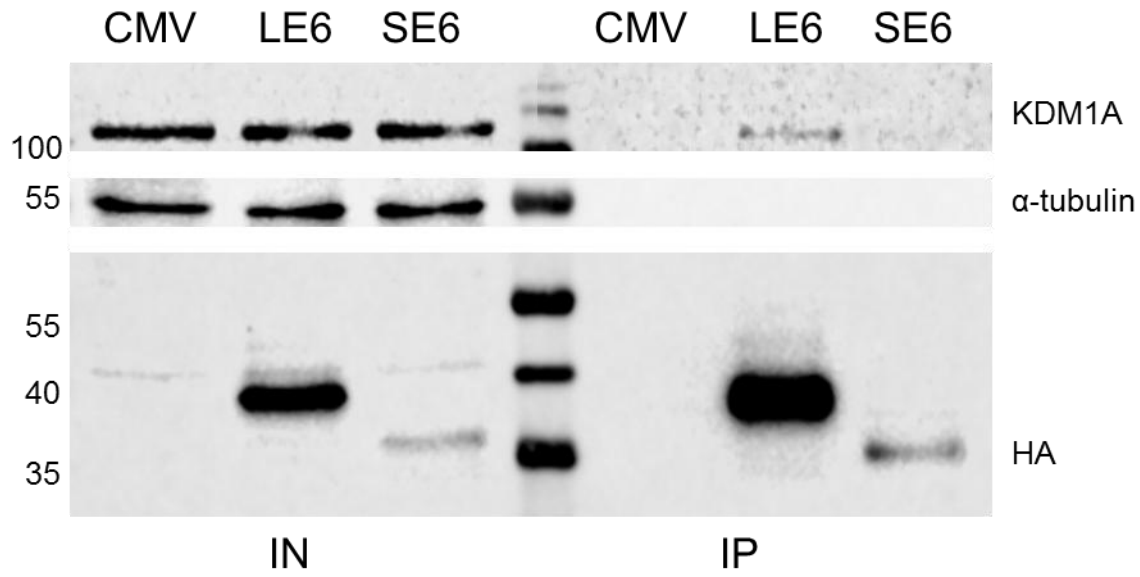

Fig. 31 CoIP of Flag_linker_HA tagged CRPV E6 proteins. Figure previously shown as Fig. 29. CRPV LE6 and SE6, as well as the empty vector (CMV), were transiently expressed in C33a cells. The western blot shows the specific band for LE6 (~40 kDa) and SE6 (~35 kDa) using an anti-HA antibody (lower panel). An HA signal was detected for all the proteins (lower panel) in both inputs (IN) and immunoprecipitates (IP) at the expected sizes. On the left, equal amounts of IN, representing an aliquot of the cell extract from transfected cells before the CoIP, and on the right are shown the IP, 1/10 of the samples resulting from the CoIP. Samples were analyzed for the presence of a reference protein using an anti-α-tubulin antibody (middle panel) and for the pull down of KDM1A (upper panel). Molecular weights are shown in kDa on the left.

As shown by the western blot, a band, although weak, was detected in the immunoprecipitate of LE6 and this validated the SILAC result concerning KDM1A.

To verify the reproducibility of LE6 interaction with KDM1A, additional CoIP experiments were performed but the interaction could not be confirmed (Supplementary results, Fig. S8).

This way, it was possible to show that there is no evident interaction between LE6 and KDM1A, although a band for KDM1A was visible in the immunoprecipitate of the SILAC samples (Fig. 31). LE6 binding to HDAC1 and HDAC2 was also evaluated, by repeating the CoIP, but no bands were detected (Supplementary results, Fig. S9).

The SILAC experiment was repeated twice, inverting the media in which cells were grown, to verify technical and biological reproducibility as shown in Table 6.

Table 6. **Culture conditions for the two SILAC experiments.** The table shows how cells were labeled in each experiment where Heavy (H), Medium (M) and Light (L) represent the three different media.

	CMV	CRPVLE6	CRPVSE6
1st SILAC	L	H	M
2nd SILAC	H	M	L

To highlight the relevant common proteins between the first and the second SILAC experiment, they were correlated and plotted as shown in Fig. 32.

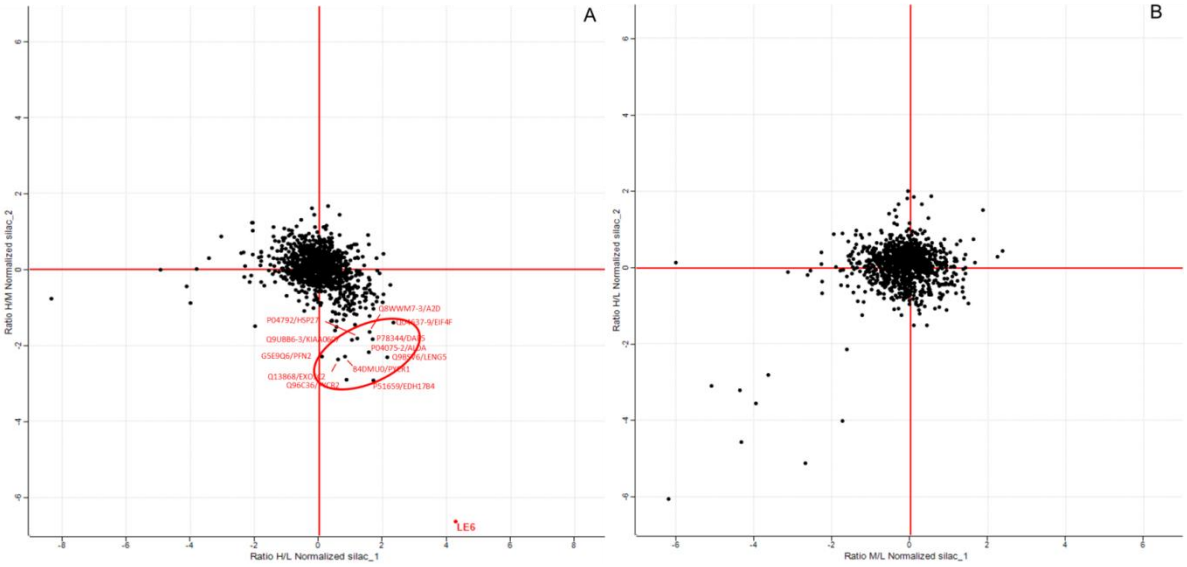

Fig. 32 Scatter plot showing correlation with inverted SILAC labels. Forward SILAC ratios (Log_2) of protein groups normalized to their respective protein were plotted against their reverse ratios. Specific binders of LE6 and SE6 are found in the right lower quadrant of each plot whereas surrounding the center of the axes are the unspecific binders. A. LE6 SILAC ratios inverted. B. SE6 SILAC ratios inverted.

The correlation analysis (Fig. 32-A) for LE6 showed that its pull down was highly reproducible, whereas this was not the case for the one of SE6 (Fig. 32-B). This is probably due to the low level of its expression (Fig. 29).

As shown in Fig. 32-A, LE6 had a high ratio, statistically distant from the distribution, which is expected from the exogenous expression of a bait protein. Moreover, statistically significant specific binders of LE6 were identified in the lower right quadrant because ratios were calculated in Log_2 and specific binding proteins showed positive ratios in the first experiment and negative ratios in the second one.

On the other hand, it was not possible to identify specific binders of SE6 as shown in Fig. 32-B where SE6 and significant proteins in the lower right quadrant were not enough distant from the distribution of nonspecific binding proteins in the center of the axes. Only in the lower left quadrant a small number of proteins were identified but they were most likely contaminants. Moreover, the intensity for the SE6 protein was the same in the CMV- and SE6-transfected cells leading to a non-significant value. Therefore, it was assumed that either the transfection or the pull down did not properly work for SE6 in both experiments.

From each experiment a list of possible proteins was determined and reproducibility was verified taking into account all the common hits between the two experiments (304) (Supplementary results, Fig. S10), leading to 19% overlap of all the possible candidates (Fig. 33).

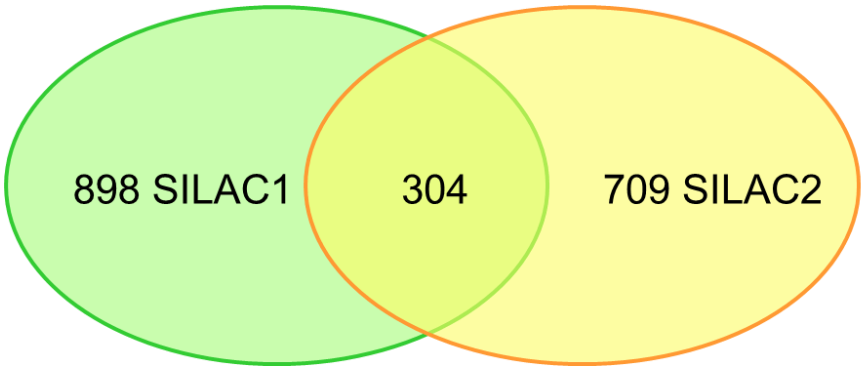

Fig. 33 Common hits between the two experiments. The list of possible candidates of the first SILAC (green) and the second SILAC (yellow) were overlapped and the common candidates were 304, shown in the intersection.

Proteins were sorted according to their ratios and p-values. Only proteins with a p-value < 0.05 and a significant ratio were analyzed and compared between the two experiments and a list of 17 possible interacting proteins is showed in Table 7.

Table 7. List of the best LE6 interacting proteins. Proteins sorted by high ratio and p-value < 0.05 in both SILAC experiments. Ratio H/L refers to the first experiment and Ratio H/M to the second. Protein IDs represent the Uniprot identification numbers.

Ratio H/L (SILAC 1)	Ratio H/M (SILAC 2)	p-value SILAC 1	p-value SILAC 2	Protein IDs	Protein Names
4,274709	-6,63279	4,92E-18	1,10E-101	LE6	
2,33674	-1,39665	1,87E-06	1,62E-03	Q04637-9	Eukaryotic translation initiation factor 4 gamma 1
2,024213	-0,6487561	2,24E-05	3,27E-02	Q9NVI7-2	ATPase family AAA domain-containing protein 3A
1,835358	-0,7399261	1,77E-04	2,95E-02	Q13263	KRAB-associated protein 1
1,468583	-0,8122322	2,64E-03	8,12E-03	O95816	BAG family molecular chaperone regulator 2
1,708894	-2,919424	5,48E-03	4,13E-07	P51659	17-beta-hydroxysteroid dehydrogenase 4
1,682933	-1,840836	6,30E-03	4,16E-05	P78344	Death-associated protein 5
1,584289	-1,645616	1,05E-02	2,31E-04	Q8WWM7-3	Ataxin-2 domain protein
1,574634	-2,18554	1,10E-02	1,86E-05	P04075-2	Fructose-bisphosphate aldolase A
1,22002	-1,811422	1,13E-02	5,44E-05	P04792	28 kDa heat shock protein
2,151794	-2,312796	1,13E-02	6,56E-05	Q9BSV6	Leukocyte receptor cluster member 5
1,471604	-1,013917	1,26E-02	1,95E-02	O00411	DNA-directed RNA polymerase, mitochondrial
1,182184	-0,7010133	1,52E-02	2,15E-02	P62280	40S ribosomal protein S11
1,451752	-0,8359862	1,99E-02	6,50E-03	Q8N163	Deleted in breast cancer gene 1 protein
1,101112	-1,056311	2,37E-02	6,50E-04	Q92616	GCN1-like protein 1
1,054223	-0,896818	3,02E-02	3,69E-02	Q9NX02	NACHT, LRR and PYD domains-containing protein 2
1,296663	-0,9981546	3,96E-02	2,13E-02	Q7KZF4	100 kDa coactivator

As shown in Table 7, all the proteins had high (positive or negative) ratios and the p-values were much lower than the 0.05 threshold, meaning that these proteins were significantly distant from the distribution of nonspecific binders and also that the probability that they are real binding proteins is very high. Moreover, as a control, LE6 was the protein with highest and lowest p-values, a feature expected from a bait protein.

Although both SILAC experiments with SE6 as bait protein did not show any reproducibility and no good expression of SE6 itself (Fig. 15, Fig. 17), a comparison was carried out. However, the analysis did not yield any meaningful result since it was not possible to identify proteins with high enough ratios and statistically significant distant from the group of proteins that represent unspecific binders.

5.1.8 Comparing SILAC with label free quantification

Finally, SILAC results were compared to the results obtained from the label free proteome analysis to determine whether relevant proteins were common to the two approaches. Only LE6 was taken into account since 38E6 was not analyzed and SE6 was not well expressed in the SILAC approach.

Comparing the results obtained from the label free and the SILAC quantifications, it is possible to identify 62 proteins (Supplementary results, Fig. S11), that were common to the two approaches.

5.1.8.1 Validation of 17-Beta-Hydroxysteroid Dehydrogenase 4 (17βHSD4) as a new promising E6 interaction partner

Since SILAC is quantitative and more standardized than the label free quantification, the results obtained with SILAC were considered more reliable than those obtained with the label free quantification. The results obtained with the two approaches were compared and 62 proteins were identified in both (Supplementary results, Fig. S11).

The final aim was to find at least one of the best LE6 interacting proteins identified by SILAC also in the label free analysis. For this purpose, protein families were analyzed in detail and the analysis was not restricted to single isoforms, since, as previously explained, large protein families rarely yield many unique peptides, which affects the analysis. Many isoforms of the 17-Beta-Hydroxysteroid Dehydrogenase protein family were present in both approaches and therefore, based on already published studies, it was decided to investigate further the protein 17-Beta-Hydroxysteroid Dehydrogenase isoform 4 (17βHSD4, Uniprot ID P51659). It is a bifunctional protein involved in the peroxisomal beta-oxidation pathway for fatty acids but it was shown that it stimulates the growth of human keratinocytes by inducing cyclin D2 [179] and inhibits oxidative stress-induced apoptosis in keratinocytes by promoting Bcl-2 expression [180].

Additional experiments were performed to determine whether the interaction between LE6 and 17βHSD4 can be validated.

First, a western blot was carried out to verify that 17βHSD4 interacts with LE6 (Fig. 34, shown also in the supplementary data as Fig. S8).

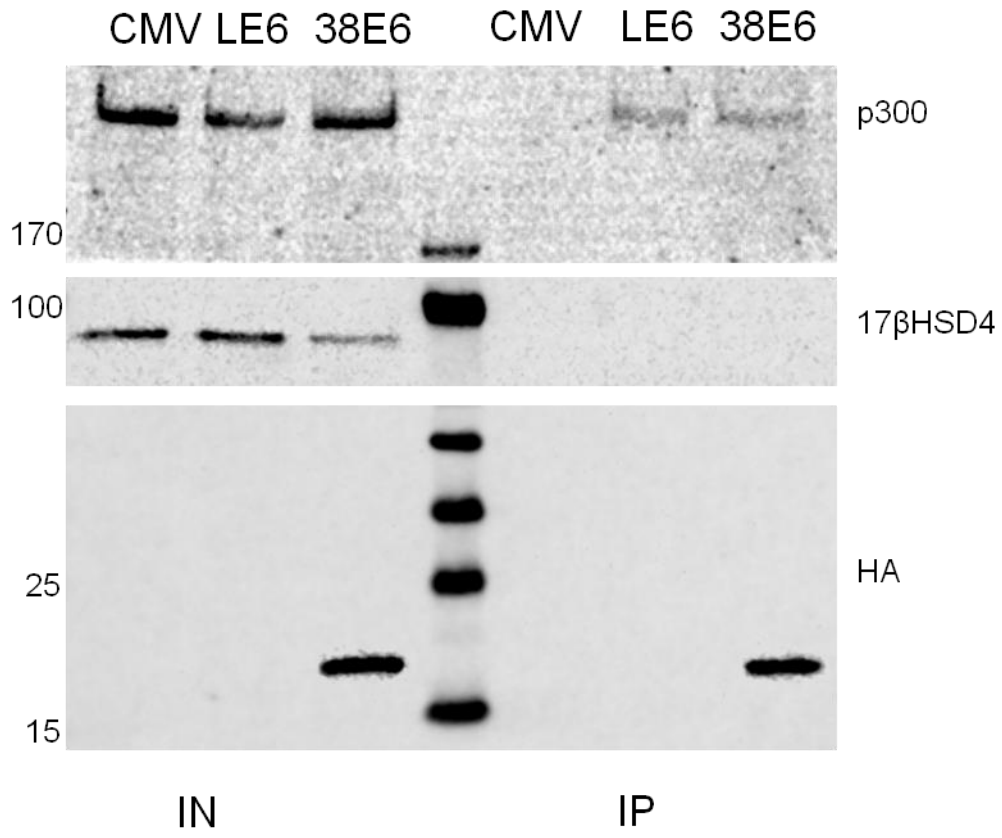

Fig. 34 Western blot to validate 17βHSD4 interaction with LE6. Figure shown also in the supplementary data as Fig. S8. HA-tagged LE6 and 38E6 were tested for the binding to p300 (upper panel, IP) and MAML1 (middle upper panel, IP), that were used as positive controls for the pull down. KDM1A was not pulled down by neither LE6 nor 38E6 (central panel), as shown before. Specific HA signals were detected for 38E6 (lower panel, 38E6 ~19 kDa) in both inputs (IN) and immunoprecipitates (IP) with the exception of LE6 (~40 kDa) that was not detectable. It was not possible to observe an interaction with 17βHSD4 (middle lower panel). CMV: pCMV-N-Flag_Linker_HA empty vector; LE6: pCMV-N-Flag_Linker_HA-CRPVLE6; 38E6: pCMV-N-Flag_Linker_HA-HPV38E6. Molecular sizes are shown in kDa on the left.

As shown by the western blot, the interaction between LE6 and 17βHSD4 could not be validated, probably due to the fact that LE6 was not expressed, as observed in the western blot. However, further investigations were performed.

An immunofluorescence assay, where C33a cells were transfected with the empty vector (CMV) or CRPVLE6 (LE6), was used to check whether the two proteins co-localize, which is a hint of their interaction (Fig. 35).

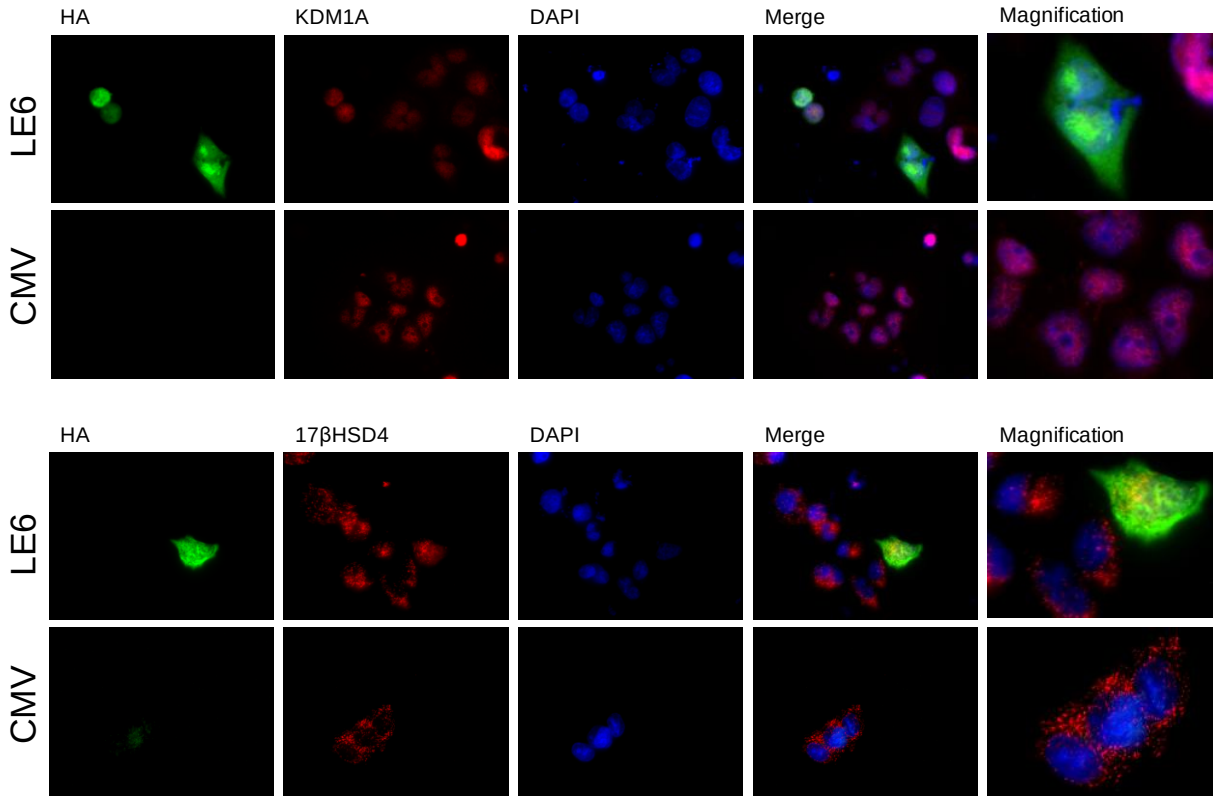

Fig. 35 Immunofluorescence showing localization of KDM1A and 17βHSD4. C33a cells were stained with an anti-HA antibody (green) and an anti-KDM1A or 17βHSD4 antibody (red). Cell nuclei were stained with DAPI (blue). Merge shows the overlays of the different stainings.

Immunofluorescence analysis showed a visible co-localization of LE6 and 17βHSD4.

Additionally, the co-localization of LE6 and KDM1A was investigated to confirm the results previously obtained by the western blot shown in Fig. 31. Similar to the prior results, no co-localization was observed (Fig. 35). CMV-transfected cells were used as a control of KDM1A or 17βHSD4 localization in the absence of LE6.

To investigate whether this co-localization corresponded to a direct interaction, a proximity ligation (PLA) assay was performed with the same antibodies (17βHSD4 and KDM1A) used for the co-localization analysis. C33a cells were transfected with CMV and LE6, and 38E6 was used as an additional control (Fig. 36 and 37).

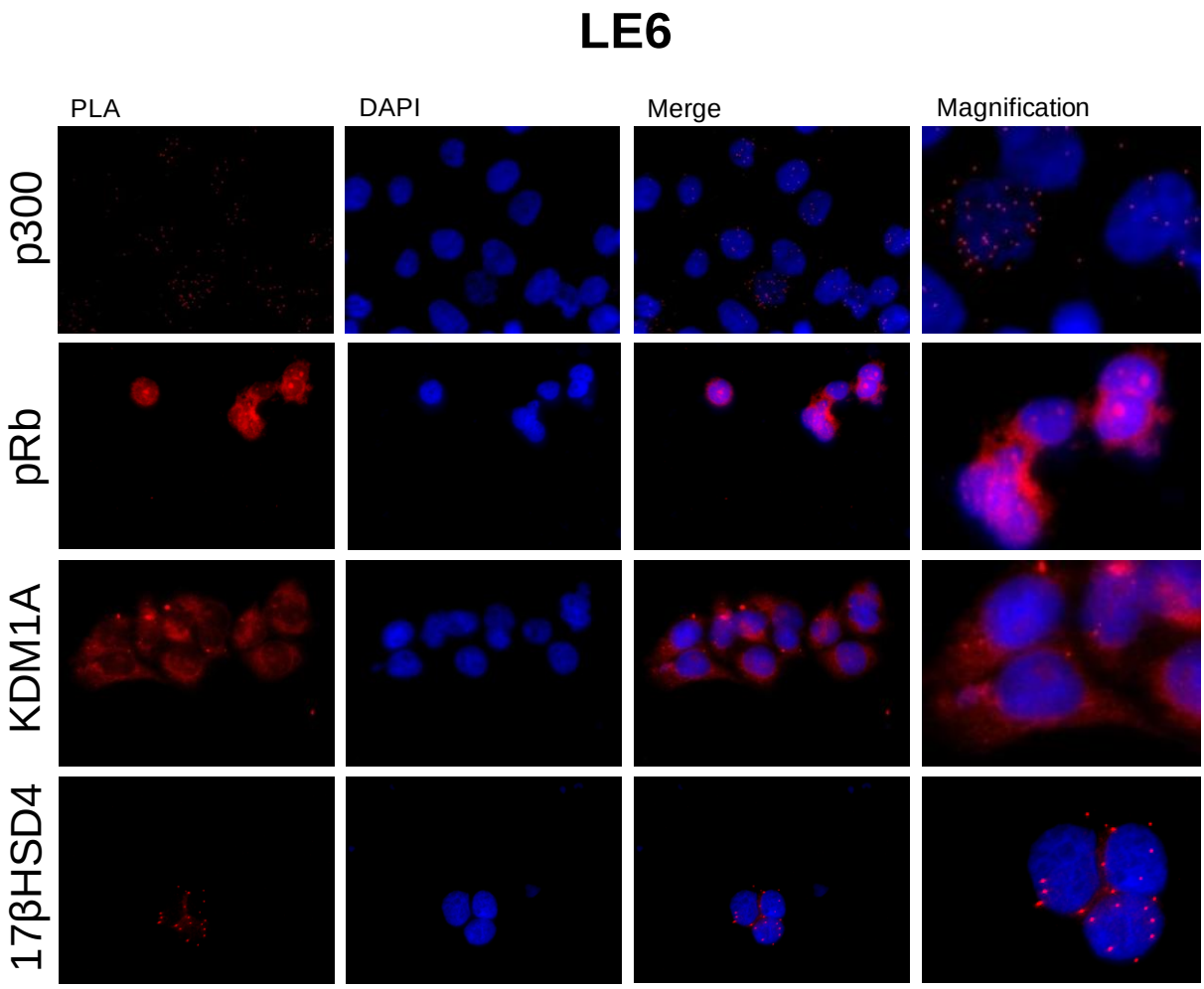

Fig. 36 LE6 interaction with KDM1A and 17βHSD4 via PLA. C33a cells were incubated with an anti-HA antibody and an anti-p300, pRb, KDM1A, 17βHSD4 antibody. Cell nuclei were stained with DAPI (blue). Red PLA dots represent single protein-protein interactions. Merge shows the overlay of the PLA and DAPI staining. The right column of images shows magnifications of the merged images.

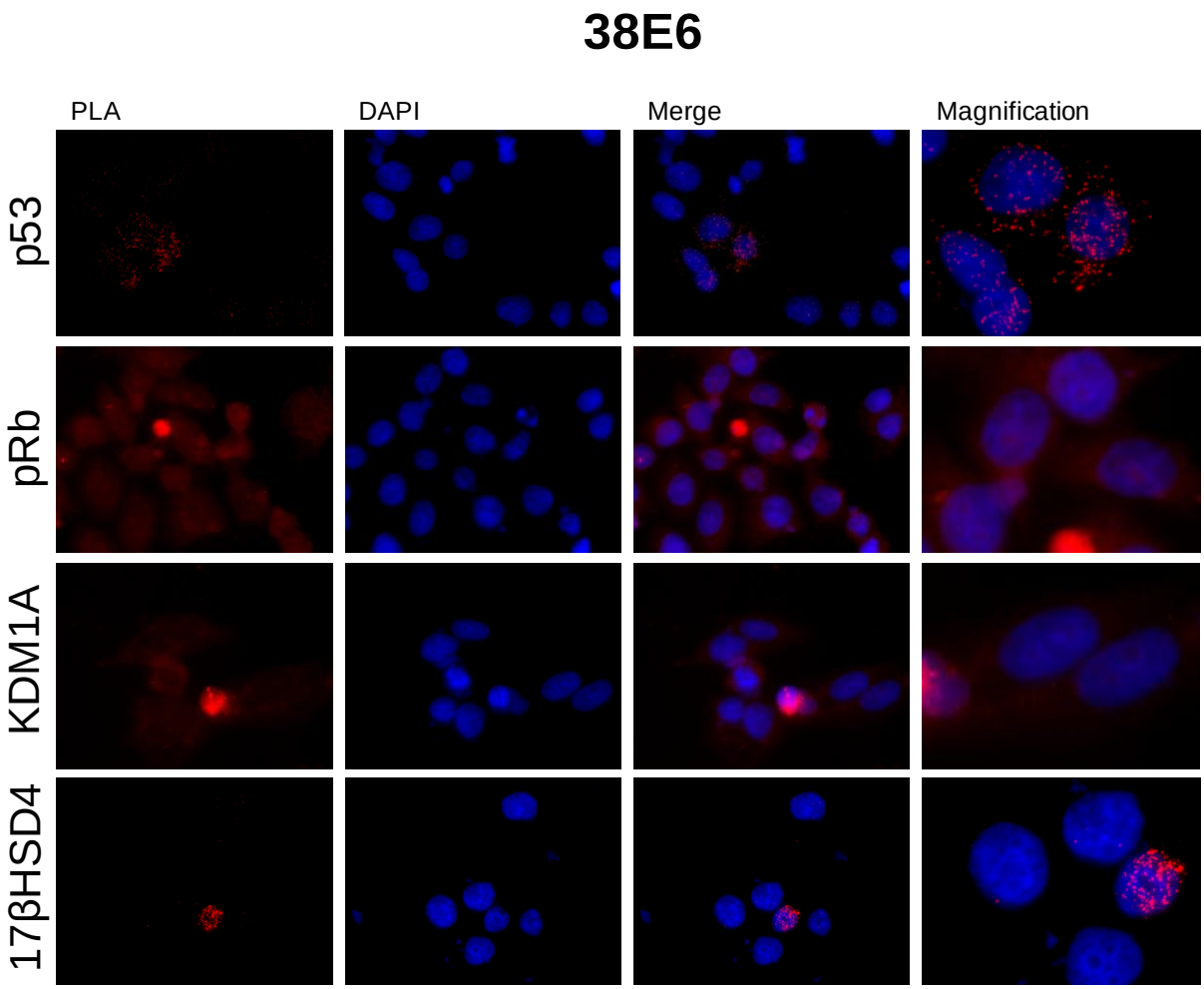

Fig. 37 38E6 interaction with KDM1A and 17βHSD4 via PLA. C33a cells were incubated with an anti-HA antibody and an anti-p53, pRb, KDM1A, 17βHSD4 antibody. Cell nuclei were stained with DAPI (blue). Red PLA dots represent single protein-protein interactions. Merge shows the overlay of the PLA and DAPI staining. The right column of images shows magnifications of the merged images.

In the immunofluorescence analysis (Fig. 35) p300 and pRb were used as positive and negative controls, respectively, for PLA signals, because it is known that LE6 interacts with p300 while it does not interact with pRb. As expected, there was a strong interaction between LE6 and p300, whereas no PLA spots were detected when the interaction between LE6 and pRb was investigated.

Concerning KDM1A, the results confirmed that there is no direct interaction with LE6, whereas 17βHSD4 showed, that it not only localized in the same cellular region as LE6 (immunofluorescence Fig. 35), but also to interact with LE6 (PLA Fig. 36), although to a lesser extent than p300.

A similar result was obtained in the case of 38E6 (Fig. 37). p53, a known interaction partner of 38E6, showed a strong interaction while no interaction with pRb was detected. KDM1A, as

well, did not show a clear interaction with 38E6, while the interaction between 38E6 and 17βHSD4 was confirmed.

In conclusion, the interaction between LE6, 38E6 and 17βHSD4 was confirmed by 3 different methods and in three independent experiments, pointing towards a role of 17βHSD4 in collaborating with cutaneous E6.

5.2 HPV31 intraviral interactome

The HR-HPV31, one of the causative agents linked to cervical cancer, was widely studied concerning viral-cellular protein interactions. This work aimed to perform a complete screening of the viral proteins to investigate how they interact with each other. A FACS-FRET approach [157] was used to elucidate the intraviral network.

5.2.1 Expression of Fluorescently labeled-proteins in the HPV-negative cell line C33a

To explore HPV31 viral-viral protein interactions, all the viral genes (E1, E2, E8^E2C, E1^E4, E5, E6, E7, L1 and L2, Fig. 38) were cloned into vectors containing either the yellow fluorescent protein (YFP) (peYFP-C1, Clontech) or the blue fluorescent protein (BFP) (pmTagBFP-C1, Clontech) tag.

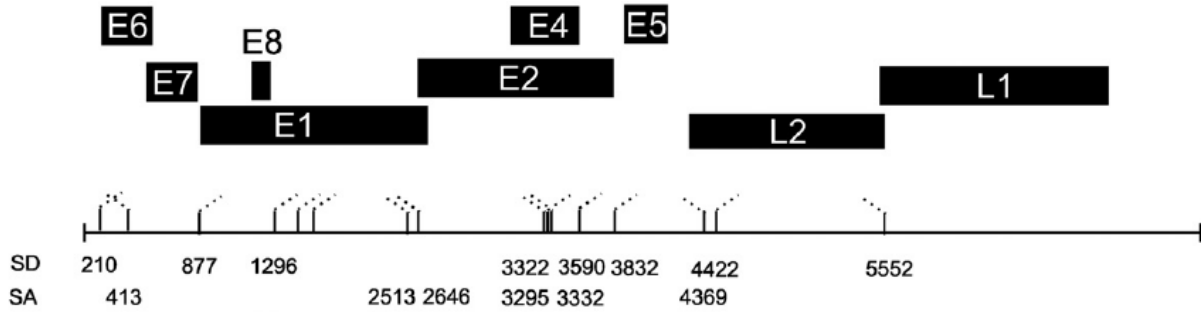

Fig. 38 Schematic overview of HPV31 genome. HPV31 linearized genome is represented on top. Below splice donor (SD) and splice acceptor (SA) sites are identified by nucleotide positions and dashed lines. Figure adapted from [181].

First, it was evaluated whether the tag had to be expressed N- or C-terminally to avoid unwanted changes in protein expression, localization and functionality. Previous experience in the lab showed that, in particular HPV 31 E1, E2 and E8^E2C were expressed and functional when the tag was located at the N-terminus. The remaining genes were cloned in both ways and then tested. A summary of the tag position is shown in Table 8.

Table 8. Fluorescent tag position for each viral protein.

N-Term YFP and BFP	E1	E2	E8^E2C	E1^E4	E5	E6	E7
C-Term YFP and BFP	L1	L2					

Except for the capsid proteins, all the other proteins were used with the N-terminal tag. Moreover, E2, L1 and L2 were codon-optimized (E2co, L1co, L2co) and for E6 a splicing mutant was created altering the splicing donor site at position 105 in the E6 ORF. The mutation led to a substitution from T to G, a silent mutation not affecting the protein sequence. This was used to avoid the synthesis of the two versions E6 and E6*, and, instead ensured the expression of full length E6.

C33a cells were transiently transfected with constructs containing the YFP-tagged viral gene sequences assuming that the BFP tag affected them in the same way, and a western blot was carried out to evaluate their expression.

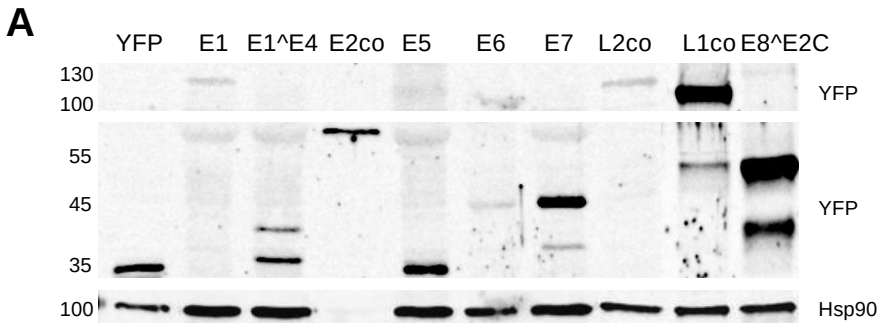

YFP	27 kDa
E1	98 kDa
E1^E4	37 kDa
E2co	77 kDa
E5	36,5 kDa
E6sm	44,7 kDa
E7	38 kDa
L2co	77 kDa
L1co	83,4 kDa
E8^E2C	47 kDa

Fig. 39 Western blot showing YFP tagged-HPV31 proteins in transiently transfected C33a cells. (A) In the lower panel, lysates were probed with an anti-Hsp90 antibody and in the middle and upper panels an anti-GFP antibody was used to detect the YFP-tagged proteins. On the left, molecular weights are indicated in kDa. (B) Expected protein molecular weights expressed in kDa. co: codon-optimized.

As shown by the western blot, all the proteins were expressed. No band for Hsp90 was present in the E2co lysate, since a cellular fractionation was performed to enhance E2 protein amount and only the nuclear fraction not expressing Hsp90 was analyzed. All the other proteins were shown to be expressed in different amounts (Fig. 39-A), but a specific band around the expected molecular weight was detected for each one (Fig. 39-B).

The next step was to test protein localization in order to verify that the tag did not affect protein localization. For this purpose immunofluorescence was performed in transiently transfected C33a cells (Fig. 40).

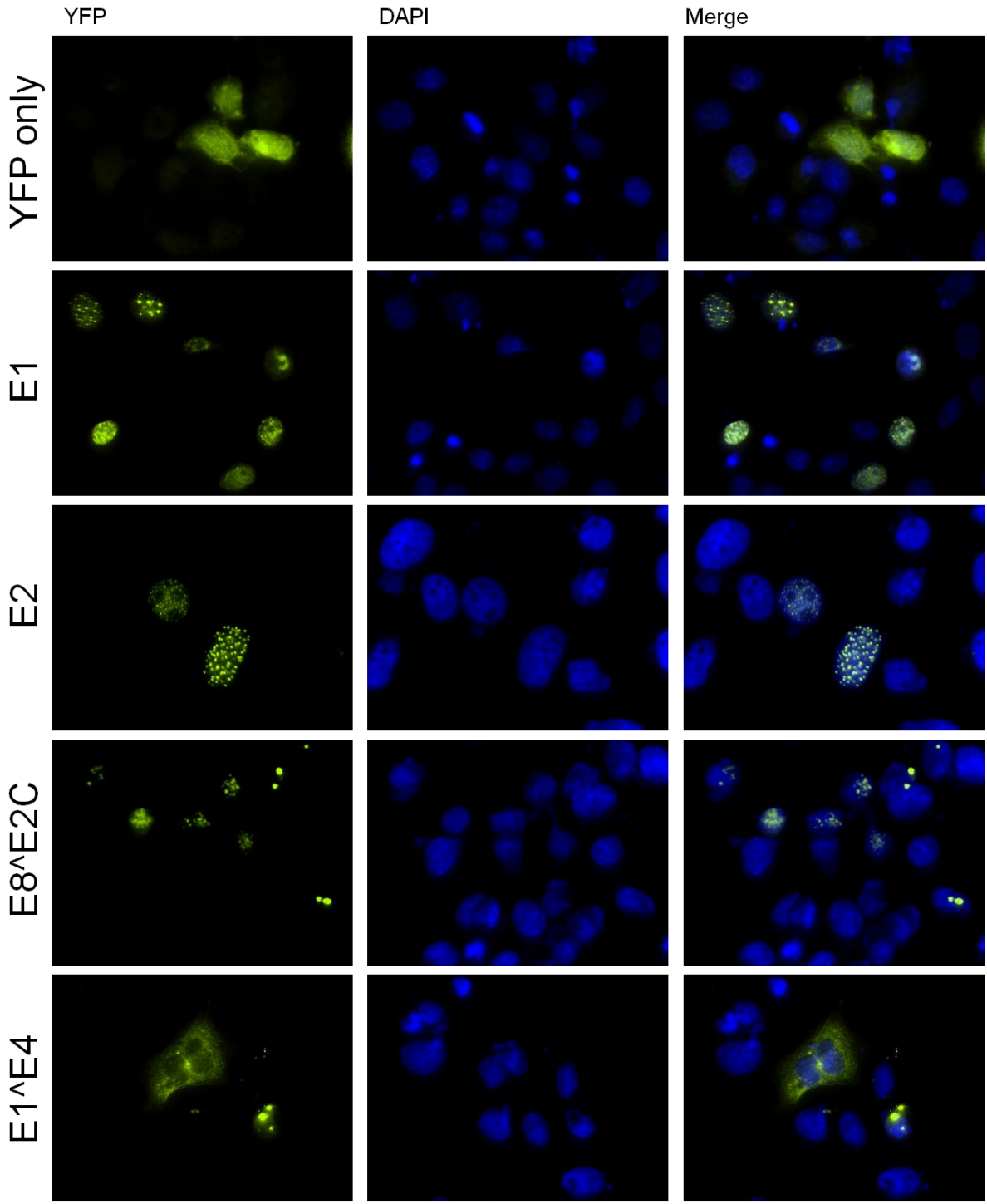

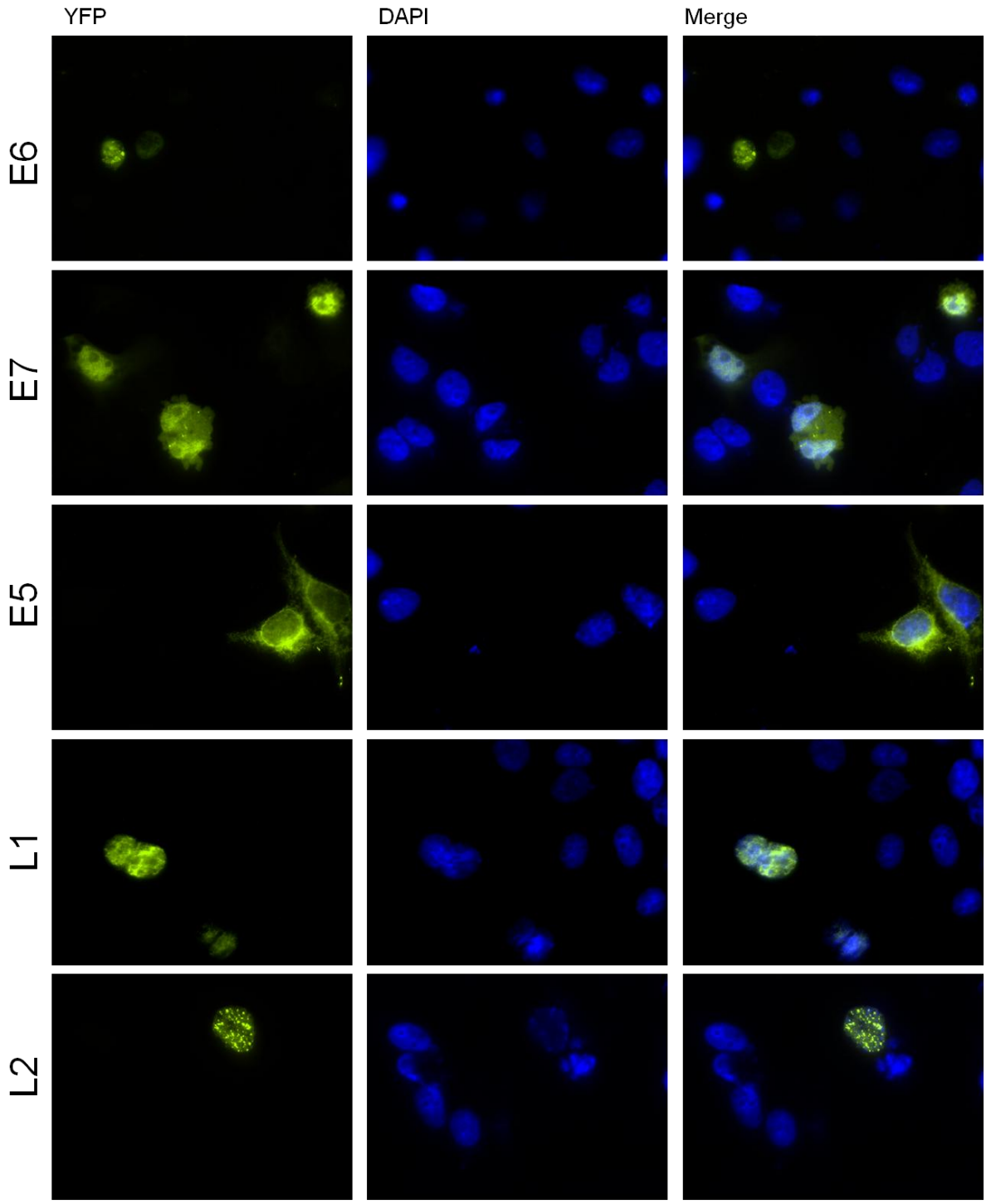

Fig. 40 Immunofluorescence showing HPV31 YFP-tagged proteins localization. C33a cells were transiently transfected with YFP- tagged proteins. On the left, the YFP (green) signal, in the middle cell nuclei stained with DAPI (blue) and on the right the overlay between YFP and the nuclei signal (Merge).

Table 9. Expected and observed HPV31 protein localization.

Proteins	Expected localization	Observed localization
E1	Nuclear (Sakakibara et al. 2011)	Nuclear
E2	Nuclear (Sakakibara et al. 2011)	Nuclear
E8^E2C	Nuclear (Stubenrauch et al. 2007)	Nuclear
E1^E4	Keratin-association (Doorbar 2013)	Cytoplasmic
E6	Nuclear and cytoplasmic (Zanier et al. 2012)	Nuclear
E7	Nuclear and cytoplasmic (Todorovic et al. 2011)	Nuclear and cytoplasmic
E5	ER, Golgi, nuclear envelope (DiMaio & Petti 2013)	Cytoplasmic
L1	Nuclear (Zhou et al. 1991)	Nuclear
L2	Nuclear (Becker et al. 2004)	Nuclear

As shown in Fig. 40 and summarized in Table 9, in transiently transfected C33a cells HPV31 proteins did not show any altered localization due to the tag. All the previously reported cellular localizations listed in the third column of Table 9 were confirmed.

5.2.2 Fluorescently tagged proteins are functional

To characterize the proteins' functionality, different assays were carried out. It was not possible to test each protein since only for some of them enough information about their role and their interactions are available. Hence functionality could only be tested for E1, E2, E8^E2C, E6 and E7.

5.2.2.1 E6 and E7

As discussed above, it is well known that HR-E6 degrades p53 by interacting with the E6AP protein. Furthermore, HR-E7 is known to bind to pRb. Both p53 and pRb are mutated in the C33a cell line, which is why the keratinocyte cell line N/Terts, which contains wild type p53 and pRb, was used to perform a CoIP experiment with YFP-tagged E6 and E7 as baits (Fig. 41).

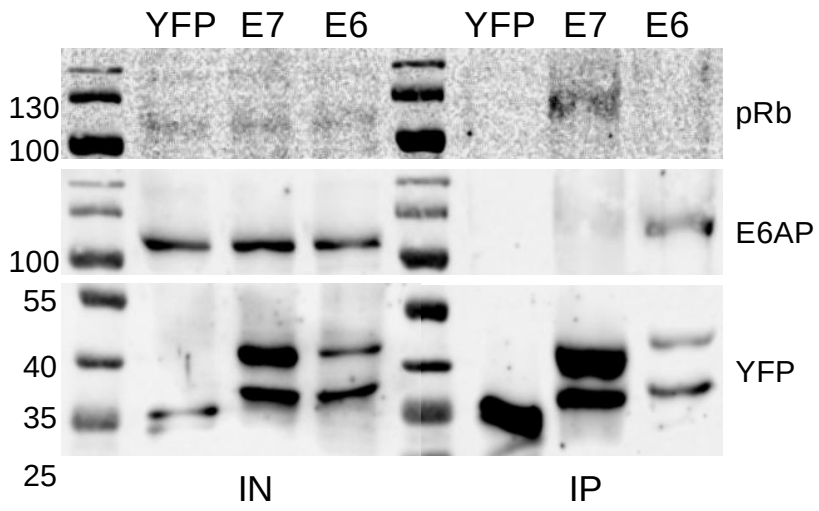

Fig. 41 CoIP showing HPV31 E6 and E7 interactions. YFP-tagged E6 and E7 were tested for the binding to pRb (upper panel, IP) and E6AP (middle panel, IP). An YFP signal was detected for all the samples (lower panel) in both inputs (IN) and immunoprecipitates (IP). Molecular sizes are shown in kDa on the left. YFP: peYFP-C1; E7: peYFP-C1+HPV31E7; E6: peYFP-C1+HPV31E6.

As demonstrated by the western blot, E7 (44 kDa) and E6 (38 kDa) proteins were well expressed, although a single YFP band was present in each sample. The western blot showed that E6 binds E6AP, whereas E7 binds pRb demonstrating that the tag did not interfere with their abilities to interact with other proteins.

5.2.2.2 E1, E2 and E8^E2C

HPV replication is finely regulated by the interplay of the three proteins E1, E2 and E8^E2C. While E1 and E2 contribute to replication and transcriptional activation, E8^E2C was shown to be a negative regulator, mainly by competing with E2 for the DNA binding site in the upstream regulatory region (URR). These functions were analyzed through a reporter assay, in which the viral tagged proteins were co-transfected with a luciferase construct under the control of the HPV31 URR (Fig. 42).

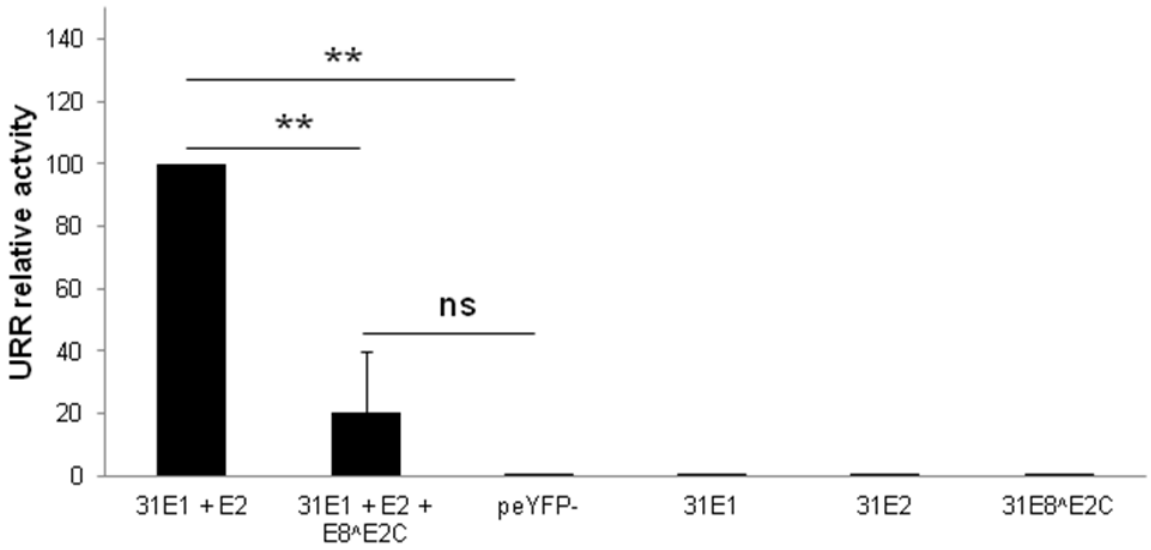

Fig. 42 Luciferase assay showing E1, E2 and E8^E2C modulation of HPV31 URR activity. C33a cells were transfected with 10 ng of the pGL 31URR-luc (HPV31 URR) vector and respectively 100, 10 and 10 ng of the expression vectors encoding for YFPE1, E2 and E8^E2C. Luciferase activity was measured after 48h. The bars represent the average and standard deviation of three independent experiments and luciferase activities are relative to the E1+E2-transfected cells. Gaussia was used as an internal transfection control. Two tailed unpaired Student's t-test:* $p < 0.05$; ** $p < 0.01$; ns: not significant.

As expected, the empty vector (peYFP-) and the single proteins did not activate transcription of the luciferase reporter gene. Conversely, the co-transfection of E1 and E2 led to a strong activation of replication and transcription, whereas when E8^E2C was transfected together with E1 and E2 a statistically significant repression of transcription activity (approximately 80%) was observed. These results indicate that the tag did not affect the proteins' function.

5.2.3 FACS-FRET screening for HPV31 intraviral interactions

After showing that the labeled proteins were expressed, correctly localized and functional, a flow cytometry-based FRET (FACS-FRET) assay was performed to discover all the interactions among HPV31 proteins. To check whether C33a cells were a suitable cell line for FACS-FRET analysis, cells were first transfected with the YFP and BFP empty control vectors either separately or both combined. Additionally, a YFP-BFP control vector was transfected containing a fusion ORF that results in a constitutive FRET signal, since the two fused proteins remain in close proximity, which is the basis for the FACS-FRET methodology. In Fig. 43, the results of this FACS-FRET adjustment experiment are shown.

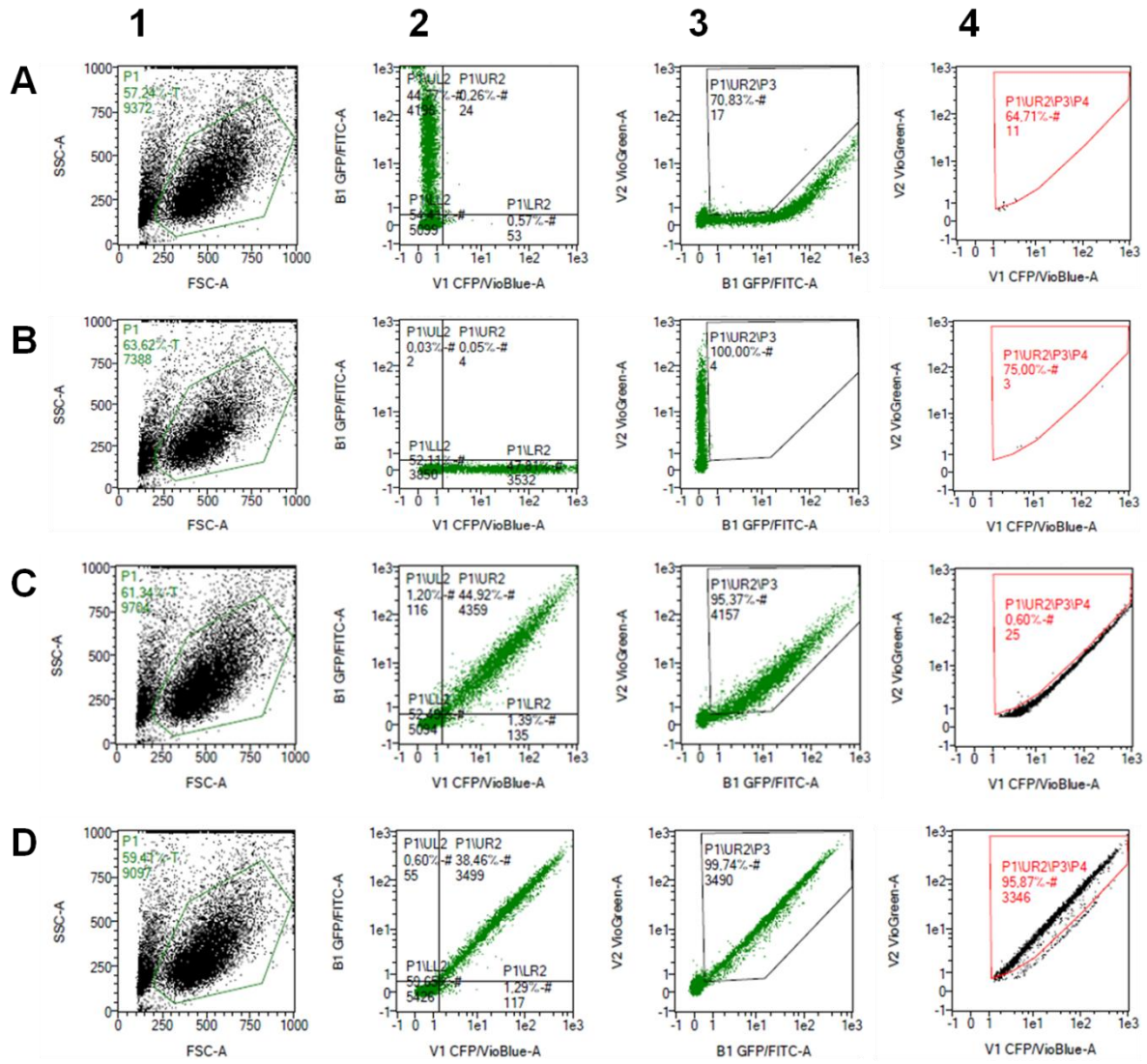

Fig. 43 Adjustment of FACS-FRET settings for C33a. A MACSQuant flow cytometer was used to measure FRET signals in C33a. Cells were transfected with the controls: YFP (A), BFP (B), YFP+BFP (C) and YFP-BFP (fusion construct giving a FRET positive signal, D). (1) FSC/SCC: along the Y-axis there is the FSC (Forward SCatter), a measure of the frontal light scattered from the cells (cell size); along the X-axis there is the SCC (Side SCatter) that measures the amount of laser beam that bounces off of particulates inside of the cell (cell complexity/granularity). (2) P1: identifies all the living cells and 4 different subpopulations: Lower Left corner (LL2, double negative); Lower Right corner (LR2, BFP positive cells); Upper Left corner (UL2, YFP positive cells); Upper Right corner (UR2, double-positive cells). (3) P3 (P1/UR2): an enlargement of the P1/UR2 where double-positive cells are gated and false positive FRET signals resulting from YFP excitation by the 405 nm laser are excluded. (4) P4: FRET-positive cells.

The four transfections (YFP, BFP, YFP+BFP, YFP-BFP) were used to adjust the gates in order to select only the FRET-positive cells, among all the double positive cells.

To identify only FRET-positive cells, the gating took into account the false positive signals deriving from the excitation of the YFP (with the 405 nm laser) and combine it with the

negative control (cells co-expressing YFP+BFP) and the positive control (cells expressing a , YFP-BFP fusion construct).

The remaining cells are evaluated for FRET signals by adjusting the gate to include cells, which are co-transfected with BFP and YFP and were FRET-negative or cells expressing the YFP-BFP fusion protein representing a FRET-positive cell population (switch into the gate in Fig. 43-4D).

Once assessed that C33a are suitable for FACS-FRET measurements, each fluorophore-tagged viral protein was tested for an interaction with itself and with each other. Two combinations were used, where both the YFP and the BFP versions of the proteins took part. Gates were adjusted according to the positive control (YFP-BFP fusion construct) were FRET-positive cells were more than 95% and to the negative control (YFP and BFP vectors co-transfection), in which cells that gave a FRET signal were less than 1%. A minimum of 500 cells in the double positive cells gate and a FRET signal of at least 10% as a cut off were also taken into consideration.

A large screening was performed using all the possible combinations to investigate previously described interactions (related not only to HPV31 but also to 16 and 18) and to discover new intraviral interactions (Fig. 44).

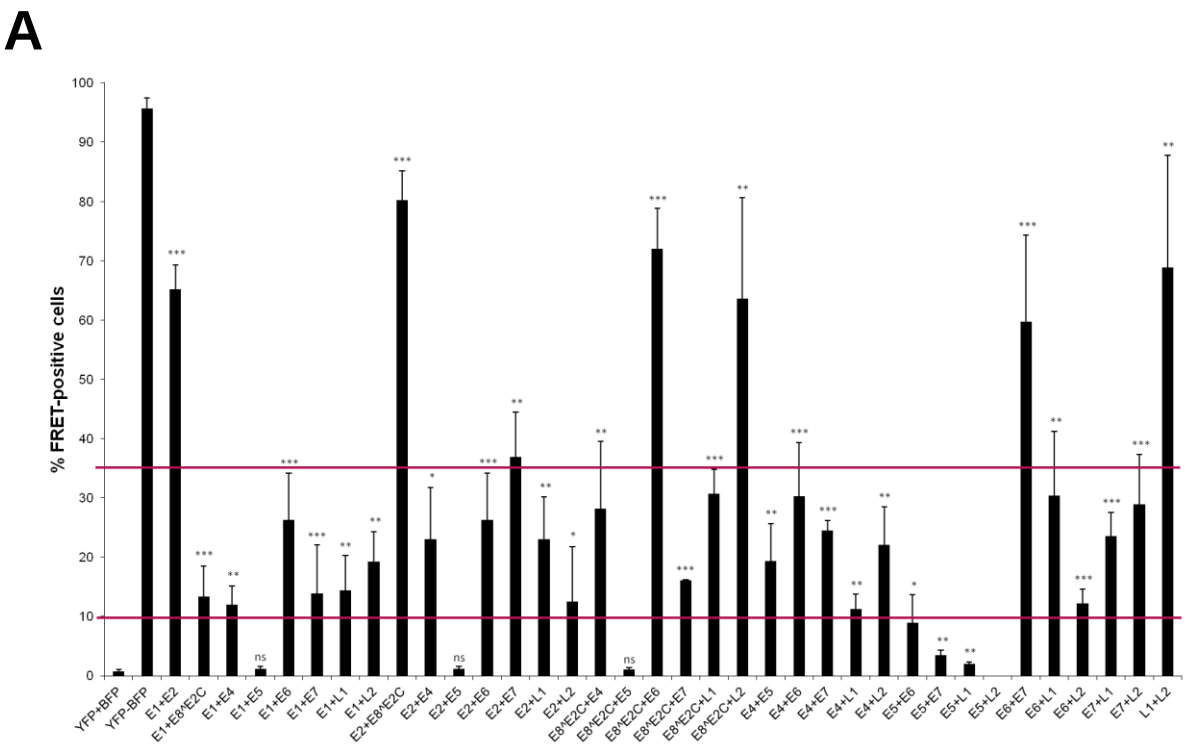

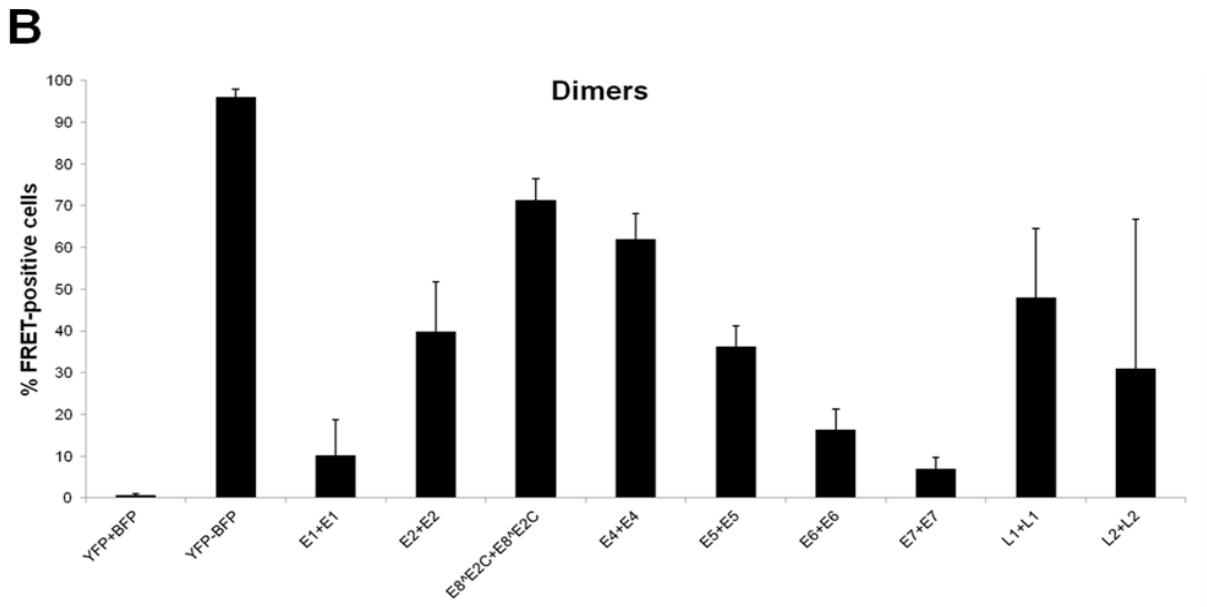

Fig. 44 FACS-FRET screening in C33a cells. Cells were transfected with YFP- and BFP- tagged proteins for hetero- (A) and homodimerization (B). The Y-axis represents the percentage of FRET-positive cells whereas the X-axis shows the combinations used. Horizontal red lines represent the 10% and 35% FRET signal cuts off. FRET Signals between 10% and 35% identify putative interactions, whereas percentages above 50% indicate strong interactions. The negative control is the co-transfection of YFP and BFP (YFP+BFP) and the positive control is the YFP-BFP fusion construct. Statistical significance was calculated with a two-tailed unpaired Student's *t* test. ns: not significant; * $p<0.05$; ** $p<0.01$; *** $p<0.001$.

As shown by the figure 44, many interactions demonstrated to be strong and statistically significant. To have a better readout of the huge dataset, more detailed analyses where performed.

A table including all the interactions already reported in literature was constructed (Table 10).

Table 10. Summary of HR-HPV published intraviral interactions

E1	[182]							
E2	[183]	[184]						
E8^E2C		[185]	[185]					
E1^E4		[186]		[187]				
E5					[188]			
E6		[189]				[190]		
E7		[191]					[192]	
L1		[193]						[48]
L2		[194]						[195]
	E1	**E2**	**E8^E2C**	**E1^E4**	**E5**	**E6**	**E7**	**L1**	**L2**

To highlight the previously known and the newly discovered protein-protein interactions, the data were presented in a table, taking into account only the statistically significant interactions and visually differentiating those previously described (orange boxes) and the new interactions (green boxes) (Table 11).

Table 11. Summarized results of FRET signals in C33a cells. Green boxes represent new interactions whereas orange boxes show interactions already described in at least one of the HR-HPV types. White boxes white are for FRET mean values below 10% and/or not significant. n: number of independent experiments; Mean: mean value of FRET; SD: standard deviations; Statistical significance (Sign.) was calculated with a two-tailed unpaired Student's *t* test. ns: not significant; * $p<0.05$; ** $p<0.01$; *** $p<0.001$.

	n	3
	Mean	10,26
E1	SD	8,38
	Sign.	ns

	n	4	4
	Mean	65,23	39,91
E2	SD	4,10	11,89
	Sign.	***	***

	n	5	5	5
	Mean	13,39	80,20	71,29
E8^E2C	SD	5,16	4,95	5,21
	Sign.	***	***	***

	n	3	3	4	3
	Mean	12,02	23,08	28,13	62,01
E1^E4	SD	6,50	8,71	11,37	6,09
	Sign.	*	*	**	***

	n	3	3	3	3	4
	Mean	3,46	4,67	1,06	19,33	36,18
E5	SD	3,05	3,26	0,34	6,33	5,04
	Sign.	ns	ns	ns	**	***

	n	4	6	3	4	3	4
	Mean	26,27	24,76	72,04	30,27	2,39	16,34
E6	SD	7,87	12,55	6,77	9,10	1,41	4,90
	Sign.	***	***	***	***	ns	***

	n	9	3	3	3	3	5	4
	Mean	13,91	36,92	21,32	24,48	3,47	59,68	6,92
E7	SD	8,15	7,51	8,27	1,74	0,81	14,60	2,77
	Sign.	***	**	*	***	**	***	**

	n	4	3	3	3	3	3	3	5
	Mean	14,37	22,99	30,72	11,25	2,05	30,43	23,57	48,08
L1	SD	5,91	7,23	4,08	2,50	0,30	10,83	4,03	16,45
	Sign.	**	**	***	**	**	**	***	***

	n	3	5	3	4	0	4	4	3	2
	Mean	19,28	12,57	63,60	22,07		12,25	28,94	68,83	30,95
L2	SD	5,04	9,25	17,04	6,48		2,32	8,36	18,96	35,83
	Sign.	**	*	**	**		***	***	**	ns

E1	**E2**	**E8^E2C**	**E1^E4**	**E5**	**E6**	**E7**	**L1**	**L2**

As shown in Table 11, most of the interactions analyzed were statistically significant (36 out of 45). All the previously reported interactions concerning E2, E8^E8C, E4, E5, E6, L1 and L2, and some of E1 and E7 were confirmed.

As shown by other groups, E2 interacts with all investigated proteins, except E5 and Table 11 shows that strong FRET signals (ranging from 12.57 and 80.20%) confirmed the already published interactions with L2, L1, E1^E4, E6, E7, E1 and E2-E2 dimerization.

For E1, FRET signals were detected for all the proteins investigated, except E5. As expected, FRET signals with E2 had the highest values, confirming a very strong interaction. E1 hexamerization was not confirmed, because the FRET value was below 10% and also non-significant.

For E8^E2C, the strongest signal, following the interaction with E2, was the homodimerization. Unpublished interactions also include E1^E4, E7, L1 and the interactions with L2 and E6.

As shown in Table 11, E1^E4 forms dimers and interacts with E2. E1^E4 is the only viral protein interacting with E5 and unreported interactions with E6, E7 and L1 were also observed.

For E5 all the FRET values were below 5% and/or not significant. The co-transfection of E5 and L2 never reached the 500 cells threshold in the double positive cells' gate, so that the values were automatically excluded from the analysis. Although the cell population analyzed was alive, it seemed that the two proteins could not be expressed at the same time.

For E6, it is known that it forms homodimers and that it interacts with E2, observations that were confirmed in this work. Additionally, new interactions were found (Table 11): E6 interacts with E1, E1^E4, L1 and L2. However, the highest FRET values were documented between E6 and E8^E2C and between E6 and E7.

By analyzing E7, new interactions with E1, E8^E2C, E1^E4, E6, L1 and L2 were detected. E7 dimerization was below the 10% threshold and could not be confirmed, differently from the already published E7-E2 interaction that is reported in Table 2.

The FACS-FRET assay confirmed that the capsid proteins, L1 and L2, interact with each other and with E2. L1 was previously shown to form dimers, differently from L2, both proven in the FACS-FRET experiments. Apart from the already reported interactions, the viral capsid proteins showed new interactions with E1, E8^E2C, E1^E4, E6 and E7.

A network map including the previously published and the interactions found via FACS-FRET was constructed with the open source program NAViGaTOR (http://ophid.utoronto.ca/navigator/) and is shown in Fig. 45.

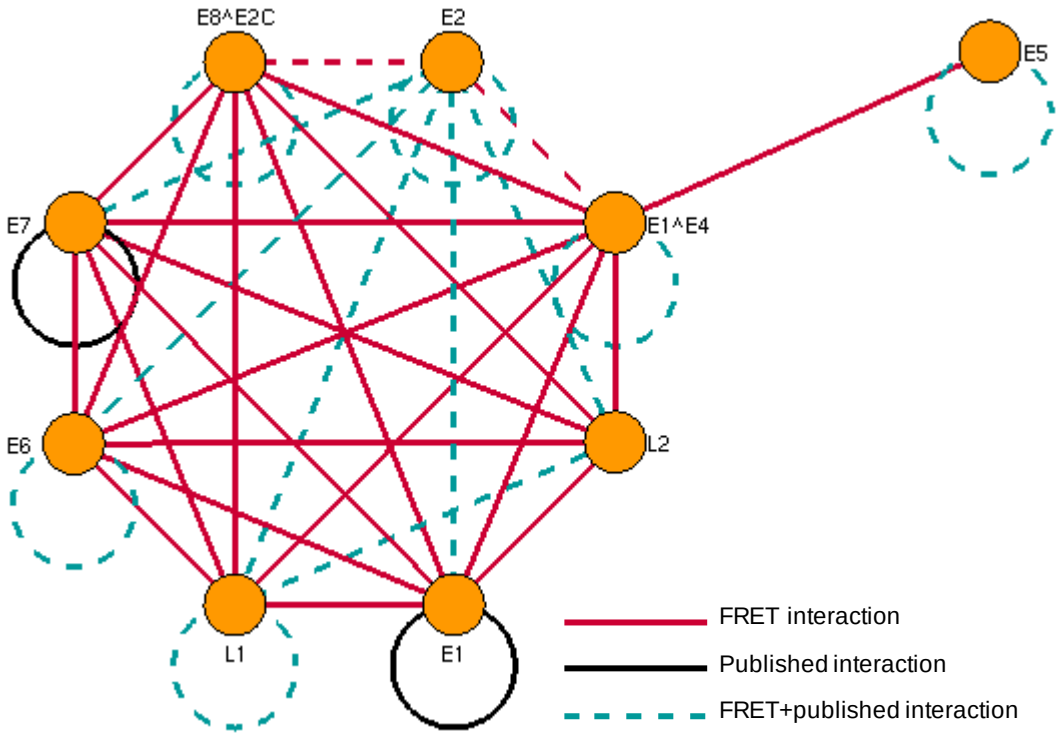

Fig. 45 The HPV31 intraviral interaction network. Red lines represent HPV31 new interactions found by FRET, black lines represent interactions reported in literature and not confirmed with the FACS-FRET assay, whereas dashed green lines show interactions both reported and confirmed by FRET. The network was generated with the program NAViGaTOR.

5.2.4 Validation of the interaction between HPV31 E6 and E7

In order to confirm the interaction between E6 and E7, a CoIP was performed. Therefore, C33a cells were transfected with YFP, BFP, YFPE6, BFPE7, YFPE7 and BFPE6 containing vectors. Then, the CoIP was performed using anti-GFP beads (able to recognize some GFP variants including YFP but not BFP) so that the YFP-tagged proteins were used as baits (Fig. 46).

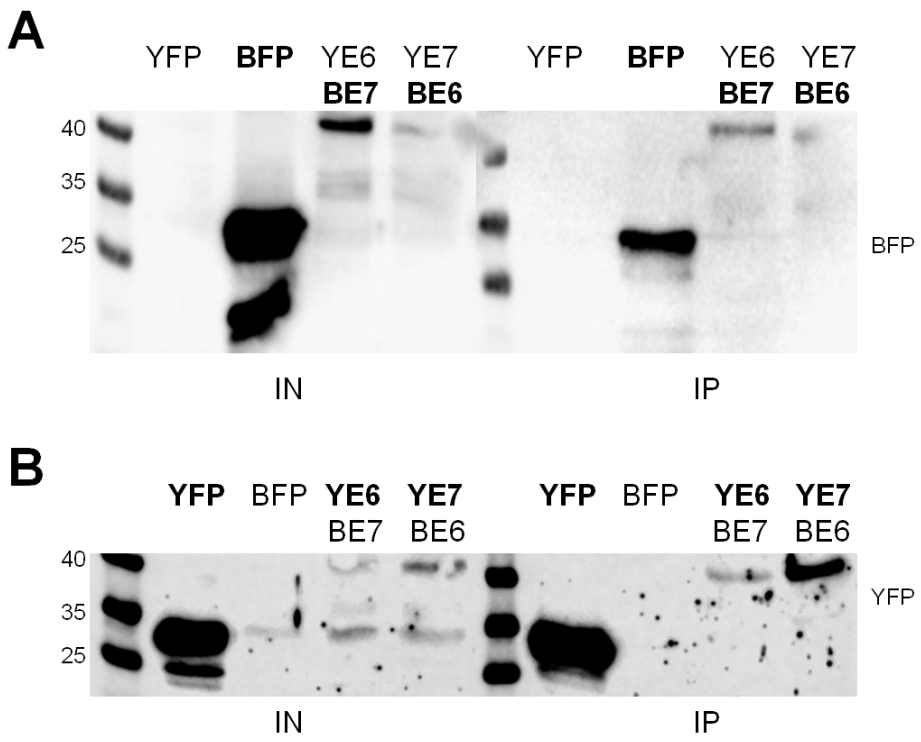

Fig. 46 CoIP showing HPV31 E6 and E7 interactions. YFP- and BFP-tagged E6 and E7 were used to perform a CoIP, where the baits were the YFP-tagged E6 and E7. YFP and BFP only containing vectors were used as negative controls. On the left (A and B) the inputs (IN) show the expression of each protein. Immunoprecipitates (IP) show the interaction between E6 and E7, in both combinations. Membranes were probed with an anti-BFP (A) and an anti-GFP (recognizing also YFP) (B) antibody. Proteins in bold are the ones detected by the antibody. YFP: peYFP-C1; BFP: pmTagBFP-C1; YFPE6: peYFP-C1+HPV31E6; YFPE7: peYFP-C1+HPV31E7; BFPE6: pmTagBFP-C1+HPV31E6; BFPE7: pmTagBFP-C1+HPV31E7. Molecular sizes are shown in kDa on the left.

As shown by the western blot analysis in Fig. 46, where the upper panel (Fig. 46-A) was incubated with an anti-BFP antibody and the lower panel (Fig. 46-B) with an anti-GFP antibody, the inputs showed that the single proteins were expressed. The immunoprecipitates showed that E6 pulled down E7 and vice versa validating the initial FACS-FRET screening results.

6. Discussion

Protein-protein interaction assays were used as tools to investigate HPV-associated carcinogenesis mechanisms. LE6 protein, as one of the oncoproteins of the Cottontail Rabbit Papillomavirus (CRPV) was analyzed to discover new host interaction partners using a proteomics approach. One of the HR-HPV types, HPV31, was studied to determine its intraviral interactome using a FACS-FRET assay.

6.1 Cutaneous E6 interaction partners

Although much is known about the high risk (HR) oncoproteins, only a limited number of studies demonstrated the involvement of the cutaneous E6 and E7 proteins in cellular transformation [64], [67], [99], [196]. Because of its similarities with the cutaneous HPVs, the Cottontail Rabbit Papillomavirus (CRPV) represents a suitable model to investigate papillomavirus-associated skin lesions [197]. By infecting the skin of New Zealand white rabbits it is possible to follow tumor formation and progression *in vivo* . For these reasons we aimed at identifying interactors of the CRPV oncoproteins LE6 and SE6, for acquiring more detailed knowledge about molecular mechanisms leading to tumorigenesis. This knowledge can subsequently be applied to study tumor formation and progression *in vivo* as well as translated to HPV-induced skin tumors. Although the infection of New Zealand white rabbits represents the best model to study HPV-related skin tumors, due to the lack of complete annotation of the rabbit genome and of a protein library, CRPV oncogenes were expressed and studied in the HPV-negative human keratinocytes cell line C33a.

Up to now, only few studies reported cutaneous E6 protein interactions with cellular targets. Some cutaneous HPVs (5, 8, 38 and others), by interacting with the Mastermind-like (MAML) family of transcription activators [75], [76], repress Notch pathway activation that was shown to act as a tumor suppressor in the skin when activated [77]–[79]. HPV38 E6 protein was also shown to interact with p53, but in contrast to HR-E6 no degradation is needed to alter its function [64], [73]. The only information available about CRPVLE6 is its interaction with the acetyltransferase p300 [63], a feature shared with HPV 5, 8 and 38 [81]. In the present study, HPV 5, 38 E6 and CRPVLE6 and SE6 were used as baits to search for previously unreported interactions. Experiments preceding the proteomic approaches confirmed the published interactions with MAML1 and p53 for HPV38 E6 and the one of LE6 and SE6 with p300 via simple CoIP.

Mucosal and cutaneous HPV E6 proteins share the characteristic of binding LXXLL peptide-containing proteins [67]. Well-studied examples of this property are E6AP for the α-HPVs and MAML1 for the β-HPVs. Since CRPV E6 resembles some characteristics of the β-HPV E6 proteins, it is reasonable to hypothesize an interaction between CRPVE6 and MAML1. This is strengthened by the fact that both LE6 and SE6 contain 8 and 6 repetitions of the Cys-X-X-Cys motif [198], respectively, a feature common to other HPV E6 proteins that, however, mostly contain just 4 motifs. However, most likely due to mismatched species-specificity, as a rabbit PV protein was expressed in human cells, the interaction between CRPV E6 and MAML1 remains unclear. Therefore, further studies in rabbit cells are needed to elucidate this interaction.

A label free quantification (LFQ) processed by liquid chromatography-mass spectrometry (LC-MS/MS) at the core facility Proteome Center of Tübingen (PCT) and subsequent bioinformatic analyses were used to select the best interaction candidates. The functional analysis showed that pathways, sites of expression and transcription factors point to and confirm an oncogenic role of the three baits LE6, SE6 and 38E6.

In more detail, the interactors identified were, indeed, found to be mostly expressed in cancer-associated cell lines. More interestingly, putative interactions with three important transcription factors, GABPA, ELK1 and NR4A2, were common to the three viral proteins investigated and they were all shown to have an impact in survival [199], poor prognosis [200], apoptosis evasion [201] and cell growth [202]. Surprisingly, LE6 and SE6 do not share any other interactions with specific transcription factors whereas 38E6 has some in common with both of them. In depth analysis showed that 38E6 and LE6 share the transcription factors E2F1, CREB1 and SPDEF, which have previously been shown to play a role in cellular growth, proliferation, survival and disease progression [203]–[205]. On the other hand KLF7, STRA13 and STAT1 are exclusive interactors of 38E6 and SE6 and they are associated with growth arrest, apoptosis and senescence in tumor cells [206]–[209]. This suggests that, while 38E6 might modulate tumorigenesis on several sides, LE6 and SE6, although closely related, might preferentially interfere with proteins involved in oncogenic or tumor suppressive mechanisms, respectively. Although additional work is needed to prove the putative interactions described so far, it is reasonable to think that the three different E6 proteins are likely to be involved in tumorigenesis and tumor progression and that the mechanisms vary depending on the respective PV.

In order to consolidate the LFQ results and to obtain a more quantitative insight, SILAC was used to perform a second run of LC-MS/MS that enabled us to exclude the detection of

unspecific binders. Observing the distribution of the data it was noted that LE6 was well expressed and highly reproducible. Therefore, the interactors of LE6 were analyzed more in depth. Interestingly, among all the possible candidates of LE6, a group of 5 proteins, all part of the NuRD complex, emerged as putative binders. Since, previous findings showed that HPV E7 interacts with components of the NuRD complex, such as HDAC1, HDAC2 and Mi2β [210], it could be speculated that E6 is also able to bind a component of the complex. However, the proteins analyzed in this study did not show any evident interaction with KDM1A, HDAC1 or HDAC2.

Proteins identified in the SILAC approach were compared to the results obtained from the LFQ. The comparison took into consideration protein families instead of single isoforms and the 17βHSD protein family was found to be represented by several isoforms in both approaches. 17βHSD4, an enzyme involved in the steroid hormone metabolism, catalyzes the conversion of the active form of estrogen, estradiol, into its inactive form estrone. Several studies reported the role of estradiol as a co-factor in HPV-associated cervical tumors [211]–[218]. Moreover, 17βHSD1, the enzyme catalyzing the reverse reaction leading to the conversion of estrone into estradiol, was found to be overexpressed in tumor tissues [219]–[221]. On the other hand, 17β-estradiol was previously shown to be involved in keratinocyte growth in a Cyclin D2-dependent manner [179] and to inhibit apoptosis by promoting Bcl-2 expression [180]. Since estradiol favors tumor progression, 17βHSD1 is overexpressed in tumor tissues and 17βHSD4 does not aid tumor growth, one might hypothesize that an inactivation or downregulation of 17βHSD4 could promote tumor progression, favoring the increase of estradiol levels. However, further research is necessary to support this thesis.

In order to validate the interaction of 17βHSD4 with LE6, immunofluorescence (IF) and proximity ligation assay (PLA) were performed and supported the interaction. 38E6, one of the most studied cutaneous viral oncoprotein, was also analyzed for the interaction with 17βHSD4, because of its high degree of overlap with LE6 concerning protein interactions. As hypothesized, the analysis supported the interaction between 38E6 and 17βHSD4.

Taken together, these data confirmed the previously reported interactions and point to new ones. Even though the screening for LE6 might be incomplete due to mismatched species-specificity of the expression system, the interaction of LE6 and human 17βHSD4 was supported by three independent methods and the results are translatable to the rabbit as human 17βHSD4 shares 90% identity with the corresponding rabbit sequence.

Further studies are needed to clarify the extent of this interaction, first by quantifying the PLA and validating the interaction also via FACS-FRET, and secondly, by expressing LE6 in a rabbit system. It could be speculated that the tumorigenic activity of LE6 might be exerted by blocking 17βHSD4 activity, thus leading to an accumulation of estradiol, that in turns promotes the expression of Cyclin D2 and Bcl-2 favoring tumor progression. Hence, it would also be of great interest to explore the function of this interaction *in vivo* by using the CRPV animal model for instance by measuring the levels of estradiol/estrone, Cyclin D2 and Bcl-2 in rabbits infected by CRPV and in rabbits where 17βHSD4 is knocked down to verify whether this two conditions are comparable and favor tumor progression. In line with the previous assumption, the overexpression of 17βHSD4 and/or increased levels of estrone, the product of 17βHSD4 metabolism, should impair tumor growth.

In conclusion, 17βHSD4 could be a novel interactor of the CRPV LE6 protein and it will need further investigation to prove its potential role in tumor growth and to demonstrate that estradiol/estrone levels play a major role in HPV-associated skin tumors, as already shown for other types of tumors [213], [214], [217]–[221].

6.2 HPV31 intraviral interactome

All large interaction studies on HPV focused on viral-host protein interactions [59], [197] so far. In order to broaden the knowledge of HPV interactions, a flow cytometry-based FRET assay (FACS-FRET) [157] was used to unravel HPV31 intra-viral protein interactions. FACS-FRET has many advantages but the most important one is that interactions can be verified in living cells, and therefore in the natural cellular compartment of the protein analyzed. Moreover, FACS-FRET is a highly reproducible, non-invasive, standardized and quantitative method. Although FRET signals can be easily quantified, signals can be influenced by various parameters as the fluorophores selected, their sterical orientation, the distance between the two interactors, expression and functionality of the tagged proteins. FRET values can be, therefore, over- or under-estimated and measures to minimize possible misreading have to be taken. However, FACS-FRET gives a strong hint of protein-protein interaction that has to be confirmed using other techniques, but it allows screening of protein interactions in thousands of living cells in a small amount of time.

Pre-analytical experiments showed that all the HPV31 fusion proteins were expressed, functional and localized to the cellular compartments where they were previously described. Among all the interactions described, the majority of these interactions was confirmed. All the

previously reported interactions concerning E2, E8^E2C, E4, E5, E6, L1 and L2, and some of E1 and E7 were confirmed.

For E2 all the interactions between E2 and L2 [194], L1 [193], E1^E4 [186], E6 [189], E7 [191], E1 [183] and E2-E2 interaction [184] were confirmed. However, the strongest interaction, although predicted but never demonstrated, was between E2 and E8^E2C. It is important to note that the strength of interaction for E2 relates as follows: E8^E2C>E1>E2. Although at low levels, E1 and E8^E2C interact with each other as well, confirming once again, that E1, E2 and E8^E2C together finely regulate HPV replication.

For E1, new interactions emerged with all the proteins investigated except E5. As expected, the interaction with E2 was the one with the highest FRET values. The already described E1 hexamerization [182], instead, could not be confirmed since FRET values were below the arbitrary 10% threshold set.

With the exception of the homodimerization [185], all other interactions observed for E8^E2C have not been described so far and comprise E1^E4, E7, L1, L2 and E6.

Concerning E1^E4, the only two interactions reported in the literature are the formation of homodimers [187] and the interaction with E2 [186]. In this work, both interactions were confirmed and new interactions were shown with E6, E7 and L1. In addition and most interestingly, E1^E4 was the only protein shown to interact with E5.

Previous studies did not highlight interactions for E5, except for its homodimerization [188], that was, however, not confirmed in the present study. Although the cells analyzed were alive in the assay, the co-expression of E5 with all the other proteins was not possible leading to values that were out of parameters set. The only interaction, never described before, is E1^E4.

The interaction between E6 with E2 [189] and E6 homodimerization [190] were also validated in this study. Previously unpublished interactions comprise E1, E1^E4, L1 and L2. However, surprisingly the highest FRET values were detected between E6 and E8^E2C and the most interesting with E7. This is the first prove that the two oncoproteins of a HR-HPV interact and this suggests a cooperation between these two proteins in carcinogenesis.

Although an E7 dimerization was previously demonstrated [192], we found that the FRET signal for E7-E7 interaction was below the 10% threshold that was arbitrarily introduced to identify only the relevant interactions. Only the interaction between E7 and E2 [191] was

confirmed. New E7 interactions found are with E1, E8^E2C, E1^E4, L1, L2 and the strongest one with E6.

Also the interaction of the capsid proteins, L1 and L2 [195], was confirmed in this work. Moreover, this study also confirmed the dimerization of L1 (Modis et al., 2002) as well as an interaction between E2 with both L1 [193] and L2 [194]. In addition, new interactions for the viral capsid proteins were identified with E1, E8^E2C, E1^E4, E6 and E7.

Almost all the proteins, with the exception of E5, were shown to interact with each other supporting the idea of a fine regulation of replication, expression and tumorigenesis. Although FACS-FRET has the great advantage of analyzing interactions in living cells, it has to be considered that proteins are expressed in a temporal, spatial and quantitative pattern during a productive HPV infection. Thus some of the detected interactions might not occur in the context of an infection. For example, E4 is the only protein demonstrated to be expressed during all the phases of the viral life cycle [29], [222], and therefore it can be speculated that the interactions found for E4 are close to representative especially considering the interaction with the capsid proteins that were reported to be expressed only in E4-positive cells [38]. However, the FACS-FRET screening provided a first overview about how the viral proteins interact with each other and further research is necessary to validate and evaluate the newly discovered interactions. As a first step, the interaction between E6 and E7 was confirmed in this work by two independent experiments and methods.

In addition, although never demonstrated so far, some reports support the idea that HPV31 E6 and E7 proteins may interact. First, HR-E6 and E7 are thought to derive from a common ancestor since the two Cys-X-X-Cys motifs present in the C-terminus of HR-E7 were supposed to undergo duplication during evolution. This might have given rise to an HR-E6 protein that contains four copies of a Cys-X-X-Cys motif, with a sequence similar to the motifs present in E7 (McLaughlin-Drubin 2009, Vande pol, 2013). Secondly, E6 and E7 were shown to form homodimers [190], [192] so it is reasonable to think that, due to the sequence similarities they might interact with each other. At last, the expression of HR-E6 and -E7 in keratinocytes was previously shown to be necessary and sufficient for immortalization and inhibition of differentiation [55], [56] and, although only E7 can immortalize the keratinocytes when expressed alone, it was also reported that the co-expression of E6 and E7 increases the efficiency of immortalization [57]. Moreover, the viral oncoproteins were shown to cooperate to favor carcinogenesis since they are involved in the regulation of several aspects of cancer onset and progression, comprising inhibition of apoptosis and cell proliferation

(Bedell et al. 1987; Vousden et al. 1988). Thus, an interaction of both proteins is both likely and reasonable.

Additional studies are needed to further confirm this interaction, using other methods such as PLA, deletion mutants to be tested in FACS-FRET and crystallography. In summary, we discovered both known and to date unknown interactions and were able to verify for the first time an interaction between the two viral oncoproteins E6 and E7.

7. Conclusions and Outlook

Despite the availability of vaccines able to prevent most cases of cervical cancers if given before a girl or woman is exposed to the virus, none of the vaccines can treat an existing HPV infection Because of their high prevalence there is, however, an urgent need to find new therapeutic alternatives in treating HPV-associated tumors. HPV, as the carcinogene or co-carcinogene of different types of cancers, including mucosal and skin tumors, needs to be therefore deeply investigated.

In this work, two different approaches to discover protein-protein interactions were used. On the one hand, a proteomics approach pointing to shed more light into cutaneous HPV-associated carcinogenesis mechanisms was used. On the other hand, a flow cytometry-based FRET assay (FACS-FRET) discovered the intraviral network of the HR type HPV31.

The data acquired so far provide a better comprehension of the molecular mechanisms by which cutaneous PVs interfere with the host. Important results include the confirmation of previously reported protein interactions as well as the identification of new interactors, where 17-Beta-Hydroxysteroid Dehydrogenase isoforms 4 (17βHSD4) looks kike a promising protein which seems to be involved in tumorigenesis and, consequently, it may prove to be a good treatment target.

The second part of the work focused on HPV31, one of the representative of the HR-HPV types. The results of the FACS-FRET allowed to have the first complete overview on the HPV31 intraviral interactome. This needs deeper investigation, but it gives an important overview on how viral proteins interact with each other and this knowledge can be translated to other HR-HPV. Knowing how viral proteins interact might help in understanding novel mechanisms involved in HPV-associated cancers, especially since the two oncoproteins E6 and E7 were shown to interact with each other for the first time. Further validation is needed to prove this interaction, but this novel finding could give new insights in new treatment options.

The findings might be used for future research to understand more in depth how cutaneous PVs cause cancer and open new possibilities for therapeutic options of PV-induced malignancies.

8. Supplementary results

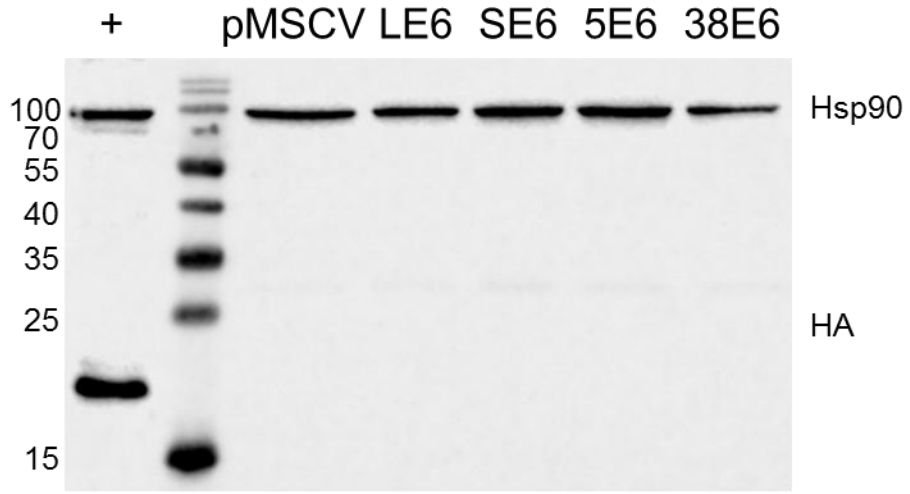

Supplementary figure S1. Western blot showing HA-tagged E6 proteins expression in stable transfected NIKS cells.
To investigate viral-host interactions of cutaneous E6 proteins, first, stable cell lines expressing HA-tagged proteins were established. E6 proteins of HPV 5, 38 and CRPV were C-terminally HA (hemagglutinin) tagged. For this, genes were cloned into a retroviral vector containing a linker followed by a triple HA tag (Materials and methods, section 4.1.10.1 Expression vectors). CRPVE6 mRNA results in two splice-variants encoding for the long (LE6) and the short (SE6) isoforms of E6. Previously Dr. Peter Muench generated a vector (pcDNA™3.1(+) CRPVLE6 M98S) containing the CRPVE6 gene with a mutation at the splicing site (substitution of methionine with serine at position 98), which ensures the exclusive production of LE6. The CRPVLE6 M98S (called simply LE6) sequence was PCR-amplified and cloned into the 3xHA-containing retroviral vector. For the expression of the labeled proteins, normal immortalized keratinocytes (NIKS) were transduced using a retroviral infection system and subsequently were kept under constant antibiotic selection, which finally resulted in stable E6-expressing cell lines. In the upper part lysates were probed with an anti-Hsp90 antibody while in the lower part an anti-HA antibody was used to detect the HA-tagged proteins. Although the presence of a housekeeping protein (Hsp90), HPV and CRPV E6 proteins could not be detected. +: positive control for HA expression; pMSCV: pMSCV_linker_3xHA empty vector; LE6: pMSCV_CRPVLE6_ linker_3xHA; SE6: pMSCV_CRPVSE6_ linker_3xHA; 5E6: pMSCV_HPV5E6_ linker_3xHA; 38E6: pMSCV_HPV38E6_ linker_3xHA. On the left, molecular weights are indicated in kDa.

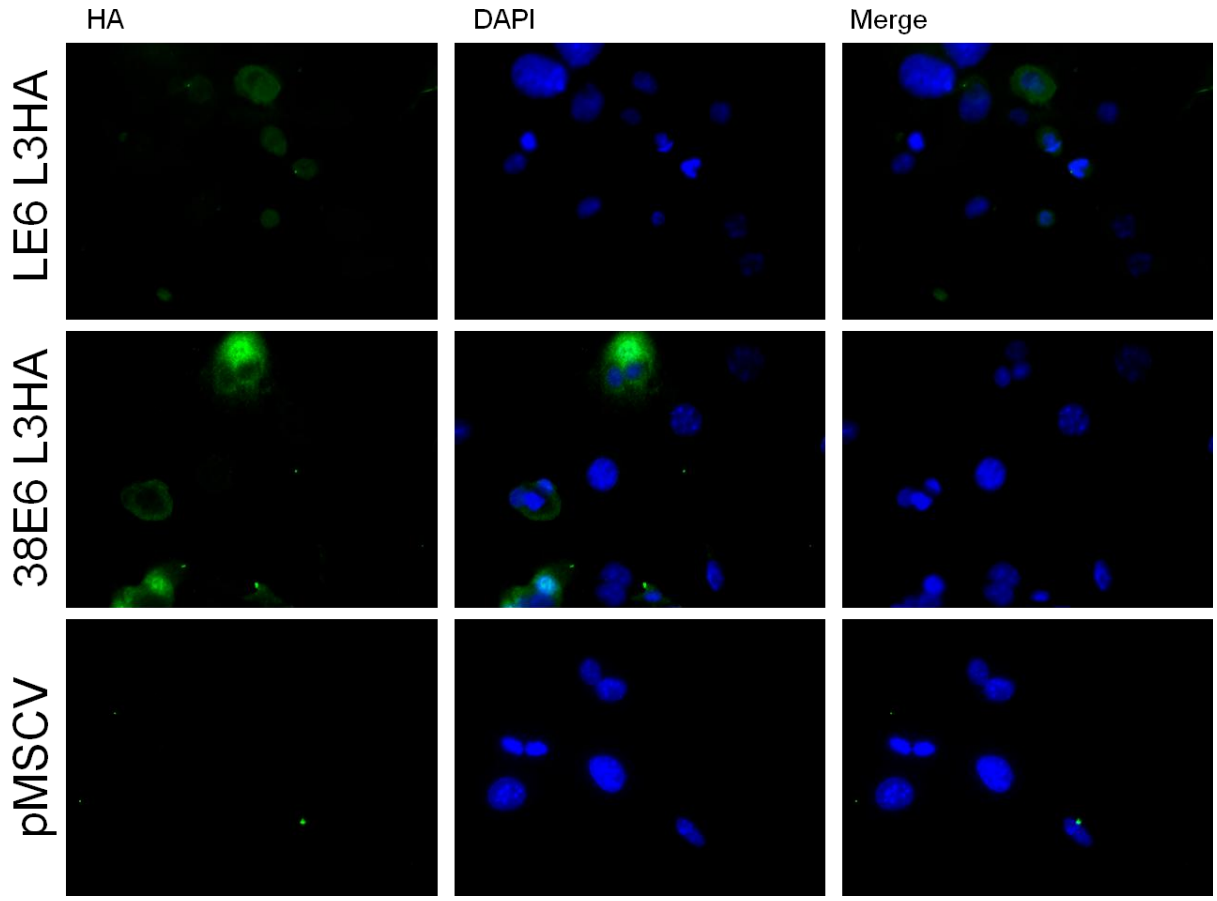

Supplementary figure S2. Immunofluorescence showing the expression of CRPVLE6 and HPV38 E6. Protein expression was examined by immunofluorescence (IF) in NIKS cells stably expressing CRPV and HPV 38 E6. Therefore, NIKS cells were stained for the presence of CRPVLE6 and HPV38 E6 using an anti-HA antibody (green). Cell nuclei were stained with DAPI (blue). Merge shows the overlay of HA and the DAPI stainings. In these cells, HA expression was detected, although this was confined to a very restricted number of cells.

Supplementary Table S3. Label free quantification (LFQ) of LE6 interaction partners. In the table are listed: LFQ ratios (LE6/CMV), posterior error probability (PEP), intensity, significance B value (Sig. B), Gene names, Protein IDs representing the Uniprot identification numbers and the protein names of the significant proteins binding to LE6. Graphical representation in results Fig. 8-A.

LE6/CMV	PEP	Intensity	LE6/CMV Sig. B	Gene Names	Protein IDs	Protein Names
12,5791	3,48E-63	9,96686	1,52E-120		LE6	
4,864	8,67E-28	9,2416	2,17E-20	HME1	P31947	14-3-3 protein sigma
8,80133	3,80E-04	8,72328	2,54E-18	H3FA	P68431	Histone H3.1
7,68448	1,97E-101	8,62822	1,66E-14	KIAA1321	Q7Z417	82 kDa FMRP-interacting protein
9,20576	1,58E-02	8,37568	5,24E-09		H0Y670	
2,65834	3,32E-57	9,11561	1,39E-07	BAP135	P78347	Bruton tyrosine kinase-associated protein 135
2,4433	0,00E+00	10,2862	1,05E-06	G22P2	P13010	86 kDa subunit of Ku antigen
2,30338	8,24E-278	9,53896	3,61E-06	SAP114	Q15459	SF3a120
6,92089	3,50E-20	8,17173	8,12E-06	HIST2H2AB	Q8IUE6	Histone H2A type 2-B
2,14906	0,00E+00	9,86804	1,31E-05	PLEC1	Q15149	Hemidesmosomal protein 1
6,57684	3,54E-135	8,49328	2,08E-05	PABP3	Q9H361	Polyadenylate-binding protein 3
2,0127	2,06E-177	9,10992	3,84E-05	CORO1C	A7MAP1	Coronin-1C_i3 protein
3,80523	6,09E-57	8,90697	5,19E-05	P53	P04637	Antigen NY-CO-13
1,95195	4,66E-151	9,14594	6,08E-05	CGI-132	Q9Y3D3	28S ribosomal protein S16, mitochondrial
1,93494	5,45E-07	9,68152	6,90E-05	RTTN	Q86VV8	Rotatin
5,91065	5,08E-53	8,08221	1,52E-04	AD-001	Q9UI30	TRM112-like protein
3,46184	6,46E-83	8,82558	1,90E-04	ALDA	J3KPS3	Fructose-bisphosphate aldolase A
5,72686	3,91E-09	7,86207	2,32E-04	PEX14	O75381	Peroxin-14
4,7913	2,19E-13	7,09548	2,36E-04	H1F3	P16402	Histone H1.3
5,16901	1,57E-02	7,54616	2,76E-04	AIP	Q9NWT8	Aurora kinase A-interacting protein
3,3109	1,25E-30	8,55951	3,25E-04	NDUFA10	E7ESZ7	Complex I-42kD
1,67761	7,52E-244	9,74603	4,18E-04	ADPRT	P09874	NAD(+) ADP-ribosyltransferase 1
5,32215	8,67E-09	8,24655	4,44E-04	MDIG	Q8IUF8	Mineral dust-induced gene protein
3,2159	3,92E-50	8,91431	4,52E-04	DDX6	P26196	ATP-dependent RNA helicase p54
5,25566	1,92E-27	8,33125	5,14E-04	MAGOH	P61326	Protein mago nashi homolog
1,64535	7,45E-142	9,50864	5,17E-04	SAP61	Q12874	SF3a60
5,31525	3,18E-09	7,92434	5,72E-04	EIF4E2	O60573	eIF4E-like protein 4E-LP
1,6214	0,00E+00	10,0114	6,03E-04	HYRC	P78527	DNA-dependent protein kinase catalytic subunit
5,12711	2,83E-20	8,24082	6,80E-04	NOC2L	Q9Y3T9	NOC2-like protein
4,93706	4,89E-04	8,40506	1,02E-03	KIAA1966	J3QR07	Putative splicing factor YT521
4,54387	5,76E-03	7,31827	1,23E-03	CBP20	P52298	20 kDa nuclear cap-binding protein
4,79271	8,84E-05	8,27969	1,37E-03	NDUFA8	P51970	Complex I-19kD
4,78859	3,78E-18	8,47748	1,38E-03	SAP62	Q15428	SF3a66
4,44282	2,21E-03	7,64177	1,54E-03	PROS26	P28070	26 kDa prosomal protein
4,43791	1,25E-06	7,6203	1,56E-03	OMP25	P57105	Mitochondrial outer membrane protein 25
2,78404	2,11E-148	8,87237	1,83E-03	UQCRC2	P22695	Complex III subunit 2
2,75224	3,58E-70	8,68049	2,01E-03	SEC23A	Q15436	Protein transport protein Sec23A

4,54003	2,62E-30	8,16152	2,25E-03	PYCR2	Q96C36	Pyrroline-5-carboxylate reductase 2
4,52944	9,23E-07	8,31867	2,30E-03	DBP2	O60231	ATP-dependent RNA helicase #3
4,56877	4,23E-08	7,93044	2,55E-03	RHOA	C9J1T2	Putative uncharacterized protein RHOA
4,51594	4,70E-16	8,05088	2,81E-03	DNAJB11	Q9UBS4	APOBEC1-binding protein 2
2,60435	4,74E-60	8,79442	3,12E-03	DDX50	Q9BQ39	ATP-dependent RNA helicase DDX50
4,3376	2,86E-43	8,39766	3,31E-03	IRA1	Q9BZK7	F-box-like/WD repeat-containing protein TBL1XR1
4,28924	2,63E-05	8,21822	3,62E-03	GBAS	O75323	Glioblastoma-amplified sequence
4,03185	2,03E-03	7,57104	3,68E-03	SPT3	O75486	SPT3-like protein
4,02565	5,04E-05	7,59647	3,73E-03	TTN	Q8WZ42-8	Connectin
3,68588	6,06E-23	7,06807	3,80E-03	DADB-118P11.2-006	A2AB10	Flotillin 1
3,65753	1,46E-04	6,89485	4,05E-03	CDIPT	B3KY94	cDNA FLJ16129 fis highly similar to CDP-diacylglycerol-inositol3-phosphatidyltransferase
3,98471	1,89E-03	7,69854	4,05E-03	MPDU1	O75352	Mannose-P-dolichol utilization defect 1 protein
2,50704	1,25E-41	8,6238	4,12E-03	NDUFS1	P28331-2	Complex I-75kD
3,96544	1,30E-03	7,42667	4,21E-03	INPP5K	Q9BT40	Inositol polyphosphate 5-phosphatase K
1,29216	6,72E-160	9,22719	4,22E-03	FACT80	Q08945	Chromatin-specific transcription elongation factor 80 kDa subunit
3,95026	3,24E-06	7,68891	4,34E-03	PRKAR1B	P31321	cAMP-dependent protein kinase type I-beta regulatory subunit
3,91241	1,27E-02	7,40358	4,68E-03	KIAA0016	Q15388	Mitochondrial 20 kDa outer membrane protein
3,58018	2,65E-09	7,22937	4,80E-03		P54819-6	
3,5659	1,77E-02	7,26252	4,95E-03	NUPL2	C9JYA1	Putative uncharacterized protein NUPL2
3,86272	9,09E-03	7,33393	5,16E-03	CYB5R3	P00387-3	Diaphorase-1
3,54532	5,39E-13	6,94077	5,17E-03	H1F2	P16403	Histone H1.2
4,16565	4,50E-06	7,9301	5,27E-03	VKORC1L1	Q8N0U8	Vitamin K epoxide reductase complex subunit 1-like protein 1
2,38737	3,02E-142	8,5741	5,73E-03	ATP6A1	P38606	Vacuolar ATPase isoform VA68
3,80382	1,45E-11	7,31601	5,79E-03	MAK16	Q9BXY0	NNP78
3,78343	1,14E-02	7,66585	6,02E-03	CCDC17	Q96LX7	Coiled-coil domain-containing protein 17
3,71115	1,18E-04	7,66523	6,92E-03	CGI-124	Q9Y3C6	Peptidyl-prolyl cis-trans isomerase-like 1
3,3881	3,48E-04	7,26708	7,22E-03	BZRP	P30536	Mitochondrial benzodiazepine receptor
3,38743	7,24E-02	7,13271	7,23E-03	ARL5B	Q96KC2	ADP-ribosylation factor-like protein 5B
3,37744	3,83E-04	6,67362	7,38E-03	POLR2G	P62487	DNA-directed RNA polymerase II subunit G
3,9659	3,91E-07	7,90927	7,41E-03	SFXN1	Q9H9B4	Sideroflexin-1
1,18131	4,42E-259	9,62782	7,53E-03	SNRPA1	P09661	U2 small nuclear ribonucleoprotein A
3,86055	3,63E-04	8,21846	7,74E-03	OGT	O15294	O-GlcNAc transferase subunit p110
3,349	5,91E-17	6,83124	7,82E-03	RAB5	P20339	Ras-related protein Rab-5A
1,16894	2,75E-110	9,13789	8,01E-03	EIF4F	E9PFM1	Eukaryotic translation initiation factor 4 gamma

						1
3,25536	1,27E-05	7,27235	9,46E-03	ANKRD46	Q86W74	Ankyrin repeat domain-containing protein 46
3,81278	2,52E-09	8,05888	9,54E-03	HSPC114	Q9Y5S9	Binder of OVCA1-1
3,80298	2,29E-10	7,87272	9,69E-03	RNP24	Q15363	Membrane protein p24A
3,78453	1,40E-06	7,79759	9,98E-03	PSMB3	P49720	Proteasome chain 13
3,77018	1,78E-14	8,10531	1,02E-02	NSUN5	Q96P11-4	NOL1/NOP2/Sun domain family member 5
3,71717	1,38E-07	7,87061	1,11E-02	RNASEP2	E9PB02	Ribonuclease P protein subunit p30
3,63943	4,14E-08	8,202	1,12E-02	PSMF1	Q92530	Proteasome inhibitor PI31 subunit
3,63667	9,84E-32	8,27665	1,12E-02	HSD17B12	Q53GQ0	17-beta-hydroxysteroid dehydrogenase 12
3,629	4,47E-03	8,35034	1,14E-02	CDO1	Q16878	Cysteine dioxygenase type 1
2,1167	3,92E-84	8,89887	1,16E-02	RO60	P10155	60 kDa SS-A/Ro ribonucleoprotein
2,11446	8,38E-15	8,78004	1,17E-02	MRP63	Q9BQC6	Ribosomal protein 63, mitochondrial
3,68267	7,76E-06	7,82563	1,17E-02	RPS21	P63220	40S ribosomal protein S21
1,08534	9,57E-207	9,82426	1,21E-02	G3BP	Q13283	ATP-dependent DNA helicase VIII
3,6636	2,50E-06	8,03491	1,21E-02	MRPL53	Q96EL3	39S ribosomal protein L53, mitochondrial
3,3862	1,90E-04	7,5784	1,25E-02	BCDIN3	Q7L2J0	7SK snRNA methylphosphate capping enzyme
3,60524	6,09E-86	7,98692	1,33E-02	MAGED1	Q9Y5V3-2	MAGE tumor antigen CCF
3,60383	2,75E-14	7,82543	1,33E-02	RCD1	Q92600	Cell differentiation protein RCD1 homolog
3,59991	1,82E-02	7,99259	1,34E-02	TRAM	Q15629	Translocating chain-associated membrane protein 1
3,32782	1,70E-05	7,56046	1,39E-02	PMC2	Q9GZR2	Exonuclease XPMC2
3,31947	1,99E-06	7,63649	1,41E-02	METT11D1	Q9H7H0-3	False p73 target gene protein
2,03752	1,13E-121	8,73556	1,41E-02	TOP2B	Q02880	DNA topoisomerase 2-beta
1,04381	5,59E-68	9,37462	1,47E-02	BAG2	O95816	BAG family molecular chaperone regulator 2
3,53966	4,72E-03	7,90462	1,47E-02	Nbla11189	Q9BSR8	Protein YIPF4
3,53135	5,09E-07	7,99257	1,49E-02	THOC3	Q96J01	hTREX45
2,01582	7,37E-28	8,58048	1,49E-02	KIAA0217	Q92615	La ribonucleoprotein domain family member 4B
3,01782	1,73E-03	7,07711	1,50E-02	MYO1C	Q12965	Myosin-Ic
3,26306	1,63E-03	7,69423	1,55E-02	COPS1	Q13098-6	COP9 signalosome complex subunit 1
3,42107	4,43E-03	8,13293	1,58E-02	KIAA0567	E5KLJ5	Dynamin-like 120 kDa protein, form S1
3,48818	5,10E-13	7,81296	1,59E-02	DNAJB12	J3KPS0	DnaJ homolog subfamily B member 12
3,23728	3,10E-12	7,29767	1,62E-02		B4E3L0	cDNA FLJ54259, highly similar to Smu-1 suppressor of mec-8 and unc-52 protein homolog
1,97937	6,15E-11	8,75721	1,62E-02	DAD1	P61803	Defender against cell death 1
3,45163	3,60E-05	7,79649	1,68E-02	IMP3	Q8TCT8	Intramembrane protease 3
3,44448	4,88E-05	8,05588	1,69E-02	MCT1	P53985	Monocarboxylate transporter 1
3,20968	1,61E-02	7,35168	1,70E-02	WIPF1	C9JB04	Putative uncharacterized

						protein WIPF1
1,94899	1,31E-97	8,93848	1,74E-02	HSPC032	Q9Y6C9	Met-induced mitochondrial protein
3,18694	6,98E-03	7,45388	1,77E-02	FCHO2	J3KNW0	FCH domain only protein 2
0,997422	0,00E+00	10,1705	1,81E-02	G22P1	P12956	70 kDa subunit of Ku antigen
3,1688	3,35E-02	7,29763	1,82E-02	GPR112	Q8IZF6	Probable G-protein coupled receptor 112
1,92081	3,71E-35	8,91995	1,86E-02	THRAP3	Q9Y2W1	Thyroid hormone receptor-associated protein 3
1,91789	1,66E-17	8,8224	1,88E-02	CGI-37	Q9Y221	60S ribosome subunit biogenesis protein NIP7 homolog
1,9093	5,26E-134	8,96458	1,92E-02	KIAA0185	Q14690	NF-kappa-B-binding protein
3,13833	3,43E-04	7,31161	1,92E-02	ITBA4	G3V1N1	NF-kappa-B-repressing factor
2,87616	1,05E-03	7,25513	1,95E-02	LENG5	E7EQB3	Leukocyte receptor cluster member 5
1,89884	1,53E-54	9,02152	1,96E-02	POLRMT	O00411	DNA-directed RNA polymerase, mitochondrial
2,86842	9,24E-03	7,18927	1,98E-02	DPY19L1	Q2PZI1	Dpy-19-like protein 1
3,11638	1,01E-03	7,65848	1,99E-02	TOMM34	Q15785	Mitochondrial import receptor subunit TOM34
2,85361	1,68E-03	5,86589	2,04E-02	GPR107	Q5VW38	Lung seven transmembrane receptor 1
2,84926	8,50E-03	7,19901	2,05E-02	TYSND1	Q2T9J0	Peroxisomal leader peptide-processing protease
1,87276	3,38E-08	8,65969	2,08E-02	NDUFS2	O75306	Complex I-49kD
0,963702	1,25E-98	9,11704	2,11E-02	DDX28	Q9NUL7	Mitochondrial DEAD box protein 28
2,81653	1,14E-03	7,04242	2,18E-02	JM4	O60831	PRA1 family protein 2
0,955966	1,18E-20	9,11998	2,18E-02	SFRS2	Q01130	Protein PR264
3,02414	6,90E-04	7,31025	2,31E-02	CGI-141	Q9Y3E0	Golgi transport 1 homolog B
3,23112	1,81E-20	8,06781	2,32E-02	SAMD1	Q6SPF0	Atherin
1,82265	9,70E-26	8,92714	2,34E-02	HSP27	P04792	28 kDa heat shock protein
2,77348	3,24E-04	6,75752	2,35E-02	RBMS3	Q6XE24	RNA-binding motif, single-stranded-interacting protein 3
2,77202	2,41E-10	7,16885	2,36E-02	KIAA1483	Q8N680	Zinc finger and BTB domain-containing protein 2
3,143	2,50E-38	8,46705	2,40E-02	HPRT	P00492	Hypoxanthine-guanine phosphoribosyltransferase
0,930701	1,38E-172	9,48524	2,43E-02	HSPC075	Q9UQ35	300 kDa nuclear matrix antigen
3,18545	3,70E-12	8,10687	2,47E-02	AFAR	O43488	AFB1 aldehyde reductase 1
3,17967	2,77E-06	7,93281	2,49E-02	ATAD1	Q8NBU5	ATPase family AAA domain-containing protein 1
2,96876	7,16E-06	7,32434	2,52E-02	UQBP	P14927	Complex III subunit 7
0,919962	4,48E-133	9,2763	2,55E-02	ATP1A1	F5H3A1	Sodium pump subunit alpha-1
3,08635	8,90E-37	8,33056	2,60E-02	PNO1	Q9NRX1	RNA-binding protein PNO1
3,14468	4,98E-08	7,84899	2,62E-02	GTF2E2	P29084	General transcription factor IIE subunit 2
0,912821	4,19E-99	9,15226	2,63E-02	LAPTM4B	Q86VI4	Lysosomal-associated transmembrane protein

						4B
0,908275	1,47E-46	9,31854	2,68E-02	UBF	P17480	Autoantigen NOR-90
2,92887	2,94E-43	7,28276	2,69E-02	C20orf99	Q9NUD5	Zinc finger CCHC domain-containing protein 3
3,12462	4,34E-21	7,7343	2,69E-02	CCNYL1	Q8N7R7	Cyclin-Y-like protein 1
1,7544	2,04E-17	8,6172	2,72E-02	PES1	O00541	Pescadillo homolog
3,05486	6,26E-24	8,14947	2,72E-02	CGI-31	Q9Y320	Cell proliferation-inducing gene 26 protein
2,68842	1,01E-03	6,93221	2,73E-02	HELLS	Q9NRZ9	Lymphoid-specific helicase
2,68196	1,92E-82	7,02584	2,76E-02	HSPC039	Q9Y5U9	Immediate early response 3-interacting protein 1
0,900884	1,49E-124	9,74744	2,76E-02	ACTBL2	Q562R1	Beta-actin-like protein 2
2,91156	1,12E-03	7,36981	2,76E-02	GLYR1	Q49A26	3-hydroxyisobutyrate dehydrogenase-like protein
2,67655	6,46E-12	6,73242	2,78E-02		F5H0M0	
3,03938	2,34E-04	8,31416	2,78E-02	BM-007	Q9NZE8	39S ribosomal protein L35, mitochondrial
2,90038	1,37E-10	7,57917	2,81E-02	SSR3	B4E2P2	cDNA FLJ52061, highly similar to Translocon-associated protein subunit gamma
1,73626	8,75E-33	8,72638	2,83E-02	CDC46	P33992	CDC46 homolog
3,08367	2,47E-06	8,12094	2,85E-02	CGI-64	H0Y8C3	Mitochondrial carrier homolog 1
3,07133	2,73E-08	7,91616	2,90E-02	POLR2B	P30876	DNA-directed RNA polymerase II 140 kDa polypeptide
3,01075	7,73E-12	8,32848	2,90E-02	SMBP	Q9HD45	EP70-P-iso
2,87578	6,74E-06	7,58831	2,92E-02	FMT	Q96DP5	Methionyl-tRNA formyltransferase, mitochondrial
2,64561	6,85E-04	6,91704	2,93E-02	CD2BP2	O95400	CD2 antigen cytoplasmic tail-binding protein 2
3,05136	4,38E-03	7,88054	2,98E-02	LSM3	P62310	U6 snRNA-associated Sm-like protein LSm3
2,86165	5,34E-02	7,42257	2,99E-02	ANKRD18B	Q8NF67	Putative uncharacterized protein FLJ00310
2,97273	7,09E-11	8,29387	3,06E-02	KIAA0650	A6NHR9	Structural maintenance of chromosomes flexible hinge domain-containing protein 1
3,02933	6,31E-17	7,95686	3,07E-02	KIAA0090	Q8N766	Uncharacterized protein KIAA0090
1,6937	4,75E-07	8,60799	3,10E-02	C8orf55	Q8WUY1	Mesenchymal stem cell protein DSCD75
2,96079	3,35E-09	8,32726	3,11E-02	LMN1	P02545	70 kDa lamin
2,58272	7,57E-03	6,86276	3,26E-02	SIR2L3	Q9NTG7	NAD-dependent deacetylase sirtuin-3, mitochondrial
0,855271	6,04E-08	10,1452	3,34E-02		P06310	Ig kappa chain V-II region RPMI 6410
2,78887	6,67E-10	7,62251	3,34E-02	MAP7D2	Q96T17-2	MAP7 domain-containing protein 2
2,90652	1,72E-33	8,37334	3,35E-02	AHAS	A1L0T0	Acetolactate synthase-like protein
2,89164	1,58E-36	8,35639	3,42E-02	ADPRT2	Q9UGN5	NAD(+) ADP-ribosyltransferase 2
0,848154	0,00E+00	10,2306	3,43E-02	INA	Q16352	66 kDa neurofilament protein
2,87704	8,45E-76	8,33614	3,49E-02	ZCCHC8	Q6NZY4	Zinc finger CCHC domain-containing protein 8

1,63856	7,96E-46	8,98526	3,49E-02	A2D	Q8WWM7-3	Ataxin-2 domain protein
1,62197	5,49E-32	9,01595	3,61E-02	NDUFA9	Q16795	Complex I-39kD
1,61538	2,58E-35	8,56862	3,66E-02	PKR2	P13861	cAMP-dependent protein kinase type II-alpha regulatory subunit
2,50474	1,11E-02	6,86248	3,71E-02	BR22	Q9P031	Coiled-coil domain-containing protein 59
0,826828	2,56E-65	10,5165	3,74E-02	H4/A	P62805	Histone H4
2,71138	3,57E-28	7,71162	3,75E-02	POLR1A	O95602	A190
2,80931	1,00E-24	8,15555	3,83E-02	HSPC124	Q9H2U2-2	Inorganic pyrophosphatase 2, mitochondrial
2,48188	3,44E-04	6,70477	3,85E-02	GIPC2	Q8TF65	PDZ domain-containing protein GIPC2
2,84514	5,91E-09	8,05614	3,93E-02	PSEC0082	Q8NBN7	Retinol dehydrogenase 13
1,58124	1,24E-08	8,78511	3,93E-02	EIF4E	P06730-2	eIF-4F 25 kDa subunit
2,82651	4,67E-07	7,89478	4,02E-02	ARC77	Q9NVC6	Activator-recruited cofactor 77 kDa component
0,807116	2,14E-27	9,37297	4,05E-02	SNRPB2	P08579	U2 small nuclear ribonucleoprotein B
2,78703	3,27E-14	7,81206	4,24E-02	KIAA0117	P42696	RNA-binding motif protein 34
0,792693	6,42E-139	9,28639	4,28E-02	CATX11	O76021	CATX-11
0,791174	2,11E-136	9,32457	4,31E-02	IARS	P41252	Isoleucine--tRNA ligase
2,40525	1,33E-03	7,04821	4,35E-02	CCDC127	Q96BQ5	Coiled-coil domain-containing protein 127
2,70715	1,12E-11	8,24932	4,38E-02	NDUFV1	P49821	Complex I-51kD
2,37872	3,14E-16	7,25563	4,54E-02	RIF1	Q5UIP0	Rap1-interacting factor 1 homolog
2,57778	1,82E-06	7,29776	4,56E-02	AAG	P29372	3-alkyladenine DNA glycosylase
0,773697	0,00E+00	9,79227	4,61E-02	DBC1	Q8N163	Deleted in breast cancer gene 1 protein
2,64973	8,65E-19	8,1233	4,72E-02	CYC1	P08574	Complex III subunit 4
2,64121	7,60E-38	8,35307	4,77E-02	NOL6	Q9H6R4	Nucleolar protein 6
2,34292	3,02E-21	7,12946	4,80E-02	BT2.1	Q7KYR7-1	Butyrophilin subfamily 2 member A1
2,67919	3,99E-37	8,07478	4,86E-02	AD-005	A5YKK6	CCR4-associated factor 1
0,758771	7,16E-76	9,37927	4,88E-02	VDAC3	F5H740	Outer mitochondrial membrane protein porin 3
1,46791	7,60E-109	8,58132	4,94E-02	MKI67	P46013	Antigen KI-67
1,46543	6,72E-34	8,7788	4,97E-02	EIF4G2	D3DQV9	Eukaryotic translation initiation factor 4 gamma, 2, isoform CRA_b

Supplementary Table S4. Label free quantification (LFQ) of SE6 interaction partners. In the table are listed: LFQ ratios (SE6/CMV), posterior error probability (PEP), intensity, significance B value (Sig. B), Gene names, Protein IDs representing the Uniprot identification numbers and the protein names of the significant proteins binding to SE6. Graphical representation in results Fig. 8-B.

SE6/CMV	PEP	Intensity	LE6/CMV Sig. B	Gene Names	Protein IDs	Protein Names
10,975	3,48E-63	9,96686	1,01E-25		LE6	
10,5616	6,59E-69	8,6343	2,75E-16		SE6	
8,89299	6,71E-31	8,98318	3,98E-12	HSPE1	P61604	10 kDa chaperonin
4,54067	1,90E-125	9,56785	9,69E-07	MDH2	P40926	Malate dehydrogenase, mitochondrial
5,43301	1,18E-03	6,84012	5,22E-06	TMEM127	C9J4H2	Putative uncharacterized protein TMEM127
3,89628	8,24E-278	9,53896	1,38E-05	SAP114	Q15459	SF3a120
6,05015	8,22E-06	7,63276	4,75E-05	LSM8	O95777	N-alpha-acetyltransferase 38, NatC auxiliary subunit
4,97634	1,45E-43	8,69873	5,23E-05	OAT	P04181	Ornithine aminotransferase, hepatic form
4,96859	2,82E-55	8,55398	5,35E-05	ACO2	A2A274	Aconitase 2, mitochondrial
4,70771	3,02E-142	8,5741	1,18E-04	ATP6A1	P38606	Vacuolar ATPase isoform VA68
4,69258	5,84E-95	8,6778	1,23E-04	SHMT2	P34897	Glycine hydroxymethyltransferase
4,55594	5,08E-36	8,9758	1,84E-04	GOT2	P00505	Aspartate aminotransferase, mitochondrial
4,47663	5,02E-30	8,55332	2,31E-04	ERO1L	Q96HE7	Endoplasmic oxidoreductin-1-like protein
5,43058	8,61E-09	7,53728	2,38E-04	NPDC1	Q5SPY9	Neural proliferation, differentiation and control, 1
4,43814	8,13E-60	8,99234	2,57E-04	CS	O75390	Citrate synthase, mitochondrial
4,41753	1,25E-30	8,55951	2,72E-04	NDUFA10	E7ESZ7	Complex I-42kD
4,19393	5,64E-17	7,1697	2,93E-04	LSM5	Q9Y4Y9	U6 snRNA-associated Sm-like protein LSm5
4,10401	1,27E-05	7,27235	3,79E-04	ANKRD46	Q86W74	Ankyrin repeat domain-containing protein 46
5,22209	2,49E-07	7,64966	3,95E-04	C19orf27	Q96GS6-2	Abhydrolase domain-containing protein FAM108A1
6,81918	3,78E-18	8,47748	4,11E-04	SAP62	Q15428	SF3a66
2,92932	7,45E-142	9,50864	4,15E-04	SAP61	Q12874	SF3a60
5,07866	3,03E-06	7,30593	5,55E-04	BRI3	O95415	Brain protein I3
4,10706	1,97E-101	8,62822	6,34E-04	KIAA1321	Q7Z417	82 kDa FMRP-interacting protein
3,86299	2,50E-05	6,78708	7,38E-04	SNX12	Q9UMY4	Sorting nexin-12
4,92716	3,13E-03	7,41581	7,86E-04	LSM4	Q9Y4Z0	Glycine-rich protein
4,88343	1,51E-14	7,54209	8,68E-04	FN14	Q9NP84	Fibroblast growth factor-inducible immediate-early response protein 14
3,98084	6,46E-83	8,82558	8,81E-04	ALDA	J3KPS3	Fructose-bisphosphate aldolase A
3,86201	2,64E-20	8,62974	1,19E-03	MPPB	O75439	Beta-MPP
3,7933	2,49E-24	8,61982	1,41E-03	GLUD	P00367	Glutamate dehydrogenase 1, mitochondrial

6,05333	1,95E-27	8,30276	1,50E-03	CYC	P99999	Cytochrome c
3,75475	6,07E-74	8,92925	1,55E-03	ALDH7A1	P49419	Aldehyde dehydrogenase family 7 member A1
3,55883	4,32E-03	7,21043	1,64E-03	CCM3	Q9BUL8	Cerebral cavernous malformations 3 protein
3,55785	3,48E-04	7,26708	1,64E-03	BZRP	P30536	Mitochondrial benzodiazepine receptor
5,91233	1,92E-27	8,33125	1,87E-03	MAGOH	P61326	Protein mago nashi homolog
6,45681	1,40E-03	7,75374	1,97E-03	MAP2K1IP1	Q9UHA4	MEK-binding partner 1
6,34976	1,70E-18	7,99084	2,31E-03	C6orf28	Q9Y333	Protein G7b
6,30676	1,23E-07	7,77732	2,46E-03	HSPC119	Q9UDW1	Complex III subunit 9
2,29287	8,66E-131	9,13615	2,70E-03	ME2	P23368	Malic enzyme 2
3,3219	2,12E-22	7,00779	2,93E-03	ATP6G	O75348	Vacuolar proton pump subunit G 1
3,31805	7,24E-02	7,13271	2,96E-03	ARL5B	Q96KC2	ADP-ribosylation factor-like protein 5B
3,29707	1,67E-22	7,01397	3,11E-03	HIAT1	Q96MC6	Hippocampus abundant transcript 1 protein
6,12232	3,45E-07	7,74262	3,22E-03	GAP43	P17677-2	Axonal membrane protein GAP-43
4,26284	1,89E-03	7,69854	3,24E-03	MPDU1	O75352	Mannose-P-dolichol utilization defect 1 protein
3,24959	4,00E-03	7,13223	3,48E-03	HLC1	O95298	Complex I-B14.5b
6,06313	1,71E-05	7,97103	3,51E-03	LSM6	P62312	U6 snRNA-associated Sm-like protein LSm6
6,05288	2,54E-10	7,99493	3,56E-03	NIF3L1BP1	Q6I9Y2	Functional spliceosome-associated protein 24
3,223	9,23E-03	6,85831	3,70E-03	C18orf2	Q7LBR1	Charged multivesicular body protein 1b
3,35566	1,87E-27	8,90909	3,96E-03	BCLAF1	Q9NYF8	Bcl-2-associated transcription factor 1
3,19144	3,97E-04	7,24988	3,98E-03	EPN3	F6QWW5	EPS-15-interacting protein 3
3,16721	8,64E-04	7,15924	4,21E-03	KIAA1115	Q9UPN7	SAPS domain family member 1
2,11872	6,78E-106	9,21155	4,28E-03	QARS	P47897	Glutamine--tRNA ligase
4,10498	5,04E-05	7,59647	4,43E-03	TTN	Q8WZ42-8	Connectin
5,32607	3,69E-10	8,42379	4,52E-03	ETFB	P38117-2	Electron transfer flavoprotein subunit beta
3,29315	9,07E-119	8,66849	4,55E-03	ACAT	P24752	Acetoacetyl-CoA thiolase
3,29044	1,91E-56	8,64715	4,58E-03	EBP1	Q9UQ80	Cell cycle protein p38-2G4 homolog
5,8402	2,52E-09	8,05888	4,80E-03	HSPC114	Q9Y5S9	Binder of OVCA1-1
3,25983	6,09E-57	8,90697	4,90E-03	P53	P04637	Antigen NY-CO-13
2,05592	3,32E-57	9,11561	5,03E-03	BAP135	P78347	Bruton tyrosine kinase-associated protein 135
5,79668	5,09E-07	7,99257	5,09E-03	THOC3	Q96J01	hTREX45
3,05457	2,39E-05	7,19195	5,44E-03	NEXN	Q0ZGT2	F-actin-binding protein
3,15304	2,11E-148	8,87237	6,17E-03	UQCRC2	P22695	Complex III subunit 2
2,98978	7,66E-03	7,19287	6,28E-03	ASCC2	B1AH60	Activating signal cointegrator 1 complex subunit 2
2,97224	3,05E-27	7,0454	6,53E-03	RAB6B	Q9NRW1	Ras-related protein Rab-6B
3,8955	1,66E-05	7,57731	6,58E-03	JTK5A	P34925-2	Tyrosine-protein kinase RYK
3,89146	2,20E-08	7,47293	6,63E-03	ATP6V1H	Q9UI12	Nef-binding protein 1
3,88441	8,55E-03	7,63737	6,72E-03	TXNDC17	Q9BRA2	14 kDa thioredoxin-related protein
5,55456	4,38E-03	7,88054	7,05E-03	LSM3	P62310	U6 snRNA-associated Sm-like protein LSm3

1,91106	5,21E-130	9,59145	7,21E-03	DBN1	A8MV58	Putative uncharacterized protein DBN1
3,07754	6,15E-11	8,75721	7,24E-03	DAD1	P61803	Defender against cell death 1
4,98854	8,84E-05	8,27969	7,25E-03	NDUFA8	P51970	Complex I-19kD
3,07372	7,50E-18	8,53145	7,30E-03	GLUR	P00390	Glutathione reductase, mitochondrial
1,90433	9,14E-21	9,31035	7,33E-03	hCG_2001850	Q32Q12	Nucleoside diphosphate kinase
1,87883	4,42E-259	9,62782	7,80E-03	SNRPA1	P09661	U2 small nuclear ribonucleoprotein A
3,79063	2,16E-05	7,48766	7,98E-03	GGH	Q92820	Conjugase
2,97973	1,25E-41	8,6238	8,86E-03	NDUFS1	P28331-2	Complex I-75kD
4,81696	1,58E-02	8,37568	9,13E-03		H0Y670	
2,75734	4,85E-09	7,23739	1,03E-02	SOD1	P00441	Superoxide dismutase [Cu-Zn]
2,89509	3,77E-113	8,76907	1,05E-02	ACTR3	P61158	Actin-like protein 3
4,67305	6,09E-10	8,3582	1,10E-02	ADK2	P54819	Adenylate kinase 2, mitochondrial
2,85157	1,56E-18	8,65379	1,15E-02	C12orf8	P30040	Endoplasmic reticulum resident protein 28
2,70029	3,09E-03	7,06524	1,16E-02	RP11-545E17.12-003	Q96GR4-3	Zinc finger, DHHC-type containing 12
4,60682	8,28E-19	8,3827	1,20E-02	PROS27	G3V5Z7	27 kDa prosomal protein
4,60427	4,47E-03	8,35034	1,20E-02	CDO1	Q16878	Cysteine dioxygenase type 1
5,13251	3,91E-09	7,86207	1,21E-02	PEX14	O75381	Peroxin-14
3,55153	2,03E-03	7,57104	1,22E-02	SPT3	O75486	SPT3-like protein
2,80311	1,39E-57	8,76926	1,26E-02	C22orf19	Q13769	Functional spliceosome-associated protein 79
3,51482	3,99E-08	7,50174	1,29E-02	EPN2	O95208	EPS-15-interacting protein 2
5,07639	4,72E-03	7,90462	1,30E-02	Nbla11189	Q9BSR8	Protein YIPF4
1,65445	1,29E-53	9,2223	1,32E-02	hCG_39182	A7YIJ8	Radixin isoform b
1,64947	6,16E-106	9,3293	1,33E-02	DDX48	P38919	ATP-dependent RNA helicase DDX48
2,60402	3,53E-07	7,17834	1,41E-02	SDF2L1	Q9HCN8	PWP1-interacting protein 8
3,442	9,15E-04	7,72908	1,46E-02	D3S1231E	B4DXJ1	cDNA FLJ56334, highly similar to SEC13-related protein
2,55086	9,68E-13	6,455	1,57E-02	BTF3	P20290	RNA polymerase B transcription factor 3
3,3772	5,58E-04	7,29953	1,63E-02	C6orf120	J3KQ97	UPF0669 protein C6orf120
1,53972	2,12E-154	9,1365	1,70E-02	VCP	P55072	15S Mg(2+)-ATPase p97 subunit
1,539	2,06E-177	9,10992	1,70E-02	CORO1C	A7MAP1	Coronin-1C_i3 protein
4,31299	2,25E-53	8,35944	1,73E-02	DHRS8	Q8NBQ5	17-beta-hydroxysteroid dehydrogenase 11
4,27672	2,62E-30	8,16152	1,81E-02	PYCR2	Q96C36	Pyrroline-5-carboxylate reductase 2
4,7938	3,67E-07	7,90116	1,81E-02	ACOT13	Q9NPJ3	Acyl-coenzyme A thioesterase 13
4,27281	4,40E-07	8,34739	1,82E-02	CPO	P36551	Coproporphyrinogen-III oxidase, mitochondrial
1,50639	1,51E-29	9,12031	1,83E-02	C1orf8	Q9BXS4	Liver membrane-bound protein
2,46794	5,85E-03	6,55302	1,84E-02	DIRC2	Q96SL1	Disrupted in renal cancer protein 2
2,57601	8,83E-32	8,55563	1,94E-02	SUCLG2	Q96I99	GTP-specific succinyl-CoA synthetase subunit beta
3,22815	5,11E-03	7,52298	2,08E-02	GCSH	P23434	Glycine cleavage system H protein, mitochondrial

4,15581	2,50E-38	8,46705	2,09E-02	HPRT	P00492	Hypoxanthine-guanine phosphoribosyltransferase
2,37266	9,05E-03	6,77243	2,21E-02	SECTM1	Q8WVN6	Protein K12
2,50177	3,71E-35	8,91995	2,22E-02	THRAP3	Q9Y2W1	Thyroid hormone receptor-associated protein 3
3,17761	1,09E-04	7,63304	2,25E-02	C14orf87	Q86SX6	Glutaredoxin-related protein 5, mitochondrial
2,35878	1,63E-06	6,60762	2,26E-02	SDC4	P31431	Amphiglycan
1,40397	2,69E-229	9,59359	2,27E-02	ATP5B	P06576	ATP synthase subunit beta, mitochondrial
1,40361	1,87E-64	9,52492	2,27E-02	BAT1	F8VQ10	56 kDa U2AF65-associated protein
3,16635	3,33E-08	7,43345	2,29E-02	GNA14	O95837	Guanine nucleotide-binding protein subunit alpha-14
3,16188	3,87E-07	7,40922	2,30E-02	LIN7C	Q9NUP9	Mammalian lin-seven protein 3
2,47707	9,80E-103	9,061	2,32E-02	HPR1	Q96FV9	hTREX84
4,05929	4,85E-09	8,24259	2,34E-02	IDH3A	P50213	Isocitrate dehydrogenase [NAD] subunit alpha, mitochondrial
2,33609	1,59E-02	7,21018	2,36E-02	FABP5	Q01469	Epidermal-type fatty acid-binding protein
2,45319	7,47E-55	8,72385	2,42E-02	CXorf3	Q8NI27	hTREX120
4,50569	2,02E-37	8,04906	2,52E-02	ANP32B	Q92688	Acidic leucine-rich nuclear phosphoprotein 32 family member B
3,10018	1,80E-02	7,56618	2,54E-02	WHIP	Q96S55	ATPase WRNIP1
3,98298	5,79E-13	8,48173	2,56E-02	PCNA	P12004	Cyclin
2,2737	9,44E-03	6,39503	2,65E-02	KIAA0257	Q92545	Protein RW1
3,9492	3,74E-33	8,19056	2,66E-02	LETM1	O95202	LETM1 and EF-hand domain-containing protein 1, mitochondrial
1,32349	1,96E-197	9,11123	2,68E-02	C20orf14	O94906	Pre-mRNA-processing factor 6
2,38742	6,77E-117	8,56886	2,72E-02	ECHS1	P30084	Enoyl-CoA hydratase 1
3,03678	4,02E-06	7,72447	2,80E-02	CDK4	P11802	Cell division protein kinase 4
3,9014	1,41E-23	8,48427	2,81E-02	ACADM	Q5T4U5	Acyl-Coenzyme A dehydrogenase, C-4 to C-12 straight chain
3,89118	4,31E-04	8,15272	2,84E-02	DER1	Q9BUN8	Degradation in endoplasmic reticulum protein 1
2,23258	4,53E-13	6,83139	2,85E-02	FAM108C1	Q6PCB6	Abhydrolase domain-containing protein FAM108C1
2,22965	1,63E-03	6,98397	2,87E-02	MER	Q12866	Proto-oncogene c-Mer
2,22028	1,17E-03	7,22889	2,91E-02	SGMS2	Q8NHU3	Phosphatidylcholine:ceramide cholinephosphotransferase 2
3,00662	6,70E-05	7,57885	2,93E-02	TM9SF1	E9PSI1	MP70 protein family member
2,21562	3,13E-03	6,64125	2,94E-02	ARFRP1	Q13795	ADP-ribosylation factor-related protein 1
2,21382	1,25E-05	6,94675	2,95E-02	DRIP92	Q9Y2X0	Mediator complex subunit 16
2,32915	1,99E-34	8,79709	3,01E-02	ACADVL	F5H2A9	Very long-chain specific acyl-CoA dehydrogenase, mitochondrial
3,82748	4,33E-21	8,24239	3,05E-02	ATP6E	P36543	Vacuolar proton pump subunit E 1

3,80811	1,00E-24	8,15555	3,12E-02	HSPC124	Q9H2U2-2	Inorganic pyrophosphatase 2, mitochondrial
4,30421	1,86E-11	8,0136	3,14E-02	GOSR1	O95249	28 kDa cis-Golgi SNARE p28
4,30009	3,91E-07	7,90927	3,15E-02	SFXN1	Q9H9B4	Sideroflexin-1
2,29522	4,96E-113	8,78671	3,19E-02	FER1L3	F8W8J4	Fer-1-like protein 3
1,23662	0,00E+00	10,1904	3,19E-02	CLH17	Q00610	Clathrin heavy chain 1
2,94361	6,90E-04	7,31025	3,21E-02	CGI-141	Q9Y3E0	Golgi transport 1 homolog B
2,28748	7,82E-90	8,67041	3,23E-02	DLD	P09622	Dihydrolipoamide dehydrogenase
2,15944	3,31E-04	7,09975	3,25E-02	CERK	Q8TCT0	Acylsphingosine kinase
2,27131	4,03E-17	8,56604	3,32E-02	ACR1	P30044	Alu corepressor 1
1,20681	2,11E-136	9,32457	3,38E-02	IARS	P41252	Isoleucine--tRNA ligase
2,24077	8,11E-47	8,78309	3,49E-02	ABCD3	E7EUE1	70 kDa peroxisomal membrane protein
2,23722	1,06E-33	8,70361	3,51E-02	INPP5E	Q10713	Alpha-MPP
2,10653	9,13E-04	7,22853	3,56E-02	MTX	Q13505	Metaxin-1
3,68244	2,86E-43	8,39766	3,58E-02	IRA1	Q9BZK7	F-box-like/WD repeat-containing protein TBL1XR1
4,17027	2,29E-10	7,87272	3,61E-02	RNP24	Q15363	Membrane protein p24A
2,85632	1,06E-07	7,35763	3,65E-02	GLXR	Q9UBQ7	Glyoxylate reductase/hydroxypyruvate reductase
2,85252	3,89E-03	7,50312	3,67E-02	PPT	P50897	Palmitoyl-protein hydrolase 1
3,65219	1,67E-09	8,14724	3,69E-02	DECR	Q16698	2,4-dienoyl-CoA reductase [NADPH]
3,64903	4,43E-03	8,13293	3,71E-02	KIAA0567	E5KLJ5	Dynamin-like 120 kDa protein, form S1
2,08216	9,30E-04	7,12746	3,71E-02	DYNLT1	P63172	Dynein light chain Tctex-type 1
2,83795	2,33E-04	7,30516	3,75E-02	IST1	A8KAH5	cDNA FLJ32696 fis, clone TESTI2000358
4,13197	3,63E-02	7,99647	3,76E-02	CXorf5	O75665	Oral-facial-digital syndrome 1 protein
2,8343	7,53E-21	7,63556	3,77E-02	IL1RL1L	Q13445	Interleukin-1 receptor-like 1 ligand
1,15052	7,44E-108	9,45281	3,77E-02	N4WBP5	Q9BT67	Breast cancer-associated protein SGA-1M
1,14485	3,00E-144	9,21492	3,81E-02	DREG	Q86SQ4	Developmentally regulated G-protein-coupled receptor
3,62111	2,27E-14	8,19973	3,82E-02	VAT1	Q99536	Synaptic vesicle membrane protein VAT-1 homolog
2,18568	1,68E-34	8,63781	3,83E-02	ETFA	P13804	Electron transfer flavoprotein subunit alpha, mitochondrial
4,10857	9,33E-10	7,89052	3,85E-02	DASS-38L18.1-001	Q96QC4	cDNA FLJ60820, highly similar to Homo sapiens MHC class I polypeptide-related sequence A (MICA), mRNA
3,59042	5,05E-07	8,12519	3,95E-02	DXS423E	Q14683	Sb1.8
2,04376	1,38E-04	7,20082	3,96E-02	SOD2	P04179	Superoxide dismutase [Mn], mitochondrial
1,12051	5,80E-84	9,12574	4,00E-02	GA11	P29992	Guanine nucleotide-binding protein G(y) subunit alpha
2,7735	0,00E+00	7,46343	4,11E-02	TUBA1	P68366	Alpha-tubulin 1
2,14066	3,43E-12	8,65706	4,12E-02	ACAA2	P42765	3-ketoacyl-CoA thiolase, mitochondrial

2,76387	6,84E-03	7,33258	4,17E-02	UBC12	P61081	NEDD8 carrier protein
2,13266	3,38E-08	8,65969	4,17E-02	NDUFS2	O75306	Complex I-49kD
3,53585	2,63E-05	8,21822	4,18E-02	GBAS	O75323	Glioblastoma-amplified sequence
2,75815	1,54E-02	7,5023	4,20E-02	ABHD10	Q9NUJ1	Abhydrolase domain-containing protein 10, mitochondrial
4,00886	2,76E-13	7,7432	4,26E-02	ATP6C	P21283	Vacuolar proton pump subunit C 1
1,998	2,01E-42	7,20303	4,28E-02	ARC100	F5GY88	Activator-recruited cofactor 100 kDa component
2,1071	9,02E-13	8,60011	4,35E-02	MIG10	P00558	Cell migration-inducing gene 10 protein
2,72869	2,29E-28	7,31608	4,38E-02	ATP6M	Q9Y5K8	Vacuolar proton pump subunit D
3,48393	8,32E-18	8,26487	4,41E-02	ARC21	O15145	Actin-related protein 2/3 complex subunit 3
1,97274	7,83E-04	7,04072	4,46E-02	MPST	J3KPV7	3-mercaptopyruvate sulfurtransferase
2,70406	2,14E-05	7,65473	4,53E-02	ARL10C	Q9NVJ2	ADP-ribosylation factor-like protein 10C
2,69598	1,81E-24	7,42354	4,58E-02	TYK2	P29597	Non-receptor tyrosine-protein kinase TYK2
1,94176	8,87E-03	7,12665	4,69E-02	C3orf28	Q96A26	E2-induced gene 5 protein
2,0579	2,58E-35	8,56862	4,70E-02	PKR2	P13861	cAMP-dependent protein kinase type II-alpha regulatory subunit
1,02727	1,39E-116	9,48637	4,75E-02	RARS	P54136	Arginine--tRNA ligase
1,02165	3,42E-148	9,35522	4,80E-02	HSP75	Q12931	Heat shock protein 75 kDa, mitochondrial
3,888	9,75E-05	8,0054	4,81E-02	EPHX	P07099	Epoxide hydratase
3,39303	1,81E-09	8,1758	4,85E-02	HMOX2	P30519	Heme oxygenase 2
1,01557	2,14E-27	9,37297	4,86E-02	SNRPB2	P08579	U2 small nuclear ribonucleoprotein B
1,91022	2,69E-06	7,13827	4,94E-02	HBP	Q9NRV9	Heme-binding protein 1
1,90774	7,57E-03	6,86276	4,96E-02	SIR2L3	Q9NTG7	NAD-dependent deacetylase sirtuin-3, mitochondrial
1,0021	0,00E+00	10,3535	4,98E-02	HSP60	P10809	60 kDa chaperonin

Supplementary Table S5. Label free quantification (LFQ) of 38E6 interaction partners. In the table are listed: LFQ ratios (38E6/CMV), posterior error probability (PEP), intensity, significance B value (Sig. B), Gene names, Protein IDs representing the Uniprot identification numbers and the protein names of the significant proteins binding to 38E6. Graphical representation in results Fig. 8-C.

38E6/CMV	PEP	Intensity	38E6/CMV Sig. B	Gene Names	Protein IDs	Protein Names
12,7027	1,70E-122	9,76094	4,86E-47		38E6	
8,76375	6,09E-57	8,90697	4,18E-10	P53	P04637	Antigen NY-CO-13
3,924	8,24E-278	9,53896	1,93E-07	SAP114	Q15459	SF3a120
6,35757	6,71E-31	8,98318	3,51E-06	HSPE1	P61604	10 kDa chaperonin
5,99199	1,92E-82	7,02584	5,37E-06	HSPC039	Q9Y5U9	Immediate early response 3-interacting protein 1
6,04021	4,38E-150	8,70875	9,50E-06	KIAA1481	Q8TF72	Protein Shroom3
6,0107	1,76E-94	8,87462	1,04E-05	CVAK104	Q6P3W7	Coated vesicle-associated kinase of 104 kDa
3,11766	7,45E-142	9,50864	1,20E-05	SAP61	Q12874	SF3a60
2,99617	1,90E-125	9,56785	2,11E-05	MDH2	P40926	Malate dehydrogenase, mitochondrial
5,56178	8,09E-150	9,10151	3,92E-05	SF1	Q15637-6	Mammalian branch point-binding protein
4,96885	1,75E-15	7,17886	1,18E-04		H7C0N4	
4,8977	5,57E-03	7,19731	1,43E-04	C17orf35	P17152	Protein PM1
2,54517	1,47E-249	9,35892	1,48E-04	XRN2	Q9H0D6	5-3 exoribonuclease 2
4,8185	1,38E-02	7,27316	1,78E-04	C11orf10	P61165	UPF0197 transmembrane protein C11orf10
2,49778	3,32E-57	9,11561	1,80E-04	BAP135	P78347	Bruton tyrosine kinase-associated protein 135
4,67835	2,62E-03	7,18475	2,59E-04	ATP5I	P56385	ATP synthase subunit e, mitochondrial
7,29957	3,78E-18	8,47748	2,74E-04	SAP62	Q15428	SF3a66
2,31901	6,78E-106	9,21155	3,64E-04	QARS	P47897	Glutamine--tRNA ligase
4,53979	5,64E-17	7,1697	3,71E-04	LSM5	Q9Y4Y9	U6 snRNA-associated Sm-like protein LSm5
4,70734	7,37E-28	8,58048	3,82E-04	KIAA0217	Q92615	La ribonucleoprotein domain family member 4B
2,21974	2,11E-136	9,32457	5,30E-04	IARS	P41252	Isoleucine--tRNA ligase
4,39671	1,97E-03	7,13707	5,34E-04	CCDC56	Q9Y2R0	Coiled-coil domain-containing protein 56
6,8338	2,86E-43	8,39766	6,03E-04	IRA1	Q9BZK7	F-box-like/WD repeat-containing protein TBL1XR1
6,72286	8,45E-76	8,33614	7,23E-04	ZCCHC8	Q6NZY4	Zinc finger CCHC domain-containing protein 8
4,345	1,87E-27	8,90909	9,12E-04	BCLAF1	Q9NYF8	Bcl-2-associated transcription factor 1
2,04313	6,16E-106	9,3293	1,01E-03	DDX48	P38919	ATP-dependent RNA helicase DDX48
5,36508	2,23E-26	7,6464	1,04E-03	CDKN2AIPNL	Q96HQ2	CDKN2A-interacting protein N-terminal-like protein
6,67635	2,52E-09	8,05888	1,26E-03	HSPC114	Q9Y5S9	Binder of OVCA1-1
6,33469	1,92E-27	8,33125	1,34E-03	MAGOH	P61326	Protein mago nashi homolog
4,15562	1,91E-56	8,64715	1,40E-03	EBP1	Q9UQ80	Cell cycle protein p38-2G4 homolog

4,13508	1,25E-30	8,55951	1,47E-03	NDUFA10	E7ESZ7	Complex I-42kD
6,5643	1,23E-07	7,77732	1,50E-03	HSPC119	Q9UDW1	Complex III subunit 9
6,25869	3,02E-20	8,12801	1,50E-03	CNOT4	F8VQP3	CCR4-associated factor 4
5,14623	2,09E-03	7,42545	1,58E-03	SEC61G	P60059	Protein transport protein Sec61 subunit gamma
3,94796	5,84E-95	8,6778	2,21E-03	SHMT2	P34897	Glycine hydroxymethyltransferase
3,78836	5,74E-09	6,75735	2,25E-03	C21orf51	P58511	Protein FAM165B
3,89361	3,02E-142	8,5741	2,48E-03	ATP6A1	P38606	Vacuolar ATPase isoform VA68
3,84649	1,97E-101	8,62822	2,74E-03	KIAA1321	Q7Z417	82 kDa FMRP-interacting protein
6,09745	1,70E-18	7,99084	2,99E-03	C6orf28	Q9Y333	Protein G7b
5,78917	8,84E-05	8,27969	3,01E-03	NDUFA8	P51970	Complex I-19kD
3,78228	1,45E-43	8,69873	3,14E-03	OAT	P04181	Ornithine aminotransferase, hepatic form
6,01797	1,71E-05	7,97103	3,35E-03	LSM6	P62312	U6 snRNA-associated Sm-like protein LSm6
3,55271	2,12E-22	7,00779	3,74E-03	ATP6G	O75348	Vacuolar proton pump subunit G 1
1,65172	4,42E-259	9,62782	3,75E-03	SNRPA1	P09661	U2 small nuclear ribonucleoprotein A
3,68872	2,82E-55	8,55398	3,80E-03	ACO2	A2A274	Aconitase 2, mitochondrial
4,62087	1,37E-10	7,57917	4,07E-03	SSR3	B4E2P2	cDNA FLJ52061, highly similar to Translocon-associated protein subunit gamma
5,48408	6,26E-24	8,14947	4,61E-03	CGI-31	Q9Y320	Cell proliferation-inducing gene 26 protein
4,52827	3,78E-04	7,34988	4,76E-03		Q8WVI0	UPF0640 protein
3,42972	1,67E-22	7,01397	4,83E-03	HIAT1	Q96MC6	Hippocampus abundant transcript 1 protein
4,49094	3,03E-06	7,30593	5,07E-03	BRI3	O95415	Brain protein I3
3,52242	2,11E-148	8,87237	5,30E-03	UQCRC2	P22695	Complex III subunit 2
5,33011	4,89E-04	8,40506	5,68E-03	KIAA1966	J3QR07	Putative splicing factor YT521
5,61692	1,40E-03	7,75374	5,82E-03	MAP2K1IP1	Q9UHA4	MEK-binding partner 1
3,31644	5,37E-03	7,09202	6,08E-03	199G4	Q9NW64	Pre-mRNA-splicing factor RBM22
4,36876	7,16E-06	7,32434	6,21E-03	UQBP	P14927	Complex III subunit 7
4,36722	8,22E-06	7,63276	6,23E-03	LSM8	O95777	N-alpha-acetyltransferase 38, NatC auxiliary subunit
3,26783	1,49E-15	7,19687	6,70E-03		Q70UQ0-4	
3,37571	3,68E-19	8,74904	7,04E-03	PRC1	O43663	Protein regulator of cytokinesis 1
5,47004	4,38E-03	7,88054	7,07E-03	LSM3	P62310	U6 snRNA-associated Sm-like protein LSm3
3,33242	1,25E-41	8,6238	7,64E-03	NDUFS1	P28331-2	Complex I-75kD
3,19884	2,13E-03	6,64181	7,67E-03	JAGN1	Q8N5M9	Protein jagunal homolog 1
5,39877	3,97E-08	7,81246	7,75E-03	HCC1	F8VZQ9	Cytokine-induced protein of 29 kDa
3,30556	8,13E-60	8,99234	8,04E-03	CS	O75390	Citrate synthase, mitochondrial
1,39268	2,69E-229	9,59359	8,21E-03	ATP5B	P06576	ATP synthase subunit beta, mitochondrial

3,16084	1,14E-03	7,04242	8,26E-03	JM4	O60831	PRA1 family protein 2
4,1589	6,99E-03	7,70936	8,71E-03	FAM51A1	Q9NWZ8	Gem-associated protein 8
3,26227	2,58E-35	8,56862	8,71E-03	PKR2	P13861	cAMP-dependent protein kinase type II-alpha regulatory subunit
1,35215	1,87E-64	9,52492	9,22E-03	BAT1	F8VQ10	56 kDa U2AF65-associated protein
1,34641	9,14E-21	9,31035	9,37E-03	hCG_2001850	Q32Q12	Nucleoside diphosphate kinase
4,07129	1,18E-04	7,66523	9,99E-03	CGI-124	Q9Y3C6	Peptidyl-prolyl cis-trans isomerase-like 1
1,31924	1,39E-116	9,48637	1,01E-02	RARS	P54136	Arginine--tRNA ligase
4,84647	6,56E-99	8,50745	1,06E-02	KIAA1671	Q9BY89	Uncharacterized protein KIAA1671
1,30027	5,21E-130	9,59145	1,07E-02	DBN1	A8MV58	Putative uncharacterized protein DBN1
4,02035	6,90E-04	7,31025	1,08E-02	CGI-141	Q9Y3E0	Golgi transport 1 homolog B
3,0186	4,10E-17	7,20003	1,08E-02	C6orf53	Q9P0S9	Transmembrane protein 14C
3,13428	3,24E-48	8,60766	1,10E-02	MCM3	P25205	DNA polymerase alpha holoenzyme-associated protein P1
5,1054	9,43E-14	7,77305	1,12E-02	ERS25	Q7Z7H5	Endoplasmic reticulum stress-response protein 25
5,09578	3,18E-09	7,92434	1,14E-02	EIF4E2	O60573	eIF4E-like protein 4E-LP
3,11024	3,71E-35	8,91995	1,15E-02	THRAP3	Q9Y2W1	Thyroid hormone receptor-associated protein 3
4,76335	1,95E-27	8,30276	1,17E-02	CYC	P99999	Cytochrome c
2,95714	1,56E-02	7,04356	1,21E-02	SFXN3	Q9BWM7	Sideroflexin-3
2,95415	9,38E-04	7,15576	1,22E-02	GSTK1	Q9Y2Q3-2	Glutathione S-transferase kappa 1
3,83566	1,25E-06	7,6203	1,43E-02	OMP25	P57105	Mitochondrial outer membrane protein 25
2,8652	4,32E-03	7,21043	1,43E-02	CCM3	Q9BUL8	Cerebral cavernous malformations 3 protein
4,58042	1,81E-09	8,1758	1,46E-02	HMOX2	P30519	Heme oxygenase 2
1,17753	3,37E-44	9,18053	1,49E-02	DARS	P14868	Aspartate--tRNA ligase
2,95337	6,15E-11	8,75721	1,51E-02	DAD1	P61803	Defender against cell death 1
4,85084	2,54E-10	7,99493	1,53E-02	NIF3L1BP1	Q6I9Y2	Functional spliceosome-associated protein 24
2,94006	2,64E-20	8,62974	1,55E-02	MPPB	O75439	Beta-MPP
2,9318	5,08E-36	8,9758	1,57E-02	GOT2	P00505	Aspartate aminotransferase, mitochondrial
1,15704	3,42E-148	9,35522	1,58E-02	HSP75	Q12931	Heat shock protein 75 kDa, mitochondrial
2,92153	5,02E-30	8,55332	1,60E-02	ERO1L	Q96HE7	Endoplasmic oxidoreductin-1-like protein
1,14576	8,66E-131	9,13615	1,62E-02	ME2	P23368	Malic enzyme 2
4,79258	5,09E-07	7,99257	1,64E-02	THOC3	Q96J01	hTREX45
4,78764	3,91E-09	7,86207	1,64E-02	PEX14	O75381	Peroxin-14
4,77135	4,72E-03	7,90462	1,68E-02	Nbla11189	Q9BSR8	Protein YIPF4
2,7677	1,62E-02	7,18761	1,71E-02	NDUFB7	P17568	Cell adhesion protein SQM1
2,87009	6,07E-74	8,92925	1,75E-02	ALDH7A1	P49419	Aldehyde

						dehydrogenase family 7 member A1
2,74134	5,95E-02	7,03711	1,79E-02	CGI-89	Q9Y397	Palmitoyltransferase ZDHHC9
4,39665	2,62E-30	8,16152	1,82E-02	PYCR2	Q96C36	Pyrroline-5-carboxylate reductase 2
1,10049	7,16E-76	9,37927	1,83E-02	VDAC3	F5H740	Outer mitochondrial membrane protein porin 3
1,08937	1,29E-53	9,2223	1,88E-02	hCG_39182	A7YIJ8	Radixin isoform b
4,35556	3,69E-10	8,42379	1,90E-02	ETFB	P38117-2	Electron transfer flavoprotein subunit beta
3,62722	5,04E-05	7,59647	1,93E-02	TTN	Q8WZ42-8	Connectin
4,64543	7,76E-06	7,82563	1,94E-02	RPS21	P63220	40S ribosomal protein S21
4,33184	2,25E-53	8,35944	1,96E-02	DHRS8	Q8NBQ5	17-beta-hydroxysteroid dehydrogenase 11
1,07256	2,06E-177	9,10992	1,96E-02	CORO1C	A7MAP1	Coronin-1C_i3 protein
2,68015	4,08E-04	6,8247	1,99E-02	CSTF2	E7EWR4	CF-1 64 kDa subunit
1,06417	0,00E+00	10,0419	2,01E-02	CG1	Q86UP2	CG-1 antigen
2,6731	8,54E-06	7,07313	2,01E-02	RP5-894H24.1-001	B1ALM5	Transmembrane protein 9
2,67194	7,55E-08	7,238	2,01E-02	EPT1	Q9C0D9	Ethanolaminephosphotransferase 1
4,2922	1,09E-14	8,42698	2,05E-02	KIAA1470	Q9P258	Protein RCC2
4,56078	4,50E-06	7,9301	2,13E-02	VKORC1L1	Q8N0U8	Vitamin K epoxide reductase complex subunit 1-like protein 1
2,74234	9,07E-119	8,66849	2,16E-02	ACAT	P24752	Acetoacetyl-CoA thiolase
1,03507	1,04E-91	9,19921	2,16E-02	CANX	B4DGP8	cDNA FLJ55574, highly similar to Calnexin
2,73211	6,46E-83	8,82558	2,19E-02	ALDA	J3KPS3	Fructose-bisphosphate aldolase A
1,02388	2,14E-27	9,37297	2,22E-02	SNRPB2	P08579	U2 small nuclear ribonucleoprotein B
1,02379	4,48E-133	9,2763	2,22E-02	ATP1A1	F5H3A1	Sodium pump subunit alpha-1
2,60114	3,83E-04	6,67362	2,27E-02	POLR2G	P62487	DNA-directed RNA polymerase II subunit G
3,5098	2,64E-11	7,44781	2,27E-02	HTRA2	O43464	High temperature requirement protein A2
1,00573	2,08E-189	9,38518	2,33E-02	EPRS	P07814	Bifunctional aminoacyl-tRNA synthetase
2,69422	2,49E-24	8,61982	2,33E-02	GLUD	P00367	Glutamate dehydrogenase 1, mitochondrial
2,69223	3,92E-50	8,91431	2,34E-02	DDX6	P26196	ATP-dependent RNA helicase p54
4,15662	2,34E-04	8,31416	2,38E-02	BM-007	Q9NZE8	39S ribosomal protein L35, mitochondrial
2,54977	2,56E-14	7,19601	2,47E-02	ECE1	P42892	Endothelin-converting enzyme 1
4,10283	4,31E-04	8,15272	2,53E-02	DER1	Q9BUN8	Degradation in endoplasmic reticulum protein 1
3,42629	2,09E-11	7,37433	2,55E-02	MBD2	Q9UBB5	Demethylase
3,42111	1,80E-02	7,56618	2,57E-02	WHIP	Q96S55	ATPase WRNIP1

0,964725	0,00E+00	10,0114	2,58E-02	HYRC	P78527	DNA-dependent protein kinase catalytic subunit
0,962739	6,04E-174	9,52214	2,59E-02	BAP	J3KPX7	B-cell receptor-associated protein BAP37
3,40722	1,27E-02	7,40358	2,62E-02	KIAA0016	Q15388	Mitochondrial 20 kDa outer membrane protein
2,50515	1,46E-04	6,89485	2,66E-02	CDIPT	B3KY94	cDNA FLJ16129 fis highly similar to CDP-diacylglycerol-inositol3-phosphatidyltransferase
0,943297	2,12E-154	9,1365	2,71E-02	VCP	P55072	15S Mg(2+)-ATPase p97 subunit
4,02986	2,63E-05	8,21822	2,73E-02	GBAS	O75323	Glioblastoma-amplified sequence
2,4868	2,74E-04	6,82791	2,74E-02	BTS	Q13286	Batten disease protein
4,01272	8,32E-18	8,26487	2,79E-02	ARC21	O15145	Actin-related protein 2/3 complex subunit 3
4,00599	8,28E-19	8,3827	2,81E-02	PROS27	G3V5Z7	27 kDa prosomal protein
4,31222	5,35E-20	8,06198	2,81E-02	KIAA1230	Q86W92	hSGT2
0,929025	6,55E-100	9,51968	2,81E-02	PHB	P35232	Prohibitin
2,46913	1,63E-10	7,26503	2,82E-02	SENP1	Q9P0U3	Sentrin/SUMO-specific protease SENP1
3,34561	1,89E-03	7,69854	2,84E-02	MPDU1	O75352	Mannose-P-dolichol utilization defect 1 protein
0,920861	4,23E-92	9,42467	2,87E-02	MDU1	P08195-4	4F2 cell-surface antigen heavy chain
3,33263	5,03E-03	7,37603	2,89E-02	SLC35F2	Q8IXU6	Solute carrier family 35 member F2
3,96729	2,50E-38	8,46705	2,93E-02	HPRT	P00492	Hypoxanthine-guanine phosphoribosyltransferase
4,22008	2,13E-23	7,78453	3,10E-02	KIAA0103	Q15006	Tetratricopeptide repeat protein 35
4,21117	6,32E-32	7,91628	3,13E-02	CARF	Q9NXV6	CDKN2A-interacting protein
3,2383	9,15E-04	7,72908	3,27E-02	D3S1231E	B4DXJ1	cDNA FLJ56334, highly similar to SEC13-related protein
0,854112	2,88E-107	9,90612	3,36E-02	ATAD3A	Q9NVI7-2	ATPase family AAA domain-containing protein 3A
0,852194	6,73E-245	9,4987	3,38E-02	PDIA6	Q15084-2	Protein disulfide isomerase P5
0,841658	1,79E-67	9,40678	3,46E-02	SNRPD1	P62314	Small nuclear ribonucleoprotein Sm D1
3,78978	1,12E-11	8,24932	3,53E-02	NDUFV1	P49821	Complex I-51kD
4,07352	2,41E-85	7,96619	3,61E-02	KIAA0095	H3BVG0	93 kDa nucleoporin
4,06671	3,45E-07	7,74262	3,63E-02	GAP43	P17677-2	Axonal membrane protein GAP-43
4,0625	2,02E-37	8,04906	3,65E-02	ANP32B	Q92688	Acidic leucine-rich nuclear phosphoprotein 32 family member B
4,04767	1,91E-03	7,89165	3,71E-02	ASF1B	Q9NVP2	Anti-silencing function protein 1 homolog B
2,39456	3,38E-08	8,65969	3,72E-02	NDUFS2	O75306	Complex I-49kD
2,37265	7,50E-18	8,53145	3,84E-02	GLUR	P00390	Glutathione reductase,

						mitochondrial
3,11061	2,38E-100	7,65889	3,85E-02	EEF1A2	Q05639	Elongation factor 1-alpha 2
0,791017	0,00E+00	10,3535	3,89E-02	HSP60	P10809	60 kDa chaperonin
3,68352	4,85E-09	8,24259	3,93E-02	IDH3A	P50213	Isocitrate dehydrogenase [NAD] subunit alpha, mitochondrial
3,67997	4,40E-07	8,34739	3,95E-02	CPO	P36551	Coproporphyrinogen-III oxidase, mitochondrial
3,08583	5,58E-04	7,29953	3,97E-02	C6orf120	J3KQ97	UPF0669 protein C6orf120
3,6699	3,50E-20	8,17173	3,99E-02	HIST2H2AB	Q8IUE6	Histone H2A type 2-B
3,07004	1,34E-26	7,52054	4,05E-02	KIAA1418	Q9NXE4-4	Neutral sphingomyelinase 3
2,30867	3,58E-70	8,68049	4,22E-02	SEC23A	Q15436	Protein transport protein Sec23A
3,60578	4,03E-15	8,33149	4,25E-02	TIAL1	Q01085-2	Nucleolysin TIAR
2,2985	4,03E-17	8,56604	4,28E-02	ACR1	P30044	Alu corepressor 1
3,90448	4,96E-85	8,09733	4,28E-02	MDH1	F5H098	Cytosolic malate dehydrogenase
3,58667	1,21E-32	8,26975	4,33E-02	HRIHFB2436	Q5VUA4	Endocrine regulatory protein
2,2838	1,03E-02	8,55751	4,37E-02	RPL39	P62891	60S ribosomal protein L39
3,88289	1,86E-11	8,0136	4,38E-02	GOSR1	O95249	28 kDa cis-Golgi SNARE p28
2,18412	8,46E-43	7,04171	4,40E-02	TBL1	O60907	F-box-like/WD repeat-containing protein TBL1X
3,00152	5,11E-03	7,52298	4,41E-02	GCSH	P23434	Glycine cleavage system H protein, mitochondrial
3,56522	6,09E-10	8,3582	4,43E-02	ADK2	P54819	Adenylate kinase 2, mitochondrial
3,86444	4,23E-04	8,00424	4,46E-02	ADAM9	Q13443	Cellular disintegrin-related protein
0,728565	0,00E+00	9,98268	4,48E-02	VDAC	P21796	Outer mitochondrial membrane protein porin 1
2,98467	3,87E-07	7,40922	4,50E-02	LIN7C	Q9NUP9	Mammalian lin-seven protein 3
0,726183	0,00E+00	10,0907	4,50E-02	MYH10	F8VTL3	Cellular myosin heavy chain, type B
0,722053	2,02E-75	9,18298	4,55E-02	ALDH10	P51648-2	Aldehyde dehydrogenase 10
3,52267	7,09E-11	8,29387	4,62E-02	KIAA0650	A6NHR9	Structural maintenance of chromosomes flexible hinge domain-containing protein 1
0,714552	2,72E-79	9,47384	4,62E-02	NIPSNAP1	Q9BPW8	Protein NipSnap homolog 1
2,95263	3,44E-02	7,51614	4,68E-02	NDUFB3	O43676	Complex I-B12
0,700503	0,00E+00	10,1904	4,77E-02	CLH17	Q00610	Clathrin heavy chain 1
2,11952	1,68E-06	6,66083	4,85E-02	HIST1H2BA	Q96A08	Histone H2B type 1-A
2,11683	6,22E-09	6,33383	4,87E-02	PIGL	Q9Y2B2	N-acetylglucosaminyl-phosphatidylinositol de-N-acetylase
3,44942	5,79E-13	8,48173	4,96E-02	PCNA	P12004	Cyclin

Supplementary Table S6. Label free quantification (LFQ) of differential interaction partners of LE6 and SE6. In the table are listed: LFQ ratios (LE6/SE6), posterior error probability (PEP), intensity, significance B value (Sig. B), Gene names, Protein IDs representing the Uniprot identification numbers and the protein names of the significant proteins binding to both LE6 and SE6, or exclusively LE6 or SE6. Graphical representation in results Fig. 9.

LE6/SE6	PEP	Intensity	LE6/SE6 Sig. B	Gene Names	Protein IDs	Protein Names
10,1324	1,49E-124	9,74744	4,14E-18	ACTBL2	Q562R1	Beta-actin-like protein 2
11,3192	3,80E-04	8,72328	1,02E-12	H3FA	P68431	Histone H3.1
-9,45144	6,59E-69	8,6343	1,11E-10		SE6	
-6,55435	1,90E-125	9,56785	9,04E-10	MDH2	P40926	Malate dehydrogenase, mitochondrial
6,82679	4,43E-44	9,13296	1,71E-08	FBL	P22087	34 kDa nucleolar scleroderma antigen
8,75709	1,03E-02	8,55751	3,12E-08	RPL39	P62891	60S ribosomal protein L39
-7,97383	6,71E-31	8,98318	5,71E-08	HSPE1	P61604	10 kDa chaperonin
-7,60818	3,63E-02	8,73607	2,29E-07	CASP7	P55210-2	Caspase 7, apoptosis-related cysteine peptidase
6,07051	6,01E-12	9,34756	7,65E-07	BTF2P44	Q13888	Basic transcription factor 2 44 kDa subunit
5,80357	7,67E-07	9,1554	2,62E-06	RPS29	P62273	40S ribosomal protein S29
-6,15742	8,13E-60	8,99234	3,06E-05	CS	O75390	Citrate synthase, mitochondrial
-5,3629	5,64E-17	7,1697	8,49E-05	LSM5	Q9Y4Y9	U6 snRNA-associated Sm-like protein LSm5
5,44432	3,46E-03	7,2179	1,35E-04	NOLA3	Q9NPE3	H/ACA ribonucleoprotein complex subunit 3
-5,132	1,18E-03	6,84012	1,63E-04	TMEM127	C9J4H2	Putative uncharacterized protein TMEM127
-7,26709	8,83E-07	8,17929	2,71E-04	SYBL1	P51809	Synaptobrevin-like protein 1
5,70268	6,13E-80	8,69808	2,78E-04	KIAA0179	Q14684	Ribosomal RNA processing protein 1 homolog B
5,19307	7,81E-05	7,16859	2,84E-04	GNG5	P63218	Guanine nucleotide-binding protein G(I)/G(S)/G(O) subunit gamma-5
4,9535	1,63E-03	7,04195	5,57E-04	ATP6	P00846	ATP synthase subunit a
-4,62901	7,66E-03	7,19287	6,21E-04	ASCC2	B1AH60	Activating signal cointegrator 1 complex subunit 2
7,16313	1,18E-02	8,38791	7,71E-04	IFITM3	Q01628	Interferon-induced transmembrane protein 3
5,22807	5,26E-134	8,96458	8,38E-04	KIAA0185	Q14690	NF-kappa-B-binding protein
4,68621	2,19E-13	7,09548	1,14E-03	H1F3	P16402	Histone H1.3
-6,20607	9,68E-08	7,58399	1,18E-03	UBTD1	Q9HAC8	Ubiquitin domain-containing protein 1
4,20713	8,67E-28	9,2416	1,23E-03	HME1	P31947	14-3-3 protein sigma
5,00624	7,60E-109	8,58132	1,37E-03	MKI67	P46013	Antigen KI-67
-4,74916	5,08E-36	8,9758	1,41E-03	GOT2	P00505	Aspartate aminotransferase, mitochondrial
-4,69406	5,02E-30	8,55332	1,61E-03	ERO1L	Q96HE7	Endoplasmic oxidoreductin-1-like protein
4,53126	1,46E-04	6,89485	1,70E-03	CDIPT	B3KY94	cDNA FLJ16129 fis highly similar to CDP-diacylglycerol-inositol3-phosphatidyltransferase

-4,66789	1,68E-34	8,63781	1,71E-03	ETFA	P13804	Electron transfer flavoprotein subunit alpha, mitochondrial
-4,6315	1,56E-18	8,65379	1,86E-03	C12orf8	P30040	Endoplasmic reticulum resident protein 28
6,61691	1,00E-49	8,47506	1,89E-03	SMNDC1	O75940	30 kDa splicing factor SMNrp
6,57773	3,35E-09	8,32726	2,01E-03	LMN1	P02545	70 kDa lamin
-6,14609	1,46E-12	8,42715	2,08E-03	CALU	O43852-3	Calumenin
-4,52422	4,39E-24	8,75897	2,39E-03	LONP1	P36776	Lon protease homolog, mitochondrial
4,72268	1,75E-17	8,87437	2,48E-03	COX5A	P20674	Cytochrome c oxidase polypeptide Va
-6,72801	1,71E-05	7,97103	2,50E-03	LSM6	P62312	U6 snRNA-associated Sm-like protein LSm6
-5,99833	4,33E-21	8,24239	2,67E-03	ATP6E	P36543	Vacuolar proton pump subunit E 1
6,20764	9,98E-03	7,60373	2,71E-03	CGI-108	Q9Y3B2	3-5 exoribonuclease CSL4 homolog
-4,46487	2,82E-55	8,55398	2,74E-03	ACO2	A2A274	Aconitase 2, mitochondrial
5,64784	2,50E-08	7,83426	2,90E-03	MRPL54	Q6P161	39S ribosomal protein L54, mitochondrial
-6,62986	5,22E-10	8,09384	2,92E-03	TM4SF8	O60637	Tetraspanin TM4-A
-6,59284	1,34E-03	7,9894	3,10E-03	ATP6C	P27449	Vacuolar proton pump 16 kDa proteolipid subunit
6,26069	3,54E-135	8,49328	3,27E-03	PABP3	Q9H361	Polyadenylate-binding protein 3
-6,5531	1,40E-03	7,75374	3,29E-03	MAP2K1IP1	Q9UHA4	MEK-binding partner 1
4,2415	5,39E-13	6,94077	3,48E-03	H1F2	P16403	Histone H1.2
6,16828	2,69E-33	8,36372	3,76E-03	TCEB1	Q15369	Elongin 15 kDa subunit
4,5048	1,65E-15	8,63329	3,85E-03	HSPC250	Q9P0M9	39S ribosomal protein L27, mitochondrial
-4,28016	1,20E-166	8,82929	4,13E-03	CDHF7	Q14517	Cadherin family member 7
4,14825	1,03E-02	6,38254	4,34E-03	TAF13	Q15543	Transcription initiation factor TFIID 18 kDa subunit
5,89416	2,32E-05	7,33216	4,42E-03	C12orf31	Q9BRT6	Protein LAPS18-like
-5,68055	5,36E-10	8,26152	4,45E-03	GLIF	P14174	Glycosylation-inhibiting factor
-4,2371	7,82E-90	8,67041	4,54E-03	DLD	P09622	Dihydrolipoamide dehydrogenase
4,11498	2,65E-09	7,22937	4,69E-03		P54819-6	
-4,21686	6,77E-117	8,56886	4,74E-03	ECHS1	P30084	Enoyl-CoA hydratase 1
5,33139	7,53E-70	8,00937	4,75E-03	RPL10L	F8W7C6	60S ribosomal protein L10-like
5,83257	5,34E-26	7,6445	4,86E-03	MRPL55	Q7Z7F7-2	39S ribosomal protein L55, mitochondrial
5,99174	1,55E-98	8,26236	4,88E-03	CGI-102	Q9NQT5	Exosome complex exonuclease RRP40
-5,59476	1,95E-27	8,30276	5,10E-03	CYC	P99999	Cytochrome c
3,73628	0,00E+00	10,2862	5,11E-03	G22P2	P13010	86 kDa subunit of Ku antigen
-4,14737	2,00E-52	8,8564	5,51E-03	AHSA1	O95433	Activator of 90 kDa heat shock protein ATPase homolog 1
-4,1428	2,64E-20	8,62974	5,56E-03	MPPB	O75439	Beta-MPP
-4,10423	9,02E-13	8,60011	6,03E-03	MIG10	P00558	Cell migration-inducing gene 10 protein
5,82991	3,73E-33	8,2675	6,16E-03	PCMT1	H7BY58	L-isoaspartyl protein carboxyl methyltransferase
-4,07691	6,07E-74	8,92925	6,39E-03	ALDH7A1	P49419	Aldehyde dehydrogenase family 7 member A1
-5,41876	5,79E-13	8,48173	6,68E-03	PCNA	P12004	Cyclin

-4,05056	9,07E-119	8,66849	6,75E-03	ACAT	P24752	Acetoacetyl-CoA thiolase
5,06855	4,88E-05	8,05588	7,03E-03	MCT1	P53985	Monocarboxylate transporter 1
5,72257	6,07E-13	8,26604	7,16E-03	BAF	O75531	Barrier-to-autointegration factor
-3,50326	1,17E-03	7,22889	8,22E-03	SGMS2	Q8NHU3	Phosphatidylcholine:ceramide cholinephosphotransferase 2
-5,04541	1,51E-14	7,54209	8,22E-03	FN14	Q9NP84	Fibroblast growth factor-inducible immediate-early response protein 14
4,09435	5,44E-34	8,94621	8,42E-03	BUB3	O43684	Mitotic checkpoint protein BUB3
-5,90888	2,54E-10	7,99493	8,57E-03	NIF3L1BP1	Q6I9Y2	Functional spliceosome-associated protein 24
5,58342	2,30E-11	8,27142	8,69E-03	TWISTNB	Q3B726	DNA-directed RNA polymerase I subunit RPA43
4,91767	2,06E-12	7,8117	8,76E-03	CNN3	Q15417	Calponin, acidic isoform
3,8302	9,24E-03	7,18927	8,90E-03	DPY19L1	Q2PZI1	Dpy-19-like protein 1
3,82689	8,21E-03	7,25356	8,97E-03	CHCHD6	J3QTA6	Coiled-coil-helix-coiled-coil-helix domain-containing protein 6
5,40311	9,09E-03	7,33393	9,15E-03	CYB5R3	P00387-3	Diaphorase-1
3,81342	3,77E-10	7,22978	9,23E-03	KCP2	Q8N6L1	Keratinocyte-associated protein 2
-5,85415	1,70E-18	7,99084	9,25E-03	C6orf28	Q9Y333	Protein G7b
5,53264	1,85E-20	8,30735	9,31E-03	CGI-117	Q9Y3C1	HBV pre-S2 trans-regulated protein 3
-4,95483	5,58E-04	7,29953	9,43E-03	C6orf120	J3KQ97	UPF0669 protein C6orf120
-3,88166	5,84E-95	8,6778	9,55E-03	SHMT2	P34897	Glycine hydroxymethyltransferase
5,36266	1,29E-03	7,69901	9,69E-03	MRPL34	Q9BQ48	39S ribosomal protein L34, mitochondrial
4,84288	1,83E-31	8,02865	9,74E-03	DCAF7	P61962	DDB1- and CUL4-associated factor 7
5,47086	8,65E-03	8,23414	1,01E-02	DNAJA4	Q8WW22-2	DnaJ homolog subfamily A member 4
4,80944	3,51E-43	7,76694	1,02E-02	CCDC137	I3L0U5	Coiled-coil domain-containing protein 137
-3,84445	3,65E-53	8,6911	1,03E-02	AE2	P04920	Anion exchange protein 2
-3,38217	2,12E-22	7,00779	1,05E-02	ATP6G	O75348	Vacuolar proton pump subunit G 1
4,71063	9,27E-03	7,78385	1,17E-02		F5GZ99	
3,42336	0,00E+00	9,86804	1,20E-02	PLEC1	Q15149	Hemidesmosomal protein 1
5,34314	1,08E-15	8,23634	1,20E-02	HDCMA18P	Q4G0J3	La ribonucleoprotein domain family member 7
5,30032	9,23E-07	8,31867	1,27E-02	DBP2	O60231	ATP-dependent RNA helicase #3
3,86255	1,75E-118	9,04328	1,28E-02	PAF53	Q9GZS1-2	DNA-directed RNA polymerase I subunit E
-4,7386	3,13E-03	7,41581	1,30E-02	LSM4	Q9Y4Z0	Glycine-rich protein
-3,27254	5,73E-04	7,15975	1,30E-02	CGI-84	Q9UQN3	Charged multivesicular body protein 2b
4,62893	7,88E-12	8,00243	1,31E-02	NOC4L	Q9BVI4	NOC4-like protein
-5,57053	1,03E-54	8,10724	1,37E-02	CMIP	Q8IY22	C-Maf-inducing protein
-3,24545	9,30E-04	7,12746	1,37E-02	DYNLT1	P63172	Dynein light chain Tctex-type 1
-4,91514	1,88E-15	8,37016	1,39E-02	CDC10	Q16181	CDC10 protein homolog
4,5805	5,15E-04	7,98945	1,40E-02	EDR	Q86TG7	Embryonal carcinoma differentiation-regulated protein
-2,21556	4,19E-152	9,38929	1,41E-02	A4	P05067	ABPP

-3,22653	1,28E-16	6,99954	1,42E-02	PNSC1	O95164	Membrane-anchored ubiquitin-fold protein
4,53983	3,27E-14	7,81206	1,48E-02	KIAA0117	P42696	RNA-binding motif protein 34
-3,6557	4,96E-113	8,78671	1,49E-02	FER1L3	F8W8J4	Fer-1-like protein 3
-4,867	1,41E-23	8,48427	1,49E-02	ACADM	Q5T4U5	Acyl-Coenzyme A dehydrogenase, C-4 to C-12 straight chain
-4,62579	2,33E-04	7,30516	1,53E-02	IST1	A8KAH5	cDNA FLJ32696 fis, clone TESTI2000358
4,9775	8,43E-04	7,71574	1,65E-02	HSPC283	Q9BYC8	39S ribosomal protein L32, mitochondrial
3,29517	0,00E+00	10,1705	1,66E-02	G22P1	P12956	70 kDa subunit of Ku antigen
5,08109	1,94E-20	8,40931	1,69E-02	ASH	P62993	Adapter protein GRB2
4,95385	1,14E-02	7,42962	1,70E-02	FLC3A	P60520	GABA(A) receptor-associated protein-like 2
-3,12585	3,09E-03	7,06524	1,72E-02	RP11-545E17.12-003	Q96GR4-3	Zinc finger, DHHC-type containing 12
-3,56239	1,45E-43	8,69873	1,78E-02	OAT	P04181	Ornithine aminotransferase, hepatic form
-4,51698	8,22E-06	7,63276	1,78E-02	LSM8	O95777	N-alpha-acetyltransferase 38, NatC auxiliary subunit
5,03827	1,30E-127	8,51868	1,78E-02	EBNA1BP2	H7C2Q8	EBNA1-binding protein 2
4,91179	7,40E-15	7,62185	1,79E-02	PP1201	Q969X1	Protein RECS1 homolog
4,38393	2,62E-15	7,96521	1,82E-02	C21orf70	Q9NSI2	Uncharacterized protein C21orf70
-4,48628	3,03E-06	7,30593	1,86E-02	BRI3	O95415	Brain protein I3
4,87594	1,57E-02	7,54616	1,88E-02	AIP	Q9NWT8	Aurora kinase A-interacting protein
3,44372	6,85E-04	6,91704	1,99E-02	CD2BP2	O95400	CD2 antigen cytoplasmic tail-binding protein 2
4,31484	7,76E-06	7,82563	2,00E-02	RPS21	P63220	40S ribosomal protein S21
4,82803	1,45E-11	7,31601	2,00E-02	MAK16	Q9BXY0	NNP78
-3,48681	1,99E-34	8,79709	2,04E-02	ACADVL	F5H2A9	Very long-chain specific acyl-CoA dehydrogenase, mitochondrial
-4,40983	2,20E-08	7,47293	2,07E-02	ATP6V1H	Q9UI12	Nef-binding protein 1
-3,02713	5,68E-03	7,16212	2,07E-02	SRCASM	O75674	Src-activating and signaling molecule protein
3,57742	1,97E-101	8,62822	2,07E-02	KIAA1321	Q7Z417	82 kDa FMRP-interacting protein
3,56398	7,29E-63	8,82316	2,12E-02	SALL4	Q9UJQ4	Sal-like protein 4
-4,36707	6,99E-07	7,48139	2,19E-02	BM-008	Q12974	HU-PP-1
-4,3664	2,49E-07	7,64966	2,19E-02	C19orf27	Q96GS6-2	Abhydrolase domain-containing protein FAM108A1
-2,99341	3,57E-03	7,16542	2,20E-02	IL17R	Q96F46	CDw217
-2,01703	3,00E-144	9,21492	2,21E-02	DREG	Q86SQ4	Developmentally regulated G-protein-coupled receptor
3,17136	6,05E-78	9,3369	2,25E-02	RIG	P62841	40S ribosomal protein S15
-5,18215	7,39E-30	8,11025	2,27E-02	ARC41	O15143	Actin-related protein 2/3 complex subunit 1B
3,37091	2,41E-10	7,16885	2,30E-02	KIAA1483	Q8N680	Zinc finger and BTB domain-containing protein 2
4,19647	1,16E-18	7,98034	2,33E-02	DNAJC7	Q99615	DnaJ homolog subfamily C member 7
4,70904	1,25E-06	7,6203	2,33E-02	OMP25	P57105	Mitochondrial outer membrane protein 25

-4,3198	8,61E-09	7,53728	2,34E-02	NPDC1	Q5SPY9	Neural proliferation, differentiation and control, 1
4,81125	5,92E-50	8,21307	2,36E-02	WDR36	Q8NI36	T-cell activation WD repeat-containing protein
3,35033	1,73E-03	7,07711	2,39E-02	MYO1C	Q12965	Myosin-Ic
-4,51361	1,54E-47	8,31479	2,40E-02	LRP12	Q9Y561	Low-density lipoprotein receptor-related protein 12
-2,94208	3,37E-07	7,08318	2,42E-02	ZDHHC18	Q9NUE0	Palmitoyltransferase ZDHHC18
3,13854	2,90E-55	9,26364	2,44E-02	C1orf33	Q9UKD2	mRNA turnover protein 4 homolog
-4,49011	6,09E-10	8,3582	2,47E-02	ADK2	P54819	Adenylate kinase 2, mitochondrial
4,66169	6,33E-05	7,66304	2,48E-02	MRPS12	O15235	28S ribosomal protein S12, mitochondrial
4,6563	1,18E-04	7,66523	2,50E-02	CGI-124	Q9Y3C6	Peptidyl-prolyl cis-trans isomerase-like 1
-5,08313	8,06E-27	8,11448	2,56E-02	ECH1	Q13011	Delta(3,5)-Delta(2,4)-dienoyl-CoA isomerase, mitochondrial
-3,35928	6,34E-34	8,62191	2,58E-02	CPD	O75976	Carboxypeptidase D
-1,93777	6,85E-237	9,63746	2,64E-02	APLP2	Q06481	Amyloid protein homolog
-3,33875	2,05E-23	8,67018	2,67E-02	PYGB	P11216	Glycogen phosphorylase, brain form
-1,93098	1,15E-170	9,1758	2,68E-02	TPI	P60174	Triosephosphate isomerase
3,25511	2,30E-12	7,06405	2,87E-02	hucep-1	O43159	Cerebral protein 1
3,25439	1,35E-02	6,99382	2,87E-02	DCAF13	Q9NV06	DDB1- and CUL4-associated factor 13
4,0069	4,54E-07	7,82092	2,95E-02	ASE1	O15446-2	A34.5
4,62526	5,64E-42	8,4304	2,96E-02	KIAA0112	Q15050	Ribosome biogenesis regulatory protein homolog
-4,94615	8,02E-13	8,04068	3,03E-02	VTI1	Q9UEU0	Vesicle transport through interaction with t-SNAREs homolog 1B
4,49643	3,49E-08	7,58307	3,05E-02	CHP	Q99653	Calcineurin B homolog
-4,32766	5,05E-07	8,12519	3,05E-02	DXS423E	Q14683	Sb1.8
3,9751	4,34E-21	7,7343	3,07E-02	CCNYL1	Q8N7R7	Cyclin-Y-like protein 1
-2,80453	3,13E-03	6,64125	3,08E-02	ARFRP1	Q13795	ADP-ribosylation factor-related protein 1
-4,92631	3,89E-49	7,97187	3,11E-02	BMPR2	Q13873	Bone morphogenetic protein receptor type II
4,47818	3,48E-04	7,40221	3,12E-02	AROS	Q86WX3	40S ribosomal protein S19-binding protein 1
4,46464	5,76E-03	7,31827	3,17E-02	CBP20	P52298	20 kDa nuclear cap-binding protein
4,56503	6,22E-19	8,16862	3,17E-02	KIAA0690	Q5JTH9	RRP12-like protein
-2,78437	7,88E-35	6,70791	3,19E-02	DER12	Q14542	36 kDa nucleolar protein HNP36
-3,23278	6,65E-54	8,57145	3,22E-02	COMT	P21964	Catechol O-methyltransferase
-2,77667	3,05E-27	7,0454	3,24E-02	RAB6B	Q9NRW1	Ras-related protein Rab-6B
-2,77571	1,67E-22	7,01397	3,24E-02	HIAT1	Q96MC6	Hippocampus abundant transcript 1 protein
3,91623	5,03E-22	8,09826	3,30E-02	WDR3	Q9UNX4	WD repeat-containing protein 3
4,51208	3,94E-16	8,15045	3,38E-02	DDX21	Q9NY93	ATP-dependent 61 kDa nucleolar RNA helicase
-3,18463	9,80E-103	9,061	3,50E-02	HPR1	Q96FV9	hTREX84
3,86008	1,56E-41	8,07646	3,53E-02	PPAN	C9J3F9	Putative uncharacterized protein PPAN
-3,99944	5,43E-03	7,72555	3,56E-02	C20orf129	Q9H4H8	Protein FAM83D

3,85347	5,65E-19	8,01098	3,56E-02	ABH5	Q6P6C2-1	Alkylated DNA repair protein alkB homolog 5
3,23246	2,24E-67	8,96215	3,59E-02	KIAA0052	P42285	ATP-dependent helicase SKIV2L2
-3,98749	3,33E-08	7,43345	3,61E-02	GNA14	O95837	Guanine nucleotide-binding protein subunit alpha-14
4,33895	2,73E-04	7,70762	3,69E-02	KPNA3	O00505	Importin alpha Q2
3,11807	5,91E-17	6,83124	3,70E-02	RAB5	P20339	Ras-related protein Rab-5A
-2,69719	1,61E-04	7,15878	3,71E-02	ANTXR1	Q9H6X2	Anthrax toxin receptor 1
-3,14978	9,44E-09	8,53168	3,71E-02	KIAA0102	E9PI68	Microsomal signal peptidase 25 kDa subunit
4,31875	1,16E-07	7,69045	3,78E-02	CCNT1	O60563	Cyclin-T1
3,78641	3,34E-06	7,80493	3,86E-02	H1F5	P16401	Histone H1.5
4,3888	1,58E-02	8,37568	3,89E-02		H0Y670	
4,38486	2,46E-22	8,45171	3,91E-02	H2AFR	Q96QV6	Histone H2A type 1-A
-1,74221	1,18E-217	9,54518	3,98E-02	DNAPTP2	Q8NC42	DNA polymerase-transactivated protein 2
-2,65296	3,81E-02	7,16125	3,99E-02	RAB33B	Q9H082	Ras-related protein Rab-33B
-3,89976	2,16E-05	7,48766	4,04E-02	GGH	Q92820	Conjugase
-4,69567	3,45E-07	7,74262	4,08E-02	GAP43	P17677-2	Axonal membrane protein GAP-43
4,33421	2,83E-20	8,24082	4,14E-02	NOC2L	Q9Y3T9	NOC2-like protein
3,71983	1,78E-14	8,10531	4,17E-02	NSUN5	Q96P11-4	NOL1/NOP2/Sun domain family member 5
3,71645	1,69E-09	8,03491	4,19E-02	EDC3	Q96F86	Enhancer of mRNA-decapping protein 3
4,22559	3,24E-06	7,68891	4,22E-02	PRKAR1B	P31321	cAMP-dependent protein kinase type I-beta regulatory subunit
4,31712	1,58E-36	8,35639	4,22E-02	ADPRT2	Q9UGN5	NAD(+) ADP-ribosyltransferase 2
-2,61291	9,05E-03	6,77243	4,27E-02	SECTM1	Q8WVN6	Protein K12
4,30173	6,94E-37	8,16643	4,29E-02	GIG38	O00422	18 kDa Sin3-associated polypeptide
-4,03918	2,27E-14	8,19973	4,35E-02	VAT1	Q99536	Synaptic vesicle membrane protein VAT-1 homolog
4,284	3,63E-04	8,21846	4,38E-02	OGT	O15294	O-GlcNAc transferase subunit p110
2,87872	6,26E-74	9,16447	4,42E-02	RBM28	Q9NW13	RNA-binding motif protein 28
-1,68962	6,78E-106	9,21155	4,43E-02	QARS	P47897	Glutamine--tRNA ligase
2,87146	1,47E-249	9,35892	4,49E-02	XRN2	Q9H0D6	5-3 exoribonuclease 2
-1,6805	9,14E-21	9,31035	4,52E-02	hCG_2001850	Q32Q12	Nucleoside diphosphate kinase
-1,67717	0,00E+00	10,3535	4,55E-02	HSP60	P10809	60 kDa chaperonin
-3,02471	1,84E-133	8,69469	4,57E-02	EHD4	Q9H223	EH domain-containing protein 4
2,99814	9,64E-05	6,99799	4,59E-02	BANP	Q8N9N5	BEN domain-containing protein 1
-3,00163	2,49E-24	8,61982	4,75E-02	GLUD	P00367	Glutamate dehydrogenase 1, mitochondrial
2,84537	1,12E-40	9,23722	4,75E-02	KIAA0264	B4DRT2	cDNA FLJ54536, highly similar to Mitochondrial 28S ribosomal protein S27
4,11872	1,27E-02	7,40358	4,77E-02	KIAA0016	Q15388	Mitochondrial 20 kDa outer membrane protein
-2,5239	7,56E-09	7,04242	4,94E-02	KIAA1734	Q9C0C9	Ubiquitin carrier protein O
4,08778	1,76E-03	7,43561	4,95E-02	TAF12	Q16514	Transcription initiation factor TFIID 20/15 kDa subunits

Supplementary Table S7. List of significant proteins detected in the first LE6 SILAC experiment. From the huge list of candidate LE6 interactors, 60 proteins were sorted according to their ratios (Ratio H/L) and p-values. In the table are shown the gene names, protein IDs (Uniprot) and the protein names of proteins detected in the first LE6 experiment. Proteins are sorted by descending ratios.

Ratio H/L	p value H/L	Gene Names	Protein IDs	Protein Names
4,255274	4,92E-18		LE6	
2,631523	1,50E-03	MTA1	Q13330	Metastasis-associated protein MTA1
2,33674	1,87E-06	EIF4F	Q04637-9	Eukaryotic translation initiation factor 4 gamma 1
2,322274	5,77E-03	BRE1B	O75150	95 kDa retinoblastoma-associated protein
2,250295	7,72E-03	C1orf28	Q6P1J9	Cell division cycle protein 73 homolog
2,191878	2,94E-04	HSPC275	D6REX3	ABP125
2,175397	1,03E-02	C20orf21	Q9BYJ9	Dermatomyositis associated with cancer putative autoantigen 1
2,151794	1,13E-02	LENG5	Q9BSV6	Leukocyte receptor cluster member 5
2,10296	1,36E-02	COCA2	P40692	DNA mismatch repair protein Mlh1
2,076901	2,24E-05	ATAD3A	Q9NVI7-2	ATPase family AAA domain-containing protein 3A
2,068293	1,55E-02	LONP	Q86WA8	Lon protease-like protein 2
2,053876	1,63E-02	MEL18	R4GMX3	DNA-binding protein Mel-18
2,022368	1,83E-02	CHD4	Q14839-2	ATP-dependent helicase CHD4
1,977023	2,15E-02	ANAPC7	Q9UJX3	Anaphase-promoting complex subunit 7
1,922046	2,61E-02	EMP	E7ESC7	Cell proliferation-inducing gene 5 protein
1,901147	2,80E-02	hCG_22498	B4DWW4	cDNA FLJ55599, highly similar to DNA replication licensing factor MCM3
1,87688	3,04E-02	EIF4E2	O60573	eIF4E-like protein 4E-LP
1,835358	1,77E-04	KAP1	Q13263	KRAB-associated protein 1
1,819096	3,68E-02	OGFR	Q9NZT2	Opioid growth factor receptor
1,816477	3,71E-02	COG6	Q9Y2V7	Component of oligomeric Golgi complex 6
1,813196	3,08E-03	BAP135	P78347	Bruton tyrosine kinase-associated protein 135
1,803599	3,87E-02	HSPC024	Q9UBK9	Androgen receptor trapped clone 27 protein
1,742869	4,70E-02	C9orf10	Q9NZB2-6	Constitutive coactivator of PPAR-gamma-like protein 1
1,708894	5,48E-03	EDH17B4	P51659	17-beta-hydroxysteroid dehydrogenase 4
1,696261	5,23E-04	RBAP48	Q09028	Chromatin assembly factor 1 subunit C
1,683921	6,26E-03	CDC47	P33993	CDC47 homolog
1,682933	6,30E-03	DAP5	P78344	Death-associated protein 5
1,598079	9,77E-03	HDAC1	Q13547	Histone deacetylase 1
1,592445	1,01E-02	GTF3C3	Q9Y5Q9	General transcription factor 3C polypeptide 3
1,591201	1,01E-02	AOF2	F6S0T5	BRAF35-HDAC complex protein BHC110
1,584289	1,05E-02	A2D	Q8WWM7-3	Ataxin-2 domain protein
1,574634	1,10E-02	ALDA	P04075-2	Fructose-bisphosphate aldolase A
1,546462	1,26E-02	POLRMT	O00411	DNA-directed RNA polymerase, mitochondrial
1,52301	1,42E-02	BCG1	Q9UNF1	11B6
1,468583	2,64E-03	BAG2	O95816	BAG family molecular chaperone regulator 2
1,451752	1,99E-02	DBC1	Q8N163	Deleted in breast cancer gene 1 protein
1,440633	2,09E-02	HC9	P25789	Macropain subunit C9
1,425459	2,25E-02	EIF2G	P41091	Eukaryotic translation initiation factor 2 subunit 3
1,418244	3,67E-03	HNRNPA0	Q13151	Heterogeneous nuclear ribonucleoprotein A0
1,377179	2,79E-02	ALDH1B1	P30837	Aldehyde dehydrogenase 5
1,303284	3,85E-02	HCFC1	A6NEM2	Putative uncharacterized protein HCFC1
1,296663	3,96E-02	SND1	Q7KZF4	100 kDa coactivator
1,271067	4,41E-02	LAS1L	Q9Y4W2	Protein LAS1 homolog
1,235482	1,13E-02	HSP27	P04792	28 kDa heat shock protein
1,23493	1,13E-02	MYH9	P35579	Cellular myosin heavy chain, type A

1,225337	1,19E-02	MYH10	P35580-3	Cellular myosin heavy chain, type B
1,215057	1,27E-02	NONO	Q15233	54 kDa nuclear RNA- and DNA-binding protein
1,202574	1,36E-02	FP17425	G8JLL9	Myosin heavy chain 14
1,19415	1,43E-02	HNRPDL	O14979	AU-rich element RNA-binding factor
1,19333	1,43E-02	NUMA	Q14980	Nuclear mitotic apparatus protein 1
1,182184	1,52E-02	RPS11	P62280	40S ribosomal protein S11
1,128095	2,05E-02	EIF3E	P60228	eIF-3 p48
1,106415	2,30E-02	WHIP	Q96S55	ATPase WRNIP1
1,101112	2,37E-02	GCN1L1	Q92616	GCN1-like protein 1
1,054223	3,02E-02	NALP2	Q9NX02	NACHT, LRR and PYD domains-containing protein 2
1,052833	3,04E-02	PAB1	P11940	Polyadenylate-binding protein 1
1,011281	3,75E-02	APP1	Q13310-3	Activated-platelet protein 1
1,000937	3,95E-02	DDX2A	P60842	ATP-dependent RNA helicase eIF4A-1
0,9942901	4,08E-02	NUP107	P57740	107 kDa nucleoporin
0,9683488	4,63E-02	RPL10L	F8W7C6	60S ribosomal protein L10-like

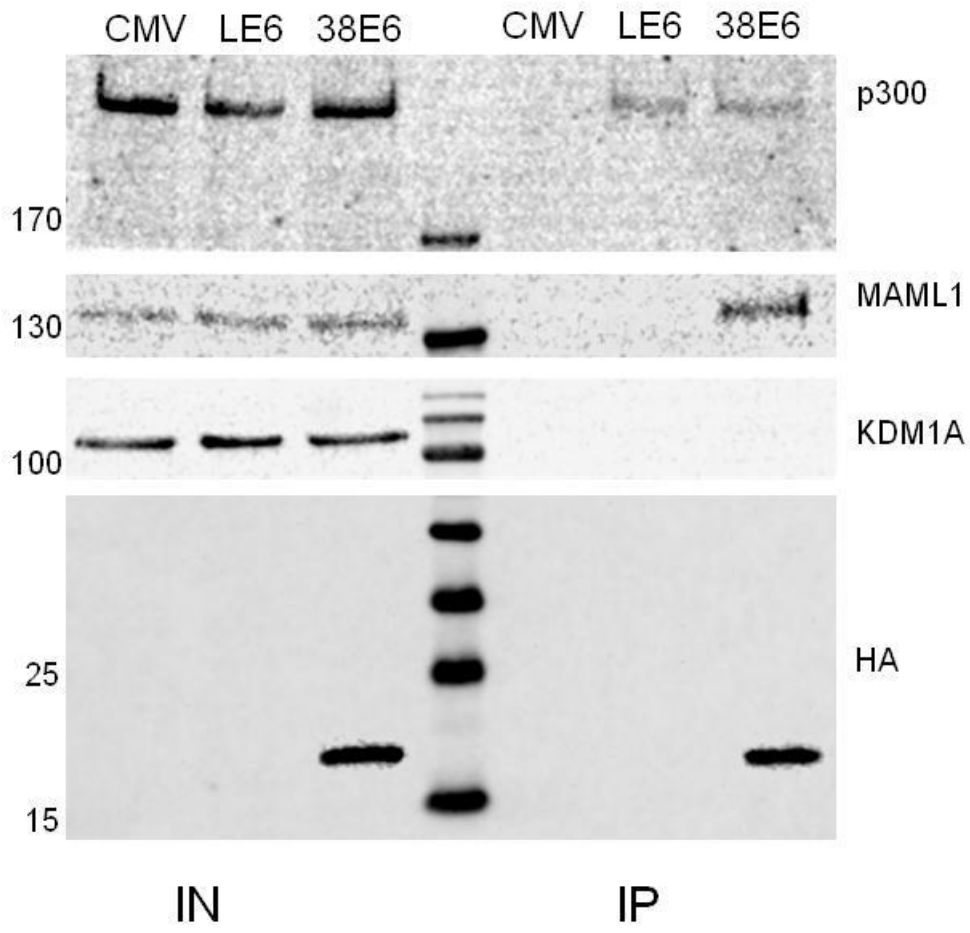

Fig. S8 Western blot to validate 17βHSD4 interaction with LE6. HA-tagged LE6 and 38E6 were tested for the binding to p300 (upper panel, IP) and MAML1 (middle upper panel, IP), that were used as positive controls for the pull down. KDM1A was not pulled down by neither LE6 nor 38E6 (central panel), as shown before. An HA signal was detected for the two proteins (lower panel) in both inputs (IN) and immunoprecipitates (IP) with the exception of LE6 and SE6 that were only visible in the IP. Molecular sizes are shown in kDa on the left. CMV: pCMV-N-Flag_Linker_HA empty vector; LE6: pCMV-N-Flag_Linker_HA-CRPVLE6; 38E6: pCMV-N-Flag_Linker_HA-HPV38E6.

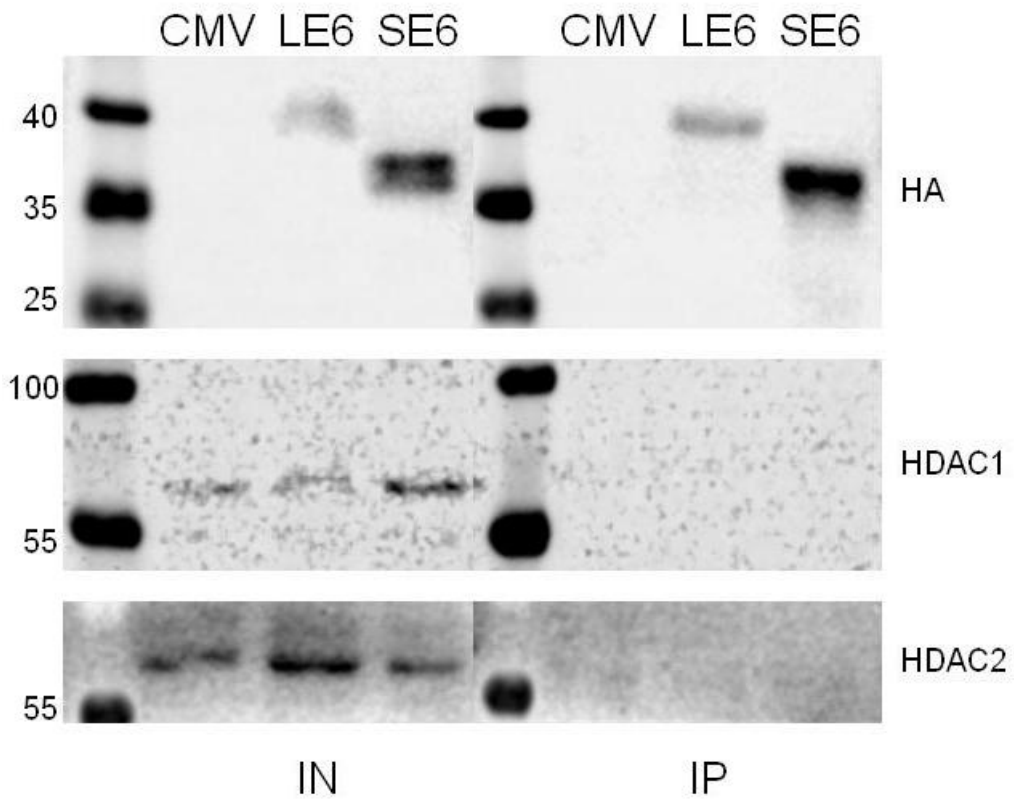

Supplementary figure S9. Western blot showing no interaction between LE6 and HDAC1 and 2. E6 HA-tagged proteins were tested for the binding to HDAC1 and HDAC2 by CoIP. KDM1A was not pulled down by LE6 and by any of the other proteins analyzed (lower panel). An HA signal was detected for all the proteins (upper panel) in both the inputs (IN) and in the immunoprecipitates (IP), whereas bands for HDAC1 and HDAC2 were detected only in the IN. Molecular sizes are shown in kDa on the left. CMV: pCMV-N-Flag_Linker_HA empty vector; LE6: pCMV-N-Flag_Linker_HA-CRPVLE6; SE6: pCMV-N-Flag_Linker_HA-CRPVSE6.

Supplementary Table S10. LE6 common hits between the two SILAC experiments. The lists of possible candidates of the first SILAC and the second SILAC experiment were compared and the common candidates were 304, sorted by descending ratios. This comparison, including also the non significant proteins, was made in order to test the reproducibility of SILAC, that in this case was 19%. In the table are shown the ratios (Ratio H/L for the first SILAC experiment and Ratio H/M for the second SILAC experiment) the p-values, the gene names, the protein IDs (Uniprot) and the protein names of all common proteins between the two SILAC experiments. Proteins are sorted by descending ratios. The significant common proteins between the two experiments are shown in results Table 7.

Ratio H/L	Ratio H/M	p-value SILAC1	p-value SILAC2	Gene Names	Protein IDs	Protein Names
4,274709	-6,63279	4,92E-18	1,10E-101		LE6	
2,33674	-1,39665	1,87E-06	1,62E-03	EIF4F	Q04637-9	Eukaryotic translation initiation factor 4 gamma 1
2,250295	-0,4113297	7,72E-03	1,63E-01	C1orf28	Q6P1J9	Cell division cycle protein 73 homolog
2,151794	-2,312796	1,13E-02	6,56E-05	LENG5	Q9BSV6	Leukocyte receptor cluster member 5
2,024213	-0,6487561	2,24E-05	3,27E-02	ATAD3A	Q9NVI7-2	ATPase family AAA domain-containing protein 3A
2,009419	-0,8581225	9,00E-02	5,26E-03	ATAD3B	Q5T9A4	ATPase family AAA domain-containing protein 3B
1,901147	-0,09525	2,80E-02	7,52E-01	hCG_22498	B4DWW4	cDNA FLJ55599, highly similar to DNA replication licensing factor MCM3
1,842456	-0,03682186	5,23E-04	7,79E-01	RBAP48	Q09028	Chromatin assembly factor 1 subunit C
1,835358	-0,7399261	1,77E-04	2,95E-02	KAP1	Q13263	KRAB-associated protein 1
1,742869	-0,6515183	4,70E-02	2,90E-01	C9orf10	Q9NZB2-6	Constitutive coactivator of PPAR-gamma-like protein 1
1,710349	-1,047428	5,21E-02	7,89E-02	CDABP0017	Q9Y5Q8-3	General transcription factor 3C polypeptide 5
1,708894	-2,919424	5,48E-03	4,13E-07	EDH17B4	P51659	17-beta-hydroxysteroid dehydrogenase 4
1,683921	-0,917243	6,26E-03	1,27E-01	CDC47	P33993	CDC47 homolog
1,682933	-1,840836	6,30E-03	4,16E-05	DAP5	P78344	Death-associated protein 5
1,644502	-0,6106313	6,37E-02	3,24E-01	MTA1L1	O94776	Metastasis-associated 1-like 1
1,598079	-0,2825615	9,77E-03	6,84E-01	HDAC1	Q13547	Histone deacetylase 1
1,597603	-0,3890544	7,32E-02	3,15E-01	NXF1	Q9UBU9	mRNA export factor TAP
1,592445	-1,219539	1,01E-02	3,93E-02	GTF3C3	Q9Y5Q9	General transcription factor 3C polypeptide 3
1,585636	-0,5412191	7,58E-02	3,88E-01	FARS	Q9Y285	CML33
1,584289	-1,645616	1,05E-02	2,31E-04	A2D	Q8WWM7-3	Ataxin-2 domain protein
1,574634	-2,18554	1,10E-02	1,86E-05	ALDA	P04075-2	Fructose-bisphosphate aldolase A
1,566718	-0,2259193	8,00E-02	5,11E-01	G3BP	Q13283	ATP-dependent DNA helicase VIII
1,537097	-0,4219598	8,71E-02	5,14E-01	FBP3	Q96I24	Far upstream element-binding protein 3
1,505637	-0,612439	9,51E-02	3,23E-01	NOC2L	Q9Y3T9	NOC2-like protein
1,471604	-1,013917	1,26E-02	1,95E-02	POLRMT	O00411	DNA-directed RNA polymerase, mitochondrial
1,470771	-0,7394202	1,05E-01	2,09E-02	CDC2L4	P50750-2	C-2K
1,468583	-0,8122322	2,64E-03	8,12E-03	BAG2	O95816	BAG family molecular chaperone regulator 2
1,464198	-0,4999322	1,07E-01	2,15E-01	ATP5L	O75964	ATP synthase subunit g, mitochondrial
1,451752	-0,8359862	1,99E-02	6,50E-03	DBC1	Q8N163	Deleted in breast cancer gene 1 protein
1,450855	-0,6110721	1,11E-01	3,24E-01	CLASP2	E7EW49	CLIP-associating protein 2

1,425459	-0,5071931	2,25E-02	8,64E-02	EIF2G	P41091	Eukaryotic translation initiation factor 2 subunit 3
1,382003	-0,6893108	1,33E-01	1,00E-01	TSPYL	Q9H0U9	Testis-specific Y-encoded-like protein 1
1,345112	-0,1239841	1,46E-01	9,57E-01	GTF2H4	Q92759	Basic transcription factor 2 52 kDa subunit
1,296663	-0,9981546	3,96E-02	2,13E-02	SND1	Q7KZF4	100 kDa coactivator
1,287591	-0,148257	1,68E-01	8,65E-01	BIG3	P61964	BMP2-induced 3-kb gene protein
1,280897	-0,05338888	1,71E-01	9,98E-01	CDA016	E7ENQ6	cDNA FLJ59191, highly similar to NADH dehydrogenase 1
1,271067	-0,8579657	4,41E-02	1,55E-01	LAS1L	Q9Y4W2	Protein LAS1 homolog
1,226077	-0,2960843	1,95E-01	4,20E-01	EIF2AK2	P19525	Eukaryotic translation initiation factor 2-alpha kinase 2
1,222619	-0,4688307	5,38E-02	2,40E-01	LUZP1	Q86V48	Leucine zipper protein 1
1,22002	-1,811422	1,13E-02	5,44E-05	HSP27	P04792	28 kDa heat shock protein
1,219401	-0,4927483	1,98E-01	2,20E-01	MAP4	E7EVA0	Microtubule-associated protein 4
1,215057	-0,1141757	1,27E-02	5,57E-01	NONO	Q15233	54 kDa nuclear RNA- and DNA-binding protein
1,194087	-0,03984416	2,10E-01	8,16E-01	PES1	O00541	Pescadillo homolog
1,192005	-1,193998	2,11E-01	4,38E-02	TARDBP	Q13148	TAR DNA-binding protein 43
1,182565	-0,03185759	6,31E-02	9,69E-01	ABCE1	P61221	2-5-oligoadenylate-binding protein
1,182184	-0,7010133	1,52E-02	2,15E-02	RPS11	P62280	40S ribosomal protein S11
1,157626	-0,1665512	2,29E-01	8,40E-01	RFC2	P35250	Activator 1 40 kDa subunit
1,131985	-1,454743	7,67E-02	1,05E-03	GNB2L1	P63244	Cell proliferation-inducing gene 21 protein
1,128095	-0,4230233	2,05E-02	1,48E-01	EIF3E	P60228	eIF-3 p48
1,115633	-0,6751664	2,51E-01	2,65E-02	PAF1	Q8N7H5	Pancreatic differentiation protein 2
1,113434	-0,9097427	2,52E-01	1,30E-01	G7A	P26640	Protein G7a
1,111566	-0,7467126	8,28E-02	7,73E-02	DDX6	P26196	ATP-dependent RNA helicase p54
1,103397	-1,162783	8,54E-02	7,97E-03	HBP	Q00341	High density lipoprotein-binding protein
1,101112	-1,056311	2,37E-02	6,50E-04	GCN1L1	Q92616	GCN1-like protein 1
1,096195	-0,6185616	8,77E-02	3,17E-01	DNAJC7	Q99615	DnaJ homolog subfamily C member 7
1,086852	-0,4734704	3,04E-02	1,12E-01	PAB1	P11940	Polyadenylate-binding protein 1
1,076285	-0,5101489	3,95E-02	9,71E-02	DDX2A	P60842	ATP-dependent RNA helicase eIF4A-1
1,054223	-0,896818	3,02E-02	3,69E-02	NALP2	Q9NX02	NACHT, LRR and PYD domains-containing protein 2
1,046002	-0,8368362	1,05E-01	5,01E-02	HMX3	I3L3A8	Modulator of non-genomic activity of estrogen receptor
1,039489	-1,862916	2,96E-01	1,39E-03	KIAA0607	Q9UBB6-3	Neurochondrin
1,022616	-0,4862263	3,75E-02	2,26E-01	APP1	Q13310-3	Activated-platelet protein 1
1,018064	-0,08074384	1,16E-01	7,28E-01	AL022311.1-001	B0QY89	Eukaryotic translation initiation factor 3, subunit E interacting protein
0,9968225	-0,9438882	1,23E-01	2,87E-02	RFC4	P35249	Activator 1 37 kDa subunit
0,9948694	-0,2337356	1,52E-01	6,74E-01	ARALAR2	Q9UJS0-2	Calcium-binding mitochondrial carrier protein Aralar2
0,9913903	-1,088838	3,26E-01	1,05E-01	BUB3	O43684	Mitotic checkpoint protein BUB3
0,986593	-0,6456156	3,30E-01	2,95E-01	BAM	Q9UQE7	Basement membrane-associated chondroitin proteoglycan
0,9769501	-0,5594943	1,21E-01	3,70E-01	EIF3G	O75821	eIF3 p42

0,9570974	-0,3924401	1,43E-01	3,12E-01	ANT3	P12236	Adenine nucleotide translocator 3
0,9557592	-0,03500262	3,50E-01	9,74E-01	ARHGEF2	V9GYM8	Rho/rac guanine nucleotide exchange factor (GEF) 2
0,9419326	-1,028322	1,50E-01	8,48E-02	OK/SW-cl.29	P04818	Thymidylate synthase
0,9382482	-0,4030458	5,34E-02	1,71E-01	D6S218E	P62269	40S ribosomal protein S18
0,9323636	-0,7194238	3,67E-01	8,72E-02	L18	Q9NXF1	Testis-expressed sequence 10 protein
0,9281239	-1,059465	1,57E-01	7,53E-02	TUBG	P23258	Gamma-1-tubulin
0,922274	-0,2418162	5,75E-02	4,90E-01	CAD	P27708	Aspartate carbamoyltransferase
0,9214364	-0,02947023	1,61E-01	8,12E-01	FAM98A	Q8NCA5	Protein FAM98A
0,9092739	-0,4550992	3,83E-01	1,26E-01	KIAA1649	Q9BY77	46 kDa DNA polymerase delta interaction protein
0,9081981	-0,1078188	1,68E-01	9,22E-01	POLR2B	P30876	DNA-directed RNA polymerase II 140 kDa polypeptide
0,9065828	-0,518949	1,69E-01	2,00E-01	RFC5	P40937	Activator 1 36 kDa subunit
0,9046575	-0,4661376	1,70E-01	2,42E-01	EIF3I	Q13347	eIF3 p36
0,9019578	-0,08133899	1,71E-01	9,59E-01	KIAA0095	Q8N1F7	93 kDa nucleoporin
0,8938282	-0,8198776	6,55E-02	8,13E-03	RPS16	P62249	40S ribosomal protein S16
0,8917302	-0,4027978	1,77E-01	2,04E-01	HRS	Q13243	Delayed-early protein HRS
0,8865891	-0,4444587	6,76E-02	2,62E-01	KIAA1835	P46060	Ran GTPase-activating protein 1
0,8831516	-0,1954012	5,63E-01	5,54E-01	SRPR	P08240	Docking protein alpha
0,8790784	-0,05752675	7,00E-02	7,66E-01	RBM14	Q96PK6	Paraspeckle protein 2
0,8684497	-2,90996	4,14E-01	1,81E-10	PYCR2	Q96C36	Pyrroline-5-carboxylate reductase 2
0,8631455	-0,2947387	1,93E-01	3,03E-01	DDX1	Q92499	ATP-dependent RNA helicase DDX1
0,8482373	-1,20553	2,02E-01	4,17E-02	hCG_19946	Q5T1Z8	Pumilio homolog 1 (Drosophila)
0,8468744	-0,9543055	2,03E-01	2,72E-02	DNAJB6	O75190	DnaJ homolog subfamily B member 6
0,8347112	-2,28736	2,11E-01	4,42E-07	PYCR1	B4DMU0	Pyrroline-5-carboxylate reductase
0,8321204	-0,7901599	4,42E-01	1,93E-01	ABCF3	Q9NUQ8	ATP-binding cassette sub-family F member 3
0,8198317	-0,2338374	4,52E-01	5,00E-01	CLINT1	Q14677-3	Clathrin interactor 1
0,8195047	-0,1525802	9,08E-02	5,59E-01	HYRC	P78527	DNA-dependent protein kinase catalytic subunit
0,8193412	-0,6007742	2,21E-01	3,33E-01	MIP224	P43686	26S protease regulatory subunit 6B
0,8152475	-0,06540045	2,24E-01	7,27E-01	C14orf166	Q9Y224	UPF0568 protein C14orf166
0,8063653	-0,4445961	4,63E-01	2,61E-01	KIAA1185	Q8N1G4	Leucine-rich repeat-containing protein 47
0,7977601	-1,186886	4,70E-01	1,89E-01	CFIM25	O43809	Cleavage and polyadenylation specificity factor 25 kDa subunit
0,7965147	-0,2053804	2,20E-01	4,53E-01	DDX47	Q9H0S4	DEAD box protein 47
0,7893537	-0,7181889	3,52E-01	2,40E-01	GOLGA2	Q08379	130 kDa cis-Golgi matrix protein
0,7861781	-0,1101371	1,42E-01	6,51E-01	OK/SW-cl.48	Q00325	Phosphate carrier protein, mitochondrial
0,7755984	-1,040794	4,88E-01	8,09E-02	CC2D1A	Q6P1N0	Coiled-coil and C2 domain-containing protein 1A
0,7724769	-1,322433	2,53E-01	2,76E-03	CDKN2	P42771-4	Cyclin-dependent kinase 4 inhibitor A
0,7700256	-0,6743833	2,55E-01	1,60E-01	BZAP45	Q7L1Q6-3	Basic leucine zipper and W2 domain-containing protein 1
0,7534333	-0,3404042	1,40E-01	5,94E-01	PSMD12	O00232	26S proteasome non-ATPase regulatory subunit 12
0,7463128	-0,1127087	2,73E-01	8,28E-01	MET	Q9NWH9	Modulator of estrogen-induced transcription

0,7349155	-0,3078764	2,81E-01	3,90E-01	ADAR	E7ENU4	136 kDa double-stranded RNA-binding protein
0,7282253	-0,1793022	2,87E-01	8,23E-01	GDI2	E7EU23	Guanosine diphosphate dissociation inhibitor 2
0,7250867	-0,0835081	5,32E-01	7,12E-01	MDS016	P82921	28S ribosomal protein S21, mitochondrial
0,724563	-0,1621698	2,90E-01	5,39E-01	POLR2E	P19388	DNA-directed RNA polymerase II 23 kDa polypeptide
0,7151905	-0,1708324	1,39E-01	5,90E-01	hCG_1784554	B3KSH1	cDNA FLJ36192 fis highly similar to Eukaryotic translation initiation factor 3 subunit 5
0,7124637	-0,2691297	2,99E-01	4,54E-01	E1BAP5	Q9BUJ2	Adenovirus early region 1B-associated protein 5
0,7010611	-0,1971202	3,09E-01	4,69E-01	C22orf28	Q9Y3I0	UPF0027 protein C22orf28
0,6927842	-0,3698369	3,16E-01	5,75E-01	DRG1	Q9Y295	Developmentally-regulated GTP-binding protein 1
0,6908193	-0,603161	3,17E-01	1,44E-01	AZI1	Q9UPN4	5-azacytidine-induced protein 1
0,6879565	-0,4525501	1,64E-01	1,31E-01	OK/SW-cl.26	P23396	40S ribosomal protein S3
0,6833821	-0,5187837	3,24E-01	2,00E-01	APG2	P34932	Heat shock 70 kDa protein 4
0,6789733	-0,6665076	3,27E-01	1,19E-01	CAPE	O95347	Chromosome-associated protein E
0,675003	-0,008870909	1,49E-01	8,46E-01	PSMD3	O43242	26S proteasome non-ATPase regulatory subunit 3
0,6738277	-0,4786678	3,88E-01	3,71E-01	SRP54	P61011	Signal recognition particle 54 kDa protein
0,6665748	-0,226088	5,84E-01	7,59E-01	NSUN2	Q08J23	NOL1/NOP2/Sun domain family member 2
0,6658475	-0,278636	1,62E-01	3,29E-01	SFRS6	Q13247	Pre-mRNA-splicing factor SRP55
0,6653928	-0,9656435	5,85E-01	1,07E-01	CYC1	P08574	Complex III subunit 4
0,663208	-0,7522183	3,41E-01	3,10E-01	DNAJ1	P25685	DnaJ homolog subfamily B member 1
0,65764	-0,3273845	1,73E-01	3,96E-01	IQGAP1	P46940	p195
0,6570912	-0,4030076	3,47E-01	3,01E-01	PRP4	O43172	PRP4 homolog
0,6546189	-0,401692	1,75E-01	1,95E-01	RPS2	P15880	40S ribosomal protein S2
0,6496614	-0,386506	2,22E-01	1,81E-01	BCLAF1	Q9NYF8	Bcl-2-associated transcription factor 1
0,6489255	-0,04149136	3,54E-01	7,92E-01	MBS	O14974	Myosin phosphatase-targeting subunit 1
0,6452405	-0,4680921	6,04E-01	1,94E-01	DIMT1	Q9UNQ2	18S rRNA dimethylase
0,6444101	-0,4137109	3,48E-01	2,90E-01	PSMC5	P62195	26S protease regulatory subunit 8
0,641546	-1,16955	6,07E-01	4,85E-02	ATP5F1	P24539	ATP synthase subunit b, mitochondrial
0,6403432	-0,07728459	3,62E-01	7,34E-01	EIF3M	Q7L2H7	Eukaryotic translation initiation factor 3 subunit M
0,6327336	-0,7722343	3,72E-01	2,04E-01	OK/SW-cl.21	P11172	OMPdecase
0,6301259	-0,1606854	9,63E-01	6,05E-01	KIF2	O00139-4	Kinesin-2
0,6295664	-0,4903345	3,72E-01	1,01E-01	KIF5B	P33176	Conventional kinesin heavy chain
0,626953	-0,5054718	1,52E-01	9,14E-02	CCG2	P62701	40S ribosomal protein S4, X isoform
0,6248028	-0,4342859	3,76E-01	1,41E-01	DDX23	Q9BUQ8	100 kDa U5 snRNP-specific protein
0,6228366	-0,1071505	1,96E-01	6,58E-01	199G4	Q9NW64	Pre-mRNA-splicing factor RBM22
0,6161695	-0,0108174	3,84E-01	8,87E-01	AP2M1	Q96CW1	Adapter-related protein complex 2 mu subunit
0,6155104	-0,8755659	6,32E-01	1,46E-01	AASDHPPT	Q9NRN7	4-phosphopantetheinyl transferase
0,6093767	-2,367359	6,38E-01	4,35E-05	EXOSC2	Q13868	Exosome complex exonuclease RRP4

0,6009358	-0,1653211	3,94E-01	5,98E-01	CKAP5	Q14008-3	Colonic and hepatic tumor over-expressed gene protein
0,5941664	-0,1480491	2,17E-01	5,12E-01	MATR3	A8MXP9	Putative uncharacterized protein MATR3
0,5941664	-0,04720429	2,52E-01	7,98E-01	KIAA0389	E7EW20	Myosin-VI
0,5918708	-0,1312816	4,08E-01	8,89E-01	COPB	P53618	Beta-coat protein
0,5869809	-0,04351208	2,24E-01	8,07E-01	ACIN1	Q9UKV3	Apoptotic chromatin condensation inducer in the nucleus
0,5847701	-0,2071779	2,24E-01	4,50E-01	ERH	P84090	Enhancer of rudimentary homolog
0,5725987	-0,1508494	6,73E-01	8,62E-01	COPB2	P35606	Beta-coat protein
0,5725017	-0,155984	2,32E-01	5,49E-01	PRPC8	Q6P2Q9	220 kDa U5 snRNP-specific protein
0,5723076	-1,515934	4,28E-01	9,75E-03	NDPKA	P15531-2	Granzyme A-activated DNase
0,5722106	-0,7975886	6,74E-01	1,88E-01	KIAA0988	Q9BTW9-4	Beta-tubulin cofactor D
0,5676428	-1,35487	4,32E-01	2,14E-02	HSD17B12	Q53GQ0	17-beta-hydroxysteroid dehydrogenase 12
0,563939	-0,1138167	2,41E-01	6,46E-01	DDX5	P17844	DEAD box protein 5
0,5582676	-0,1448873	2,26E-01	5,75E-01	ARC34	O15144	Actin-related protein 2/3 complex subunit 2
0,5530656	-0,3646635	4,48E-01	3,41E-01	FDFT1	P37268	Farnesyl-diphosphate farnesyltransferase
0,5472524	-0,8251334	6,98E-01	1,72E-01	PEX14	O75381	Peroxin-14
0,5419112	-0,4905373	3,69E-01	4,39E-01	CPR3	O60884	Cell cycle progression restoration gene 3 protein
0,5413166	-0,3156301	2,60E-01	2,63E-01	HSPA1	P08107	Heat shock 70 kDa protein 1/2
0,5408208	-0,5254133	4,60E-01	6,51E-01	ABCF2	Q75MJ1	ATP-binding cassette, sub-family F (GCN20), member 2, isoform CRA_d
0,5307699	-1,175371	4,71E-01	4,73E-02	HEATR2	Q86Y56	HEAT repeat-containing protein 2
0,5307699	-0,07512481	4,71E-01	7,37E-01	POLR2H	P52434	DNA-directed RNA polymerase II subunit H
0,5301707	-0,1294814	4,27E-01	6,08E-01	ACTR3	P61158	Actin-like protein 3
0,5216539	-0,2576488	2,76E-01	3,64E-01	BAT1	F8VQ10	56 kDa U2AF65-associated protein
0,516822	-0,08701293	2,65E-01	7,04E-01	ILF2	Q12905	Interleukin enhancer-binding factor 2
0,5155106	-0,2359087	4,88E-01	4,98E-01	ARPC1A	Q92747	Actin-related protein 2/3 complex subunit 1A
0,5139959	-0,113364	7,31E-01	6,77E-01	TCEB2	Q15370-2	Elongin 18 kDa subunit
0,5075155	-0,2477481	7,38E-01	7,30E-01	PSMC1	P62191	26S protease regulatory subunit 4
0,5073125	-1,609068	4,97E-01	3,13E-04	HSPC	O14818	Proteasome subunit alpha type-7
0,5060941	-1,124692	7,39E-01	5,83E-02	COPS4	D6RAX7	COP9 signalosome complex subunit 4
0,4897484	-0,3532843	5,16E-01	2,18E-01	PRP31	Q8WWY3	Pre-mRNA-processing factor 31
0,4833644	-0,898108	5,24E-01	3,67E-02	WDR18	Q9BV38	WD repeat-containing protein 18
0,4730076	-0,09332488	3,23E-01	7,08E-01	KIAA0727	O94832	Myosin-Id
0,4703026	-0,2797391	7,76E-01	3,26E-01	MYBBP1A	Q9BQG0-2	Myb-binding protein 1A
0,4699901	-0,03791745	3,26E-01	7,84E-01	SMU1	Q2TAY7	Smu-1 suppressor of mec-8 and unc-52 protein homolog
0,468114	-0,05389804	5,41E-01	9,98E-01	PRI	P13489	Placental ribonuclease inhibitor
0,4642501	-0,3791322	3,31E-01	3,44E-01	KIAA0221	Q92900	ATP-dependent helicase RENT1
0,458172	-0,352529	2,26E-01	3,54E-01	MTPAP	Q9NVV4-2	mtPAP
0,4528063	-0,4956745	3,59E-01	9,74E-02	PLEC1	Q15149	Hemidesmosomal protein 1
0,4512243	-0,1260923	5,61E-01	8,96E-01	CAP	Q01518	Adenylyl cyclase-associated protein 1

0,4413773	-1,106467	8,05E-01	1,13E-02	RPUSD4	Q96CM3	RNA pseudouridylate synthase domain-containing protein 4
0,4408458	-0,4284105	8,06E-01	5,07E-01	BAP28	Q9H583	HEAT repeat-containing protein 1
0,4398891	-0,3512768	9,57E-01	5,97E-01	GRWD	Q9BQ67	Glutamate-rich WD repeat-containing protein 1
0,4369081	-0,2665416	2,47E-01	3,47E-01	RPL17	P18621-3	60S ribosomal protein L17
0,4312485	-0,5221155	3,66E-01	8,19E-02	ANT2	P05141	Adenine nucleotide translocator 2
0,4292143	-1,340258	5,87E-01	2,43E-03	POH1	O00487	26S proteasome non-ATPase regulatory subunit 14
0,4269625	-1,355202	8,20E-01	2,14E-02	PPP2R5D	Q14738	PP2A B subunit isoform B56-delta
0,4247072	-0,08341635	5,92E-01	9,56E-01	FTP3	P55795	FTP-3
0,420725	-0,3207744	5,97E-01	2,64E-01	PLRG1	A8MW61	Putative uncharacterized protein PLRG1
0,418136	-0,02494212	4,02E-01	8,60E-01	FXR1	P51114	Fragile X mental retardation syndrome-related protein 1
0,4138107	-0,3001286	3,80E-01	2,96E-01	RPL24	P83731	60S ribosomal protein L24
0,4104497	-1,366429	6,10E-01	2,03E-02	AAAS	Q9NRG9	Adracalin
0,4062101	-0,1366007	4,18E-01	5,93E-01	ACTR2	P61160-2	Actin-like protein 2
0,4031586	-0,525995	3,97E-01	3,90E-01	SNX3	O60493	Protein SDP3
0,4003193	-0,2322265	4,00E-01	5,17E-01	PAB2	Q86U42	Nuclear poly(A)-binding protein 1
0,399882	-0,2695644	3,00E-01	3,42E-01	OK/SW-cl.82	P62244	40S ribosomal protein S15a
0,3923174	-1,363048	6,32E-01	2,06E-02	SLC20A3	P53007	Citrate transport protein
0,3906677	-0,08955901	4,75E-01	6,98E-01	EEF2	P13639	Elongation factor 2
0,3875831	-0,7446564	4,15E-01	7,15E-03	CDC2	P06493	Cell division control protein 2 homolog
0,3873625	-0,4609455	4,15E-01	5,74E-01	CNN2	B4DUT8	cDNA FLJ52765, highly similar to Calponin-2
0,3827226	-0,08071329	4,20E-01	7,19E-01	STAU	O95793	Double-stranded RNA-binding protein Staufen homolog 1
0,3811726	-0,1480171	4,21E-01	7,60E-01	PRO1677	Q7Z2W4	Zinc finger antiviral protein
0,3807295	-0,2289595	4,37E-01	4,10E-01	DDX48	P38919	ATP-dependent RNA helicase DDX48
0,3800644	-0,4638874	4,42E-01	1,23E-01	THRAP3	Q9Y2W1	Thyroid hormone receptor-associated protein 3
0,3792882	-0,1347621	6,48E-01	5,97E-01	MRPS25	P82663	28S ribosomal protein S25, mitochondrial
0,3703876	-0,2757514	8,80E-01	4,45E-01	PDHA1	P08559-4	PDHE1-A type I
0,3674829	-0,7622405	8,83E-01	2,10E-01	KIAA1972	Q96DX4	RING finger and SPRY domain-containing protein 1
0,3606452	-0,4768998	6,72E-01	4,53E-01	KIAA0251	H3BND4	Pyridoxal-dependent decarboxylase domain-containing protein 1
0,3598585	-0,1868858	6,73E-01	5,66E-01	PPP1CB	P62140	Serine/threonine-protein phosphatase PP1-beta catalytic subunit
0,3588463	-0,002772615	4,49E-01	9,07E-01	ARC20	P59998-3	Actin-related protein 2/3 complex subunit 4
0,3572705	-0,6722437	6,53E-01	1,08E-01	CSNK1D	H7BYT1	Casein kinase I isoform delta
0,3561438	-0,09326333	8,95E-01	9,42E-01	KIAA1101	O95747	Oxidative stress-responsive 1 protein
0,3482324	-0,3852242	6,49E-01	5,57E-01	KIAA1352	Q9P2J5	Leucine--tRNA ligase
0,3478923	-0,3659644	6,88E-01	5,80E-01	C8orf2	O94905	Endoplasmic reticulum lipid raft-associated protein 2
0,3478923	-0,1866887	4,62E-01	5,66E-01	C17orf85	Q53F19	Protein ELG
0,3434647	-0,126549	4,76E-01	3,90E-01	CAPZA2	P47755	CapZ alpha-2
0,3428961	-0,3012481	4,68E-01	4,14E-01	C1orf77	Q9Y3Y2-3	Uncharacterized protein C1orf77

0,3422133	-0,3058241	9,09E-01	6,54E-01	CYFIP1	Q7L576	Cytoplasmic FMR1-interacting protein 1
0,3325074	-0,02876362	4,81E-01	8,43E-01	KPNB1	Q14974	Importin subunit beta-1
0,3287216	-0,1014434	4,80E-01	6,30E-01	ADTB2	P63010-2	Adapter-related protein complex 2 beta subunit
0,3249257	-0,1784857	7,18E-01	8,99E-01	DEF3	P78332	Lung cancer antigen NY-LU-12
0,3221589	-0,09572784	9,31E-01	9,39E-01	CDC10	Q16181	CDC10 protein homolog
0,315798	-0,08696698	4,70E-01	7,03E-01	DDX17	H3BLZ8	DEAD box protein 17
0,3119681	-0,3964602	8,34E-01	1,78E-01	FUBP2	Q92945	Far upstream element-binding protein 2
0,3076617	-0,2632653	7,41E-01	7,09E-01	SFRS4	Q08170	Pre-mRNA-splicing factor SRP75
0,3036931	-0,4517212	5,18E-01	4,63E-01	HSP105	Q92598	Antigen NY-CO-25
0,3036931	-0,1249277	5,18E-01	6,18E-01	ADTAA	O95782	100 kDa coated vesicle protein A
0,3026407	-0,4245522	7,47E-01	3,04E-01	LDC2	Q15287	RNA-binding protein with serine-rich domain 1
0,3002995	-0,1335746	5,62E-01	5,99E-01	AQR	O60306	Intron-binding protein aquarius
0,2994792	-0,1229782	5,23E-01	6,16E-01	ASCC3L1	O75643	Activating signal cointegrator 1 complex subunit 3-like 1
0,2961931	-0,08578761	5,28E-01	6,39E-01	GIG38	O00422	18 kDa Sin3-associated polypeptide
0,2930173	-0,0323002	6,46E-01	9,70E-01	ASNS	O43776	Asparagine--tRNA ligase
0,2899525	-0,2388339	5,37E-01	3,93E-01	ASF	J3KTL2	Alternative-splicing factor 1
0,2843957	-0,2157808	5,44E-01	4,34E-01	PTB	P26599-3	57 kDa RNA-binding protein PPTB-1
0,2828548	-0,3994828	7,73E-01	5,40E-01	ERC55	F8WCY5	Calcium-binding protein ERC-55
0,2827364	-0,2969348	7,74E-01	4,19E-01	RBM4	Q9BWF3	Lark homolog
0,2766753	-0,05427247	5,54E-01	7,67E-01	DC37	P82914	28S ribosomal protein S15, mitochondrial
0,2679552	-0,03194612	5,66E-01	8,35E-01	CGI-132	Q9Y3D3	28S ribosomal protein S16, mitochondrial
0,2665168	-0,07897503	7,95E-01	9,62E-01	UNQ9342/PRO34047	Q6UXN9	Swd2
0,2515676	-0,04568457	5,93E-01	8,11E-01	HNRNPC	P07910-2	Heterogeneous nuclear ribonucleoproteins C1/C2
0,2481705	-0,09690002	9,91E-01	7,03E-01	EXOSC4	Q9NPD3	Exosome complex exonuclease RRP41
0,2454957	-0,1234968	5,98E-01	6,28E-01	RP11-373M8.1-002	E9PCT1	Putative uncharacterized protein SRRM1
0,245374	-0,04650377	5,98E-01	8,00E-01		J3QR07	
0,2451305	-0,4363928	8,24E-01	2,69E-01	CDC40	O60508	Cell division cycle 40 homolog
0,2382977	-0,09518836	9,81E-01	9,40E-01	AFAR	O43488	AFB1 aldehyde reductase 1
0,2370741	-0,3006438	6,09E-01	2,95E-01	HSP70B	P17066	Heat shock 70 kDa protein 6
0,2367069	-0,209278	9,40E-01	7,82E-01	SPNR	Q96SI9	Spermatid perinuclear RNA-binding protein
0,2342561	-0,2647378	6,13E-01	3,50E-01	HSC70	P11142	Heat shock 70 kDa protein 8
0,2261386	-0,1740678	8,50E-01	8,30E-01	PSMC6	P62333	26S protease regulatory subunit 10B
0,2258919	-0,1460842	6,25E-01	5,72E-01	CALM	H0Y7A7	Calmodulin
0,2245343	-0,0987218	6,26E-01	6,77E-01	RPL28	P46779	60S ribosomal protein L28
0,2107629	-0,2353821	9,52E-01	4,98E-01	KIAA0179	Q14684	Ribosomal RNA processing protein 1 homolog B
0,2063932	-0,5739177	8,77E-01	1,62E-01	DPM1	H0Y368	Dolichyl-phosphate mannosyltransferase polypeptide 1, catalytic subunit
0,2045164	-0,01152983	8,82E-01	9,06E-01	FHOD2	Q96PY5-3	Formin homology 2 domain-containing protein 2
0,2018848	-0,084808	8,84E-01	7,09E-01	HDCMD11P	P82673	28S ribosomal protein S28, mitochondrial

0,2016338	-0,3116137	5,63E-01	4,01E-01	HSPC206	Q8NEY8	Gastric cancer antigen Ga50
0,1991226	-0,05972046	6,25E-01	7,68E-01	OTT	Q96T37	One-twenty two protein 1
0,19131	-0,3442635	8,98E-01	3,63E-01	COPA	P53621-2	Alpha-coat protein
0,1851053	-0,2182962	9,26E-01	7,69E-01	DXS1179E	P41743	Atypical protein kinase C-lambda/iota
0,1791288	-0,1834249	6,94E-01	5,30E-01	CKAP4	Q07065	63 kDa membrane protein
0,1741506	-0,3089483	6,06E-01	2,56E-01	RPL11	P62913	60S ribosomal protein L11
0,1708224	-0,1417007	9,26E-01	5,41E-01	MRPS5	P82675	28S ribosomal protein S5, mitochondrial
0,169925	-0,1070572	9,10E-01	6,87E-01	MRL3	E7ETU7	39S ribosomal protein L3, mitochondrial
0,1655583	-0,2853896	7,14E-01	3,17E-01	ALY	E9PB61	Ally of AML-1 and LEF-1
0,1623389	-0,4681519	9,03E-01	4,63E-01	LETM1	O95202	LETM1 and EF-hand domain-containing protein 1, mitochondrial
0,153935	-0,2245869	9,50E-01	7,61E-01	ADE2	P22234-2	AIR carboxylase
0,1515991	-0,137251	9,53E-01	6,40E-01	DDX39	O00148	ATP-dependent RNA helicase DDX39
0,1474369	-0,126612	9,59E-01	5,92E-01	FRG1	Q14331	FSHD region gene 1 protein
0,1409095	-0,158526	7,52E-01	5,46E-01	KIAA0105	Q15007	Female-lethal(2)D homolog
0,1403861	-0,02211194	7,53E-01	8,60E-01	SPTAN1	A6NG51	Putative uncharacterized protein SPTAN1
0,1268407	-0,3017816	8,66E-01	6,59E-01	C10orf2	Q96RR1	Progressive external ophthalmoplegia 1 protein
0,1180938	-0,06342424	7,87E-01	7,56E-01	EPRS	P07814	Bifunctional aminoacyl-tRNA synthetase
0,1115655	-2,298176	9,91E-01	7,31E-05	PFN2	G5E9Q6	Putative uncharacterized protein PFN2
0,1050075	-0,078716	7,91E-01	5,29E-01	FMR1L2	P51116	Fragile X mental retardation syndrome-related protein 2
0,1042025	-0,23545	9,81E-01	7,46E-01	DDX36	Q9H2U1	DEAH box protein 36
0,103934	-0,2578212	9,80E-01	4,69E-01	KIF23	Q02241	Kinesin-like protein 5
0,1036654	-0,06469113	8,38E-01	7,44E-01	HNRNPF	P52597	Heterogeneous nuclear ribonucleoprotein F
0,1024567	-0,1506733	9,78E-01	6,20E-01	KIAA0052	P42285	ATP-dependent helicase SKIV2L2
0,09531686	-0,07160316	8,23E-01	7,40E-01	C3orf5	P82650	28S ribosomal protein S22, mitochondrial
0,09423606	-0,2998621	9,67E-01	3,48E-01	BCAS2	O75934	Breast carcinoma-amplified sequence 2
0,09044699	-0,1746376	7,66E-01	5,30E-01	CGI-201	Q9BZJ0	Crooked neck homolog
0,08990479	-0,4198159	9,55E-01	5,16E-01	CTNNB	P35222	Beta-catenin
0,0889556	-0,1278253	9,59E-01	6,12E-01	IK	Q13123	Cytokine IK
0,08460858	-0,213136	9,53E-01	4,39E-01	AP17	M0QYZ2	Adapter-related protein complex 2 sigma subunit
0,08351974	-0,1579786	9,52E-01	5,47E-01	PBSCF	P62306	Sm protein F
0,07915612	-0,5581129	8,45E-01	6,39E-02	KIAA0536	Q13523	PRP4 kinase
0,07587489	-0,05282013	8,15E-01	9,99E-01	EMC19	E5RJR5	Cyclin-A/CDK2-associated protein p19
0,07573799	-0,8838215	8,15E-01	1,42E-01	SAKS1	Q04323-2	SAPK substrate protein 1
0,07573799	-0,185868	9,41E-01	8,13E-01	MSS1	P35998	26S protease regulatory subunit 7
0,07423148	-0,5744547	8,57E-01	5,72E-02	DNAJ2	P31689	DnaJ homolog subfamily A member 1
0,07189995	-0,9445267	9,36E-01	2,86E-02	CDKN2	Q8N726	Cyclin-dependent kinase inhibitor 2A, isoform 4
0,07025199	-0,4081865	8,90E-01	1,59E-01	C20orf14	O94906	Pre-mRNA-processing factor 6
0,06295063	-0,3755715	8,75E-01	5,68E-01	MARS	P56192	Methionine--tRNA ligase
0,06115411	-0,04494017	9,21E-01	8,04E-01	MRPS34	C9JJ19	Putative uncharacterized protein MRPS34
0,05727703	-0,455752	9,15E-01	4,76E-01	LMN1	P02545	70 kDa lamin
0,05533457	-0,3679366	8,87E-01	2,08E-01	ATP5C	P36542	ATP synthase subunit gamma, mitochondrial

0,04865466	-0,431423	8,97E-01	3,70E-01	LDHB	P07195	LDH heart subunit
0,044464	-0,1273052	9,04E-01	8,95E-01	CRM1	O14980	Chromosome region maintenance 1 protein homolog
0,04404436	-0,2810883	9,05E-01	3,24E-01	KIAA0663	O75152	Zinc finger CCCH domain-containing protein 11A
0,0321009	-0,4759563	8,80E-01	4,54E-01	MRPP1	Q7L0Y3	HBV pre-S2 trans-regulated protein 2
0,01292609	-0,08897574	9,55E-01	7,15E-01	PSA	Q9Y617	Phosphohydroxythreonine aminotransferase
0,00776951	-0,2093114	8,47E-01	4,24E-01	C21orf101	P82932	28S ribosomal protein S6, mitochondrial
0,00532814	-0,08228566	8,44E-01	7,04E-01	KIAA0264	B4DRT2	cDNA FLJ54536, highly similar to Mitochondrial 28S ribosomal protein S27
0,00173013	-0,3759646	9,73E-01	5,68E-01	EZR	P15311	Cytovillin
0,00158601	-0,07240693	7,41E-01	7,42E-01	ADTAB	O94973-2	100 kDa coated vesicle protein C

Supplementary Table S11. Comparison between SILAC and LFQ. Proteins detected in the two SILAC experiments and the LFQ proteome analysis were overlapped to make the analysis more stringent and detect only the strong LE6 binders detected in both approaches. and Finally, SILAC results were compared to the results obtained from the label free proteome analysis to determine whether relevant proteins were common to the two approaches. In the Table of 62 proteins are shown only protein IDs (Uniprot) and protein names.

Protein IDs	Protein names
B0QY89	Eukaryotic translation initiation factor 3, subunit E interacting protein
E5RJR5	Cyclin-A/CDK2-associated protein p19
E9PCT1	Putative uncharacterized protein SRRM1
J3QR07	Putative splicing factor YT521
LE6	LE6
O00411	DNA-directed RNA polymerase, mitochondrial
O00541	Pescadillo homolog
O14818	Proteasome subunit alpha type-7
O43488	AFB1 aldehyde reductase 1
O43684	Mitotic checkpoint protein BUB3
O60306	Intron-binding protein aquarius
O60508	Cell division cycle 40 homolog
O75381	Peroxin-14
O75821	eIF3 p42
O95202	LETM1 and EF-hand domain-containing protein 1, mitochondrial
O95816	BAG family molecular chaperone regulator 2
P02545	70 kDa lamin
P04792	28 kDa heat shock protein
P04818	Thymidylate synthase
P06493	Cell division control protein 2 homolog
P08574	Complex III subunit 4
P12236	Adenine nucleotide translocator 3
P15311	Cytovillin
P23258	Gamma-1-tubulin
P26196	ATP-dependent RNA helicase p54
P30876	DNA-directed RNA polymerase II 140 kDa polypeptide
P33993	CDC47 homolog
P35222	Beta-catenin
P35249	Activator 1 37 kDa subunit
P42285	ATP-dependent helicase SKIV2L2
P46940	p195
P51116	Fragile X mental retardation syndrome-related protein 2
P53007	Citrate transport protein
P60228	eIF-3 p48
P78527	DNA-dependent protein kinase catalytic subunit
Q00341	High density lipoprotein-binding protein
Q13283	ATP-dependent DNA helicase VIII
Q14008-3	Colonic and hepatic tumor over-expressed gene protein
Q15149	Hemidesmosomal protein 1
Q15287	RNA-binding protein with serine-rich domain 1
Q2TAY7	Smu-1 suppressor of mec-8 and unc-52 protein homolog
Q53GQ0	17-beta-hydroxysteroid dehydrogenase 12
Q75MJ1	ATP-binding cassette, sub-family F (GCN20), member 2, isoform CRA_d
Q86V48	Leucine zipper protein 1
Q86Y56	HEAT repeat-containing protein 2
Q8N163	Deleted in breast cancer gene 1 protein

Q8WWM7-3	Ataxin-2 domain protein
Q92759	Basic transcription factor 2 52 kDa subunit
Q92900	ATP-dependent helicase RENT1
Q96C36	Pyrroline-5-carboxylate reductase 2
Q99615	DnaJ homolog subfamily C member 7
Q9BQG0-2	Myb-binding protein 1A
Q9BV38	WD repeat-containing protein 18
Q9NUQ8	ATP-binding cassette sub-family F member 3
Q9NVV4-2	mtPAP
Q9NYF8	Bcl-2-associated transcription factor 1
Q9NZB2-6	Constitutive coactivator of PPAR-gamma-like protein 1
Q9UBU9	mRNA export factor TAP
Q9UJS0-2	Calcium-binding mitochondrial carrier protein Aralar2
Q9Y2W1	Thyroid hormone receptor-associated protein 3
Q9Y3D3	28S ribosomal protein S16, mitochondrial
Q9Y3T9	NOC2-like protein

9. References

[1] E.-M. de Villiers, C. Fauquet, T. R. Broker, H.-U. Bernard, and H. zur Hausen, “Classification of papillomaviruses.,” *Virology*, vol. 324, no. 1, pp. 17–27, Jun. 2004.

[2] D. Bzhalava, P. Guan, S. Franceschi, J. Dillner, and G. Clifford, “A systematic review of the prevalence of mucosal and cutaneous human papillomavirus types.,” *Virology*, vol. 445, no. 1–2, pp. 224–31, Oct. 2013.

[3] I. G. Bravo and M. Félez-Sánchez, “Papillomaviruses: viral evolution, cancer and evolutionary medicine.,” *Evol. Med. public Heal.*, vol. 2015, no. 1, pp. 32–51, Jan. 2015.

[4] N. Muñoz, F. X. Bosch, S. de Sanjosé, R. Herrero, X. Castellsagué, K. V Shah, P. J. F. Snijders, and C. J. L. M. Meijer, “Epidemiologic classification of human papillomavirus types associated with cervical cancer.,” *N. Engl. J. Med.*, vol. 348, no. 6, pp. 518–27, Feb. 2003.

[5] S. de Sanjose, W. G. Quint, L. Alemany, D. T. Geraets, J. E. Klaustermeier, B. Lloveras, S. Tous, A. Felix, L. E. Bravo, H.-R. Shin, C. S. Vallejos, P. A. de Ruiz, M. A. Lima, N. Guimera, O. Clavero, M. Alejo, A. Llombart-Bosch, C. Cheng-Yang, S. A. Tatti, E. Kasamatsu, E. Iljazovic, M. Odida, R. Prado, M. Seoud, M. Grce, A. Usubutun, A. Jain, G. A. H. Suarez, L. E. Lombardi, A. Banjo, C. Menéndez, E. J. Domingo, J. Velasco, A. Nessa, S. C. B. Chichareon, Y. L. Qiao, E. Lerma, S. M. Garland, T. Sasagawa, A. Ferrera, D. Hammouda, L. Mariani, A. Pelayo, I. Steiner, E. Oliva, C. J. Meijer, W. F. Al-Jassar, E. Cruz, T. C. Wright, A. Puras, C. L. Llave, M. Tzardi, T. Agorastos, V. Garcia-Barriola, C. Clavel, J. Ordi, M. Andújar, X. Castellsagué, G. I. Sánchez, A. M. Nowakowski, J. Bornstein, N. Muñoz, F. X. Bosch, and Retrospective International Survey and HPV Time Trends Study Group, “Human papillomavirus genotype attribution in invasive cervical cancer: a retrospective cross-sectional worldwide study,” *Lancet Oncol.*, vol. 11, no. 11, pp. 1048–1056, Nov. 2010.

[6] S. Collins, S. Mazloomzadeh, H. Winter, P. Blomfield, A. Bailey, L. S. Young, and C. B. J. Woodman, “High incidence of cervical human papillomavirus infection in women during their first sexual relationship.,” *BJOG*, vol. 109, no. 1, pp. 96–8, Jan. 2002.

[7] S. Franceschi, R. Herrero, G. M. Clifford, P. J. F. Snijders, A. Arslan, P. T. H. Anh, F. X. Bosch, C. Ferreccio, N. T. Hieu, E. Lazcano-Ponce, E. Matos, M. Molano, Y.-L.

Qiao, R. Rajkumar, G. Ronco, S. de Sanjosé, H.-R. Shin, S. Sukvirach, J. O. Thomas, C. J. L. M. Meijer, and N. Muñoz, “Variations in the age-specific curves of human papillomavirus prevalence in women worldwide.,” *Int. J. Cancer*, vol. 119, no. 11, pp. 2677–84, Dec. 2006.

[8] T. Iftner, S. Eberle, A. Iftner, B. Holz, N. Banik, W. Quint, and A.-N. Straube, “Prevalence of low-risk and high-risk types of human papillomavirus and other risk factors for HPV infection in Germany within different age groups in women up to 30 years of age: an epidemiological observational study.,” *J. Med. Virol.*, vol. 82, no. 11, pp. 1928–39, Nov. 2010.

[9] A.-B. Moscicki, M. Schiffman, S. Kjaer, and L. L. Villa, “Chapter 5: Updating the natural history of HPV and anogenital cancer.,” *Vaccine*, vol. 24 Suppl 3, p. S3/42-51, Aug. 2006.

[10] A. G. Ostör, “Natural history of cervical intraepithelial neoplasia: a critical review.,” *Int. J. Gynecol. Pathol.*, vol. 12, no. 2, pp. 186–92, Apr. 1993.

[11] M. R. E. McCredie, K. J. Sharples, C. Paul, J. Baranyai, G. Medley, R. W. Jones, and D. C. G. Skegg, “Natural history of cervical neoplasia and risk of invasive cancer in women with cervical intraepithelial neoplasia 3: a retrospective cohort study.,” *Lancet. Oncol.*, vol. 9, no. 5, pp. 425–34, May 2008.

[12] S. Jeon, B. L. Allen-Hoffmann, and P. F. Lambert, “Integration of human papillomavirus type 16 into the human genome correlates with a selective growth advantage of cells.,” *J. Virol.*, vol. 69, no. 5, pp. 2989–97, May 1995.

[13] M. Dürst, L. Gissmann, H. Ikenberg, and H. zur Hausen, “A papillomavirus DNA from a cervical carcinoma and its prevalence in cancer biopsy samples from different geographic regions.,” *Proc. Natl. Acad. Sci. U. S. A.*, vol. 80, no. 12, pp. 3812–5, Jun. 1983.

[14] S. Jablonska, J. Dabrowski, and K. Jakubowicz, “Epidermodysplasia verruciformis as a model in studies on the role of papovaviruses in oncogenesis.,” *Cancer Res.*, vol. 32, no. 3, pp. 583–9, Mar. 1972.

[15] G. Orth, “Epidermodysplasia verruciformis: a model for understanding the oncogenicity of human papillomaviruses.,” *Ciba Found. Symp.*, vol. 120, pp. 157–74, Jan. 1986.

[16] M. Dubina and G. Goldenberg, “Viral-associated nonmelanoma skin cancers: a

review.," *Am. J. Dermatopathol.*, vol. 31, no. 6, pp. 561–73, Aug. 2009.

[17] B. Ö. Cakir, P. Adamson, and C. Cingi, "Epidemiology and economic burden of nonmelanoma skin cancer.," *Facial Plast. Surg. Clin. North Am.*, vol. 20, no. 4, pp. 419–22, Nov. 2012.

[18] V. Madan, J. T. Lear, and R.-M. Szeimies, "Non-melanoma skin cancer.," *Lancet*, vol. 375, no. 9715, pp. 673–85, Feb. 2010.

[19] I. Nindl, M. Gottschling, and E. Stockfleth, "Human papillomaviruses and non-melanoma skin cancer: basic virology and clinical manifestations.," *Dis. Markers*, vol. 23, no. 4, pp. 247–59, Jan. 2007.

[20] B. Aldabagh, J. G. C. Angeles, A. R. Cardones, and S. T. Arron, "Cutaneous squamous cell carcinoma and human papillomavirus: is there an association?," *Dermatol. Surg.*, vol. 39, no. 1 Pt 1, pp. 1–23, Jan. 2013.

[21] S. Euvrard, J. Kanitakis, M. Faure, and A. Claudy, "[Human papillomavirus and skin carcinoma in organ transplants. Recent studies].," *Ann. Dermatol. Venereol.*, vol. 128, no. 11, pp. 1252–5, Nov. 2001.

[22] O. Forslund, T. Iftner, K. Andersson, B. Lindelof, E. Hradil, P. Nordin, B. Stenquist, R. Kirnbauer, J. Dillner, E.-M. de Villiers, and Viraskin Study Group, "Cutaneous human papillomaviruses found in sun-exposed skin: Beta-papillomavirus species 2 predominates in squamous cell carcinoma.," *J. Infect. Dis.*, vol. 196, no. 6, pp. 876–83, Sep. 2007.

[23] A. Antonsson, "Review: antibodies to cutaneous human papillomaviruses.," *J. Med. Virol.*, vol. 84, no. 5, pp. 814–22, May 2012.

[24] S. J. Weissenborn, I. Nindl, K. Purdie, C. Harwood, C. Proby, J. Breuer, S. Majewski, H. Pfister, and U. Wieland, "Human Papillomavirus-DNA Loads in Actinic Keratoses Exceed those in Non-Melanoma Skin Cancers," *J. Invest. Dermatol.*, vol. 125, no. 1, pp. 93–97, Jul. 2005.

[25] H. Pfister, "Chapter 8: Human papillomavirus and skin cancer.," *J. Natl. Cancer Inst. Monogr.*, no. 31, pp. 52–6, Jan. 2003.

[26] H. zur Hausen, "Papillomaviruses and cancer: from basic studies to clinical application.," *Nat. Rev. Cancer*, vol. 2, no. 5, pp. 342–50, May 2002.

[27] S. Hong and L. A. Laimins, “Regulation of the life cycle of HPVs by differentiation and the DNA damage response.,” *Future Microbiol.*, vol. 8, no. 12, pp. 1547–57, Dec. 2013.

[28] M. A. Ozbun and C. Meyers, “Temporal Usage of Multiple Promoters during the Life Cycle of Human Papillomavirus Type 31b,” *J. Virol.*, vol. 72, no. 4, pp. 2715–2722, Apr. 1998.

[29] J. Doorbar, W. Quint, L. Banks, I. G. Bravo, M. Stoler, T. R. Broker, and M. A. Stanley, “The biology and life-cycle of human papillomaviruses.,” *Vaccine*, vol. 30 Suppl 5, pp. F55-70, Nov. 2012.

[30] C. Johansson and S. Schwartz, “Regulation of human papillomavirus gene expression by splicing and polyadenylation.,” *Nat. Rev. Microbiol.*, vol. 11, no. 4, pp. 239–51, Apr. 2013.

[31] J. Doorbar, “Molecular biology of human papillomavirus infection and cervical cancer.,” *Clin. Sci. (Lond).*, vol. 110, no. 5, pp. 525–41, May 2006.

[32] P. J. Masterson, M. A. Stanley, A. P. Lewis, and M. A. Romanos, “A C-Terminal Helicase Domain of the Human Papillomavirus E1 Protein Binds E2 and the DNA Polymerase alpha -Primase p68 Subunit,” *J. Virol.*, vol. 72, no. 9, pp. 7407–7419, Sep. 1998.

[33] S. Titolo, A. Pelletier, F. Sauve, K. Brault, E. Wardrop, P. W. White, A. Amin, M. G. Cordingley, and J. Archambault, “Role of the ATP-Binding Domain of the Human Papillomavirus Type 11 E1 Helicase in E2-Dependent Binding to the Origin,” *J. Virol.*, vol. 73, no. 7, pp. 5282–5293, Jul. 1999.

[34] A. A. McBride, “The papillomavirus E2 proteins.,” *Virology*, vol. 445, no. 1–2, pp. 57–79, Oct. 2013.

[35] G. Steger and S. Corbach, “Dose-dependent regulation of the early promoter of human papillomavirus type 18 by the viral E2 protein.,” *J. Virol.*, vol. 71, no. 1, pp. 50–8, Jan. 1997.

[36] A. A. McBride, “Replication and partitioning of papillomavirus genomes.,” *Adv. Virus Res.*, vol. 72, pp. 155–205, Jan. 2008.

[37] J. Doorbar, A. Parton, K. Hartley, L. Banks, T. Crook, M. Stanley, and L. Crawford,

"Detection of novel splicing patterns in a HPV16-containing keratinocyte cell line.," *Virology*, vol. 178, no. 1, pp. 254–62, Sep. 1990.

[38] L. Florin, C. Sapp, R. E. Streeck, and M. Sapp, "Assembly and translocation of papillomavirus capsid proteins.," *J. Virol.*, vol. 76, no. 19, pp. 10009–14, Oct. 2002.

[39] S. Roberts, I. Ashmole, S. M. Rookes, and P. H. Gallimore, "Mutational analysis of the human papillomavirus type 16 E1--E4 protein shows that the C terminus is dispensable for keratin cytoskeleton association but is involved in inducing disruption of the keratin filaments.," *J. Virol.*, vol. 71, no. 5, pp. 3554–62, May 1997.

[40] A. Venuti, F. Paolini, L. Nasir, A. Corteggio, S. Roperto, M. S. Campo, and G. Borzacchiello, "Papillomavirus E5: the smallest oncoprotein with many functions.," *Mol. Cancer*, vol. 10, p. 140, Jan. 2011.

[41] E. S. Hwang, T. Nottoli, and D. Dimaio, "The HPV16 E5 protein: expression, detection, and stable complex formation with transmembrane proteins in COS cells.," *Virology*, vol. 211, no. 1, pp. 227–33, Aug. 1995.

[42] K. Crusius, E. Auvinen, B. Steuer, H. Gaissert, and A. Alonso, "The human papillomavirus type 16 E5-protein modulates ligand-dependent activation of the EGF receptor family in the human epithelial cell line HaCaT.," *Exp. Cell Res.*, vol. 241, no. 1, pp. 76–83, May 1998.

[43] S. W. Straight, B. Herman, and D. J. McCance, "The E5 oncoprotein of human papillomavirus type 16 inhibits the acidification of endosomes in human keratinocytes.," *J. Virol.*, vol. 69, no. 5, pp. 3185–92, May 1995.

[44] K. Crusius, I. Rodriguez, and A. Alonso, "The human papillomavirus type 16 E5 protein modulates ERK1/2 and p38 MAP kinase activation by an EGFR-independent process in stressed human keratinocytes.," *Virus Genes*, vol. 20, no. 1, pp. 65–9, Jan. 2000.

[45] X. Wang, C. Meyers, H.-K. Wang, L. T. Chow, and Z.-M. Zheng, "Construction of a full transcription map of human papillomavirus type 18 during productive viral infection.," *J. Virol.*, vol. 85, no. 16, pp. 8080–92, Aug. 2011.

[46] A. B. Raff, A. W. Woodham, L. M. Raff, J. G. Skeate, L. Yan, D. M. Da Silva, M. Schelhaas, and W. M. Kast, "The evolving field of human papillomavirus receptor research: a review of binding and entry.," *J. Virol.*, vol. 87, no. 11, pp. 6062–72, Jun.

2013.

[47] M. Sapp and M. Bienkowska-Haba, “Viral entry mechanisms: human papillomavirus and a long journey from extracellular matrix to the nucleus.,” *FEBS J.*, vol. 276, no. 24, pp. 7206–16, Dec. 2009.

[48] C. B. Buck, P. M. Day, and B. L. Trus, “The papillomavirus major capsid protein L1.,” *Virology*, vol. 445, no. 1–2, pp. 169–74, Oct. 2013.

[49] M. Sapp and P. M. Day, “Structure, attachment and entry of polyoma- and papillomaviruses.,” *Virology*, vol. 384, no. 2, pp. 400–9, Mar. 2009.

[50] J. T. Schiller, P. M. Day, and R. C. Kines, “Current understanding of the mechanism of HPV infection.,” *Gynecol. Oncol.*, vol. 118, no. 1 Suppl, pp. S12-7, Jun. 2010.

[51] J. W. Wang and R. B. S. Roden, “L2, the minor capsid protein of papillomavirus.,” *Virology*, vol. 445, no. 1–2, pp. 175–86, Oct. 2013.

[52] N. A. Hamid, C. Brown, and K. Gaston, “The regulation of cell proliferation by the papillomavirus early proteins.,” *Cell. Mol. Life Sci.*, vol. 66, no. 10, pp. 1700–17, May 2009.

[53] M. A. Bedell, K. H. Jones, and L. A. Laimins, “The E6-E7 region of human papillomavirus type 18 is sufficient for transformation of NIH 3T3 and rat-1 cells.,” *J. Virol.*, vol. 61, no. 11, pp. 3635–40, Nov. 1987.

[54] K. H. Vousden, J. Doniger, J. A. DiPaolo, and D. R. Lowy, “The E7 open reading frame of human papillomavirus type 16 encodes a transforming gene.,” *Oncogene Res.*, vol. 3, no. 2, pp. 167–75, Sep. 1988.

[55] M. S. Barbosa and R. Schlegel, “The E6 and E7 genes of HPV-18 are sufficient for inducing two-stage in vitro transformation of human keratinocytes.,” *Oncogene*, vol. 4, no. 12, pp. 1529–32, Dec. 1989.

[56] K. Münger, W. C. Phelps, V. Bubb, P. M. Howley, and R. Schlegel, “The E6 and E7 genes of the human papillomavirus type 16 together are necessary and sufficient for transformation of primary human keratinocytes.,” *J. Virol.*, vol. 63, no. 10, pp. 4417–21, Oct. 1989.

[57] C. L. Halbert, G. W. Demers, and D. A. Galloway, “The E7 gene of human papillomavirus type 16 is sufficient for immortalization of human epithelial cells.,” *J.*

Virol., vol. 65, no. 1, pp. 473–8, Jan. 1991.

[58] O. Rozenblatt-Rosen, R. C. Deo, M. Padi, G. Adelmant, M. A. Calderwood, T. Rolland, M. Grace, A. Dricot, M. Askenazi, M. Tavares, S. J. Pevzner, F. Abderazzaq, D. Byrdsong, A.-R. Carvunis, A. A. Chen, J. Cheng, M. Correll, M. Duarte, C. Fan, M. C. Feltkamp, S. B. Ficarro, R. Franchi, B. K. Garg, N. Gulbahce, T. Hao, A. M. Holthaus, R. James, A. Korkhin, L. Litovchick, J. C. Mar, T. R. Pak, S. Rabello, R. Rubio, Y. Shen, S. Singh, J. M. Spangle, M. Tasan, S. Wanamaker, J. T. Webber, J. Roecklein-Canfield, E. Johannsen, A.-L. Barabási, R. Beroukhim, E. Kieff, M. E. Cusick, D. E. Hill, K. Münger, J. A. Marto, J. Quackenbush, F. P. Roth, J. A. DeCaprio, and M. Vidal, "Interpreting cancer genomes using systematic host network perturbations by tumour virus proteins.," *Nature*, vol. 487, no. 7408, pp. 491–5, Jul. 2012.

[59] E. A. White and P. M. Howley, "Proteomic approaches to the study of papillomavirus-host interactions.," *Virology*, vol. 435, no. 1, pp. 57–69, Jan. 2013.

[60] S. Duensing, L. Y. Lee, A. Duensing, J. Basile, S. Piboonniyom, S. Gonzalez, C. P. Crum, and K. Munger, "The human papillomavirus type 16 E6 and E7 oncoproteins cooperate to induce mitotic defects and genomic instability by uncoupling centrosome duplication from the cell division cycle.," *Proc. Natl. Acad. Sci. U. S. A.*, vol. 97, no. 18, pp. 10002–7, Aug. 2000.

[61] Y. Zhang, S. Fan, Q. Meng, Y. Ma, P. Katiyar, R. Schlegel, and E. M. Rosen, "BRCA1 interaction with human papillomavirus oncoproteins.," *J. Biol. Chem.*, vol. 280, no. 39, pp. 33165–77, Sep. 2005.

[62] R. A. Katzenellenbogen, E. M. Egelkrout, P. Vliet-Gregg, L. C. Gewin, P. R. Gafken, and D. A. Galloway, "NFX1-123 and poly(A) binding proteins synergistically augment activation of telomerase in human papillomavirus type 16 E6-expressing cells.," *J. Virol.*, vol. 81, no. 8, pp. 3786–96, Apr. 2007.

[63] P. Muench, S. Probst, J. Schuetz, N. Leiprecht, M. Busch, S. Wesselborg, F. Stubenrauch, and T. Iftner, "Cutaneous papillomavirus E6 proteins must interact with p300 and block p53-mediated apoptosis for cellular immortalization and tumorigenesis.," *Cancer Res.*, vol. 70, no. 17, pp. 6913–24, Sep. 2010.

[64] I. Cornet, V. Bouvard, M. S. Campo, M. Thomas, L. Banks, L. Gissmann, J. Lamartine, B. S. Sylla, R. Accardi, and M. Tommasino, "Comparative analysis of transforming properties of E6 and E7 from different beta human papillomavirus types.," *J. Virol.*, vol.

86, no. 4, pp. 2366–70, Feb. 2012.

[65] K. M. Bedard, M. P. Underbrink, H. L. Howie, and D. A. Galloway, “The E6 oncoproteins from human betapapillomaviruses differentially activate telomerase through an E6AP-dependent mechanism and prolong the lifespan of primary keratinocytes.,” *J. Virol.*, vol. 82, no. 8, pp. 3894–902, Apr. 2008.

[66] M. S. Barbosa, D. R. Lowy, and J. T. Schiller, “Papillomavirus polypeptides E6 and E7 are zinc-binding proteins.,” *J. Virol.*, vol. 63, no. 3, pp. 1404–7, Mar. 1989.

[67] S. B. Vande Pol and A. J. Klingelhutz, “Papillomavirus E6 oncoproteins.,” *Virology*, vol. 445, no. 1–2, pp. 115–37, Oct. 2013.

[68] M. Scheffner, B. A. Werness, J. M. Huibregtse, A. J. Levine, and P. M. Howley, “The E6 oncoprotein encoded by human papillomavirus types 16 and 18 promotes the degradation of p53.,” *Cell*, vol. 63, no. 6, pp. 1129–36, Dec. 1990.

[69] M. Scheffner, T. Takahashi, J. M. Huibregtse, J. D. Minna, and P. M. Howley, “Interaction of the human papillomavirus type 16 E6 oncoprotein with wild-type and mutant human p53 proteins.,” *J. Virol.*, vol. 66, no. 8, pp. 5100–5, Aug. 1992.

[70] C. J. Sherr, “Principles of tumor suppression.,” *Cell*, vol. 116, no. 2, pp. 235–46, Jan. 2004.

[71] F. Murray-Zmijewski, E. A. Slee, and X. Lu, “A complex barcode underlies the heterogeneous response of p53 to stress.,” *Nat. Rev. Mol. Cell Biol.*, vol. 9, no. 9, pp. 702–12, Sep. 2008.

[72] M. Scheffner, J. M. Huibregtse, R. D. Vierstra, and P. M. Howley, “The HPV-16 E6 and E6-AP complex functions as a ubiquitin-protein ligase in the ubiquitination of p53.,” *Cell*, vol. 75, no. 3, pp. 495–505, Nov. 1993.

[73] R. Accardi, W. Dong, A. Smet, R. Cui, A. Hautefeuille, A.-S. Gabet, B. S. Sylla, L. Gissmann, P. Hainaut, and M. Tommasino, “Skin human papillomavirus type 38 alters p53 functions by accumulation of deltaNp73.,” *EMBO Rep.*, vol. 7, no. 3, pp. 334–40, Mar. 2006.

[74] N. A. Wallace, K. Robinson, and D. A. Galloway, “Beta human papillomavirus E6 expression inhibits stabilization of p53 and increases tolerance of genomic instability.,” *J. Virol.*, vol. 88, no. 11, pp. 6112–27, Jun. 2014.

[75] N. Brimer, C. Lyons, A. E. Wallberg, and S. B. Vande Pol, “Cutaneous papillomavirus E6 oncoproteins associate with MAML1 to repress transactivation and NOTCH signaling.,” *Oncogene*, vol. 31, no. 43, pp. 4639–46, Oct. 2012.

[76] M. J. A. Tan, E. A. White, M. E. Sowa, J. W. Harper, J. C. Aster, and P. M. Howley, “Cutaneous β-human papillomavirus E6 proteins bind Mastermind-like coactivators and repress Notch signaling.,” *Proc. Natl. Acad. Sci. U. S. A.*, vol. 109, no. 23, pp. E1473-80, Jun. 2012.

[77] G. P. Dotto, “Notch tumor suppressor function.,” *Oncogene*, vol. 27, no. 38, pp. 5115–23, Sep. 2008.

[78] M. Nicolas, A. Wolfer, K. Raj, J. A. Kummer, P. Mill, M. van Noort, C. Hui, H. Clevers, G. P. Dotto, and F. Radtke, “Notch1 functions as a tumor suppressor in mouse skin.,” *Nat. Genet.*, vol. 33, no. 3, pp. 416–21, Mar. 2003.

[79] A. Proweller, L. Tu, J. J. Lepore, L. Cheng, M. M. Lu, J. Seykora, S. E. Millar, W. S. Pear, and M. S. Parmacek, “Impaired notch signaling promotes de novo squamous cell carcinoma formation.,” *Cancer Res.*, vol. 66, no. 15, pp. 7438–44, Aug. 2006.

[80] J. M. Meyers, J. M. Spangle, and K. Munger, “The human papillomavirus type 8 E6 protein interferes with NOTCH activation during keratinocyte differentiation.,” *J. Virol.*, vol. 87, no. 8, pp. 4762–7, Apr. 2013.

[81] H. L. Howie, J. I. Koop, J. Weese, K. Robinson, G. Wipf, L. Kim, and D. A. Galloway, “Beta-HPV 5 and 8 E6 promote p300 degradation by blocking AKT/p300 association.,” *PLoS Pathog.*, vol. 7, no. 8, p. e1002211, Aug. 2011.

[82] H. Zimmermann, R. Degenkolbe, H. U. Bernard, and M. J. O’Connor, “The human papillomavirus type 16 E6 oncoprotein can down-regulate p53 activity by targeting the transcriptional coactivator CBP/p300.,” *J. Virol.*, vol. 73, no. 8, pp. 6209–19, Aug. 1999.

[83] M. C. Thomas and C.-M. Chiang, “E6 oncoprotein represses p53-dependent gene activation via inhibition of protein acetylation independently of inducing p53 degradation.,” *Mol. Cell*, vol. 17, no. 2, pp. 251–64, Jan. 2005.

[84] T. Kiyono, A. Hiraiwa, M. Fujita, Y. Hayashi, T. Akiyama, and M. Ishibashi, “Binding of high-risk human papillomavirus E6 oncoproteins to the human homologue of the Drosophila discs large tumor suppressor protein.,” *Proc. Natl. Acad. Sci. U. S. A.*, vol.

94, no. 21, pp. 11612–6, Oct. 1997.

[85] B. A. Glaunsinger, S. S. Lee, M. Thomas, L. Banks, and R. Javier, “Interactions of the PDZ-protein MAGI-1 with adenovirus E4-ORF1 and high-risk papillomavirus E6 oncoproteins.,” *Oncogene*, vol. 19, no. 46, pp. 5270–80, Nov. 2000.

[86] M. Thomas, R. Laura, K. Hepner, E. Guccione, C. Sawyers, L. Lasky, and L. Banks, “Oncogenic human papillomavirus E6 proteins target the MAGI-2 and MAGI-3 proteins for degradation.,” *Oncogene*, vol. 21, no. 33, pp. 5088–96, Aug. 2002.

[87] S. S. Lee, B. Glaunsinger, F. Mantovani, L. Banks, and R. T. Javier, “Multi-PDZ domain protein MUPP1 is a cellular target for both adenovirus E4-ORF1 and high-risk papillomavirus type 18 E6 oncoproteins.,” *J. Virol.*, vol. 74, no. 20, pp. 9680–93, Oct. 2000.

[88] P. Muench, T. Hiller, S. Probst, A.-M. Florea, F. Stubenrauch, and T. Iftner, “Binding of PDZ proteins to HPV E6 proteins does neither correlate with epidemiological risk classification nor with the immortalization of foreskin keratinocytes,” *Virology*, vol. 387, no. 2, pp. 380–387, 2009.

[89] K. Van Doorslaer, R. DeSalle, M. H. Einstein, and R. D. Burk, “Degradation of Human PDZ-Proteins by Human Alphapapillomaviruses Represents an Evolutionary Adaptation to a Novel Cellular Niche.,” *PLoS Pathog.*, vol. 11, no. 6, p. e1004980, Jun. 2015.

[90] M. Thomas and L. Banks, “Human papillomavirus (HPV) E6 interactions with Bak are conserved amongst E6 proteins from high and low risk HPV types.,” *J. Gen. Virol.*, vol. 80 (Pt 6), pp. 1513–7, Jun. 1999.

[91] M. P. Underbrink, H. L. Howie, K. M. Bedard, J. I. Koop, and D. A. Galloway, “E6 proteins from multiple human betapapillomavirus types degrade Bak and protect keratinocytes from apoptosis after UVB irradiation.,” *J. Virol.*, vol. 82, no. 21, pp. 10408–17, Nov. 2008.

[92] M. Filippova, L. Parkhurst, and P. J. Duerksen-Hughes, “The human papillomavirus 16 E6 protein binds to Fas-associated death domain and protects cells from Fas-triggered apoptosis.,” *J. Biol. Chem.*, vol. 279, no. 24, pp. 25729–44, Jun. 2004.

[93] D. Pim, P. Massimi, and L. Banks, “Alternatively spliced HPV-18 E6* protein inhibits E6 mediated degradation of p53 and suppresses transformed cell growth.,” *Oncogene*,

vol. 15, no. 3, pp. 257–64, Jul. 1997.

[94] A. J. Klingelhutz and A. Roman, “Cellular transformation by human papillomaviruses: lessons learned by comparing high- and low-risk viruses.,” *Virology*, vol. 424, no. 2, pp. 77–98, Mar. 2012.

[95] W. C. Phelps, C. L. Yee, K. Münger, and P. M. Howley, “The human papillomavirus type 16 E7 gene encodes transactivation and transformation functions similar to those of adenovirus E1A.,” *Cell*, vol. 53, no. 4, pp. 539–47, May 1988.

[96] K. H. Vousden and P. S. Jat, “Functional similarity between HPV16E7, SV40 large T and adenovirus E1a proteins.,” *Oncogene*, vol. 4, no. 2, pp. 153–8, Feb. 1989.

[97] W. C. Phelps, K. Münger, C. L. Yee, J. A. Barnes, and P. M. Howley, “Structure-function analysis of the human papillomavirus type 16 E7 oncoprotein.,” *J. Virol.*, vol. 66, no. 4, pp. 2418–27, Apr. 1992.

[98] J. R. Gage, C. Meyers, and F. O. Wettstein, “The E7 proteins of the nononcogenic human papillomavirus type 6b (HPV-6b) and of the oncogenic HPV-16 differ in retinoblastoma protein binding and other properties.,” *J. Virol.*, vol. 64, no. 2, pp. 723–30, Feb. 1990.

[99] A. Schmitt, J. B. Harry, B. Rapp, F. O. Wettstein, and T. Iftner, “Comparison of the properties of the E6 and E7 genes of low- and high-risk cutaneous papillomaviruses reveals strongly transforming and high Rb-binding activity for the E7 protein of the low-risk human papillomavirus type 1.,” *J. Virol.*, vol. 68, no. 11, pp. 7051–9, Nov. 1994.

[100] H. Pfister and J. Ter Schegget, “Role of HPV in cutaneous premalignant and malignant tumors.,” *Clin. Dermatol.*, vol. 15, no. 3, pp. 335–47, Jan. 1997.

[101] D. W. Goodrich, N. P. Wang, Y.-W. Qian, E. Y.-H. P. Lee, and W.-H. Lee, “The retinoblastoma gene product regulates progression through the G1 phase of the cell cycle,” *Cell*, vol. 67, no. 2, pp. 293–302, Oct. 1991.

[102] N. Dyson, P. M. Howley, K. Münger, and E. Harlow, “The human papilloma virus-16 E7 oncoprotein is able to bind to the retinoblastoma gene product.,” *Science*, vol. 243, no. 4893, pp. 934–7, Feb. 1989.

[103] E. A. White, M. E. Sowa, M. J. A. Tan, S. Jeudy, S. D. Hayes, S. Santha, K. Münger, J. W. Harper, and P. M. Howley, “Systematic identification of interactions between

host cell proteins and E7 oncoproteins from diverse human papillomaviruses.," *Proc. Natl. Acad. Sci. U. S. A.*, vol. 109, no. 5, pp. E260-7, Jan. 2012.

[104] K.-W. Huh, J. DeMasi, H. Ogawa, Y. Nakatani, P. M. Howley, and K. Münger, "Association of the human papillomavirus type 16 E7 oncoprotein with the 600-kDa retinoblastoma protein-associated factor, p600.," *Proc. Natl. Acad. Sci. U. S. A.*, vol. 102, no. 32, pp. 11492–7, Aug. 2005.

[105] K. Huh, X. Zhou, H. Hayakawa, J.-Y. Cho, T. A. Libermann, J. Jin, J. W. Harper, and K. Munger, "Human papillomavirus type 16 E7 oncoprotein associates with the cullin 2 ubiquitin ligase complex, which contributes to degradation of the retinoblastoma tumor suppressor.," *J. Virol.*, vol. 81, no. 18, pp. 9737–47, Sep. 2007.

[106] D. Holland, K. Hoppe-Seyler, B. Schuller, C. Lohrey, J. Maroldt, M. Dürst, and F. Hoppe-Seyler, "Activation of the enhancer of zeste homologue 2 gene by the human papillomavirus E7 oncoprotein.," *Cancer Res.*, vol. 68, no. 23, pp. 9964–72, Dec. 2008.

[107] M. E. McLaughlin-Drubin, C. P. Crum, and K. Münger, "Human papillomavirus E7 oncoprotein induces KDM6A and KDM6B histone demethylase expression and causes epigenetic reprogramming.," *Proc. Natl. Acad. Sci. U. S. A.*, vol. 108, no. 5, pp. 2130–5, Mar. 2011.

[108] X. Liu, A. Dakic, R. Chen, G. L. Disbrow, Y. Zhang, Y. Dai, and R. Schlegel, "Cell-restricted immortalization by human papillomavirus correlates with telomerase activation and engagement of the hTERT promoter by Myc.," *J. Virol.*, vol. 82, no. 23, pp. 11568–76, Dec. 2008.

[109] C. A. Moody and L. A. Laimins, "Human papillomavirus oncoproteins: pathways to transformation.," *Nat. Rev. Cancer*, vol. 10, no. 8, pp. 550–60, Aug. 2010.

[110] P. Rous and J. W. Beard, "The progression to carcinoma of virus-induced rabbit papillomas (Shope)," *J. Exp. Med.*, vol. 62, no. 4, pp. 523–48, Sep. 1935.

[111] R. E. Shope and E. W. Hurst, "Infectious papillomatosis of rabbits: with a note on the histopathology.," *J. Exp. Med.*, vol. 58, no. 5, pp. 607–24, Oct. 1933.

[112] S. Jeckel, E. Huber, F. Stubenrauch, and T. Iftner, "A transactivator function of cottontail rabbit papillomavirus e2 is essential for tumor induction in rabbits.," *J. Virol.*, vol. 76, no. 22, pp. 11209–15, Nov. 2002.

[113] J. T. Syverton, “The Pathogenesis of the rabbit papilloma-to-carcinoma sequence,” *Ann. N. Y. Acad. Sci.*, vol. 54, no. 6, pp. 1126–1140, Jul. 1952.

[114] I. Giri, O. Danos, and M. Yaniv, “Genomic structure of the cottontail rabbit (Shope) papillomavirus.,” *Proc. Natl. Acad. Sci. U. S. A.*, vol. 82, no. 6, pp. 1580–4, Mar. 1985.

[115] J. Xi, “Master thesis.” 2014.

[116] M. S. Barbosa and F. O. Wettstein, “Transcription of the cottontail rabbit papillomavirus early region and identification of two E6 polypeptides in COS-7 cells.,” *J. Virol.*, vol. 61, no. 9, pp. 2938–42, Oct. 1987.

[117] O. Danos, E. Georges, G. Orth, and M. Yaniv, “Fine structure of the cottontail rabbit papillomavirus mRNAs expressed in the transplantable VX2 carcinoma.,” *J. Virol.*, vol. 53, no. 3, pp. 735–41, Mar. 1985.

[118] T. Ganzenmueller, M. Matthaei, P. Muench, M. Scheible, A. Iftner, T. Hiller, N. Leiprecht, S. Probst, F. Stubenrauch, and T. Iftner, “The E7 protein of the cottontail rabbit papillomavirus immortalizes normal rabbit keratinocytes and reduces pRb levels, while E6 cooperates in immortalization but neither degrades p53 nor binds E6AP.,” *Virology*, vol. 372, no. 2, pp. 313–24, Mar. 2008.

[119] P. Drobni, N. Mistry, N. McMillan, and M. Evander, “Carboxy-fluorescein diacetate, succinimidyl ester labeled papillomavirus virus-like particles fluoresce after internalization and interact with heparan sulfate for binding and entry,” *Virology*, vol. 310, no. 1, pp. 163–172, May 2003.

[120] T. Giroglou, L. Florin, F. Schäfer, R. E. Streeck, and M. Sapp, “Human papillomavirus infection requires cell surface heparan sulfate.,” *J. Virol.*, vol. 75, no. 3, pp. 1565–70, Feb. 2001.

[121] S. Sarrazin, W. C. Lamanna, and J. D. Esko, “Heparan sulfate proteoglycans.,” *Cold Spring Harb. Perspect. Biol.*, vol. 3, no. 7, Jul. 2011.

[122] S. Shafti-Keramat, A. Handisurya, E. Kriehuber, G. Meneguzzi, K. Slupetzky, and R. Kirnbauer, “Different heparan sulfate proteoglycans serve as cellular receptors for human papillomaviruses.,” *J. Virol.*, vol. 77, no. 24, pp. 13125–35, Dec. 2003.

[123] T. D. Culp, L. R. Budgeon, M. P. Marinkovich, G. Meneguzzi, and N. D. Christensen, “Keratinocyte-secreted laminin 5 can function as a transient receptor for human

papillomaviruses by binding virions and transferring them to adjacent cells.," *J. Virol.*, vol. 80, no. 18, pp. 8940–50, Sep. 2006.

[124] T. D. Culp, L. R. Budgeon, and N. D. Christensen, "Human papillomaviruses bind a basal extracellular matrix component secreted by keratinocytes which is distinct from a membrane-associated receptor.," *Virology*, vol. 347, no. 1, pp. 147–59, Mar. 2006.

[125] K. D. Scheffer, F. Berditchevski, and L. Florin, "The tetraspanin CD151 in papillomavirus infection.," *Viruses*, vol. 6, no. 2, pp. 893–908, Feb. 2014.

[126] L. Florin, M. Sapp, and G. A. Spoden, "Host-cell factors involved in papillomavirus entry.," *Med. Microbiol. Immunol.*, vol. 201, no. 4, pp. 437–48, Nov. 2012.

[127] T. D. Culp and N. D. Christensen, "Kinetics of in vitro adsorption and entry of papillomavirus virions.," *Virology*, vol. 319, no. 1, pp. 152–61, Mar. 2004.

[128] L. Pelkmans and A. Helenius, "Insider information: what viruses tell us about endocytosis," *Curr. Opin. Cell Biol.*, vol. 15, no. 4, pp. 414–422, Aug. 2003.

[129] P. M. Day, D. R. Lowy, and J. T. Schiller, "Papillomaviruses infect cells via a clathrin-dependent pathway.," *Virology*, vol. 307, no. 1, pp. 1–11, Mar. 2003.

[130] J. L. Smith, S. K. Campos, and M. A. Ozbun, "Human papillomavirus type 31 uses a caveolin 1- and dynamin 2-mediated entry pathway for infection of human keratinocytes.," *J. Virol.*, vol. 81, no. 18, pp. 9922–31, Sep. 2007.

[131] M. Schelhaas, B. Shah, M. Holzer, P. Blattmann, L. Kühling, P. M. Day, J. T. Schiller, and A. Helenius, "Entry of human papillomavirus type 16 by actin-dependent, clathrin- and lipid raft-independent endocytosis.," *PLoS Pathog.*, vol. 8, no. 4, p. e1002657, Jan. 2012.

[132] G. Spoden, K. Freitag, M. Husmann, K. Boller, M. Sapp, C. Lambert, and L. Florin, "Clathrin- and caveolin-independent entry of human papillomavirus type 16--involvement of tetraspanin-enriched microdomains (TEMs).," *PLoS One*, vol. 3, no. 10, p. e3313, Jan. 2008.

[133] Gary R. Whittaker, Michael Kann, and A. Helenius, "VIRAL ENTRY INTO THE NUCLEUS," Nov. 2003.

[134] J. L. Smith, S. K. Campos, A. Wandinger-Ness, and M. A. Ozbun, "Caveolin-1-dependent infectious entry of human papillomavirus type 31 in human keratinocytes

proceeds to the endosomal pathway for pH-dependent uncoating.," *J. Virol.*, vol. 82, no. 19, pp. 9505–12, Oct. 2008.

[135] K. H. Müller, G. A. Spoden, K. D. Scheffer, R. Brunnhöfer, J. K. De Brabander, M. E. Maier, L. Florin, and C. P. Muller, "Inhibition by cellular vacuolar ATPase impairs human papillomavirus uncoating and infection.," *Antimicrob. Agents Chemother.*, vol. 58, no. 5, pp. 2905–11, May 2014.

[136] H.-C. Selinka, T. Giroglou, and M. Sapp, "Analysis of the infectious entry pathway of human papillomavirus type 33 pseudovirions.," *Virology*, vol. 299, no. 2, pp. 279–287, Aug. 2002.

[137] P. M. Day, C. D. Thompson, R. M. Schowalter, D. R. Lowy, and J. T. Schiller, "Identification of a role for the trans-Golgi network in human papillomavirus 16 pseudovirus infection.," *J. Virol.*, vol. 87, no. 7, pp. 3862–70, Apr. 2013.

[138] A. Lipovsky, A. Popa, G. Pimienta, M. Wyler, A. Bhan, L. Kuruvilla, M.-A. Guie, A. C. Poffenberger, C. D. S. Nelson, W. J. Atwood, and D. DiMaio, "Genome-wide siRNA screen identifies the retromer as a cellular entry factor for human papillomavirus.," *Proc. Natl. Acad. Sci. U. S. A.*, vol. 110, no. 18, pp. 7452–7, Apr. 2013.

[139] L. Florin, K. A. Becker, C. Lambert, T. Nowak, C. Sapp, D. Strand, R. E. Streeck, and M. Sapp, "Identification of a dynein interacting domain in the papillomavirus minor capsid protein l2.," *J. Virol.*, vol. 80, no. 13, pp. 6691–6, Jul. 2006.

[140] M. A. Schneider, G. A. Spoden, L. Florin, and C. Lambert, "Identification of the dynein light chains required for human papillomavirus infection.," *Cell. Microbiol.*, vol. 13, no. 1, pp. 32–46, Jan. 2011.

[141] L. Florin, F. Schäfer, K. Sotlar, R. E. Streeck, and M. Sapp, "Reorganization of nuclear domain 10 induced by papillomavirus capsid protein l2.," *Virology*, vol. 295, no. 1, pp. 97–107, Mar. 2002.

[142] P. M. Day, C. C. Baker, D. R. Lowy, and J. T. Schiller, "Establishment of papillomavirus infection is enhanced by promyelocytic leukemia protein (PML) expression.," *Proc. Natl. Acad. Sci. U. S. A.*, vol. 101, no. 39, pp. 14252–7, Sep. 2004.

[143] M. Lazarczyk, P. Cassonnet, C. Pons, Y. Jacob, and M. Favre, "The EVER proteins as a natural barrier against papillomaviruses: a new insight into the pathogenesis of human papillomavirus infections.," *Microbiol. Mol. Biol. Rev.*, vol. 73, no. 2, pp. 348–

70, Jun. 2009.

[144] M. A. Stanley, M. R. Pett, and N. Coleman, “HPV: from infection to cancer.,” *Biochem. Soc. Trans.*, vol. 35, no. Pt 6, pp. 1456–60, Dec. 2007.

[145] B. P. Lucey, W. A. Nelson-Rees, and G. M. Hutchins, “Henrietta Lacks, HeLa Cells, and Cell Culture Contamination,” Oct. 2009.

[146] M. N. Ruesch, F. Stubenrauch, and L. A. Laimins, “Activation of papillomavirus late gene transcription and genome amplification upon differentiation in semisolid medium is coincident with expression of involucrin and transglutaminase but not keratin-10.,” *J. Virol.*, vol. 72, no. 6, pp. 5016–24, Jun. 1998.

[147] J. G. Rheinwald and H. Green, “Serial cultivation of strains of human epidermal keratinocytes: the formation of keratinizing colonies from single cells.,” *Cell*, vol. 6, no. 3, pp. 331–43, Nov. 1975.

[148] M. Scheffner, K. Münger, J. C. Byrne, and P. M. Howley, “The state of the p53 and retinoblastoma genes in human cervical carcinoma cell lines.,” *Proc. Natl. Acad. Sci. U. S. A.*, vol. 88, no. 13, pp. 5523–7, Jul. 1991.

[149] F. Friedl, I. Kimura, T. Osato, and Y. Ito, “Studies on a new human cell line (SiHa) derived from carcinoma of uterus. I. Its establishment and morphology.,” *Proc. Soc. Exp. Biol. Med.*, vol. 135, no. 2, pp. 543–5, Nov. 1970.

[150] F. L. Graham, J. Smiley, W. C. Russell, and R. Nairn, “Characteristics of a human cell line transformed by DNA from human adenovirus type 5.,” *J. Gen. Virol.*, vol. 36, no. 1, pp. 59–74, Jul. 1977.

[151] B. L. Allen-Hoffmann, S. J. Schlosser, C. A. Ivarie, C. A. Sattler, L. F. Meisner, and S. L. O’Connor, “Normal growth and differentiation in a spontaneously immortalized near-diploid human keratinocyte cell line, NIKS.,” *J. Invest. Dermatol.*, vol. 114, no. 3, pp. 444–55, Mar. 2000.

[152] S. Swift, J. Lorens, P. Achacoso, and G. P. Nolan, “Rapid production of retroviruses for efficient gene delivery to mammalian cells using 293T cell-based systems.,” *Curr. Protoc. Immunol.*, vol. Chapter 10, p. Unit 10.17C, May 2001.

[153] R. A. Pattillo, R. O. Hussa, M. T. Story, A. C. Ruckert, M. R. Shalaby, and R. F. Mattingly, “Tumor antigen and human chorionic gonadotropin in CaSki cells: a new

epidermoid cervical cancer cell line.," *Science*, vol. 196, no. 4297, pp. 1456–8, Jun. 1977.

[154] C. M. Stoscheck and G. Carpenter, "Biology of the A-431 cell: a useful organism for hormone research.," *J. Cell. Biochem.*, vol. 23, no. 1–4, pp. 191–202, Jan. 1983.

[155] E. Huber, D. Vlasny, S. Jeckel, F. Stubenrauch, and T. Iftner, "Gene profiling of cottontail rabbit papillomavirus-induced carcinomas identifies upregulated genes directly Involved in stroma invasion as shown by small interfering RNA-mediated gene silencing.," *J. Virol.*, vol. 78, no. 14, pp. 7478–89, Jul. 2004.

[156] M. Jones, I. R. Dry, D. Frampton, M. Singh, R. K. Kanda, M. B. Yee, P. Kellam, M. Hollinshead, P. R. Kinchington, E. A. O'Toole, and J. Breuer, "RNA-seq analysis of host and viral gene expression highlights interaction between varicella zoster virus and keratinocyte differentiation.," *PLoS Pathog.*, vol. 10, no. 1, p. e1003896, Jan. 2014.

[157] C. Banning, J. Votteler, D. Hoffmann, H. Koppensteiner, M. Warmer, R. Reimer, F. Kirchhoff, U. Schubert, J. Hauber, and M. Schindler, "A flow cytometry-based FRET assay to identify and analyse protein-protein interactions in living cells.," *PLoS One*, vol. 5, no. 2, p. e9344, Jan. 2010.

[158] F. Stubenrauch, A. M. Colbert, and L. A. Laimins, "Transactivation by the E2 protein of oncogenic human papillomavirus type 31 is not essential for early and late viral functions.," *J. Virol.*, vol. 72, no. 10, pp. 8115–23, Oct. 1998.

[159] J. S. Lea, N. Sunaga, M. Sato, G. Kalahasti, D. S. Miller, J. D. Minna, and C. Y. Muller, "Silencing of HPV 18 oncoproteins With RNA interference causes growth inhibition of cervical cancer cells.," *Reprod. Sci.*, vol. 14, no. 1, pp. 20–8, Jan. 2007.

[160] L. T. M. J. L. and D. G. S. Dieffenbach C.W., "General Concepts of Primer Design," *Genome Research*, 1993. [Online]. Available: http://www.nature.com/scitable/content/general-concepts-of-primer-design-8942407. [Accessed: 26-Apr-2015].

[161] M. W. Pfaffl, "A new mathematical model for relative quantification in real-time RT-PCR.," *Nucleic Acids Res.*, vol. 29, no. 9, p. e45, May 2001.

[162] F. M. B. R. K. R. E. M. D. D. S. J. G. S. J. A. S. K. Ausubel, "Current Protocols in Molecular Biology," *Greene Publ. Assoc. Interscience, New York*, 1990.

[163] J. Cox, M. Y. Hein, C. A. Luber, I. Paron, N. Nagaraj, and M. Mann, “Accurate proteome-wide label-free quantification by delayed normalization and maximal peptide ratio extraction, termed MaxLFQ.,” *Mol. Cell. Proteomics*, vol. 13, no. 9, pp. 2513–26, Sep. 2014.

[164] B. Schwanhäusser, D. Busse, N. Li, G. Dittmar, J. Schuchhardt, J. Wolf, W. Chen, and M. Selbach, “Global quantification of mammalian gene expression control.,” *Nature*, vol. 473, no. 7347, pp. 337–42, May 2011.

[165] J. Cox and M. Mann, “MaxQuant enables high peptide identification rates, individualized p.p.b.-range mass accuracies and proteome-wide protein quantification.,” *Nat. Biotechnol.*, vol. 26, no. 12, pp. 1367–72, Dec. 2008.

[166] S.-E. Ong, “Stable Isotope Labeling by Amino Acids in Cell Culture, SILAC, as a Simple and Accurate Approach to Expression Proteomics,” *Mol. Cell. Proteomics*, vol. 1, no. 5, pp. 376–386, May 2002.

[167] H. C. Harsha, H. Molina, and A. Pandey, “Quantitative proteomics using stable isotope labeling with amino acids in cell culture.,” *Nat. Protoc.*, vol. 3, no. 3, pp. 505–16, Jan. 2008.

[168] S.-E. Ong and M. Mann, “A practical recipe for stable isotope labeling by amino acids in cell culture (SILAC).,” *Nat. Protoc.*, vol. 1, no. 6, pp. 2650–60, Jan. 2006.

[169] S.-E. Ong and M. Mann, “Mass spectrometry-based proteomics turns quantitative.,” *Nat. Chem. Biol.*, vol. 1, no. 5, pp. 252–62, Oct. 2005.

[170] B. Macek, I. Mijakovic, J. V Olsen, F. Gnad, C. Kumar, P. R. Jensen, and M. Mann, “The serine/threonine/tyrosine phosphoproteome of the model bacterium Bacillus subtilis.,” *Mol. Cell. Proteomics*, vol. 6, no. 4, pp. 697–707, Apr. 2007.

[171] J. Cox, I. Matic, M. Hilger, N. Nagaraj, M. Selbach, J. V Olsen, and M. Mann, “A practical guide to the MaxQuant computational platform for SILAC-based quantitative proteomics.,” *Nat. Protoc.*, vol. 4, no. 5, pp. 698–705, Jan. 2009.

[172] J. Cox, N. Neuhauser, A. Michalski, R. A. Scheltema, J. V Olsen, and M. Mann, “Andromeda: a peptide search engine integrated into the MaxQuant environment.,” *J. Proteome Res.*, vol. 10, no. 4, pp. 1794–805, Apr. 2011.

[173] Y. Benjamini and Y. Hochberg, “Controlling the false discovery rate: a practical and

powerful approach to multiple testing," *J. R. Stat. Soc. Ser. B …*, 1995.

[174] T. Förster, "Zwischenmolekulare Energiewanderung und Fluoreszenz," *Ann. Phys.*, vol. 437, no. 1–2, pp. 55–75, 1948.

[175] C. G. dos Remedios and P. D. Moens, "Fluorescence resonance energy transfer spectroscopy is a reliable 'ruler' for measuring structural changes in proteins. Dispelling the problem of the unknown orientation factor.," *J. Struct. Biol.*, vol. 115, no. 2, pp. 175–85, Jan. 1995.

[176] R. Y. Tsien, "The green fluorescent protein.," *Annu. Rev. Biochem.*, vol. 67, pp. 509–44, Jan. 1998.

[177] E. A. White, R. E. Kramer, M. J. A. Tan, S. D. Hayes, J. W. Harper, and P. M. Howley, "Comprehensive analysis of host cellular interactions with human papillomavirus E6 proteins identifies new E6 binding partners and reflects viral diversity.," *J. Virol.*, vol. 86, no. 24, pp. 13174–86, Dec. 2012.

[178] A. Benito-Martin and H. Peinado, "FunRich proteomics software analysis, let the fun begin!," *Proteomics*, vol. 15, no. 15, pp. 2555–6, Aug. 2015.

[179] N. Kanda and S. Watanabe, "17beta-estradiol stimulates the growth of human keratinocytes by inducing cyclin D2 expression.," *J. Invest. Dermatol.*, vol. 123, no. 2, pp. 319–28, Aug. 2004.

[180] N. Kanda and S. Watanabe, "17beta-estradiol inhibits oxidative stress-induced apoptosis in keratinocytes by promoting Bcl-2 expression.," *J. Invest. Dermatol.*, vol. 121, no. 6, pp. 1500–9, Dec. 2003.

[181] S. Poppelreuther, T. Iftner, and F. Stubenrauch, "A novel splice donor site at nt 1534 is required for long-term maintenance of HPV31 genomes," *Virology*, vol. 370, no. 1, pp. 93–101, 2008.

[182] E. J. Enemark and L. Joshua-Tor, "Mechanism of DNA translocation in a replicative hexameric helicase.," *Nature*, vol. 442, no. 7100, pp. 270–5, Jul. 2006.

[183] L. E. King, E. S. Dornan, M. M. Donaldson, and I. M. Morgan, "Human papillomavirus 16 E2 stability and transcriptional activation is enhanced by E1 via a direct protein-protein interaction.," *Virology*, vol. 414, no. 1, pp. 26–33, May 2011.

[184] R. S. Hegde and E. J. Androphy, "Crystal structure of the E2 DNA-binding domain

from human papillomavirus type 16: implications for its DNA binding-site selection mechanism.," *J. Mol. Biol.*, vol. 284, no. 5, pp. 1479–89, Dec. 1998.

[185] M. Dreer, J. Fertey, S. van de Poel, E. Straub, J. Madlung, B. Macek, T. Iftner, and F. Stubenrauch, "Interaction of NCOR/SMRT Repressor Complexes with Papillomavirus E8^E2C Proteins Inhibits Viral Replication.," *PLoS Pathog.*, vol. 12, no. 4, p. e1005556, Apr. 2016.

[186] C. Davy, P. McIntosh, D. J. Jackson, R. Sorathia, M. Miell, Q. Wang, J. Khan, Y. Soneji, and J. Doorbar, "A novel interaction between the human papillomavirus type 16 E2 and E1^E4 proteins leads to stabilization of E2," *Virology*, vol. 394, no. 2, pp. 266–275, Nov. 2009.

[187] Q. Wang, H. Griffin, S. Southern, D. Jackson, A. Martin, P. McIntosh, C. Davy, P. J. Masterson, P. A. Walker, P. Laskey, M. B. Omary, and J. Doorbar, "Functional analysis of the human papillomavirus type 16 E1=E4 protein provides a mechanism for in vivo and in vitro keratin filament reorganization.," *J. Virol.*, vol. 78, no. 2, pp. 821–33, Jan. 2004.

[188] D. DiMaio and L. M. Petti, "The E5 proteins.," *Virology*, vol. 445, no. 1–2, pp. 99–114, Oct. 2013.

[189] H. S. Grm, P. Massimi, N. Gammoh, and L. Banks, "Crosstalk between the human papillomavirus E2 transcriptional activator and the E6 oncoprotein.," *Oncogene*, vol. 24, no. 33, pp. 5149–64, Aug. 2005.

[190] K. Zanier, A. ould M'hamed ould Sidi, C. Boulade-Ladame, V. Rybin, A. Chappelle, A. Atkinson, B. Kieffer, and G. Travé, "Solution structure analysis of the HPV16 E6 oncoprotein reveals a self-association mechanism required for E6-mediated degradation of p53.," *Structure*, vol. 20, no. 4, pp. 604–17, Apr. 2012.

[191] N. Gammoh, H. S. Grm, P. Massimi, and L. Banks, "Regulation of human papillomavirus type 16 E7 activity through direct protein interaction with the E2 transcriptional activator.," *J. Virol.*, vol. 80, no. 4, pp. 1787–97, Mar. 2006.

[192] M. E. McLaughlin-Drubin and K. Münger, "The human papillomavirus E7 oncoprotein.," *Virology*, vol. 384, no. 2, pp. 335–44, Feb. 2009.

[193] A. Siddiqa, K. C. Léon, C. D. James, M. F. Bhatti, S. Roberts, and J. L. Parish, "The human papillomavirus type 16 L1 protein directly interacts with E2 and enhances E2-

dependent replication and transcription activation.," *J. Gen. Virol.*, vol. 96, no. 8, pp. 2274–85, Aug. 2015.

[194] P. M. Day, R. B. Roden, D. R. Lowy, and J. T. Schiller, "The papillomavirus minor capsid protein, L2, induces localization of the major capsid protein, L1, and the viral transcription/replication protein, E2, to PML oncogenic domains.," *J. Virol.*, vol. 72, no. 1, pp. 142–50, Jan. 1998.

[195] R. L. Finnen, K. D. Erickson, X. S. Chen, and R. L. Garcea, "Interactions between papillomavirus L1 and L2 capsid proteins.," *J. Virol.*, vol. 77, no. 8, pp. 4818–26, Apr. 2003.

[196] S. Caldeira, I. Zehbe, R. Accardi, I. Malanchi, W. Dong, M. Giarrè, E.-M. de Villiers, R. Filotico, P. Boukamp, and M. Tommasino, "The E6 and E7 proteins of the cutaneous human papillomavirus type 38 display transforming properties.," *J. Virol.*, vol. 77, no. 3, pp. 2195–206, Feb. 2003.

[197] J. Haedicke and T. Iftner, "Human papillomaviruses and cancer," *Radiother. Oncol.*, vol. 108, no. 3, pp. 397–402, 2013.

[198] J. B. Harry and F. O. Wettstein, "Transforming Properties of the Cottontail Rabbit Papillomavirus Oncoproteins LE6 and SE6 and of the E8 Protein," *J. Virol.*, vol. 70, no. 6, pp. 3355–3362, 1996.

[199] N. Ke, G. Claassen, D.-H. Yu, A. Albers, W. Fan, P. Tan, M. Grifman, X. Hu, K. Defife, V. Nguy, B. Meyhack, A. Brachat, F. Wong-Staal, and Q.-X. Li, "Nuclear hormone receptor NR4A2 is involved in cell transformation and apoptosis.," *Cancer Res.*, vol. 64, no. 22, pp. 8208–12, Nov. 2004.

[200] Y. Han, H. Cai, L. Ma, Y. Ding, X. Tan, Y. Liu, T. Su, Y. Yu, W. Chang, H. Zhang, C. Fu, and G. Cao, "Nuclear orphan receptor NR4A2 confers chemoresistance and predicts unfavorable prognosis of colorectal carcinoma patients who received postoperative chemotherapy," *Eur. J. Cancer*, vol. 49, no. 16, pp. 3420–3430, 2013.

[201] R. J. A. Bell, H. T. Rube, A. Kreig, A. Mancini, S. D. Fouse, R. P. Nagarajan, S. Choi, C. Hong, D. He, M. Pekmezci, J. K. Wiencke, M. R. Wrensch, S. M. Chang, K. M. Walsh, S. Myong, J. S. Song, and J. F. Costello, "Cancer. The transcription factor GABP selectively binds and activates the mutant TERT promoter in cancer.," *Science*, vol. 348, no. 6238, pp. 1036–9, May 2015.

[202] T. Oikawa and T. Yamada, “Molecular biology of the Ets family of transcription factors,” *Gene*, vol. 303, pp. 11–34, 2003.

[203] D. Engelmann and B. M. Pützer, “The dark side of E2F1: in transit beyond apoptosis.,” *Cancer Res.*, vol. 72, no. 3, pp. 571–5, Feb. 2012.

[204] Y.-T. Siu and D.-Y. Jin, “CREB − a real culprit in oncogenesis,” *FEBS J.*, vol. 274, no. 13, pp. 3224–3232, Jul. 2007.

[205] E. D. Pleasance, R. K. Cheetham, P. J. Stephens, D. J. McBride, S. J. Humphray, C. D. Greenman, I. Varela, M.-L. Lin, G. R. Ordóñez, G. R. Bignell, K. Ye, J. Alipaz, M. J. Bauer, D. Beare, A. Butler, R. J. Carter, L. Chen, A. J. Cox, S. Edkins, P. I. Kokko-Gonzales, N. A. Gormley, R. J. Grocock, C. D. Haudenschild, M. M. Hims, T. James, M. Jia, Z. Kingsbury, C. Leroy, J. Marshall, A. Menzies, L. J. Mudie, Z. Ning, T. Royce, O. B. Schulz-Trieglaff, A. Spiridou, L. A. Stebbings, L. Szajkowski, J. Teague, D. Williamson, L. Chin, M. T. Ross, P. J. Campbell, D. R. Bentley, P. A. Futreal, and M. R. Stratton, “A comprehensive catalogue of somatic mutations from a human cancer genome,” *Nature*, vol. 463, no. 7278, pp. 191–196, Jan. 2010.

[206] J. Kaczynski, T. Cook, and R. Urrutia, “Sp1- and Krüppel-like transcription factors,” *Genome Biol.*, vol. 4, no. 2, p. 206, 2003.

[207] H. Sun and R. Taneja, “Stra13 expression is associated with growth arrest and represses transcription through histone deacetylase (HDAC)-dependent and HDAC-independent mechanisms.,” *Proc. Natl. Acad. Sci. U. S. A.*, vol. 97, no. 8, pp. 4058–63, Apr. 2000.

[208] F. Sato, U. K. Bhawal, T. Yoshimura, and Y. Muragaki, “DEC1 and DEC2 Crosstalk between Circadian Rhythm and Tumor Progression.,” *J. Cancer*, vol. 7, no. 2, pp. 153–9, 2016.

[209] S. Pensa, G. Regis, D. Boselli, F. Novelli, and V. Poli, “STAT1 and STAT3 in Tumorigenesis: Two Sides of the Same Coin?,” 2013.

[210] A. Brehm, S. J. Nielsen, E. A. Miska, D. J. McCance, J. L. Reid, A. J. Bannister, and T. Kouzarides, “The E7 oncoprotein associates with Mi2 and histone deacetylase activity to promote cell growth.,” *EMBO J.*, vol. 18, no. 9, pp. 2449–58, May 1999.

[211] J. M. Arbeit, P. M. Howley, and D. Hanahan, “Chronic estrogen-induced cervical and vaginal squamous carcinogenesis in human papillomavirus type 16 transgenic mice.,”

Proc. Natl. Acad. Sci. U. S. A., vol. 93, no. 7, pp. 2930–5, Apr. 1996.

[212] T. Brake and P. F. Lambert, “Estrogen contributes to the onset, persistence, and malignant progression of cervical cancer in a human papillomavirus-transgenic mouse model,” *Proc. Natl. Acad. Sci.*, vol. 102, no. 7, pp. 2490–2495, Feb. 2005.

[213] Y. Huang, J. Li, L. Xiang, D. Han, X. Shen, and X. Wu, “17β-Oestradiol activates proteolysis and increases invasion through phosphatidylinositol 3-kinase pathway in human cervical cancer cells,” *Eur. J. Obstet. Gynecol. Reprod. Biol.*, vol. 165, no. 2, pp. 307–312, Dec. 2012.

[214] Q. Wang, X. Li, L. Wang, Y.-H. Feng, R. Zeng, and G. Gorodeski, “Antiapoptotic Effects of Estrogen in Normal and Cancer Human Cervical Epithelial Cells,” *Endocrinology*, vol. 145, no. 12, pp. 5568–5579, Dec. 2004.

[215] M. Ruutu, N. Wahlroos, K. Syrjanen, B. Johansson, and S. Syrjanen, “Effects of 17beta-estradiol and progesterone on transcription of human papillomavirus 16 E6/E7 oncogenes in CaSki and SiHa cell lines,” *Int. J. Gynecol. Cancer*, vol. 16, no. 3, pp. 1261–1268, May 2006.

[216] I. Correa, M. A. Cerbón, A. M. Salazar, J. D. Solano, A. García-Carrancá, and A. Quintero, “Differential p53 Protein Expression Level in Human Cancer-Derived Cell Lines After Estradiol Treatment,” *Arch. Med. Res.*, vol. 33, no. 5, pp. 455–459, Sep. 2002.

[217] D. A. Elson, R. R. Riley, A. Lacey, G. Thordarson, F. J. Talamantes, and J. M. Arbeit, “Sensitivity of the cervical transformation zone to estrogen-induced squamous carcinogenesis.,” *Cancer Res.*, vol. 60, no. 5, pp. 1267–75, Mar. 2000.

[218] L. Newfield, H. L. Bradlow, D. W. Sepkovic, and K. Auborn, “Estrogen metabolism and the malignant potential of human papillomavirus immortalized keratinocytes.,” *Proc. Soc. Exp. Biol. Med.*, vol. 217, no. 3, pp. 322–6, Mar. 1998.

[219] E. Keleş, M. Lianeri, and P. P. Jagodziński, “Apicidin suppresses transcription of 17β-hydroxysteroid dehydrogenase type 1 in endometrial adenocarcinoma cells,” *Mol. Biol. Rep.*, vol. 38, no. 5, pp. 3355–3360, Jun. 2011.

[220] H. Drzewiecka, B. Gałęcki, D. Jarmołowska-Jurczyszyn, A. Kluk, W. Dyszkiewicz, and P. P. Jagodziński, “Increased expression of 17-beta-hydroxysteroid dehydrogenase type 1 in non-small cell lung cancer,” *Lung Cancer*, vol. 87, no. 2, pp. 107–116, Feb.

2015.

[221] C.-Y. Zhang, J. Chen, D.-C. Yin, and S.-X. Lin, “The Contribution of 17beta-Hydroxysteroid Dehydrogenase Type 1 to the Estradiol-Estrone Ratio in Estrogen-Sensitive Breast Cancer Cells,” *PLoS One*, vol. 7, no. 1, p. e29835, Jan. 2012.

[222] M. A. Stanley, “Epithelial cell responses to infection with human papillomavirus.,” *Clin. Microbiol. Rev.*, vol. 25, no. 2, pp. 215–22, Apr. 2012.

10. Abbreviations

aa	amino acid
APS	Ammoniumpersulfate
ATP	adenosine triphosphate
BCC	Basal cell carcinoma
bp	base pair
BFP	Blue fluorescent protein
BPV	Bovine papillomavirus
BSA	Bovine serum albumin
cAMP	Cyclic adenosine monophosphate
CAPS	N-cyclohexyl-3-aminopropanesulfonic acid
CBP	CREB-binding protein
cDNA	Complementary DNA
CIN	Cervical intraepithelial neoplasia
co	Codon-optimized
CoIP	Co-immunoprecipitaion
CREB	cAMP responsive element binding protein
CRPV	Cottontail rabbit papillomavirus
CS	Calf serum
Ct	Threshold cycle
DAPI	4’,6-Diamidino-2-phenylindol
DBD	DNA-binding domain
DMEM	Dulbecco´s Modified Eagle Medium
DMSO	Dimethyl sulfoxide
dNTP	Deoxyribonucleotide triphosphate
ds	double-stranded
DTT	Dithiothreitol
E6AP	E6-associated protein, E3 ubiquitin ligase

ECM	Extracellular matrix
EGF	Epidermal Growth Factor
ER	Endoplasmic reticulum
EV	Epidermodysplasia verruciformis
FACS	Fluorescence Activated Cell Sorting
FBS	Fetal bovine serum
FCS	Fetal calf serum
Fig	Figure
FITC	Fluorescein isothiocyanate
FRET	Förster/fluorescence resonance energy transfer
FSC	Forward SCatter
GFP	Green fluorescent protein
h	Hours
HA	Human influenza hemagglutinin
HPV	Human papillomavirus
HR-HPV	High risk-HPV
HRP	Horseradish peroxidase
HSPG	Heparan sulfate proteoglycan
ICC	Immunocytochemistry
IF	Immunofluorescence
IN	Input
IP	Immunoprecipitate
kDa	Kilodalton
LC	Liquid Chromatography
LCR	Long control region
LE6	Long E6
LR-HPV	Low risk-HPV
luc	Luciferase
M	Molar

MCLB	Mammalian cell lysis buffer
MCS	Multiple cloning site
Met/Ac	Methanol/Acetone
min	Minutes
mRNA	Messenger RNA
MS	Mass Spectrometry
NMSC	Non-melanoma skin cancer
NP40	4-Nonylphenyl-polyethylene glycol
nt	Nucleotide
OD	Optical density
ORF	Open reading frame
pAE	Early polyadenylation site
pAL	Late polyadenylation site
PBS	Phosphate buffered saline
PBS-T	PBS-Tween
PCR	Polimerase chain reaction
PDZ	PSD-95, Discs-large, ZO-1
PFA	Paraformaldehyde
PV	papillomavirus
qPCR	Quantitative PCR
RLU	Relative light units
rpm	Rotations per minute
RT	Room temperature
s	Seconds
SCC	Squamous cell carcinoma
SD	Standard deviation
SDS-PAGE	Sodium Dodecyl Sulphate – PolyAcrylamide Gel Electrophoresis
SE6	Short E6
SILAC	Stable isotope labeling by/with amino acids in cell culture

siRNA	small interfering RNA
SSC	Side SCatter
TBS	Tris-buffered saline
TBS-T	TBS-tween
TEMED	Tetramethylethylendiamine
Tm	Melting temperature
Tris	Trishydroxymethylaminomethan
URR	Upstream regulatory region
YFP	Yellow fluorescent protein
WT	Wildtype

11. Academic CV

Dec. 2011 - Dec. 2015 **PhD in Life Science, University Hospital Tübingen**
Institute of Medical Virology, Division of Experimental Virology (AG Iftner)

Dissertation title: "Global examination of papillomavirus protein-protein interactions: The intraviral interactome of HPV31 and the cellular binding partners of cutaneous papillomaviruses"

Jan.2008 - Jan. 2010 **MSc Degree in Medical, Molecular and Cellular Biotechnology**
(2 years graduation)
Final Mark: 110/110 cum laude (with honors)

"Role of glutamate metabotropic receptor mGlu4 in a model of transient focal cerebral ischemia"

Oct. 2004 - Oct. 2007 **Bachelor's degree in Biotechnology (3 years graduation)**

"Study of glutamate metabotropic receptor mGlu4 in medulloblastoma's cellular cultures"

12. Acknowledgements

I am deeply grateful to Prof. Dr. Thomas Iftner for giving me the great opportunity to work on my PhD in his group and for the guidance and support received during these years.

Many thanks to Prof. Dr. Peter G. Kremsner for being my second supervisor and for evaluating my PhD thesis

A special thank you goes to Dr. Juliane Haedicke- Jarboui and Dr. Mohamed Ali Jarboui who helped me in correcting my PhD thesis as well as in daily life issues.

Thanks to Prof. Dr. Frank Stubenrauch for his help and for all the scientific discussions.

My gratitude goes to the Proteome Center of Tübingen (PCT), especially to Prof. Dr. Boris Macek and to Dr. Ana Velic for their support in the proteomics experiments and their help in writing my PhD thesis.

Thanks to Prof. Schindler's group for the help in the FACS-FRET experiments.

Many thanks to Dr. Karl Munger for providing the pCMV vectors to Prof. Dr. Scott Vande pol for the Notch responsive luciferase vectors.

A great thank-you goes to Dr. Maria Delcuratolo, Dr. Olga Rataj and Jin Xi who supported me during the work in the lab but also as friends in real life. We shared a lot of happy and hard moments together, but with your support everything was easier.

A great thanks to the Tübingeros, for making life in Tübingen more like "at home".

I would like to thank my family and my friends who supported me throughout these years, showing me their unconditional love and demonstrating me that 1000 km are not that far in the end.

Last but not least I give my full gratitude to Dario, who became my husband during the PhD period and who stood by me step by step, encouraging and supporting me as only the love of a life can do.